

APPENDIX 2.10.7 PENETRATION TEST AS PER 10 CFR 71.71(C)-(10)

1. INTRODUCTION

The penetration test is carried out using a 6 kg (13 lb.), 3.2 cm (1.25 in.) diameter bar with hemispherical end dropped from 1 meter (40 in.) height onto the exposed surface of the F-294 package. The analytical assessment of the penetration test is presented herein.

2. ANALYSIS

Figure 2.10.7-F1 is reproduced from Figure 2 of Shieh's paper Ref.[26]. It shows the non-dimensional incipient puncture energy $V_c = [V_c / (\sigma_u t^3)]$ and punch displacement $U_c = \delta_c / t$ as functions of d/t for various values of d/D for both stainless steel and carbon steel plates not backed by lead. R. S. Shieh recommends that the use of these curves in puncture-safe design of circular flat steel cask plate should be made only after reducing the puncture energy absorbing capacity by 30% to allow a margin of safety for inaccuracy, uncertainties etc.

$$V_c = [V_c / (\sigma_u t^3)] \quad \text{..... Equation 1}$$

$$U_c = \delta_c / t \quad \text{..... Equation 2}$$

where

V_c = non-dimensional incipient puncture energy parameter.

V_c = incipient puncture energy in.-lb.

σ_u = ultimate strength of steel psi

t = thickness of steel plate or shell

d = punch diameter, in.

D = diameter of the plate or shell

2.1 PUNCTURE ANALYSIS OF TOP FIRESHIELD

Equations 1 and 2 are applied to the top fireshield case. The parameters are:

σ_u = ultimate strength of steel psi = 65,000 psi for AISI 1020 steel

t = thickness of steel plate or shell = 0.5 in.

d = punch diameter, in. = 1.25 in.

D = diameter of the plate or shell = 30 in.

d/t = 1.25/0.5 = 2.5

d/D = 1.25/30 = 0.0416

From Figure 2.10.7-F1, at $d/t = 2.5$ and $d/D = 0.0416$ (rounded up to 0.07), $V_c = 5.5$

Therefore

$$\begin{aligned} V_c &= (100\% - 30\%) * V_c * \sigma_u * t^3 \\ &= 0.7 * 5.5 * 65,000 * 0.5^3 \\ &= 0.7 * 44,687 \text{ in.-lb.} \\ &= 31,280 \text{ in.-lb.} \end{aligned}$$

The energy available to puncture

$$\begin{aligned} E_{\text{available}} &= \text{weight of the puncture bar} * \text{drop height} \\ &= 13 \text{ lb.} * 40 \text{ in.} \\ &= 520 \text{ in.-lb.} \end{aligned}$$

As the computed incipient puncture energy (31,280 in.-lb.) required for the top fireshield plate (0.5 in. thick) to puncture is much greater than the energy available (520 in.-lb.) to puncture, the top fireshield plate shall not be punctured.

2.2 CARBON STEEL 1/4 IN. THICK PLATE

Equations 1 and 2 are applied to the 1/4 in. thick carbon steel plate case. The parameters are

$$\begin{aligned}\sigma_u &= \text{ultimate strength of steel psi} = 65,000 \text{ psi for AISI 1020 steel} \\ t &= \text{thickness of steel plate} = 0.25 \text{ in.} \\ d &= \text{punch diameter, in.} = 1.25 \text{ in.} \\ D &= \text{diameter of the plate or shell} = 30 \text{ in.} \\ d/t &= 1.25/0.25 = 5. \\ d/D &= 1.25/30 = 0.0416\end{aligned}$$

From Figure 2.10.7-F1, at $d/t = 5$. and $d/D = 0.0416$ (rounded up to 0.07), $V_c = 26$

Therefore

$$\begin{aligned}V_c &= (100\% - 30\%) * V_c * \sigma_c * t^3 \\ &= 0.7 * 26 * 65,000 * 0.25^3 \\ &= 0.7 * 26,406 \text{ in.-lb.} \\ &= 18,480 \text{ in.-lb.}\end{aligned}$$

The energy available to puncture

$$\begin{aligned}pE_{\text{available}} &= \text{weight of the puncture bar} * \text{drop height} \\ &= 13 \text{ lb.} * 40 \text{ in.} \\ &= 520 \text{ in.-lb.}\end{aligned}$$

As the computed incipient puncture energy (18,480 in.-lb.) required for the 0.25 in. thick plate to puncture is much greater than the energy available (520 in.-lb.) to puncture, the 0.25 in. thick plate shall not be punctured.

2.3 0.25 IN THICK SHELL OF CYLINDRICAL FIRESHIELD

No empirical puncture data for steel shell, not backed by lead, exist today.

Therefore it is assumed that curvature of the shell shall offer as much resistance to puncture as the flat plate as the shell is stiffer for same d/t , d/D ratios.

The full-scale F-294 test packaging was subjected to five (5) puncture pin tests for the hypothetical accident conditions of transport tests. This is presented in Chapter 2, Appendix 2.10.12. The puncture pin is 6 in. diameter and 26 in. in height. The initial impact energy is 21,482 lb. x 36 in. height = 773,352 in.-lb. The cylindrical fireshield was subjected to two (2) puncture tests. In the worst case, the double shell of the cylindrical fireshield was torn and the amount of opening was 21 in².

In the normal conditions of transport penetration test for the F-294, the initial impact energy for a bar (13 lb. weight) dropped from a 40-inch free height onto an F-294 package is only 520 in.-lb.

As 520 in.-lb. impact energy (for normal conditions) is so small in comparison with the impact energy of 773,352 in.-lb. (for accident conditions), it is concluded that the 0.25 inch thick shell of the cylindrical fireshield will not puncture when subjected to the penetration test.

3. SUMMARY

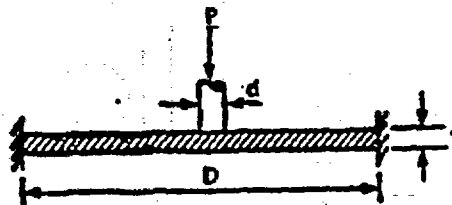
3.1 THE SUB-COMPONENTS THAT SURROUND THE F-294 CONTAINER ARE:

1. top fireshield (integral with the crush shield)
2. cylindrical fireshield
3. bottom skid

As both top and bottom carbon steel plates are 0.5 in. thick, they will resist puncture, when F-294 package is subject to the penetration test.

As the cylindrical fireshield shell is 0.25 in. thick, it will resist puncture when the F-294 package is subject to the penetration test.

Figure 2.10.7-F1
Non-dimensional Incipient Puncture Energy V_c and Punch Displacement U_c
as Function of d/t for Various Values of d/D
 (Reproduced from Fig. 2 of Shieh's paper Ref. [26])



1319

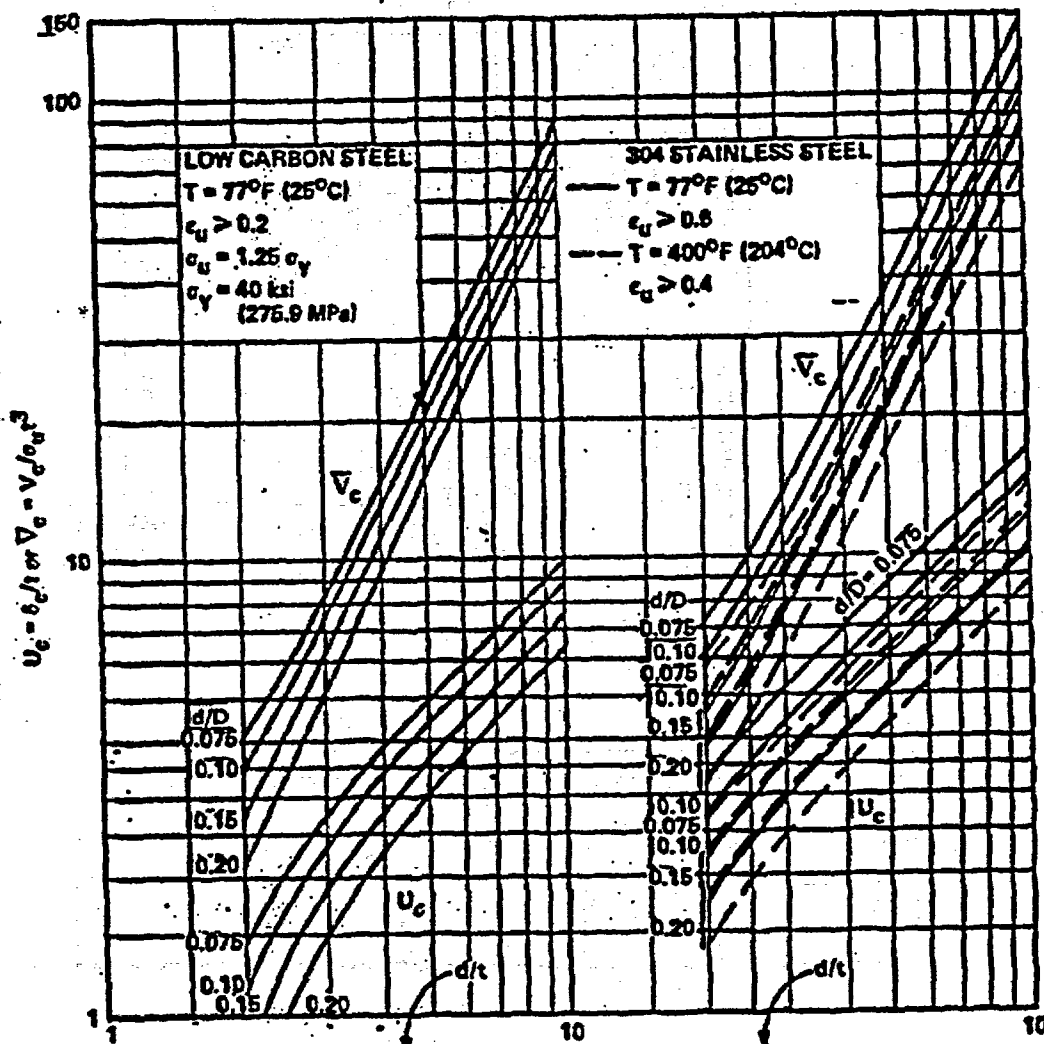
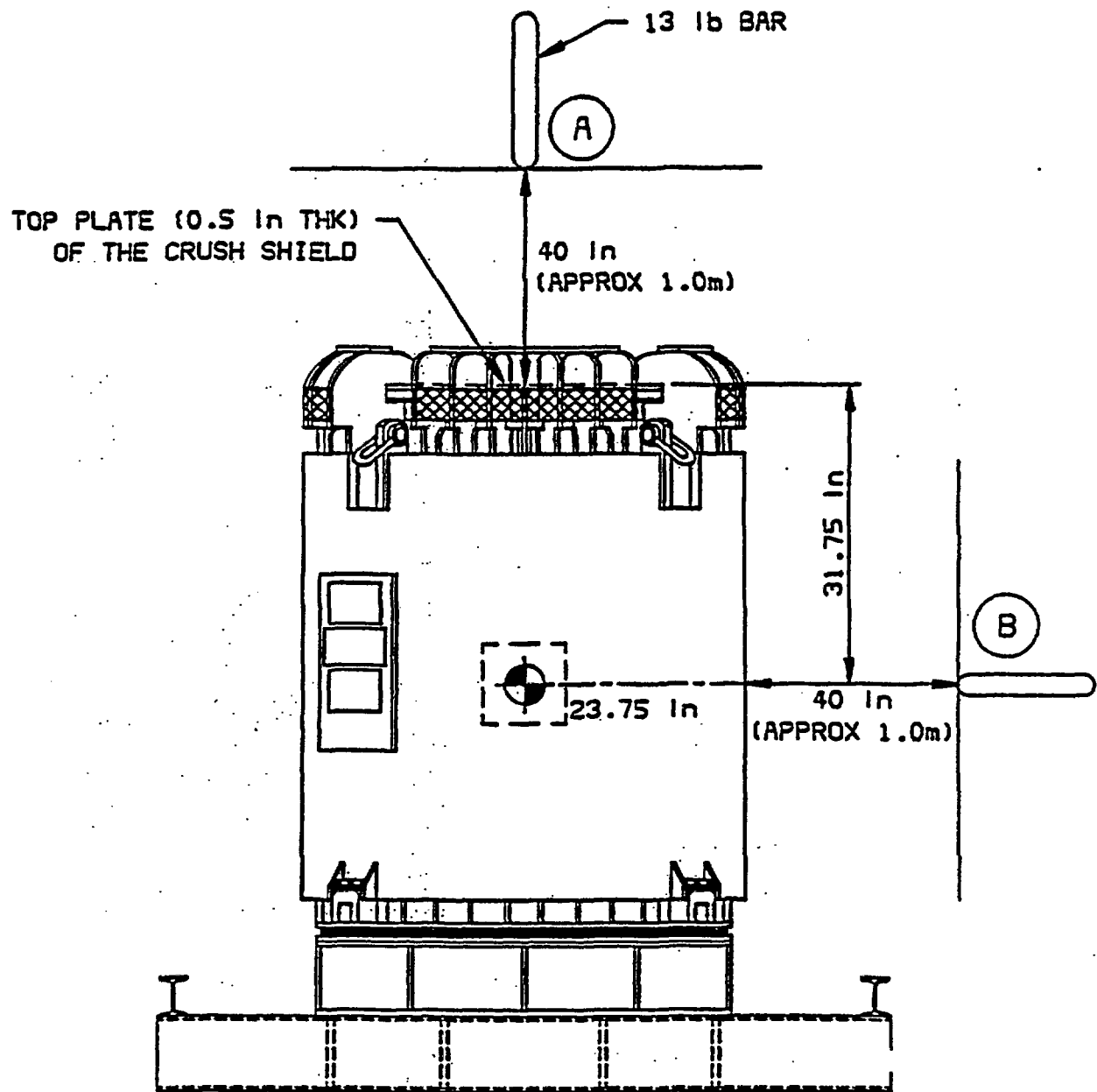


Figure 2. Nondimensional Incipient Puncture Energy V_c and Punch Displacement U_c as Functions of d/t for Various Values of d/D

Figure 2.10.7-F2
F-294 Subject to Penetration Test



APPENDIX 2.10.8

COMPRESSION TEST AS PER 10 CFR 71.71 (c)-(9)

1. INTRODUCTION

As the F-294 package weight of 21,000 lb. is greater than 5000 kg (11,000 lb.), 10 CFR 71.71 (c)-(9) does not apply to the F-294. The Regulations for the Safe Transport of Radioactive Material (IAEA TS-R-1) do require that the F-294 package withstand a compressive load uniformly applied to the top and bottom of the package for a period of 24 hours, equal to the greater of:

- i) five times the weight of the package;

$$5 * 21,000 \text{ lb.} = 105,000 \text{ lb., OR}$$
- ii) the equivalent of 13 kilopascals (2 lb./in²) multiplied by the vertically projected area of the package;

$$\begin{aligned} \text{Vertically projected area} &= 78 \text{ in.} * 78 \text{ in.} \\ &= 6084 \text{ in}^2 \end{aligned}$$

Therefore,

$$\text{Load} = 2 \text{ lb./in}^2 * 6064 \text{ in}^2 = 12,128 \text{ lb.}$$

Therefore, the applied load shall be 105,000 lb.

An analytical assessment is presented for demonstration of F-294's ability to withstand the compressive load equal to 5 x the weight of the F-294 package.

2. ANALYSIS

2.1 COMPRESSIVE STRESS IN THE OUTER SHELL OF THE CONTAINER

The problem can be simplified by making a conservative assumption that all the compressive load is borne by 0.5 in. thick stainless steel outer shell of the container only, with no support credited for the external cooling fins and the lead shielding. See Figures 2.10.8-F1 and 2.10.8-F2 respectively.

The stainless steel shell is treated as a thin-walled circular pipe, of length 24 in. and OD = 36 in., under longitudinal compression. the formula for critical unit compressive stress σ_c , given by Roark (Table XVI, Case 25 of Ref.[4]), for ends unrestrained, is

$$\sigma_c = 0.3 * E * t / r$$

where

$$\begin{aligned} \sigma_c &= \text{unit compressive stress, psi} \\ E &= \text{Modulus of Elasticity, psi} \\ t &= \text{wall thickness of shell or pipe, inches} \\ r &= \text{mean radius of pipe, inches} \\ \sigma_c &= 0.3 * 28 * 10^6 * 0.5 / 17.5 \\ &= 0.24 * 10^6 \text{ psi} \end{aligned}$$

The formula is most accurate for very long tubes but is applicable if the length is several times greater than $1.72 \sqrt{rt} = 1.72 \sqrt{(17.5 * 0.5)} = 5.1 \text{ in.}$, which is the length of a half-wave of buckling

The compressive load capability P_c is then

$$\begin{aligned} P_c &= \sigma_c * A \\ &= 0.24 * 10^6 * \pi * 35 * 0.5 \\ &= 13.19 * 10^6 \text{ lb.} \end{aligned}$$

The critical buckling load P_c of $13.19 * 10^6$ lb. is well above the actual applied load of 105,000 lb. It is therefore concluded that the F-294 container will easily sustain compressive loads of 5 times its own weight, applied on top and bottom for 24 hours at room temperature or 38°C ambient.

2.2 COMPRESSIVE STRESS IN THE EXTERNAL COOLING FINS

Material of fins = ss304L

Number of fins = 36

Size of fins = 0.375 in. minimum thickness x 4 in. width

Compressive stress at top of the fins, σ_c

$$\begin{aligned}\sigma_c &= 5 * W/A_{fins} \\ &= 5 * 21,000/[36 * 0.375 * 4] \\ &= 1,944 \text{ psi}\end{aligned}$$

The compressive stress is well within the yield stress 25,000 psi for ss304L.

2.3 COMPRESSIVE STRESS IN THE FLANGES OF CHANNELS OF THE SKID

Material of the channel = ASTM A-36

Channel section = 3.5 * 8 * 78 in.

$$\begin{aligned}\text{compressive stress, } \sigma_c &= 5 * W/A_{flanges} \\ &= 5 * 21,000/[4 * 78 * 3] \\ &= 112 \text{ psi}\end{aligned}$$

The compressive stress is well within the yield stress of 36,000 psi. of the channel material.

Figure 2.10.8-F1
F-294 Package under Compression

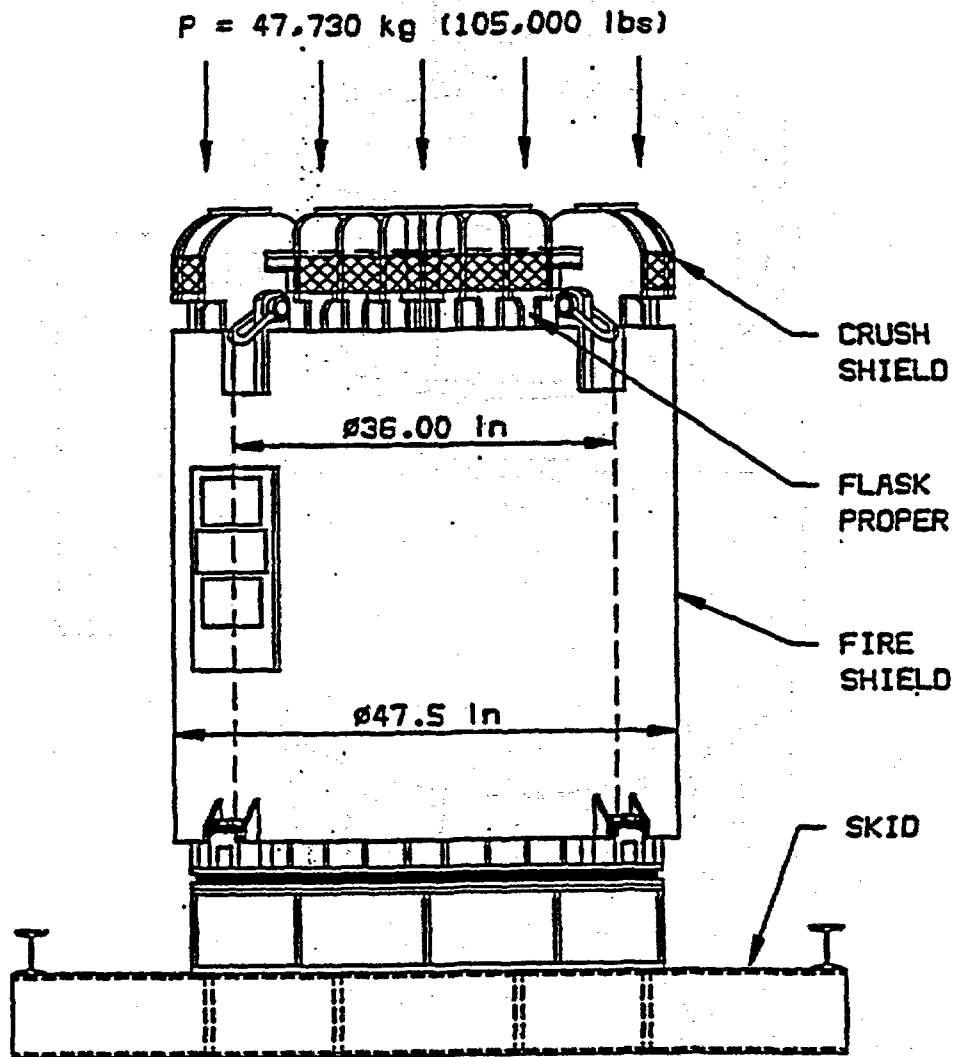
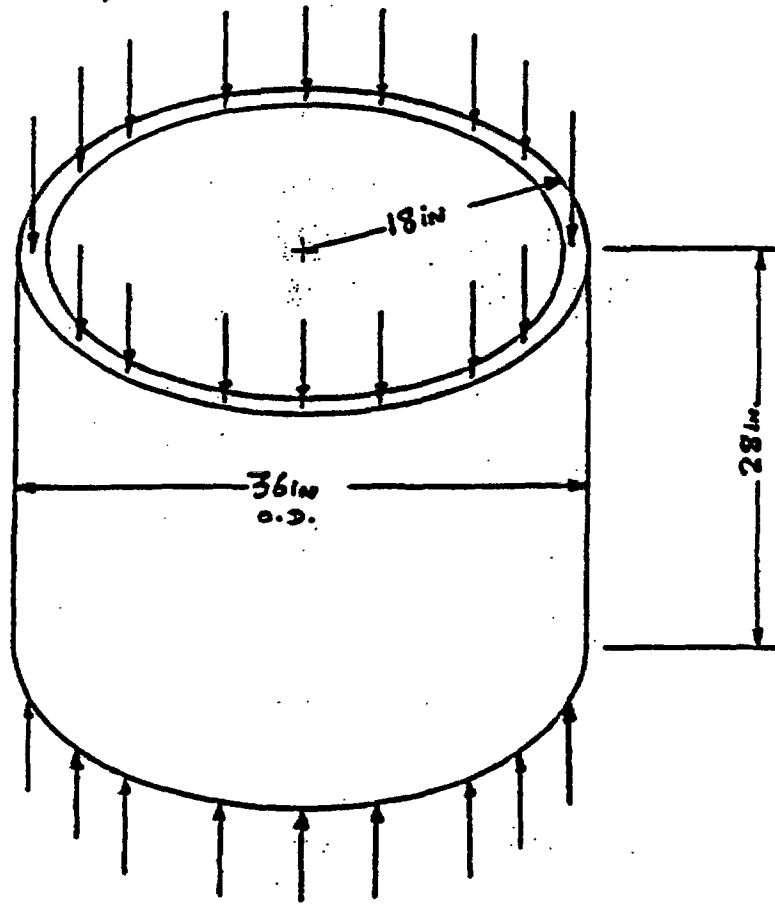


Figure 2.10.8-F2
Container Shell under Compressive Load



APPENDIX 2.10.9

ANALYTICAL ASSESSMENT OF F-294 PACKAGE SUBJECT TO 30-FT DROP TEST

CONTENTS

1.	INTRODUCTION	5
2.	SUMMARY OF THE ANALYSIS OF DROP TEST IN END, SIDE AND CORNER ORIENTATIONS	9
3.	TOP END DROP	12
3.1	MODE OF IMPACT	12
3.2	POTENTIAL ENERGY DUE TO 30-FT DROP HEIGHT OF THE PACKAGE	12
3.3	GEOMETRICAL DATA FOR IMPACT LIMITING FINS	12
3.4	ENERGY ABSORBED BY 0.5 IN. THICK CRUSH SHIELD FINS	12
3.4.1	<i>Fin Type #1 Parameters</i>	12
3.4.2	<i>Energy Absorbed Per Fin at Zero Degree Loading Angle</i>	12
3.4.3	<i>Energy Absorbed by 28, 0.5 in. Thick Fins of the Crush Shield (EA₁)</i>	13
3.5	ENERGY ABSORBED BY 0.375 IN. THICK CONTAINER FINS	13
3.5.1	<i>Fin Type #2 Parameters</i>	13
3.5.2	<i>Energy Absorbed per fin at Zero Degrees Loading Angle</i>	13
3.5.3	<i>Energy absorbed by 24, 0.375 in. thick fins of the container fins (EA₂)</i>	13
3.6	ENERGY ABSORBED BY 0.5 IN. THICK CONTAINER FINS	13
3.6.1	<i>Fin Type #3 Parameters</i>	13
3.6.2	<i>Energy Absorbed Per Fin at Zero Degrees Loading Angle</i>	13
3.6.3	<i>Energy Absorbed by 8, 0.5 in. Thick Fins of the Container (EA₃)</i>	14
3.7	TOTAL ENERGY ABSORBED, EA _T	14
3.8	ESTIMATE OF PEAK FORCE AND G-LOADS	14
3.8.1	<i>Crush Shield</i>	14
3.8.2	<i>Container top fins (0.375 in. thick)</i>	15
3.8.3	<i>Container top fins (0.5 in. thick)</i>	15
3.8.4	<i>Cumulative Total Peak Force</i>	15
3.8.5	<i>Estimate of G-loads</i>	15
3.9	LEAD SLUMP IN THE TOP END IMPACT	16
4.	SIDE DROP	30
4.1	SIDE DROP #1	30
4.1.1	<i>Mode of Impact</i>	30
4.1.2	<i>Potential Energy of F-294 Package</i>	30
4.1.3	<i>Energy Absorption, G-Loads for 1st Stage</i>	30
4.1.4	<i>Energy absorption, G-loads for 2nd stage</i>	34
4.1.5	<i>Energy absorption, G-loads for 3rd stage</i>	39
4.1.6	<i>Energy Balance, Peak Force, G-load so Far</i>	43
4.1.7	<i>Energy Absorbed by Cask Shell and Lead. Estimate of Lead Movement or Slump</i>	44
4.1.8	<i>Summary</i>	45
4.2	SIDE DROP #2	46
4.2.1	<i>Mode of Impact</i>	46
4.2.2	<i>Energy absorption, G-loads for 1st stage</i>	46
4.2.3	<i>Energy Absorbed by Two Structural Elements: 1st Stage</i>	48
4.2.4	<i>Ratio of 1st stage energy Absorbed/Initial Potential Energy</i>	48
4.2.5	<i>Summary of Energy Absorbed in Side Drop #2</i>	48
4.2.5	<i>Peak Force and G-loads</i>	49
4.3	IMPLICATIONS OF PEAK FORCE AND G-LOAD ON THE INTEGRITY OF CONTAINER AND INTERNALS	50
4.3.1	<i>Integrity of SS304L Shell Around Lead Shielding</i>	50

5. TOP CORNER DROP	64
5.1 MODE OF IMPACT	64
5.2 ENERGY ABSORPTION, G-LOADS FOR 1ST STAGE	64
5.2.1 <i>Energy Absorbed by the Fins of the Crush Shield</i>	64
5.2.2 <i>Energy Absorbed by Top Fins of the Container</i>	67
5.3 TOTAL ENERGY ABSORBED, EXCLUSIVE OF EFFECTS OF REINFORCING STRUCTURAL MEMBERS	71
5.4 EFFECT OF REINFORCING MEMBERS ON THE IMPACT RESISTANCE	72
5.4.1 <i>Load Spreading Structural Members</i>	72
5.4.2 <i>2nd Moment of Area of Fin Area A0 About XX</i>	72
5.5 TOTAL ENERGY ABSORBED, INCLUSIVE OF LOAD SPREADING EFFECTS.....	72
5.6 ESTIMATE OF PEAK FORCES AND EFFECT OF PEAK FORCE ON THE CONTAINER SHELL.....	73
5.6.1 <i>Estimate of Peak Force</i>	73
5.6.2 <i>Estimate G-Load During Peak Force Duration</i>	75
5.6.3 <i>Effect of Peak Force on the SS Shell Directly Under the Foot of the Lift Lug Fin</i>	75
5.7 SUMMARY OF RESULTS SO FAR.....	76
5.8 ENERGY ABSORBED BY THE CASK	76
5.8.1 <i>Impact Areas and Volumes</i>	76
5.8.2 <i>Dynamic Properties of Material</i>	77
5.8.3 <i>Energy Absorbed by Cask Top Plug/Container Corner</i>	77
5.8.4 <i>Footprint G-Loads</i>	78
5.9 SUMMARY OF ENERGY BREAKDOWN, PEAK FORCE, G-LOADS AT EACH STAGE.....	78
5.9.1 <i>Energy Balance</i>	78
5.9.2 <i>Peak Force and G-loads</i>	79
5.9.3 <i>Displacements</i>	79
6. BOTTOM CORNER DROP	89
6.1 MODE OF IMPACT	89
6.2 ENERGY ABSORPTION, G-LOADS FOR 1ST STAGE	89
6.2.1 <i>Energy Absorption Contribution by one Channel of the Shipping Skid</i>	89
6.2.2 <i>Peak Forces in the Shipping Skid</i>	91
6.2.3 <i>Energy Absorption Contribution by One Channel of the Fixed Skid</i>	92
6.2.4 <i>Peak Forces in the Fixed Skid</i>	94
6.2.5 <i>Energy Absorbed, G-loads for the Container Bottom Fins</i>	95
6.2.6 PEAK FORCES IN THE BOTTOM CONTAINER FINS.....	99
6.3 ENERGY, PEAK FORCES, G-LOADS SUMMARY AT END OF 1ST STAGE	99
6.4 2ND STAGE: SECONDARY BOUNCE.....	100
6.5 3RD STAGE: TOP SIDE CORNER OF CONTAINER IMPACT	100
6.5.1 <i>Energy Absorption by Fins of Crush Shield</i>	100
6.5.2 <i>Peak Force for Crush Shield</i>	103
6.5.3 <i>Energy Absorbed by Top/Side Fins of the Container</i>	103
6.5.4 <i>Peak forces for Top Container Fins</i>	105
6.5.5 <i>Summarize 3rd Stage</i>	106
6.6 ENERGY ABSORPTION, G-LOADS FOR 4TH STAGE.....	106
6.6.1 <i>Energy Absorption by External Cooling Fins on the Container</i>	106
6.6.2 <i>Peak forces for Side Container Fins</i>	107
6.6.3 <i>Energy Absorbed by the Cylindrical Fireshield</i>	108
6.6.4 <i>Summarize 4th Stage</i>	110
6.7 ENERGY ABSORBED BY CASK SHELL AND LEAD ESTIMATE OF LEAD MOVEMENT OR SLUMP	110
6.8 SUMMARY OF ENERGY BALANCE AND PEAK FORCES IN BOTTOM CORNER DROP.....	111

7. BOTTOM END DROP	117
7.1 MODE OF IMPACT	117
7.2 ENERGY ABSORPTION CONTRIBUTION BY FOUR CHANNELS OF THE SHIPPING SKID.....	117
7.2.1 Energy Absorbed by the Webs of the Channels.....	117
7.3 ENERGY ABSORPTION CONTRIBUTION BY EIGHT GUSSETS OF THE SHIPPING SKID.....	118
7.3.1 Energy Absorbed by the Gussets of the Shipping Skid	118
7.4 ENERGY ABSORBED BY THE SHIPPING SKID ALONE	118
7.5 ESTIMATE OF PEAK FORCES AND G-LOADS	119
7.6 SUMMARY FOR BOTTOM END DROP	119
8. TRANSNUCLEAIRE DATA FROM REF. [37] WITH REFERENCE TO 15-TON DUPONT CASK DROP DATA.....	122
8.1 MEASUREMENTS MADE ON A 15-TON PACKAGING.....	122
8.2 APPLICATION OF THIS TEST DATA TO F-294.....	122
9. SPECIAL ISSUES	122
9.1 CRUSH SHIELD RETENTION DURING 30-FT DROP.....	122
9.2 CYLINDRICAL FIRESHIELD RETENTION DURING 30-FT DROP TEST	124

This page left blank intentionally.

1. INTRODUCTION

The F-294 package can be dropped in any of the four basic free drop orientations, as per Figure 2.10.9-F1. The drop orientations are identified as

- Orientation #1.1 – End Drop - Top
- Orientation #1.2 – End Drop - Bottom
- Orientation #2 – Side Drop
- Orientation #3.1 – Corner Drop - Top
- Orientation #3.2 – Corner Drop - Bottom
- Orientation #4 – Oblique Drop - Side Corner

To cushion the impact during a 30-ft drop test, the F-294 package has a top crush shield. The crush shield assembly is as shown in Figure 2.10.9-F2. There are seven fins in each of four quadrant segments; 28 fins in total spaced around the circumference. Eight of the 28 fins have extension legs located on the assembly within the container side cooling fins. This method assists in trapping the crush shield assembly within the container assembly, thereby ensuring that the crush shield will not "fly away" upon impact.

Within the crush shield assembly is a top fireshield sub-assembly consisting of "KAOWOOL" insulation sandwiched between two carbon steel plates. The fins of the crush shield are joined to a ring collar and a donut ring. The crush shield assembly sits flush on the container top fins and is bolted at eight locations (two fasteners per location) to the container top fins; four on the mounting pads on top of the container and four on the side container fins adjacent to the lift lug fins. There are eight top fasteners and eight side fasteners connecting the crush shield to the container top fins.

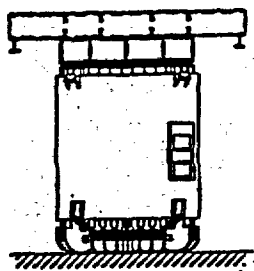
In addition, the external fins on the container, the fixed skid, the shipping skid - all these serve as energy absorbing devices during a 30-ft drop test. Depending upon the drop orientation, only some of the energy absorbing devices come into play.

The analytical structural assessment of the F-294 package and, in particular, the energy absorbing elements of the package, subjected to 30-ft drop test for end, side, corner drop orientations are presented here. The methodology for performing the energy absorption by the fins is based on Davis as per Ref. [18]. Table 2.10.9-T1 outlines the flowchart describing the logic behind fin energy absorption calculations.

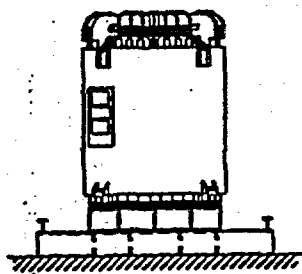
Table 2.10.9-T1
Flow Chart: Methodology for Fin Impact Energy Absorption Calculations
(Block Chart of Fin Analysis)

Step 0	Begin
Step 1	Identify type of fin; classify type #1 fin; assume x% crush
Step 2	Fin geometrical parameters: width or loaded length (b), thickness (t), height (h)
Step 3	From Davis Fin data/figures, for a specific fin height (h) and fin loading angle (0°, 10°), select multiplier (na) proportional to x% crush). Select a
Step 4	Calculate static plastic moment (m_p); $m_p = \sigma_y bt^2/4$, where σ_y = static yield stress value of the fin material
Step 5	Energy absorbed by a fin loaded at loading angle (0°, 10° etc.) $e_a = na \times m_p$
Step 6	Total energy absorbed by type #1 fins: $e_t = \text{number of type \#1 fins} \times e_a$
Step 7	If there is more than one type of fin, repeat steps 1 through 6 for each different type of fin.
Step 8	Compare total aggregate energy absorbed (Σe_t) by all fins of the package versus the 30-ft free drop energy of the package (e_o)
Step 9	If $e_t > e_o$, then x% crush as per 1st step is incorrect (too high); If $e_t < e_o$, then x% crush as per 1st step is incorrect (too low); If $x\% > 45\%$, go to step 10; otherwise use a better value of x% and repeat steps 3 through 9
Step 10	Check point
Step 11	Now estimate the peak force resulting from fin impact
Step 12	For each type of fin, and each fin loading angle, for each fin ratio [h/t], from Davis data/figures select peak force per linear inch of fin parameter (ft.-lb./in)
Step 13	p , peak force per fin = $f \times \text{loaded length of fin (b)}$
Step 14	Total aggregate peak force of all fins $p_a = \Sigma p$
Step 15	Estimate G-load; $G\text{-load} = p_a/w_{F-294}$, where w_{F-294} is weight of F-294 container
Step 16	Stop
Step 17	End

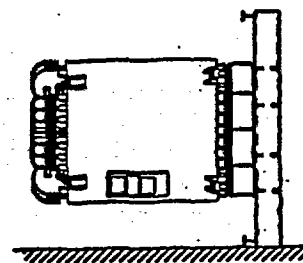
Figure 2.10.9-F1
F-294 Drop Test Orientations



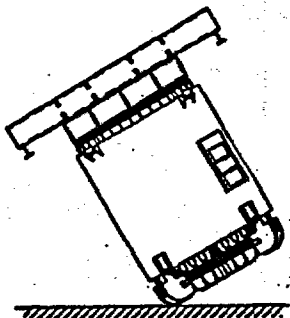
DROP ORIENTATION
#1.1
TOP END DROP



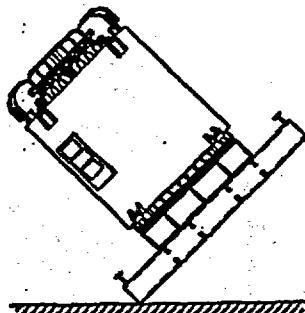
DROP ORIENTATION
#1.2
BOTTOM END DROP



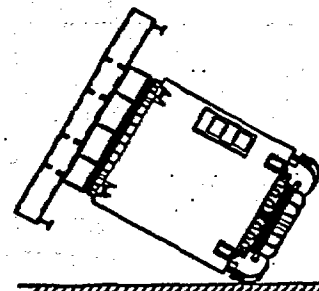
DROP ORIENTATION
#2
SIDE DROP



DROP ORIENTATION
#3.1
TOP CORNER DROP



DROP ORIENTATION
#3.2
BOTTOM CORNER DROP

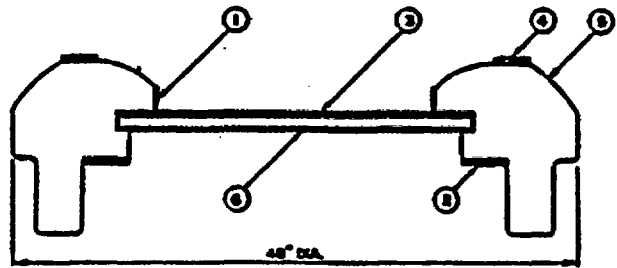
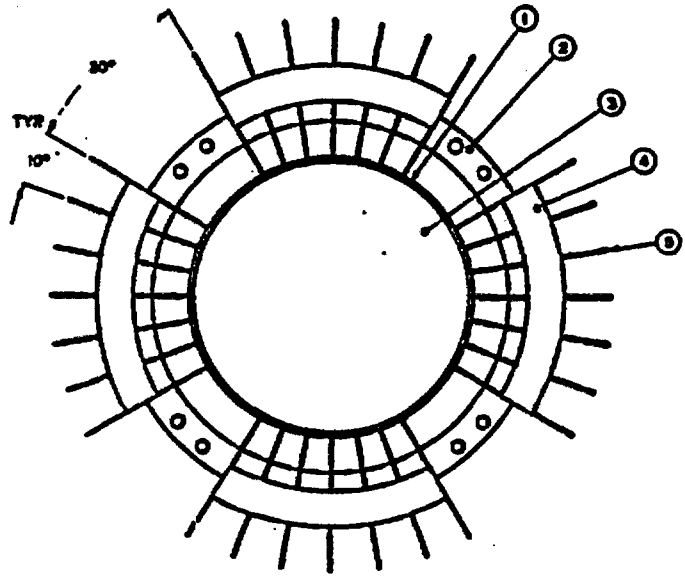
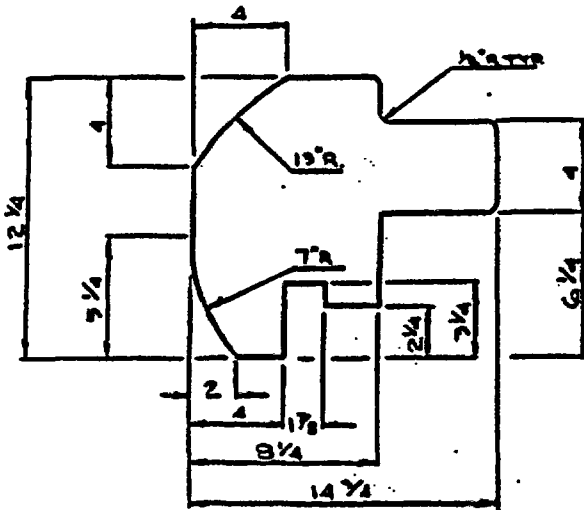


DROP ORIENTATION
#4
OBLIQUE

Figure 2.10.9-F2
F-294 Crush Shield Impact Limiter

CRUSH SHIELD (REF. DWG. NO. F029403-010)

- ① 1" x 3" x 33-3/16 DIA C.S. BAND
- ② 1" C.S. LOAD SPREADER & MOUNTING PLATE
- ③ 1" C.S. TOP PLATE
- ④ 1" C.S. STIFFENER
- ⑤ 1" C.S. FIN (TOTAL FINS-20)
- ⑥ 1" C.S. BOTTOM PLATE



2. SUMMARY OF THE ANALYSIS OF DROP TEST IN END, SIDE AND CORNER ORIENTATIONS

Table 2.10.9-T2 summarizes the impact data of the F-294 package subject to 30-ft free drop test.

In top end drop, 7.74×10^6 in.-lb. of energy is absorbed by the crush shield and the container fins. This represents 104% of the 30-ft drop energy. None of the energy is absorbed in the cask shell and lead shielding ;consequently resulting in almost minimal lead slump. We conservatively assigned a value of 0.4 in. max lead slump. The G-load = 200 g's at the impact point. The crush shield displaces down by about 1.8 in.

In side drop # 1, 8.875×10^6 in.-lb. of energy is absorbed. This represents 110% of the 30-ft drop energy. 36% of 30-ft drop energy is absorbed in the cask shell and lead resulting in lead slump of 0.6 in. max. The G-load range is 100 g's -520 g's at the impact point.

In side drop #2, 9.178×10^6 in.-lb. of energy is absorbed. This represents 121% of the 30-ft drop energy. 36% of 30-ft drop energy is absorbed in the cask shell and lead resulting in lead slump of 0.6 in. max. The G-load range is 100 g's -500 g's at the impact point.

In top corner drop, 7.9×10^6 in.-lb. of energy is absorbed. This represents 104% of the 30-ft drop energy. 41% of 30-ft drop energy is absorbed in the cask top corner; resulting in lead displacement of 1.125 in. max. The G-load range is 315 g's -338 g's at the impact point.

In bottom corner drop, 7.8×10^6 in.-lb. of energy is absorbed. This represents 103% of the 30-ft drop energy. The 10% of 30-ft drop energy shall be absorbed by the cask shell and lead; resulting in negligible lead displacement. The G-load range is 104 g's-530 g's at the impact point.

In bottom end drop, 7.9×10^6 in.-lb. of energy is absorbed by the crush shield and the container fins. This represents 104% of the 30-ft drop energy. None of the energy is absorbed in the cask shell and lead shielding ;consequently resulting in almost minimal lead slump. We conservatively assigned a value of 0.4 in. max lead slump. The G-load = 334 g's at the impact point.

The impact energy absorption elements of the F-294 package will crush about 1.8 to 5.0 in. The F-294 package will be subjected to G-loads at the impact point in the range $100 \leq G \leq 530$. At locations away from the impact point the deceleration G-loads shall be lower in magnitude compared to G-loads at the impact point; such a measure is given in section 8. Therefore, the deceleration loads to which sub-components are subjected are known. The estimated energy absorption range suggests that sufficient absorption capability exists and the crush shield design is adequate. The top corner drop appears to be the "worst" drop test orientation.

It is demonstrated that the structural integrity of the F-294 container will be maintained when the F-294 package is subjected to 30-ft drop test; the outer stainless steel jacket surrounding the lead shielding shall not be breached. In the absence of actual post-drop deformation data of F-294, Figure 2.10.9-F3 provides a postulated displacement at three distinct vectors (horizontal, vertical, 33° radial from vertical) around the F-294 container which can be used for post-accident shielding evaluation in Chapter 5.

The retention of the crush shield and the cylindrical fireshield has also been examined in section 9 and demonstrated to be sound.

The determination of the maximum damaging drop test orientation of the F-294 transport package is presented in Chapter 2, Appendix 2.10.11.

Table 2.10.9-T2
Summary of Impact Data of F-294 Package Subjected to 30-Ft Free Drop

Designated Orientation	Drop Orientation	Initial Energy E_0 (in.-lb.) $\times 10^6$	Energy Absorbed EAT (in.-lb.) $\times 10^6$	Ratio E_{AT}/E_0	Peak Force lb. $\times 10^6$	G-Loads g's	Crush Distance in.	Lead "slump" or displacement
1.1	Top End Drop	7.56	7.74	102%	4.2	200	3.825 in.	0.4 in.
1.2	Bottom End	7.56	7.9	104%	3.9	400	1.8 in.	0.4 in.
2.1	Side Drop #1	7.56	8.875	110%	10.8	520	2 to 4 in.	0.6 in.
2.2	Side Drop #2	7.56	9.178	121%	9.9	500	2 to 4 in.	0.6 in.
3.1	Top Corner	7.56	7.9	104%	7.1	338	5 in.	1.125 in.
3.2	Bottom Corner	7.56	7.8	103%	10.6	530	2 to 4 in.	0. in.

FIGURE WITHHELD UNDER 10 CFR 2.390

3. TOP END DROP

3.1 MODE OF IMPACT

See Figure 2.10.9-F4

1. The top collar of the crush shield impacts the unyielding surface first.
2. The fins of the crush shield start buckling in a double hinge manner, restrained against by the mounting pad on top container fins.
3. As the container top fins are marginally less stiff than the crush shield fins, the container top fins will absorb part of the impact and the balance shall be absorbed by the crush shield fins until all the potential energy E_0 is fully absorbed. The container fins will start "buckling" coincidentally with the crush shield fins.

3.2 POTENTIAL ENERGY DUE TO 30-FT DROP HEIGHT OF THE PACKAGE

The potential energy due to 30-ft drop height of the package, E_0

$$\begin{aligned} E_0 &= W_{F-294} * H \\ &= 21,000 * 30 * 12 \\ &= 7,560,000 \text{ in.-lb.} \end{aligned}$$

where

$$\begin{aligned} W_{F-294} &= \text{weight of F-294 package, 21,000 lb.} \\ H &= \text{drop test height} = 30 \text{ feet} \end{aligned}$$

3.3 GEOMETRICAL DATA FOR IMPACT LIMITING FINS

See for geometrical data.

3.4 ENERGY ABSORBED BY 0.5 IN. THICK CRUSH SHIELD FINS

3.4.1 Fin Type #1 Parameters

- Effective height, h = 9. in.
- Thickness, t = 0.5 in.
- Loaded length, b = 6 in.
- material = CR C1020
- % of crush = 22.5%

3.4.2 Energy Absorbed Per Fin at Zero Degree Loading Angle

$$\begin{aligned} EA_{\text{FIN TYPE \#1}} &= N * M_p \\ &= 10.5 * \sigma_Y * bt^2 / 4 \\ &= 10.5 * 46,000 * 6 * (0.5)^2 / 4 \\ &= 181,125 \text{ in.-lb. per fin} \end{aligned}$$

where

$$\begin{aligned} EA_{\text{FIN TYPE \#1}} &= \text{Energy absorbed per fin in.-lb.} \\ N &= \text{Empirical parameter relating [absorbed energy/plastic moment] to} \\ &\quad \text{[deformation/original height] for a mild steel fin.} \\ &= 10.5 \text{ from Figure 2.10.9-F6.1.} \\ M_p &= \text{Plastic Moment in.-lb.} \\ &= \sigma_Y * bt^2 / 4 \\ \sigma_Y &= \text{yield stress of C1020 steel} = 46000 \text{ psi.} \end{aligned}$$

3.4.3 Energy Absorbed by 28, 0.5 in. Thick Fins of the Crush Shield (EA₁)

$$\begin{aligned} EA_1 &= 28 * 181,125 \\ &= 5.0568 * 10^6 \text{ in.-lb.} \end{aligned}$$

3.5 ENERGY ABSORBED BY 0.375 IN. THICK CONTAINER FINS

3.5.1 Fin Type #2 Parameters

- Effective height, h = 8. in.
- Thickness, t = 0.375 in.
- Loaded length, b = 8 in.
- material = ss304L
- % of crush = 22.5%

3.5.2 Energy Absorbed per fin at Zero Degrees Loading Angle

$$\begin{aligned} EA_{\text{FIN TYPE \#2}} &= N * M_p \\ &= 10 * \sigma_Y * bt^2 / 4 \\ &= 10 * 25,000 * 8 * (0.375)^2 / 4 \\ &= 70,266 \text{ in.-lb. per fin} \end{aligned}$$

where

$$\begin{aligned} EA_{\text{FIN TYPE \#2}} &= \text{Energy absorbed per fin in.-lb.} \\ N &= \text{Empirical parameter relating [absorbed energy/plastic moment] to} \\ &\quad \text{[deformation/original height] for a mild steel fin.} \\ &= 10. \text{ from Figure 2.10.9-F6.1, for 8 in. fin height, 22.5\% crush} \\ M_p &= \text{Plastic Moment in.-lb.} \\ &= \sigma_Y * bt^2 / 4 \\ \sigma_Y &= \text{yield stress of ss304L steel} = 25000 \text{ psi.} \end{aligned}$$

3.5.3 Energy absorbed by 24, 0.375 in. thick fins of the container fins (EA₂)

$$\begin{aligned} EA_2 &= \text{Number of fins} * EA_{\text{FIN TYPE \#2}} \\ &= 24 * 70,266 \\ &= 1.686 * 10^6 \text{ in.-lb.} \end{aligned}$$

3.6 ENERGY ABSORBED BY 0.5 IN. THICK CONTAINER FINS

3.6.1 Fin Type #3 Parameters

- Effective height, h = 8. in.
- Thickness, t = 0.5 in.
- Loaded length, b = 8 in.
- material = ss304L
- % of crush = 22.5%

3.6.2 Energy Absorbed Per Fin at Zero Degrees Loading Angle

$$\begin{aligned} EA_{\text{FIN TYPE \#3}} &= N * M_p \\ &= 10 * \sigma_Y * bt^2 / 4 \\ &= 10 * 25,000 * 8 * (0.5)^2 / 4 \\ &= 125,000 \text{ in.-lb. per fin} \end{aligned}$$

where

$EA_{\text{FIN TYPE \#3}}$	= Energy absorbed per fin in.-lb.
N	= Empirical parameter relating [absorbed energy/plastic moment] to [deformation/original height] for a mild steel fin. = 10 from Figure 2.10.9-F6.1, for 8 in. fin height, 22.5% crush
M_p	= Plastic Moment in.-lb. = $\sigma_Y * bt^2 / 4$
σ_Y	= yield stress of ss304L steel = 25,000 psi.

3.6.3 Energy Absorbed by 8, 0.5 in. Thick Fins of the Container (EA_3)

$$\begin{aligned} EA_3 &= \text{Number of fins} \times EA_{\text{FIN TYPE \#3}} \\ &= 8 * 125,000 \\ &= 1.0 * 10^6 \text{ in.-lb.} \end{aligned}$$

3.7 TOTAL ENERGY ABSORBED, EA_T

$$\begin{aligned} EA_T &= EA_1 + EA_2 + EA_3 \\ &= (5.0568 + 1.686 + 1.0) * 10^6 \text{ in.-lb.} \\ &= 7.7428 * 10^6 \text{ in.-lb.} \end{aligned}$$

The total energy absorbed, by the crush shield fins and the container fins, is computed to be $EA_T = 7.7428 * 10^6$ in.-lb., without taking credit of the reinforcing structural members. As the total computed energy absorbed $EA_T (7.7428 * 10^6 \text{ in.-lb.}) \geq E_0 (7.56 * 10^6 \text{ in.-lb.})$, the initial required potential energy of the F-294 package, the F-294 in the top end drop orientation has been demonstrated to have the full capability of absorbing all the required energy due to 30-ft free drop test for top end drop orientation.

The resulting total deformation (crush) = 3.825 in. In other words, the crush shield is displaced in towards the container by distance of 3.825 in. The 3.825 in. displacement results from:

- deformation of the crush shield is 22.5% of 9 in. = 2.025 in. PLUS
- deformation of the top container fins 22.5% of 8.0 in = 1.8 in.

The estimate of resulting G-loads is given in the following section.

In the above computation, only the non-braced fins were individually considered and their energy summed to arrive at the cumulative energy absorbed by the crush shield or the container fins. In reality, the crush shield fins are joined by a number of structural members (i.e., donut ring, etc.). The contribution of the braced fins is quantified by a factor, $F_{[\text{COMPOSITE}/\text{NON-COMPOSITE}]}$ which is estimated in section 5.4.

3.8 ESTIMATE OF PEAK FORCE AND G-LOADS

Data from Ref. [18] is used to estimate peak force; also see Figure 2.10.9-F7.1.

3.8.1 Crush Shield

$$[\text{height of fin}/\text{thickness of fin}] = 9.0/0.5 = 18$$

From Figure 2.10.9-F7.1, peak force, $P_1 = 10,000$ lb. per in. of loaded length of fin per fin.

$$\begin{aligned} \text{Total peak force, } FP_1 &= \text{peak force} * \text{loaded length per fin} * \text{number of fins} \\ &= P_1 \times b \times 28 \\ &= 10,000 * 6 * 28 \\ &= 1.68 * 10^6 \text{ lb.} \end{aligned}$$

3.8.2 Container top fins (0.375 in. thick)

$$[\text{height of fin}/\text{thickness of fin}] = 8.0/0.375 = 21.3$$

From Figure 2.10.9-F7.1, peak force, $P_2 = 8,000$ lb. per in. of loaded length of fin per fin.

$$\begin{aligned} \text{Total peak force, } FP_2 &= \text{peak force} * \text{loaded length per fin} * \text{number of fins} \\ &= P_2 * b * 24 \\ &= 8,000 * 8 * 24 \\ &= 1.536 * 10^6 \text{ lb.} \end{aligned}$$

3.8.3 Container top fins (0.5 in. thick)

$$[\text{height of fin}/\text{thickness of fin}] = 8.0/0.5 = 16$$

From Figure 2.10.9-F7.1, Peak force = 15,000 lb. per in. of loaded length of fin per fin.

$$\begin{aligned} \text{Total peak force, } FP_3 &= \text{peak force} * \text{loaded length per fin} * \text{number of fins} \\ &= P_3 * b * 8 \\ &= 15,000 * 8 * 8 \\ &= 0.96 * 10^6 \text{ lb.} \end{aligned}$$

3.8.4 Cumulative Total Peak Force

The cumulative sum of discrete peak forces is:

$$\begin{aligned} \Sigma FP &= FP_1 + FP_2 + FP_3 \\ &= (1.68 + 1.536 + 0.96) * 10^6 \text{ lb.} \\ &= 4.176 * 10^6 \text{ lb.} \end{aligned}$$

3.8.5 Estimate of G-loads

It is possible to estimate G-loads based on peak forces calculated using DAVIS method - Ref. [18]. The cumulative Peak force $\Sigma FP = 4.176 * 10^6$ lb., exclusive of stiffening factors due to stiffening structural members.

Therefore

$$\begin{aligned} G_1 &= \Sigma FP / W_{F-294} \\ &= 4.176 * 10^6 \text{ lb.} / 21,000 \text{ lb.} \\ &= 199 \text{ g's.} \end{aligned}$$

Another method of estimating G-load is based on the linear method as per Ref. [33]. This method assumes the package is cushioning with linear elasticity and no bottoming out.

$$G_2 = 2H/s$$

where

$$\begin{aligned} H &= \text{drop test height} = 30 \text{ feet} = 360 \text{ in.} \\ s &= \text{total crush distance} = \\ &= \text{crush shield} + \text{container fins} \\ &= 22.5\% * 9 \text{ in.} + 22.5\% * 8 \text{ in.} \\ &= 2.025 + 1.8 \\ &= 3.825 \text{ in.} \\ G_2 &= 2 * 360 / 3.825 \\ &= 188 \text{ g's} \end{aligned}$$

3.8.5.1 Summary of G-load Range

Based on above calculations, during the hypothetical 30-ft drop test and specifically in the top end drop orientation, the F-294 Package shall be subjected to a G-load range of 188 g's ≤ G-load ≤ 199 g's at the impact point. At locations away from the impact point but within the container, the G-loads are reduced. See Transnuclaire Ref. [37] for Dupont 15 ton flask in Appendix 2.10.10.

At 120 cm. from the impact zone of 25 cm., the G-loads were 50% or lower. Based on this, the G-loads on F-294 the cavity end plate, a distance of 80 cm. from the impact point, are in the range of 0.6 x 200 g's = 120 g's. This G-load data shall be used to evaluate stresses on the cavity end plate.

3.9 LEAD SLUMP IN THE TOP END IMPACT

An end drop of a cask in which lead is not bonded to the steel shell will cause the lead to settle, thus crating a void in the end opposite the point of impact (see Figure 2.10.9-F8). An analysis of such an impact, based on the energy absorbed by the lead (as a result of its deformation) and by the outer steel shell (as a result of its circumferential strain from internal lead pressure) has been made [Ref. [25]].

The change in the lead volume in an impact may be estimated from equation:

$$\Delta V = RWH / (t_s \sigma_s + R \sigma_{pb}) \dots \dots \dots \text{Equation 1}$$

For negligible changes in the outer radius, R, and the inner radius of lead, r, the change in the height of the lead column, ΔH, is

$$\Delta H = \Delta V / [\pi(R^2 - r^2)] \dots \dots \dots \text{Equation 2}$$

combining equations 1 and 2 yields

$$\Delta H = RWH / [\pi((R^2 - r^2)(t_s \sigma_s - R \sigma_{pb})] \dots \dots \dots \text{Equation 3}$$

where

- ΔH = amount of lead slump, in.
- R = outer radius of lead cylinder = 17.5 in.
- r = inner radius of lead cylinder = 6.25 in.
- t_s = thickness of ss304 shell = 0.5 in.
- H = drop test height = 30-ft = 360 in.
- W_{F-294} = weight of the F-294 container = 21,000 lb.
- σ_s = dynamic flow stress of steel = 50,000 psi
- σ_{pb} = dynamic flow stress of lead = 5,000 psi

As noted earlier, equation 3 is based on an unbonded lead condition since neither the support provided by steel shells nor the possibility of collapse of the inner shell by buckling is taken into account. For an end impact of a cylindrical cask having non-buffered ends (without any shock absorbers), the amount of lead slump is:

$$\begin{aligned} \Delta H &= RWH / [\pi((R^2 - r^2)(t_s \sigma_s - R \sigma_{pb})] \\ &= 17.5 \times 21,000 \times 360 / [\pi(17.5^2 - 6.25^2) (0.5 \times 50,000 + 17.5 \times 5,000)] \\ &= 17.5 \times 21,000 \times 360 / 839.5 \times 112,500 \\ &= 1.4 \text{ in.} \end{aligned}$$

In the end impact, all (100%) of the potential energy attributed to 30-ft drop height of the package has been shown to be absorbed by 1) the crush shield and 2) the fins on the container (see Appendix 2.10). Consequently, there is no unabsorbed energy remaining; therefore, neither the container lead shielding nor the container shells are called upon to absorb impact energy.

Therefore, the estimate of lead slump $\Delta H = 1.4$ in. based on the cask *without shock absorbers*, absorbing all the PE due to 30-ft as impact energy, is *grossly conservative*. In addition the lead shielding is normally bonded to the steel shell, which further mitigates the lead slump.

For purposes of shielding calculations in post-hypothetical accident conditions situation, the effective $\Delta H_{\text{effective}} = 25\%$ of $1.4 = 0.375$ in. is *arbitrarily selected*, the factor of 25% is an allowance for uncertainties in the calculations.

Figure 2.10.9-F4
F-294 in Top End Drop Orientation

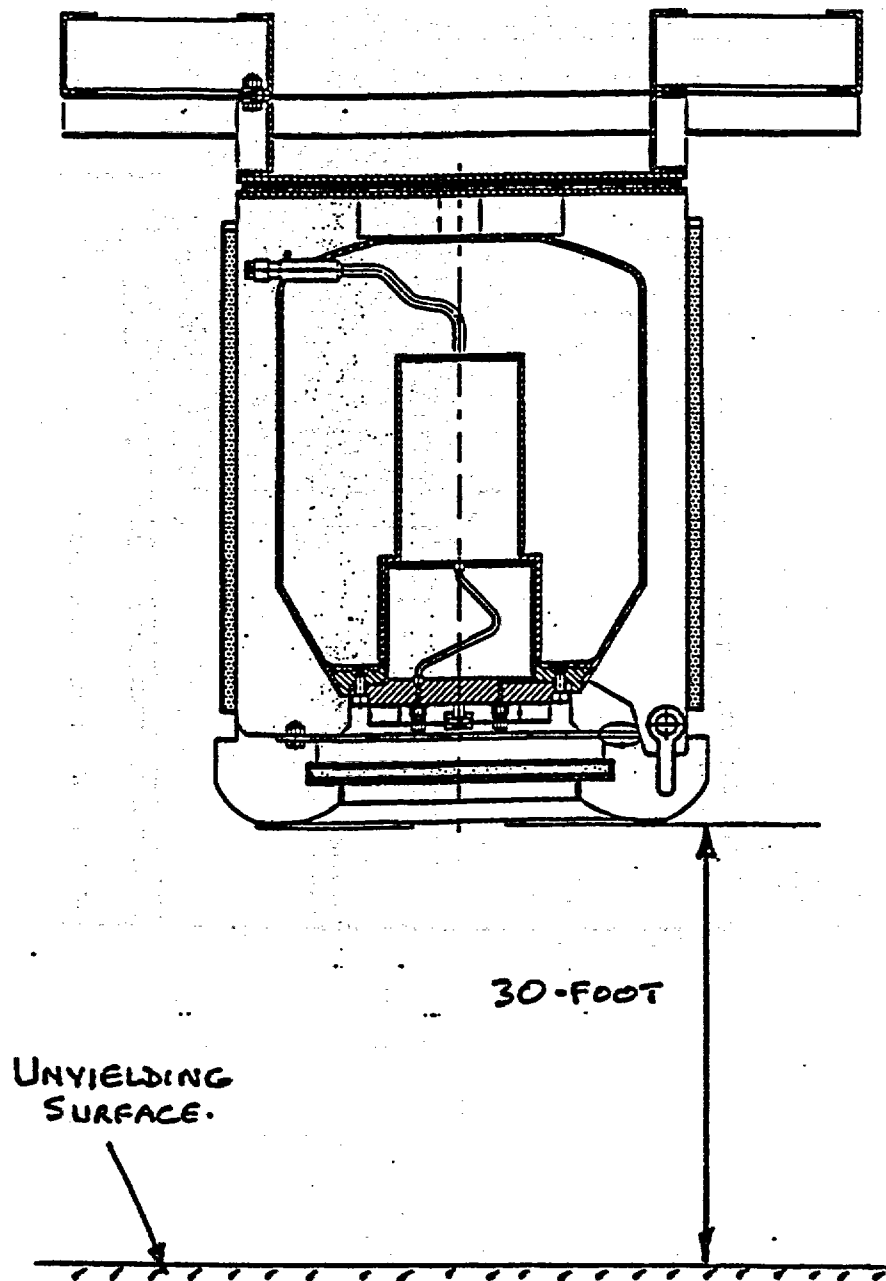


Figure 2.10.9-F5
Geometrical Data of the Crush Shield Fin # in the Top End Drop

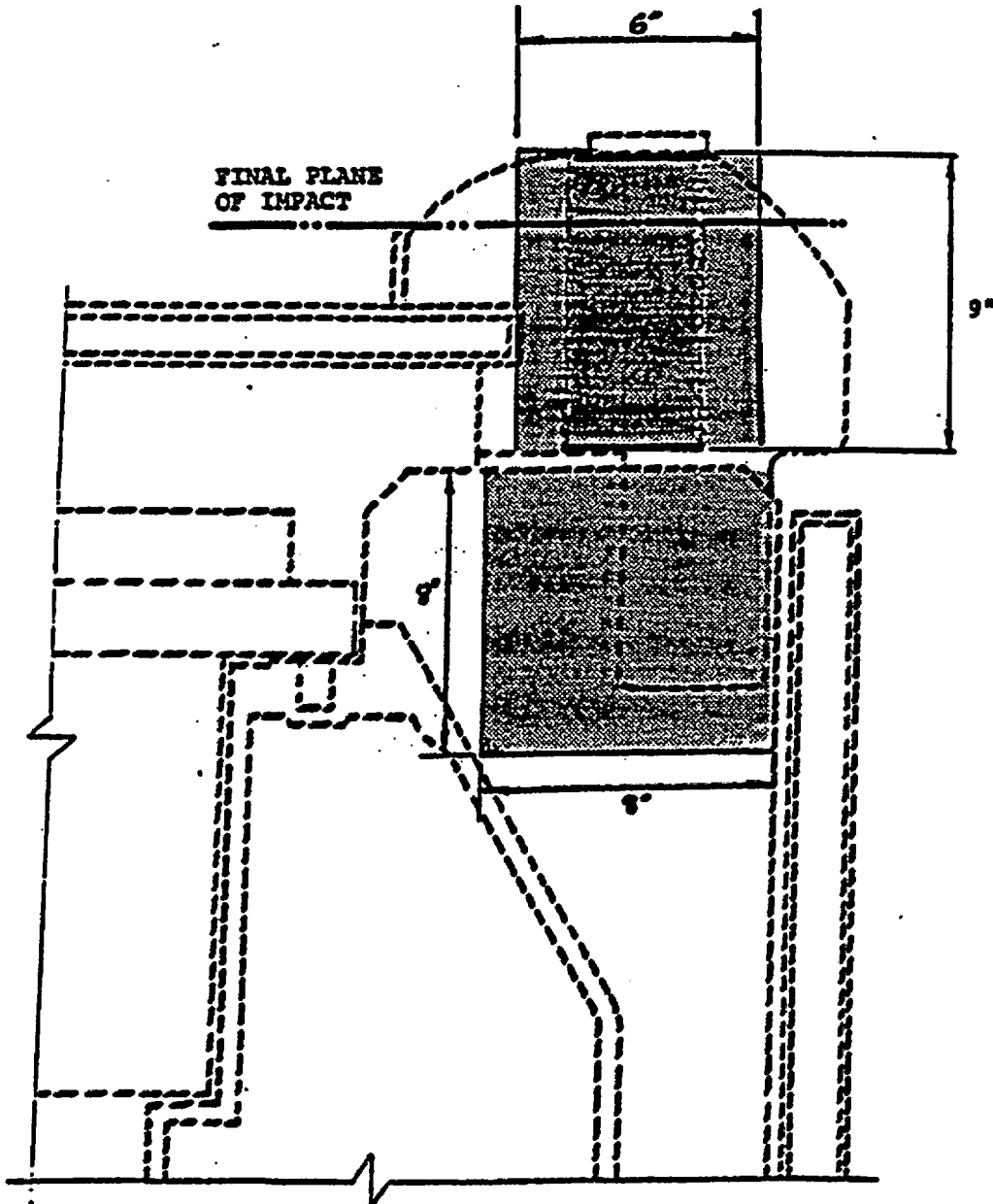


Figure 2.10.9-F6.1
 Parameter [Absorbed Energy/Plastic Moment] versus Parameter
 [Deformation/Original Height] for Fin impacting at 0°
 (Data appended from Ref. [18])

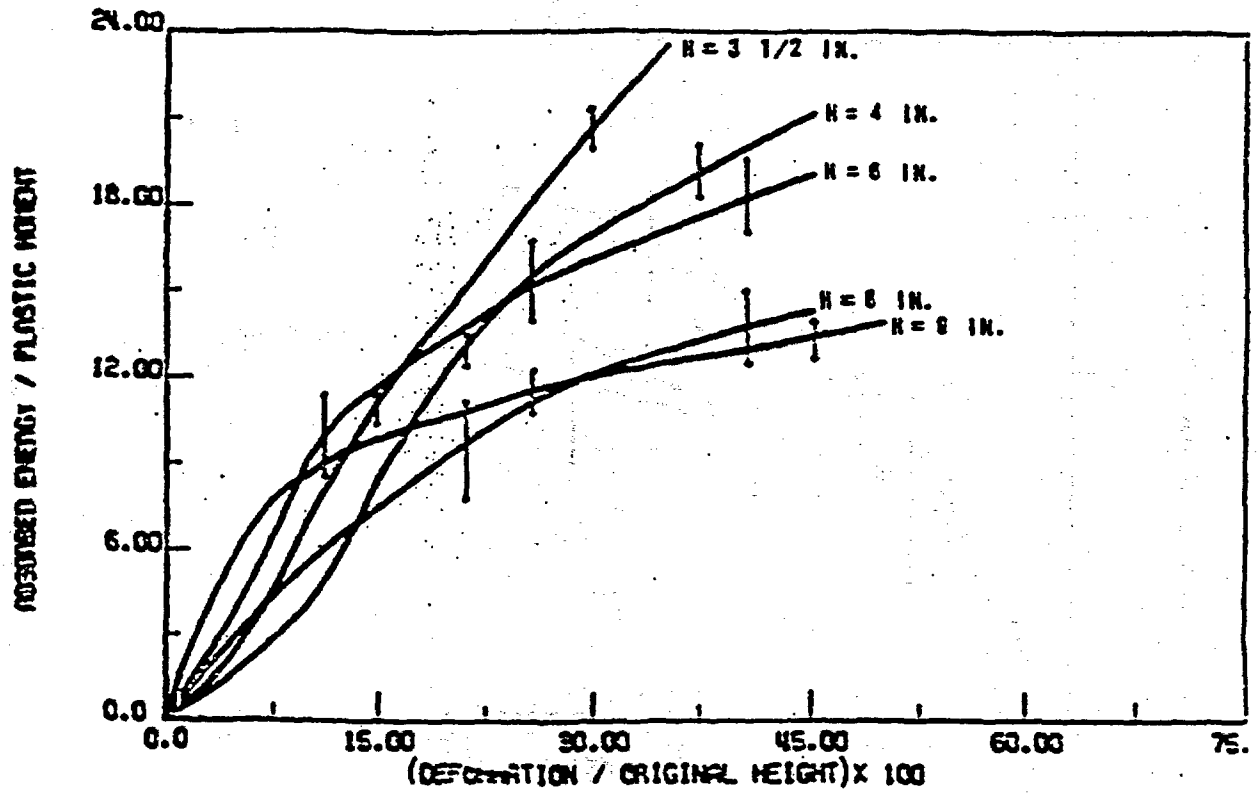


Figure 2.10.9-F6.2
Parameter [Absorbed Energy/Plastic Moment] versus Parameter
[Deformation/Original Height] for Fin impacting at 10°
 (Data appended from Ref. [18])

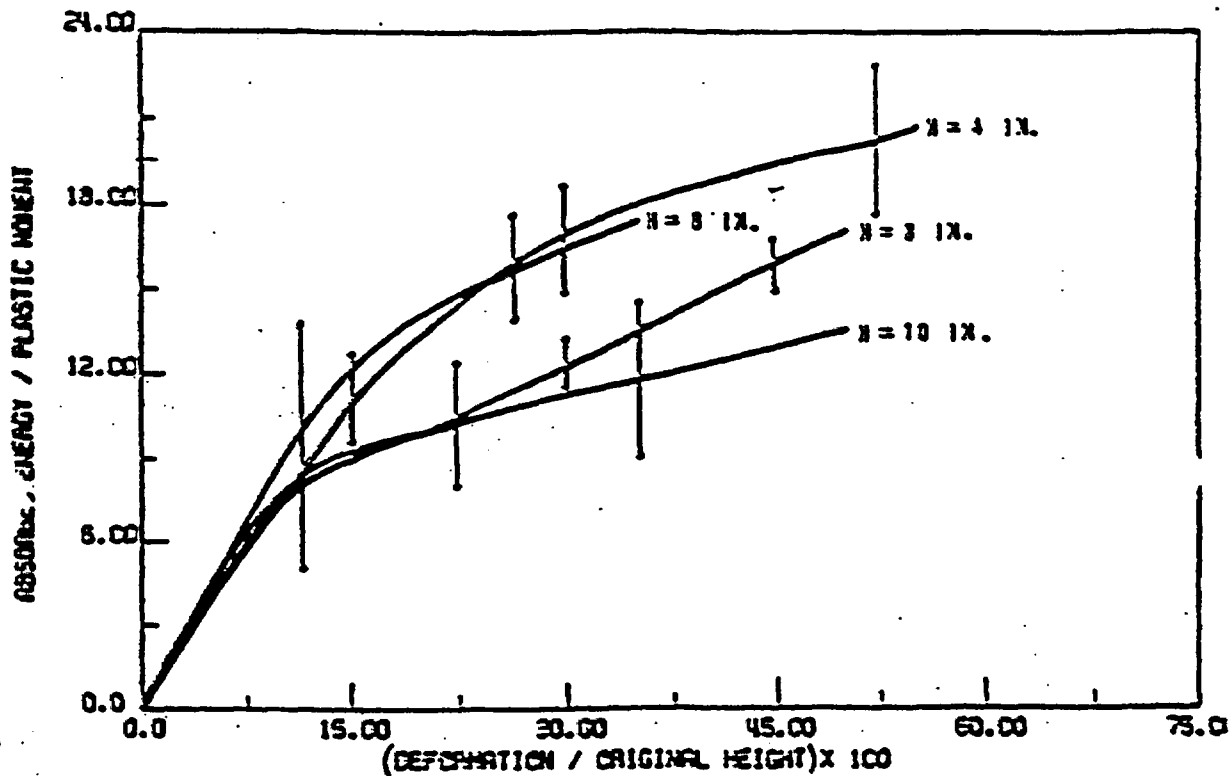


Figure 2.10.9-F6.3
Parameter [Absorbed Energy/Plastic Moment] versus Parameter
[Deformation/Original Height] for Fin impacting at 20°
(Data appended from Ref. [18])

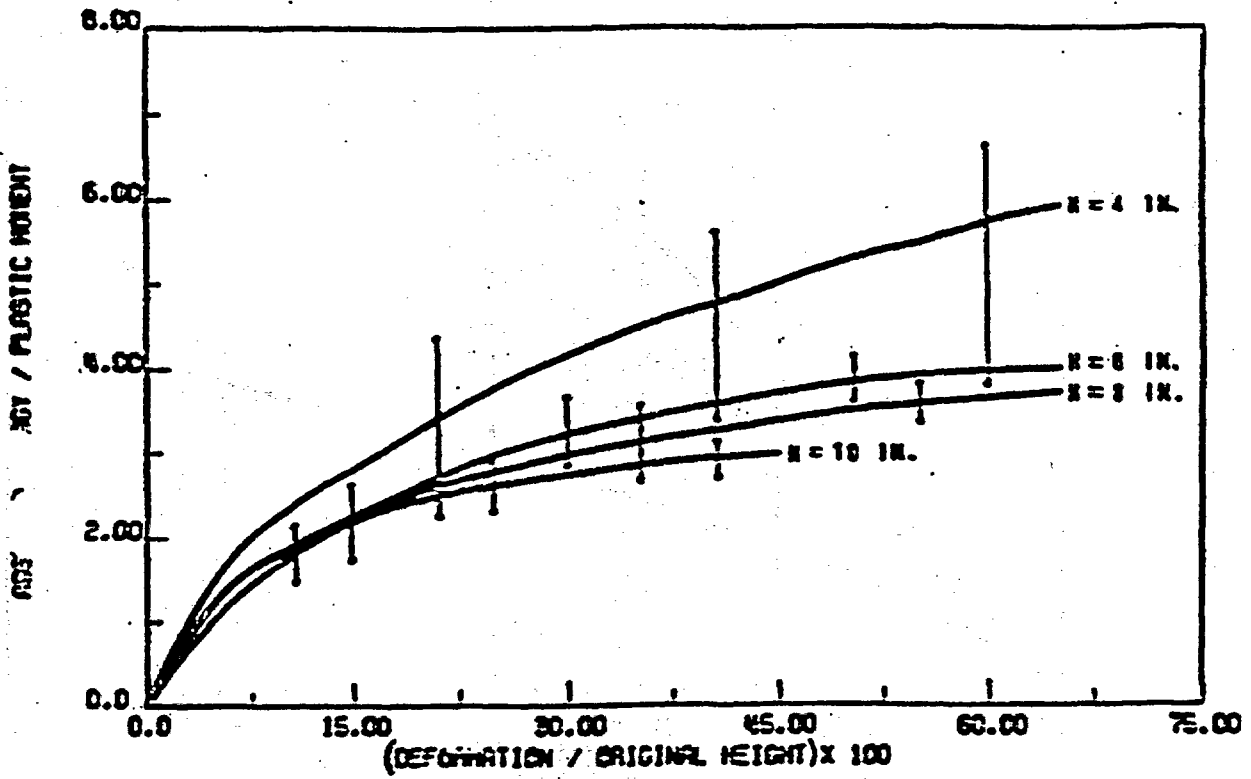


Figure 2.10.9-F6.4
Parameter [Absorbed Energy/Plastic Moment] versus Parameter
[Deformation/Original Height] for Fin impacting at 30°
 (Data appended from Ref. [18])

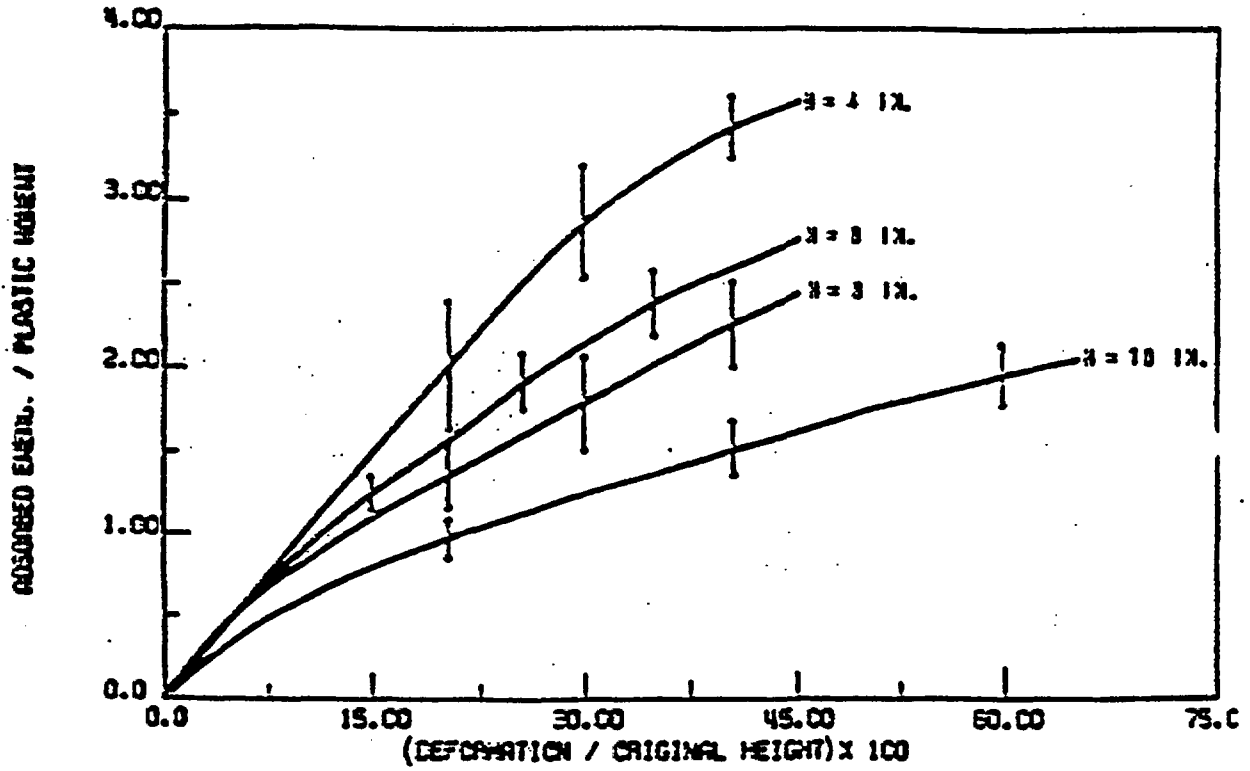


Figure 2.10.9-F6.5
Parameter [Absorbed Energy/Plastic Moment] versus Parameter
[Deformation/Original Height] for Fin impacting at 40°
(Data appended from Ref. [18])

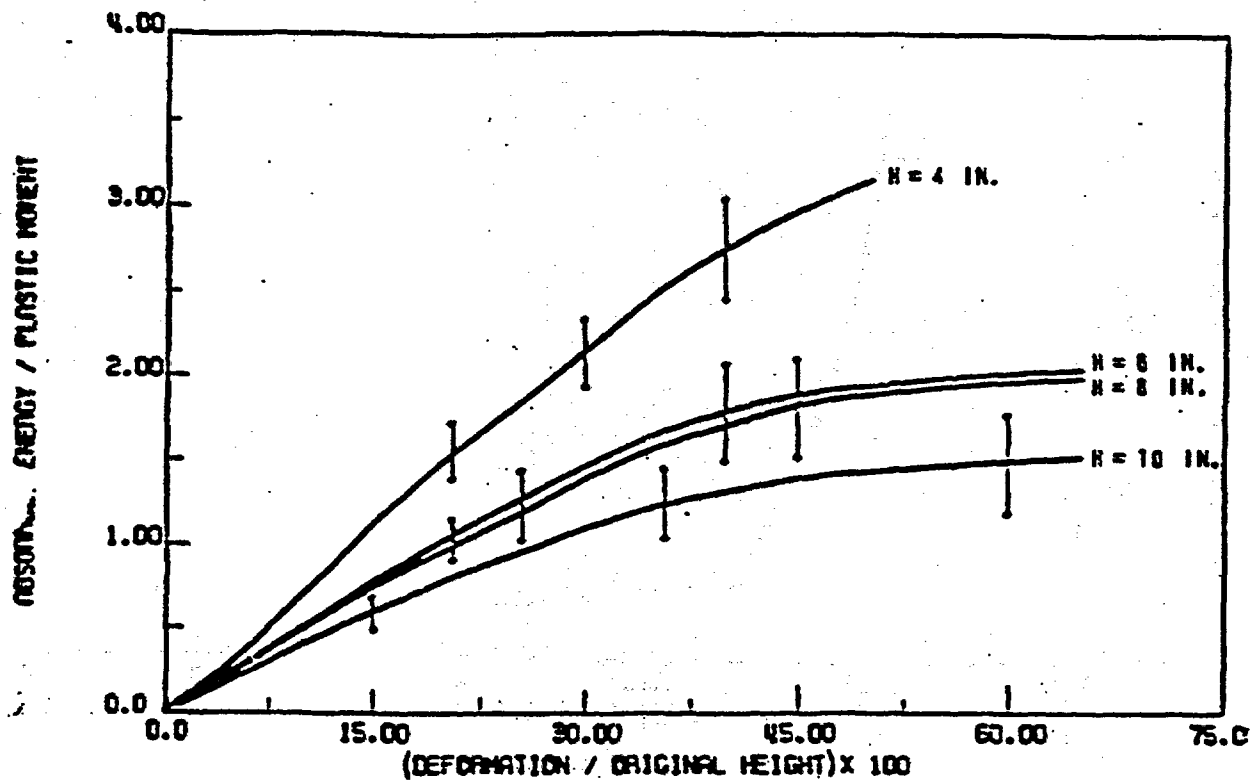


Figure 2.10.9-F7.1
Parameter [Peak force] versus Parameter [height/thickness] for Fin Impacting at 0°
(Data appended from Ref. [18])

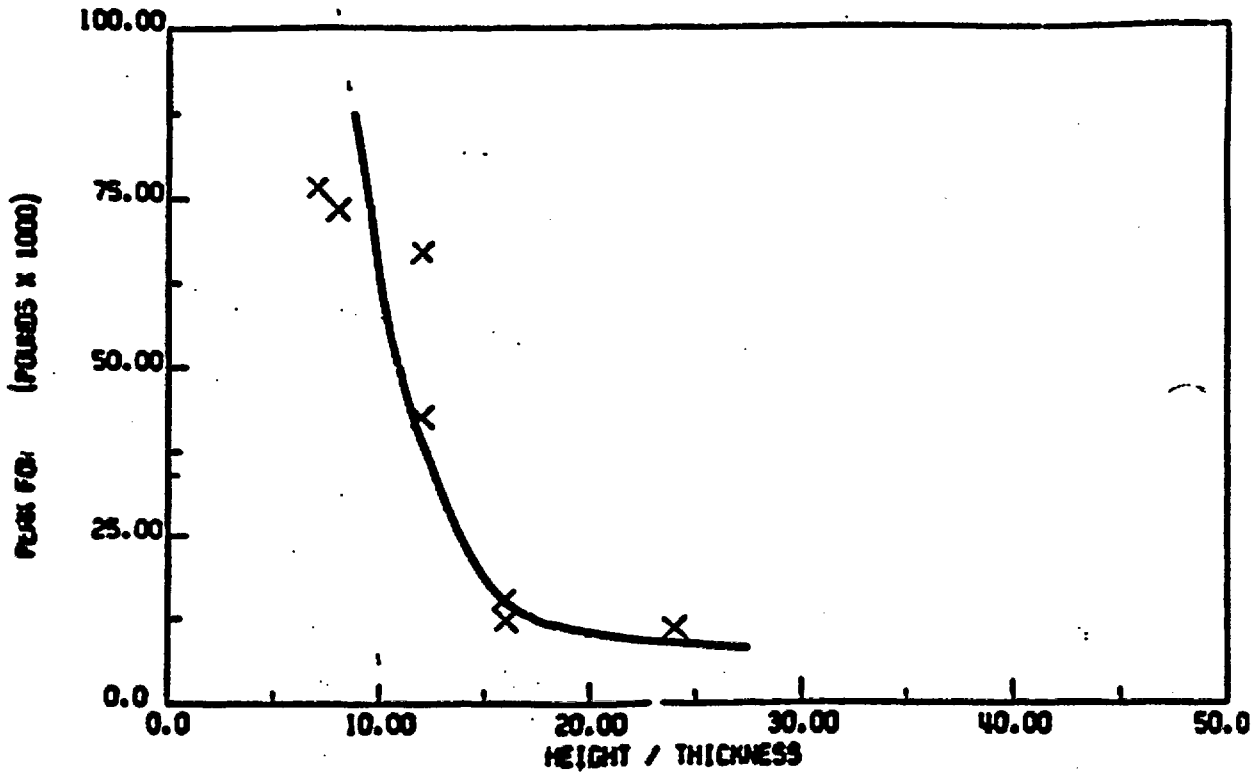


Figure 2.10.9-F7.2
Parameter [Peak Force] versus Parameter [height/thickness] for Fin Impacting at 10°
(Data appended from Ref. [18])

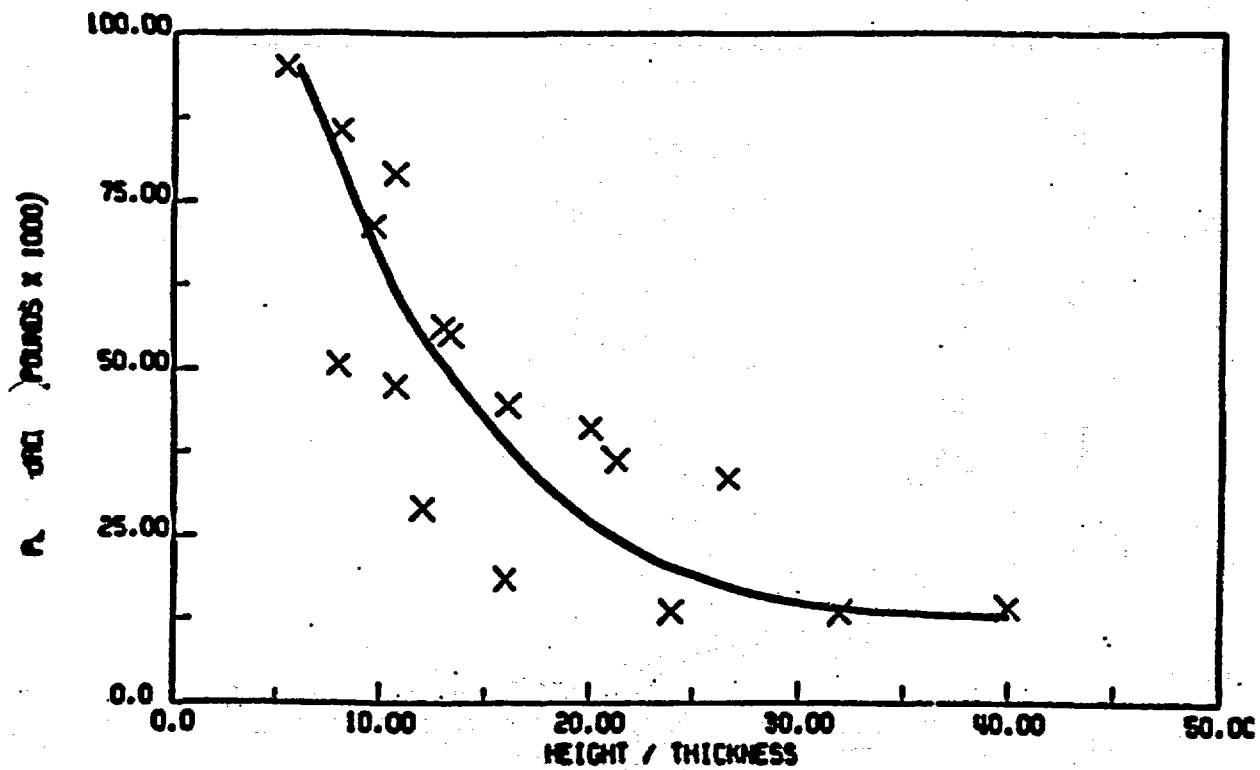


Figure 2.10.9-F7.3
Parameter [Peak force] versus Parameter [height/thickness] for Fin Impacting at 20°
(Data appended from Ref. [18])

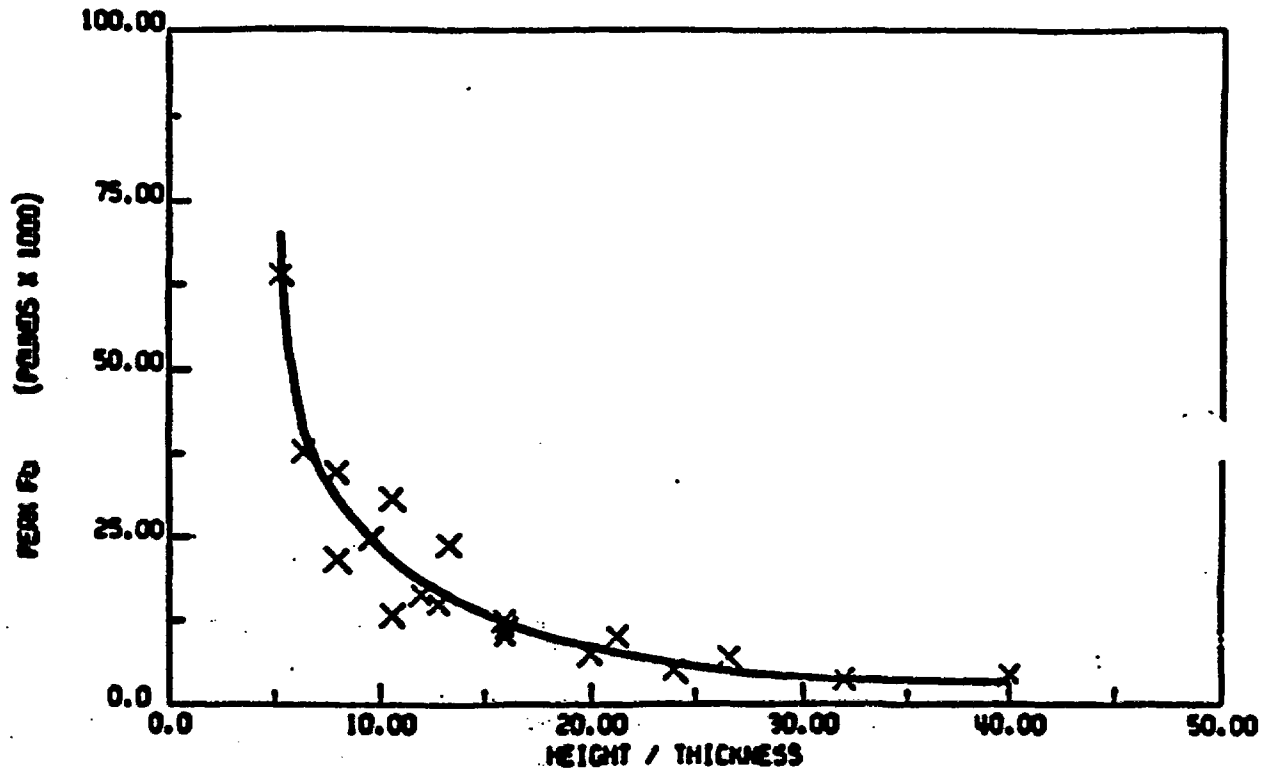


Figure 2.10.9-F7.4
Parameter [Peak force] versus Parameter [height/thickness] for Fin Impacting at 30°
(Data appended from Ref. [18])

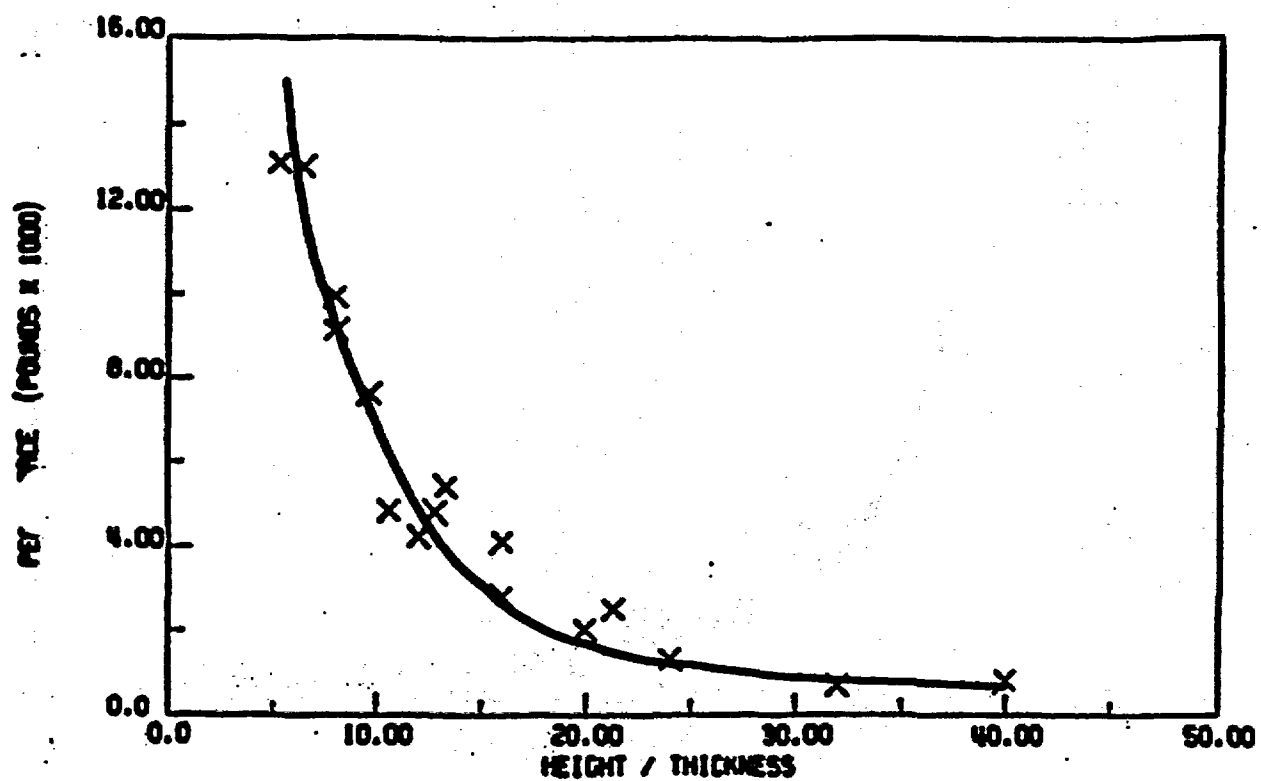


Figure 2.10.9-F7.5
Parameter [Peak force] versus Parameter [height/thickness] for Fin Impacting at 40°
(Data appended from Ref. [18])

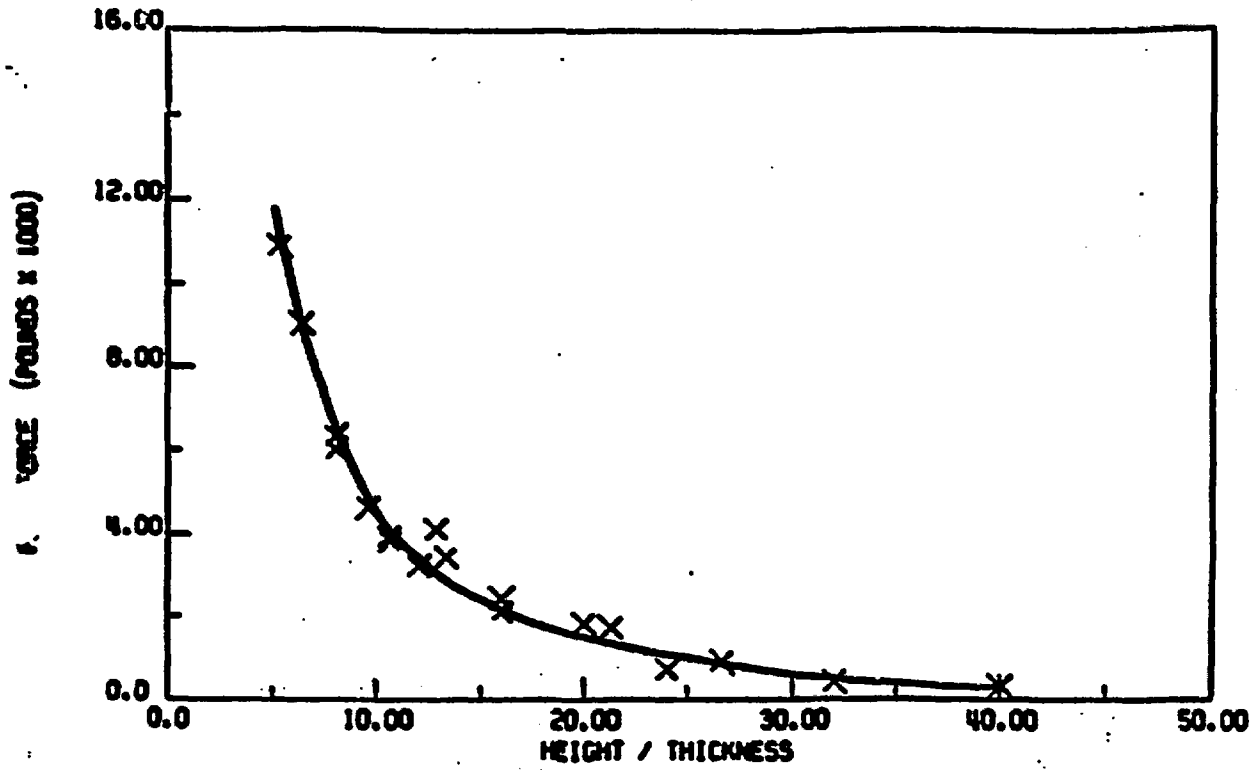
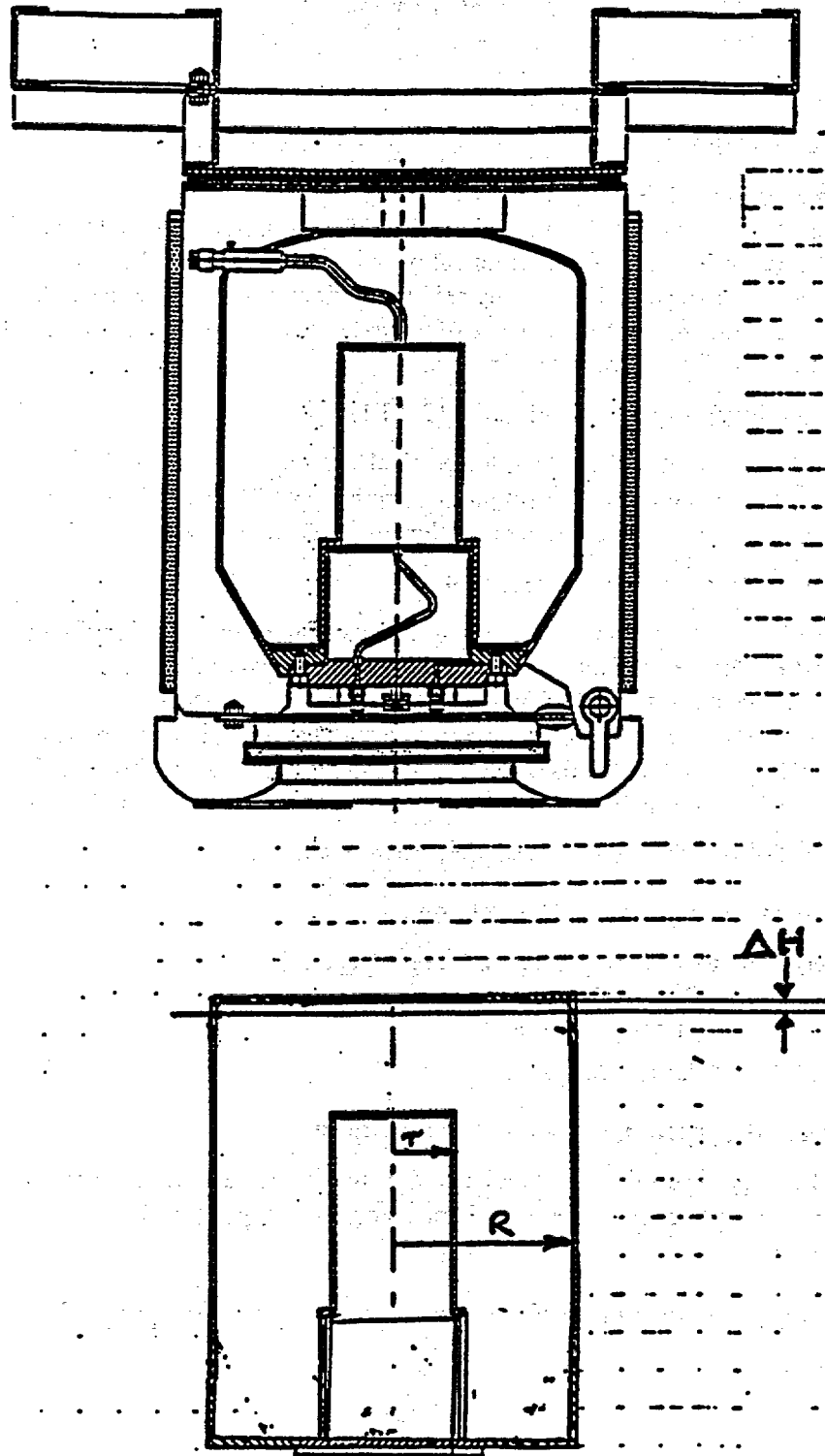


Figure 2.10.9-F8
Lead Slump in the Top End Drop



4. SIDE DROP

There are two mutually perpendicular side drops to consider: side drop #1 (see Figure 2.10.9-F9) and side drop #2 (see Figure 2.10.9-F10). Side drop #1 is orthogonal to side drop #2. Side drop #1 analysis is presented in section 4.1; side drop #2 analysis is presented in section 4.2.

4.1 SIDE DROP #1

4.1.1 Mode of Impact

First stage (primary) impact. See Figure 2.10.9-F11.

The entire 78-inch length of the 8 x 3 structural channel of the shipping skid and the ends of two I-beams impact the unyielding surface first. The four gusset plates within the channel will crush and the I-beam will deform. The bolts (connecting the shipping skid to the fixed skid) will be sheared; consequently the shipping skid will be detached from the balance of the package assembly. The balance of the package will rotate around the CG for the secondary impact.

Second stage (secondary) impact. See Figure 2.10.9-F11.

After the F-294 container rotates, the side of the crush shield impacts the unyielding surface at approximately 15°. As the secondary impact progresses the top of the cylindrical fireshield impacts the unyielding surface. As the impact progresses, the container top fins are crushed.

Third stage (tertiary) impact. See Figure 2.10.9-F11.

After the container has absorbed as much energy as it is capable of in 1st and 2nd stages, the container shall be subjected to secondary rebound. The height of the secondary rebound shall be proportional to the elastic portion of the energy absorbed by the container during 2nd stage. After the secondary rebound, the remaining momentum causes the container to rotate about CG and impact on the bottom end of the cylindrical fireshield, followed by the fixed skid, and finally the side external fins of the container. Any remaining unabsorbed energy shall be absorbed by the cask shell and lead until the container comes to rest.

Energy absorption, G-loads for each stage shall be carried out.

4.1.2 Potential Energy of F-294 Package

The potential energy due to 30-ft drop height of the package, E_0

$$\begin{aligned} E_0 &= W_{F-294} * H \\ &= 21,000 * 30 * 12 \\ &= 7,560,000 \text{ in.-lb.} \end{aligned}$$

4.1.3 Energy Absorption, G-Loads for 1st Stage

There are two (2) energy absorption structural elements that can be analyzed. These are

1. Four gusset plates between two channels of the shipping skid.
2. I-beams

4.1.3.1 Energy Absorption by Four Gusset Plates of the Shipping Skid

See Figure 2.10.9-F12.

- i) Fin Parameters
- Effective height, $h = 19.5$ in.
 - Thickness, $t = 0.75$ in.
 - Loaded length, $b = 8$ in.
 - material = ASTM A-36
 - % of crush = 45%
 - fin loading angle = 0°
- ii) Energy absorbed by one fin at 0° loading angle.

$$\begin{aligned} E_A &= N * M_P \\ &= 9 * \sigma_Y * bt^2 / 4 \\ &= 9 * 36,000 * 8 * (0.75)^2 / 4 \\ &= 364,500 \text{ in.-lb. per fin} \end{aligned}$$

where

$$\begin{aligned} E_A &= \text{Energy absorbed per fin in.-lb.} \\ N &= \text{Empirical parameter relating [absorbed energy/plastic moment] to} \\ &\quad \text{[deformation/original height] for a mild steel fin.} \\ &= 9 \text{ from Figure 2.10.9-F6.1, for 9-in. fin height, 45\% crush. Note: data for 19.5 in. height} \\ &\quad \text{fin does not exist; so 9-in. fin height data is extrapolated and} \\ N &= 9. \\ M_P &= \text{Plastic Moment in.-lb.} \\ &= \sigma_Y * bt^2 / 4 \\ \sigma_Y &= \text{yield stress of ASTM A-36 steel} = 36000 \text{ psi.} \end{aligned}$$

- iii) Energy absorbed by 4, 0.75 in. thick fins
- $$\begin{aligned} E_{A_{\text{GUSSET}}} &= 4 * 364,500 \\ &= 1.458 * 10^6 \text{ in.-lb.} \end{aligned}$$

4.1.3.2 Energy Absorption by Two I-beam Overhang

This energy absorption is an approximation as the effect of cross I-beams is difficult to account for. Each I-beam overhang member is treated as a discrete fin - one web fin and two flange fins.

A Web Fin

See Figure 2.10.9-F12.

- Effective height, $h = 10$ in. (actual height = 17 in.)
- Thickness, $t = 0.25$ in.
- Loaded length, $b = 4$ in.
- material = ASTM A-36
- % of crush* = 22.5%
- loading angle = 0° (angle of inclination to the unyielding surface)

* This implies only bending (single hinge failure mode) of fin only.

$$\begin{aligned} M_P &= \sigma_Y bt^2 / 4 \\ &= 36,000 * 4 * (0.25)^2 / 4 \\ &= 2,250 \text{ in.-lb.} \\ N &= 9 \text{ (Figures 2.10.9-F6.1 \& 6.2 at 22.5\%, 10 in. fin height)} \\ E_{A_{\text{WEB FIN}}} &= N * M_P \\ &= 9 * 2,250 \\ &= 20,250 \text{ in.-lb.} \end{aligned}$$

B Two Flange Fins

See Figure 2.10.9-F12.

- Effective height, $h = 10$ in. (actual height = 17 in.)
- Thickness, $t = 0.375$ in.
- Loaded length, $b = 4$ in.
- material = ASTM A-36
- % of crush* = 22.5%
- loading angle = 0° (angle of inclination to the unyielding surface)

* This implies only bending (single hinge failure mode) of fin only.

$$\begin{aligned} M_p &= \sigma_Y b t^2 / 4 \\ &= 36,000 \times 4 \times (0.375)^2 / 4 \\ &= 5,060 \text{ in.-lb.} \end{aligned}$$

$$N = 9 \text{ (Figures 2.10.9-F6.1 \& 6.2 22.5\%, 10 in. height)}$$

$$\begin{aligned} EA_{\text{FLANGE FIN}} &= N \times M_p \\ &= 9 \times 5,060 \\ &= 45,540 \text{ in.-lb. per flange per I-beam} \end{aligned}$$

As there are two flange fins per I-beam,

$$EA_{\text{FLANGE}} = 2 \times 45,540 = 91,080 \text{ in.-lb.}$$

Therefore, per I-beam end, the energy absorption is

$$\begin{aligned} EA_{\text{I-BEAM}} &= EA_{\text{FLANGE}} + EA_{\text{WEB FIN}} \\ &= 91,080 + 20,250 \text{ in.-lb.} \\ &= 111,330 \text{ in.-lb. per I-beam end} \end{aligned}$$

As there are two I beam ends impacting at the same time,

$$\begin{aligned} EA_{\text{I-BEAM ENDS}} &= \text{Number of I-beam ends} \times EA_{\text{I-BEAM}} \\ &= 2 \times 111,330 \\ &= 273,200 \text{ in.-lb.} \\ &= 0.223 \times 10^6 \text{ in.-lb.} \end{aligned}$$

4.1.3.3 First Stage: Energy Absorbed by Two Structural Elements

The total energy absorbed by four gussets and two I-beam ends is

$$\begin{aligned} pEA_{\text{T, 1st stage}} &= \Sigma EA_{\text{GUSSET}} + EA_{\text{I-BEAM ENDS}} \\ &= (1.458 + 0.223) \times 10^6 \text{ in.-lb.} \\ &= 1.681 \times 10^6 \text{ in.-lb.} \end{aligned}$$

4.1.3.4 Ratio of First Stage Energy Absorbed/Initial Potential Energy

$$\begin{aligned} EA_{\text{T, 1st stage}}/E_0 &= 1.681 \times 10^6 / 7.56 \times 10^6 \\ &= 22.2\% \end{aligned}$$

It is estimated that 22.2% of the initial potential energy of F-294 package subjected to 30-ft free drop is absorbed in the first stage of the drop.

4.1.3.5 Estimate of Peak Force and G-load

4.1.3.5.1 Gusset Plate

[Height of the fin/thickness of the fin] = $10/0.75 = 13.3$

Peak force, $P = 37500$ lb. per in. per fin (Figure 2.10.9-F7.1)

Peak force in gusset plates, FP_{gusset}

$$\begin{aligned} FP_{\text{gusset}} &= \text{unit peak force} \times \text{loaded length} \times \text{number of fins} \\ &= P \times b \times 4 \\ &= 37,500 \times 8 \times 4 \\ &= 1.2 \times 10^6 \text{ lb.} \end{aligned}$$

4.1.3.5.2 I-beam

Web of the I-beam

[Height of fin/thickness of web] = $10/0.25 = 40$

From Fig 2.10.9-F7.1, Unit Peak force, $P_2 = 8,000$ lb. per in. of loaded length per fin.

Flange of the I-beam

[Height of fin/thickness of flange] = $10/0.375 = 26.7$

From Fig 2.10.9-F7.1, unit peak force, $P_2 = 8,000$ lb. per in. of loaded length per fin.

The container weight is acting over 4 in. web length and 4 in. of each flange width. The loaded length of each I-beam = $4 + 2 \times 4 = 12$ in.

Peak force $FP_{\text{I-beam}}$

$$\begin{aligned} FP_{\text{I-beam}} &= \text{unit peak force} \times \text{loaded length} \times \text{number of I-beam ends} \\ &= 8,000 \times 12 \times 2 \\ &= 0.192 \times 10^6 \text{ lb.} \end{aligned}$$

4.1.3.5.3 Channel face

A channel has two flanges and one web; each flange is 3.5 inch high x 0.5 in thick. The flanges are considered "fins" for estimating peak forces.

[Height of fin/thickness of fin] = $3.5/0.5 = 7$

From Figure 2.10.9-F7.1, Unit Peak force, $P_1 = 75,000$ lb. per inch of loaded length per fin

Effective loaded length of channel face

$$\begin{aligned} &= [\text{full span of channel} \\ &+ \text{span over which container load acts}]/2 \\ &= [78 + 48]/2 \\ &= 63 \end{aligned}$$

Number of flanges per channel face impacting = 2

Peak force, $FP_{\text{channel face}}$

$$\begin{aligned} FP_{\text{channel face}} &= \text{Unit Peak Force} \times \text{loaded length} \times \text{number of flanges per channel face} \\ &\quad \text{impacting} \\ &= 8000 \times 63 \times 2 \\ FP_{\text{channel face}} &= 9.45 \times 10^6 \text{ lb.} \end{aligned}$$

4.1.3.6 Total Peak Force, ΣFP

$$\begin{aligned} \Sigma FP &= FP_{\text{gusset}} + FP_{\text{I-beam ends}} + FP_{\text{channel face}} \\ &= 1.2 \times 10^6 + 0.192 \times 10^6 + 9.45 \times 10^6 \text{ lb.} \\ &= 10.842 \times 10^6 \text{ lb.} \end{aligned}$$

4.1.3.7 G-load

It is possible to estimate G-load based on peak force calculated using DAVIS method - Ref. [18].

The cumulative Peak force $\Sigma FP = 10.842 * 10^6$ lb., exclusive of stiffening factors due to stiffening structural members.

Therefore,

$$\begin{aligned} G_1 &= \Sigma FP / W_{F-294} \\ &= 10.842 * 10^6 \text{ lb.} / 21,000 \text{ lb.} \\ &= 516 \text{ g's} \end{aligned}$$

4.1.4 Energy absorption, G-loads for 2nd stage

There are three (3) energy absorption structural elements that can be analyzed. These are:

1. A top/side sector of the crush shield
2. A top/side sector of the cylindrical fireshield
3. A top/side sector of the container external cooling fins

4.1.4.1 Energy Absorption by Fins of Crush Shield

Refer to Figure 2.10.9-F13 for layout and numbering of crush shield fins.

How many fins are in the zone of impact? See Figure 2.10.9-F13. It is estimated from the graphical data, that seven (7) fins (0.5 in. thick) come into play.

What is the loading angle for each fin?

$$\theta = \beta \times \cos \alpha$$

where

θ = fin loading angle ($^{\circ}$)

β = angle between vertical axis and fin n

α = angle between impact pad and the longitudinal axis of the package.

Table 2.10.9-T3 lists the appropriate θ , loading angles for all the fins of the crush shield, as calculated in the following example; e.g.,

For Fins #3 and #4 (i.e., 0.5 in. thick fin)

$$\theta = \beta \times \cos \alpha$$

$$\theta = 10 \times \cos 15^{\circ}$$

$$\theta = 9.5^{\circ}$$

Table 2.10.9-T3
Fin Data for the Crush Shield Fins in Side Drop #1: 2nd Stage

Type of Fins	Designated #	No. of Fins	Loading Angle, θ	Parameter N
0.5 in.	#4	1	0 $^{\circ}$	14
0.5 in.	#3, #5	2	9.5 $^{\circ}$	14
0.5 in.	#2, #6	2	19.0 $^{\circ}$	3
0.5 in.	#1, #7	2	28.5 $^{\circ}$	2.5

i) Fin #4,

- Effective height, $h = 8$ in.
- Thickness, $t = 0.5$ in.
- Loaded length, $b = 9$ in.
- material = C-1020
- % of crush = 45%
- loading angle = 0° (angle of inclination to the unyielding surface)

Therefore, at crush of 45%, for fin height of 8 in., fin inclination angle of 0° , from Figure 2.10.9-F6.1, the parameter [absorbed energy/plastic moment], $N = 14$.

$$\begin{aligned} EA_{\text{FINS \#4}} &= N \times \sigma_Y \times b \times t^2 / 4 \\ &= 14 \times 46,000 \times 9 \times (0.5)^2 / 4 \\ &= 0.362 \times 10^6 \text{ in.-lb.} \end{aligned}$$

ii) Fins #3 and #5

- Effective height, $h = 8$ in.
- Thickness, $t = 0.5$ in.
- Loaded length, $b = 9$ in.
- material = C-1020
- % of crush = 45%
- loading angle = 9.5° (angle of inclination to the unyielding surface)

Therefore, at crush of 45%, for fin height of 8 in., fin inclination angle of 9.5° , from Figure 2.10.9-F6.2, the parameter [absorbed energy/plastic moment], $N = 14$

$$\begin{aligned} EA_{\text{FINS \#3,\#5}} &= 2 \times 14 \times \sigma_Y \times b \times t^2 / 4 \\ &= 2 \times 14 \times 46,000 \times 9 \times (0.5)^2 / 4 \\ &= 2 \times 0.362 \times 10^6 \\ &= 0.724 \times 10^6 \text{ in.-lb.} \end{aligned}$$

iii) Fins #2 and #6

For Fins #2 and #6 (i.e., 0.5 in. thick fin)

$$\begin{aligned} \theta &= \beta \times \cos \alpha \\ \theta &= 20 \times \cos 15^\circ \\ \theta &= 19.^\circ \end{aligned}$$

- Effective height, $h = 8$ in.
- Thickness, $t = 0.5$ in.
- Loaded length, $b = 9$ in.
- material = C-1020
- % of crush = 45%
- loading angle = 19° (angle of inclination to the unyielding surface)

Therefore, at crush of 45%, for fin height of 8 in., fin inclination angle of 34° , from Figure 2.10.9-F6.3, the parameter [absorbed energy/plastic moment], $N = 3$

$$\begin{aligned} EA_{\text{FINS \#2,\#6}} &= 2 \times N \times \sigma_Y \times b \times t^2 / 4 \\ &= 2 \times 3 \times 46,000 \times 9 \times (0.5)^2 / 4 \\ &= 2 \times 77,625 \\ &= 155,250 \text{ in.-lb.} \end{aligned}$$

iv) Fins #1 and #7

For Fins #1 and #7 (i.e., 0.5 in. thick fin)

$$\theta = \beta \times \cos \alpha$$

$$\theta = 30 \times \cos 15^\circ$$

$$\theta = 28.5^\circ$$

- Effective height, $h = 8$ in.
- Thickness, $t = 0.5$ in.
- Loaded length, $b = 9$ in.
- material = C-1020
- % of crush = 45%
- loading angle = 28.5° (angle of inclination to the unyielding surface)

Therefore, at crush of 45%, for fin height of 8 in., fin inclination angle of 9.5° , from Figures 2.10.9-F6.4, the parameter [absorbed energy/plastic moment], $N = 2.5$

$$\begin{aligned} EA_{\text{FINS \#1, \#7}} &= 2 \times 2.5 \times \sigma_Y \times b \times t^2 / 4 \\ &= 2 \times 2.5 \times 46,000 \times 9 \times (0.5)^2 / 4 \\ &= 2 \times 64,687 \times 10^6 \\ &= 0.129 \times 10^6 \text{ in.-lb.} \end{aligned}$$

Therefore, the sum of energy absorbed by all the fins is:

$$\begin{aligned} EA_{\text{crush shield fins}} &= [EA_{\text{FINS \#4}} + EA_{\text{FINS \#3, \#5}} + EA_{\text{FINS \#2, \#6}} + EA_{\text{FINS \#1, \#7}}] \\ &= [0.362 + 0.724 + 0.155 + 0.129] \times 10^6 \text{ in.-lb.} \\ &= 1.37 \times 10^6 \text{ in.-lb.} \end{aligned}$$

4.1.4.2 Energy Absorbed by Top/Side Fins of the Container

Refer to Figure 2.10.9-F13 for layout and numbering of container fins.

There are three types of fins on the top of the container 1) 1.25 in. thick 2) 0.5 in. thick 3) 0.375 in. thick. The container lift lug fin and the 0.5 in. thick fin adjacent to the lift lug fin do not come into play as they are just outside the zone of impact. Lift lug fin is at 45° to the shipping skid. Refer to Figure 2.10.9-F13 for depiction of effective fin parameters etc.

How many fins are in the zone of impact? See Figure 2.10.9-F13. It is estimated from the graphical data, that six fins (3/8 in. thick) come into play.

What is the loading angle for each fin?

$$\theta = \beta \times \cos \alpha$$

where

$$\theta = \text{fin loading angle } (^\circ)$$

$$\beta = \text{angle between fin 1 and fin n}$$

$$\alpha = \text{angle between impact pad and the longitudinal axis of the package.}$$

Table 2.10.9-T4 lists the appropriate θ , loading angles for all the fins of the container, as calculated in the following example;

For Fins #5 and #6 (i.e., 0.375 inch fin)

$$\theta = \beta \times \cos \alpha$$

$$\theta = 5 \times \cos 15^\circ$$

$$\theta = 5^\circ$$

For Fins #4 and #7 (i.e., 0.375 in. thick fin)

$$\theta = \beta \times \cos \alpha$$

$$\theta = 15 \times \cos 15^\circ$$

$$\theta = 14.5^\circ$$

For Fins #3 and #8 (i.e., 0.375 in. thick fin)

$$\theta = \beta \times \cos \alpha$$

$$\theta = 25 \times \cos 15^\circ$$

$$\theta = 24.5^\circ$$

Table 2.10.9-T4
Container Fin Data for Side Drop #1: 2nd Stage

Type of Fin	Designated # Fin Number	Number of Fins	Loading Angle, θ	Parameter N
0.375 in. fin	5, 6	2	5°	17
0.375 in. fin	4, 7	2	14.5°	10
0.375 in. fin	3, 8	2	24.5°	3

i) Fins #5 and #6

- Effective height, $h = 6$ in.
- Thickness, $t = 0.375$ in.
- Loaded length, $b = 12$ in.
- material = ss304L
- % of crush = 35%
- loading angle = 5° (angle of inclination to the unyielding surface)

Therefore, at crush of 45%, for fin height of 6 in., fin inclination angle of 5°, from Figure 2.10.9-F6.1 & F6.2, the parameter [absorbed energy/plastic moment], $N = 17$.

$$\begin{aligned} EA_{\text{FINS \#5,\#6}} &= 2 \times N \times \sigma_Y \times b \times t^2 / 4 \\ &= 2 \times 17 \times 25,000 \times 12 \times (0.375)^2 / 4 \\ &= 2 \times 179,000 \\ &= 358,000 \text{ in.-lb.} \end{aligned}$$

ii) Fins #4 and #7

- Effective height, $h = 6$ in.
- Thickness, $t = 0.375$ in.
- Loaded length, $b = 12$ in.
- material = ss304L
- % of crush = 35%
- loading angle = 14.5° (angle of inclination to the unyielding surface)

Therefore, at crush of 35%, for fin height of 6 in., fin inclination angle of 14.5°, from Figures 2.10.9-F6.2 & F6.3, the parameter [absorbed energy/plastic moment], $N = 10$.

$$\begin{aligned} EA_{\text{FINS \#4,\#7}} &= 2 \times N \times \sigma_Y \times b \times t^2 / 4 \\ &= 2 \times 10 \times 25,000 \times 12 \times (0.375)^2 / 4 \\ &= 2 \times 105,000 \\ &= 210,000 \text{ in.-lb.} \end{aligned}$$

iii) Fins #3 and #8

- Effective height, $h = 6$ in.
- Thickness, $t = 0.375$ in.
- Loaded length, $b = 12$ in.
- material = ss304L
- % of crush = 35%
- loading angle = 24.5° (angle of inclination to the unyielding surface)

Therefore, at crush of 35%, for fin height of 6 in., fin inclination angle of 24.5° , from Figures 2.10.9-F6.3 and 2.10.9-F6.4, the parameter [absorbed energy/plastic moment], $N = 3$.

$$\begin{aligned} EA_{\text{FINS \#3,\#8}} &= 2 \times N \times \sigma_Y \times b \times t^2 / 4 \\ &= 2 \times 3 \times 25,000 \times 12 \times (0.375)^2 / 4 \\ &= 2 \times 31,000 \\ &= 62,000 \text{ in.-lb.} \end{aligned}$$

Therefore the sum of energy absorbed by all the fins is

$$\begin{aligned} EA_{\text{container fins}} &= [EA_{\text{FINS \#5, \#6}} + EA_{\text{FINS \#4, \#7}} + EA_{\text{FINS \#3, \#8}}] \\ &= [0.358 + 0.210 + 0.062] \times 10^6 \text{ in.-lb.} \\ &= 0.63 \times 10^6 \text{ in.-lb.} \end{aligned}$$

4.1.4.3 Estimate of Peak Force, G-loads for 2nd Stage

4.1.4.3.1 Estimate of Peak Force

Peak force is evaluated using Ref. [18]. It should be noted that, during impact, this "peak" force is only experienced by the F-294 package for an extremely short time (in the order of less than 100 milliseconds).

a) For crush shield fins (0.5 in. thick)

1. [height of fin/ thickness of fin] = $8/0.5 = 16$
2. fin loading angle = $0^\circ, 9.5^\circ, 14.5^\circ, 24.5^\circ$
- 3.1 For fin #4 at fin loading angle = 0° , unit peak force $P_1 = 12,500$ lb. per in of loaded length per fin (see Figure 2.10.9-F7.1)
- 3.2 For fins #3 and #5 at fin loading angle = 9.5° , unit peak force $P_2 = 37,000$ lb. per in of loaded length per fin (see Figure 2.10.9-F7.2). (9.5°)
- 3.3 For fins #2 and #6 at fin loading angle = 14.5° , Unit peak force $P_3 = 20,000$ lb. per in of loaded length per fin (See Figure 2.10.9-F7.2 & F7.3). (24°)
- 3.4 For fins #1 and #7 at fin loading angle = 24.5° , Unit peak force $P_4 = 8,000$ lb. per inch of loaded length per fin (see Figures 2.10.9-F7.3 and 2.10.9-R7.4). (24.5°)
4. Loaded length of the fin = 9 in.
5. Total peak force experienced by the package due to impact of the crush shield;

$$\begin{aligned} \Sigma FP_{\text{CRUSH SHIELD}} &= \text{loaded length} \times \Sigma [\text{unit peak force} \times \text{number of fins}] \\ &= 9 \times [P_1 \times 1 + P_2 \times 2 + P_3 \times 2 + P_4 \times 2] \\ &= 9 \times [12,500 \times 1 + 37,000 \times 2 + 20,000 \times 2 + 8,000 \times 2] \\ &= 9 \times [143,500] \\ &= 1.291 \times 10^6 \text{ lb.} \end{aligned}$$

b) For container fins (0.375 in. thick)

1. [height of fin/thickness of fin] = $6/0.375 = 16$
2. Fin loading angle = $5^\circ, 14.5^\circ, 25^\circ$
- 3.1 For fins #5 and #6 with fin loading angle = 5° , unit peak force $P_1 = 20,000$ lb. per inch of loaded length per fin (see Figure 2.10.9-F7.3) (19°)
- 3.2 For fins #4 and #7 with fin loading angle = 14.5° , unit peak force $P_2 = 20,000$ lb. per in of loaded length per fin (see Figures 2.10.9-F7.2 and 2.10.9-F7.3) (28.5°)
- 3.3 For fins #3 and #8 with fin loading angle = 24.5° , unit peak force $P_3 = 8,000$ lb. per inch of loaded length per fin (see Figures 2.10.9-F7.2 and 2.10.9-F7.3) (28.5°)
4. Loaded length of the fin = 12 in.
5. Total peak force experienced by the package due to impact of the 0.375-inch thick top fins of the container;

$$\begin{aligned}\Sigma FP_{0.375 \text{ FINS, CONTAINER}} &= \text{loaded length} \times \Sigma [\text{unit peak force} \times \text{number of fins}] \\ &= 12 \times [P_1 \times 2 + P_2 \times 2 + P_3 \times 2] \\ &= 12 \times [20,000 \times 2 + 2 \times 20,000 + 2 \times 8,000] \\ &= 12 \times [96,000] \\ &= 1.152 \times 10^6 \text{ lb.}\end{aligned}$$

The total peak force, ΣFP

$$\begin{aligned}\Sigma FP &= FP_{\text{CRUSH SHIELD}} + FP_{0.375 \text{ FIN CONTAINER}} \\ &= [1.291 + 1.152] \times 10^6 \text{ lb.} \\ &= 2.416 \times 10^6 \text{ lb.}\end{aligned}$$

4.1.4.3.2 Estimate G-load during peak force duration

a) Based on Davis's method (Ref. [18]) of estimating peak forces, the G-load is

$$\begin{aligned}G &= \Sigma FP / W_{F-294} \\ &= 2.4 \times 10^6 / 21,000 \\ &= 114 \text{ g's.}\end{aligned}$$

In the side corner drop orientation, the container is subjected to a G-load of 114 g's.

4.1.5 Energy absorption, G-loads for 3rd stage

There are three (3) energy absorption structural elements. These are:

1. A bottom/side sector of the cylindrical fireshield
2. A bottom/side sector of the fixed skid
3. A bottom/side sector of the container external cooling fins.

Of these, 1) and 3) shall be considered herein.

4.1.5.1 Energy Absorption by External Cooling Fins on the Container

See Figure 2.10.9-F14.

i) Fins #5 and #6 Parameters

- Effective height, h = 4 in.
- Thickness, t = 0.375 in.
- Loaded length, b = 32 in.
- material = ss304L
- % of crush = 30%
- loading angle = 5° (angle of inclination to the unyielding surface)

Therefore, at crush of 30%, for fin height of 4 in., from Figures 2.10.9-F6.1 and 2.10.9-F6.2, the parameter [absorbed energy/plastic moment], $N = 16$

$$\begin{aligned} EA_{\text{FINS}\#5,6} &= 2 \times N \times M_p \\ &= 2 \times 16 \times [\sigma_y \times b \times t^2 / 4] \\ &= 2 \times 16 \times [25,000 \times 32 \times (0.375)^2 / 4] \\ &= 0.9 \times 10^6 \text{ in.-lb.} \end{aligned}$$

ii) Fins #4 and #7

- Effective height, $h = 4$ in.
- Thickness, $t = 0.375$ in.
- Loaded length, $b = 32$ in.
- material = ss304L
- % of crush = 30%
- loading angle = 15° (angle of inclination to the unyielding surface)

Therefore, at crush of 30%, for fin height of 4 in., fin inclination angle of 15° , from Figures 2.10.9-F6.2 and 2.10.9-F6.3, the parameter [absorbed energy/plastic moment], $N = 10$

$$\begin{aligned} EA_{\text{FINS}\#4,\#7} &= 2 \times N \times \sigma_y \times b \times t^2 / 4 \\ &= 2 \times 10 \times 25,000 \times 32 \times (0.375)^2 / 4 \\ &= 2 \times 0.281 \times 10^6 \\ &= 0.562 \times 10^6 \text{ in.-lb.} \end{aligned}$$

iii) Fins #3 and #8

- Effective height, $h = 4$ in.
- Thickness, $t = 0.375$ in.
- Loaded length, $b = 32$ in.
- material = ss304L
- % of crush = 30%
- loading angle = 25° (angle of inclination to the unyielding surface)

Therefore, at crush of 30%, for fin height of 4 in., fin inclination angle of 25° , from Figures 2.10.9-F6.2 and 2.10.9-F6.3, the parameter [absorbed energy/plastic moment], $N = 3$

$$\begin{aligned} EA_{\text{FINS}\#3,\#8} &= 2 \times N \times \sigma_y \times b \times t^2 / 4 \\ &= 2 \times 3 \times 25,000 \times 32 \times (0.375)^2 / 4 \\ &= 2 \times 0.084 \times 10^6 \\ &= 0.168 \times 10^6 \text{ in.-lb.} \end{aligned}$$

Cumulative energy absorbed by external cooling fins

$$\begin{aligned} \Sigma EA_{\text{FINS}} &= EA_{\text{FINS}\#5,\#6} + EA_{\text{FINS}\#4,\#7} + EA_{\text{FINS}\#3,\#8} \\ &= (0.900 + 0.562 + 0.168) \times 10^6 \text{ in.-lb.} \\ &= 1.63 \times 10^6 \text{ in.-lb.} \end{aligned}$$

4.1.5.2 Energy Absorbed by the Cylindrical Fireshield

In the second stage of the impact we had neglected to estimate the energy absorbed by the cylindrical fireshield. In the third stage the cylindrical fireshield side is impacted. Second and third stage impact of the fireshield shall be combined and analyzed here. (see Figure 2.10.9-F15).

A cylindrical fireshield is a cylindrical shell which is deformed by some amount in the side impact. A simple model is given here:

Step 1

The radius R_0 decreases to R_i

$$\begin{aligned} \text{the strain is } \epsilon &= [R_0 - R_i] / R_0 \\ &= \Delta / R_0 \end{aligned}$$

Step 2

The stress, σ = function (ϵ)

Step 3

The compressive stress $\sigma_c = 1.6 \times \sigma$

Step 4

The crushed area $A_{\text{crush}} = L \times c$

$$c = 2 [\Delta (2R_0 - \Delta)]^{0.5}$$

Therefore, $A_{\text{crush}} = L \times c$

$$A_{\text{crush}} = L \times 2 [\Delta (2R_0 - \Delta)]^{0.5}$$

Step 5

Mean crushed area $A_{\text{mean crush}} = A_{\text{crush}} / 2$

Step 6

Mean Impact force

$$F_c = \sigma_c \times A_{\text{mean crush}}$$

Step 7

Work done

$$U = F_c \times \Delta$$

Step 8

$$G\text{-load} = F_c / W_{F-294 \text{ LESS SKID}}$$

Plugging in the data:

$$\Delta = 0.1 \text{ in.}$$

$$R_0 = 23.75 \text{ in.}$$

$$L = 30.0 \text{ in.}$$

$$\sigma = 32,000 + [23,000/20] \times \epsilon (\%)$$

we find

$$\epsilon = 0.1/23.75 = 0.00421$$

$$\sigma = 32,000 + [23,000/20] \times \epsilon (\%)$$

$$= 32,000 + [23,000/20] \times 0.421$$

$$= 32,000 + 484$$

$$= 32,484 \text{ psi}$$

$$\sigma_c = 1.6 \times \sigma$$

$$= 1.6 \times \text{psi}$$

$$= 51,974 \text{ psi}$$

$$\begin{aligned}
 c &= 2 [\Delta (2R_0 - \Delta)]^{0.5} \\
 &= 2 [0.1 (2 \times 23.75 - 0.1)]^{0.5} \\
 &= 4.35 \text{ in.} \\
 L &= 30 \text{ in.} \\
 A_{\text{crush}} &= L \times c \\
 &= 30. \times 4.35 \\
 &= 130.5 \text{ in}^2 \\
 A_{\text{mean crush}} &= A_{\text{crush}} / 2 \\
 &= 130.5/2 \\
 &= 65.35 \text{ in}^2
 \end{aligned}$$

Mean Impact force

$$\begin{aligned}
 F_c &= \sigma_c \times A_{\text{mean crush}} \\
 &= 51,974 \text{ psi} \times 65.25 \\
 &= 3.391 \times 10^6 \text{ lb.}
 \end{aligned}$$

Work done

$$\begin{aligned}
 U &= F_c \times \Delta \\
 &= 3.391 \times 10^6 \text{ lb.} \times 0.1 \text{ in.} \\
 &= 0.339 \times 10^6 \text{ in.-lb.}
 \end{aligned}$$

Hence, it is estimated that for a small deformation of 0.1 in. over a length of 30 in., the energy absorbed by the cylinder is 0.339×10^6 in.-lb.

4.1.5.3 Peak Force and G-loads in the 3rd Stage

4.1.5.3.1 External Cooling Fins

[Height of the fin/thickness of the fin]= $4/0.375 = 10.6$

Peak force, $P_1 = 55000$ lb. per in. per fin (Figures 2.10.9-F7.1 and 2.10.9-F7.2)

Peak force in cooling fins, FP_{FINS}

Fin at 5°

$$\begin{aligned}
 FP_{\text{FIN}\#5,6} &= \text{unit peak force} \times \text{loaded length} \times \text{number of fins} \\
 &= P_1 \times b \times 2 \\
 &= 55,000 \times 32 \times 2 \\
 &= 3.52 \times 10^6 \text{ lb.}
 \end{aligned}$$

Fin at 15°

Peak force, $P_2 = 35,000$ lb. per in. per fin (Figures 2.10.9-F7.2 and 2.10.9-F7.3)

$$\begin{aligned}
 FP_{\text{FIN}\#4,\#7} &= \text{unit peak force} \times \text{loaded length} \times \text{number of fins} \\
 &= P_2 \times b \times 2 \\
 &= 35000 \times 32 \times 2 \\
 &= 2.24 \times 10^6 \text{ lb.}
 \end{aligned}$$

Fin at 25°

Peak force, $P_3 = 13,000$ lb. per in. per fin (Figures 2.10.9-F7.3 and 2.10.9-F7.4)

$$\begin{aligned}
 FP_{\text{FIN}\#3,\#35} &= \text{unit peak force} \times \text{loaded length} \times \text{number of fins} \\
 &= P_3 \times b \times 2 \\
 &= 13,000 \times 32 \times 2 \\
 &= 0.832 \times 10^6 \text{ lb.}
 \end{aligned}$$

4.1.5.3.2 Peak forces in the Cylindrical Fireshield

$$\begin{aligned}\text{Mean Impact force, } F_c &= \sigma_c \times A_{\text{mean crush}} \\ &= 51,974 \text{ psi} \times 65.25 \\ &= 3.391 \times 10^6 \text{ lb.}\end{aligned}$$

4.1.5.3.3 Total Peak Force, ΣFP

$$\begin{aligned}\Sigma FP &= FP_{\text{cooling fins}} + F_{\text{cylindrical fireshield}} \\ &= 6.592 \times 10^6 + 3.391 \times 10^6 \text{ lb.} \\ &= 9.983 \times 10^6 \text{ lb.}\end{aligned}$$

4.1.5.3.4 G-load

It is possible to estimate G-load based on peak force calculated using Davis method (Ref. [18]).

The cumulative Peak force $\Sigma FP = 9.983 \times 10^6 \text{ lb.}$, exclusive of stiffening factors due to stiffening structural members.

Therefore

$$\begin{aligned}G_1 &= \Sigma FP / W_{F-294} \\ &= 9.983 \times 10^6 \text{ lb.} / 20,020 \text{ lb.} \\ &= 500 \text{ g's.}\end{aligned}$$

4.1.6 Energy Balance, Peak Force, G-load so Far

4.1.6.1 Energy Balance

1st Stage

$$EA_{T,1st \text{ stage}} = 1.681 \times 10^6 \text{ in.-lb.}$$

2nd Stage

$$\begin{aligned}EA_{\text{crush shield fins}} &= 1.37 \times 10^6 \text{ in.-lb.} \\ EA_{\text{container fins}} &= 0.63 \times 10^6 \text{ in.-lb.} \\ EA_{\text{cyl. fireshield}} &= \text{not accounted for}\end{aligned}$$

3rd Stage

$$\begin{aligned}EA_{\text{fins}} &= .63 \times 10^6 \text{ in.-lb.} \\ EA_{\text{cyl. fireshield}} &= 0.339 \times 10^6 \text{ in.-lb.}\end{aligned}$$

Total energy absorbed so far $5.65 \times 10^6 \text{ in.-lb.}$

$$\% \text{ absorbed} = 5.65 \times 10^6 / 7.56 \times 10^6 = 74.7\%$$

$$\% \text{ not absorbed} = 25.3\%$$

The 25.3% of 30-ft drop energy shall be taken up by the cask shell and lead. This is presented in section 4.1.5.

4.1.6.2 Peak Force and G-loads

1 st stage: Peak force = $10.842 \times 10^6 \text{ lb.}$, G-load = 516 g's.

2 nd stage: Peak force = $2.1 \times 10^6 \text{ lb.}$, G-load = 100 g's.

3 rd stage: Peak force = $9.991 \times 10^6 \text{ lb.}$, G-load = 500 g's

4.1.7 Energy Absorbed by Cask Shell and Lead. Estimate of Lead Movement or Slump

When the container without the fins is approximated to a cylindrical cask with flat end plates dropped in side drop orientation, the container will absorb energy upon impact in three ways:

1. by deformation of end plates
2. by movement of lead
3. by deformation of cylindrical outer shell.

A relatively small amount of energy is absorbed in bending the steel shell at the point of impact and is, therefore, neglected in this analysis. Such a model is presented in Figure 2.10.9-F16.

Shappert (Ref. [8], page 59) has provided a method of estimating the amount of lead movement for such a cask. We shall apply formula as per Ref. [8], page 59, to estimate lead movement in the F-294 container. It should be noted that 75% of the energy absorption has been accounted for in section 4.1.4; consequently only the remaining 25% of the potential energy due to 30-ft height of the package is required to be considered. However, 25% factor shall be increased to, say, 36% of 30-ft drop height energy to provide a conservative estimate of the lead slump.

The formula is:

$$WH/t_sRL\sigma_s = [F_1(\theta)][R/t_s(\sigma_{pb}/\sigma_s) + 2(R/L)(t_e/t_s)] + F_2(\theta)$$

where

W = effective cask weight = 21,000 lb. - $W_{skid} = 21,000 - 980 = 20,020$ lb.

H = effective drop height = 36% of 30 feet = 129.6 in.

$F_1(\theta) = \theta - 1/2(\sin 2\theta)$

$F_2(\theta) = \sin\theta(2 - \cos\theta) - \theta$

R = the outer shell radius = 18 in.

t_s = the outer shell thickness = 0.5 in.

L = length of the shell = 50.25 - 6.0 = 44.25 in.

σ_s = the dynamic flow stress of ss304 shell, psi = 50,000 psi

σ_{pb} = the dynamic flow stress in lead = 5,000 psi

t_e = thickness of ss304 end plate = 0.5 in.

θ = the angle defined in Figure 2.7.1.2-ii)-F12, degrees.

Above formula is based on assumptions that the yield point stress of the ss304 end piece is the same as that of the ss304 shell and that the end pieces are of equal thickness. In order to use above formula, the angle θ and the cask geometry must be known. The angle θ may be determined from Figure 2.10.9-F17 (reproduced from Ref. [8], Shappert, page 61), which is based on above formula. The maximum displacement of shielding represented by the outer shell flattening, δ , may be calculated by $\delta = R(1 - \cos\theta)$

Calculate Non-dimensional Resistance Parameter #1.

$$\begin{aligned} & [R/t_s(\sigma_{pb}/\sigma_s) + 2(R/L)(t_e/t_s)] \\ & [18/0.5(5,000/50,000) + 2(18/44.25)(0.5/0.5)] \\ & [3.6 + 0.8135] \\ & [4.4135] \end{aligned}$$

Calculate Non-dimensional Energy Parameter #2.

$$\begin{aligned} & [WH/t_sRL\sigma_s] \\ & [20,020 \times 129.6 / (0.5 \times 18 \times 44.25 \times 50,000)] \\ & [0.1303] \end{aligned}$$

Use nomograph as per Figure 2.10.9-F17, with Parameter #1 = 4.4135 and parameter #2 = 0.1303. Connect the line between the two parameters and read the value of $\theta = 20^\circ$.

See Figure 2.10.9-F18.

$$\begin{aligned}\delta &= R(1 - \cos\theta) \\ \delta &= 18(1 - \cos(20^\circ)) \\ \delta &= 18(1 - 0.939) \\ \delta &= 1.086 \text{ in.}\end{aligned}$$

Now $\delta = t_s + \Delta_{\text{lead}}$

where

$$\begin{aligned}t_s &= \text{thickness of flattened ss304 shell} = 0.5 \\ \Delta_{\text{lead}} &= \text{amount of lead shielding displaced} \\ \Delta_{\text{lead}} &= \delta - t_s \\ &= 1.086 - 0.5 \\ &= 0.586 \text{ in.}\end{aligned}$$

To summarize, in the side drop orientation, it is estimated that the amount of lead shielding displaced in the F-294 container is 0.586 in., which represents approximately 1.5 half-value layers of lead shielding for cobalt-60.

4.1.8 Summary

- In side drop #1, the energy of 30-ft drop is absorbed as per Table 2.10.9-T5:
- Peak force and G-loads
1st stage: Peak force = 10.842×10^6 lb., G-load = 516 g's.
2nd stage: Peak force = 2.1×10^6 lb., G-load = 100 g's.
3rd stage: Peak force = 9.991×10^6 lb., G-load = 500 g's
- The estimated lead slump, based on the assumptions in section 4.1.5 is 0.6 in. which represent 1.5 half value layer for lead shielding of cobalt-60. This amount of lead shielding displacement is shown in Figure 2.10.9-F3 at horizontal centerline.
- The structural integrity of stainless steel shell is examined in section 4.3.

Table 2.10.9-T5
Energy Balance in Side Drop #1

Stage	Structural Element	Energy Absorbed x 10^6 in.-lb.	% of 30-Ft Drop Energy
1st	shipping skid	1.681	22.2%
2nd	crush shield fins	1.37	18.1%
2nd	container fins	0.63	8.3%
3rd	cylindrical fireshield	0.339	4.4%
3rd	container fins	1.63	21.5%
3rd	cask shell and lead	2.721	36.0%
Total		8.875	110.5%

4.2 SIDE DROP #2

In Side Drop #1, the entire 78-inch length of the shipping skid channel and the ends of two I-beams impact against the unyielding surface initially. Side Drop #2 (Figure 2.10.9-F9) is orthogonal to side drop #1. In Side Drop #2, the ends of the skid channels impact against the unyielding surface and the full length of one I-beam impacts at the same time. Therefore, the first stage of the drop is different for side drop #1 and side drop #2; but the 2nd stage and the 3rd stage of the drop are identical for both side drop #1 and side drop #2.

4.2.1 Mode of Impact

1st Stage

The sequence of events is as follows:

1. The ends of the four channel members impact first; the channels deform. The impact is transmitted to the cross I-beams, gussets, fixed skid, fixed skid gussets, bolts etc.
2. Due to high deceleration loads, the bolts will shear and the shipping skid will separate from the balance of the package.

2nd Stage

As per previous description, see section 4.1.4

3rd Stage

As per previous description, see section 4.1.5

Energy absorption, peak force, G-loads in the 1st stage shall be re-examined. For stages 2 and 3, previous data in sections 4.1.4 and 4.1.5 apply.

4.2.2 Energy absorption, G-loads for 1st stage

There are two (2) energy absorption structural elements that can be analyzed. These are:

1. Four gusset plates between two channels of the shipping skid.
2. I-beams.

4.2.2.1 Energy Absorption by Four Channel Members Overhang

This energy absorption is an approximation, as the effect of cross I-beams and gusset plates is difficult to account for. Each channel member is treated as a discrete fin - one web fin and two flange fins.

A Web Fin

See Figure 2.10.9-F19.

- Effective height, $h = 10$ in. (actual height = 17 in.)
- Thickness, $t = 0.43$ in.
- Loaded length, $b = 8$ in.
- material = ASTM A-36
- % of crush* = 22.5%
- loading angle = 0° (angle of inclination to the unyielding surface)

* This implies only bending (single hinge failure mode) of fin only.

$$\begin{aligned} M_P &= \sigma_Y bt^2 / 4 \\ &= 36,000 \times 8 \times (0.43)^2 / 4 \\ &= 13,310 \text{ in.-lb.} \end{aligned}$$

$$N = 9 \text{ (Figures 2.10.9-F6.1 and 2.10.9-F6.2 at 22.5\%, 10 in. fin height)}$$

$$\begin{aligned} EA_{\text{WEB FIN}} &= N \times M_P \\ &= 9 \times 13,310 \\ &= 120,000 \text{ in.-lb.} \end{aligned}$$

B Two Flange Fins

See Figure 2.10.9-F19.

- Effective height, $h = 10$ in. (actual height = 17 in.)
- Thickness, $t = 0.5$ in.
- Loaded length, $b = 3.5$ in.
- material = ASTM A-36
- % of crush* = 22.5%
- loading angle = 0° (angle of inclination to the unyielding surface)

* This implies only bending (single hinge failure mode) of fin only.

$$\begin{aligned} M_p &= \sigma_Y b t^2 / 4 \\ &= 36,000 \times 3.5 \times (0.5)^2 / 4 \\ &= 7,875 \text{ in.-lb.} \end{aligned}$$

$$\begin{aligned} N &= 9 \text{ (Figures 2.10.9-F6.1 and 2.10.9-F6.2) } 22.5\%, 10 \text{ in. height)} \\ EA_{\text{FLANGE FIN}} &= N \times M_p \\ &= 9 \times 7,875 \\ &= 70,875 \text{ in.-lb. per fin} \end{aligned}$$

As there are two flange fins per channel end,

$$EA_{\text{FLANGE}} = 2 \times 70,875 = 141,750 \text{ in.-lb.}$$

Therefore, per channel end, the energy absorption is

$$\begin{aligned} EA_{\text{CHANNEL}} &= EA_{\text{FLANGE}} + EA_{\text{WEB FIN}} \\ &= 141,750 + 120,000 \text{ in.-lb.} \\ &= 261,750 \text{ in.-lb. per channel end} \end{aligned}$$

As there are four channel ends impacting at the same time,

$$\begin{aligned} EA_{\text{CHANNEL ENDS}} &= \text{number of channel ends} \times EA_{\text{CHANNEL}} \\ &= 4 \times 261,750 \\ &= 1.047 \times 10^6 \text{ in.-lb.} \end{aligned}$$

$$\begin{aligned} EA_T &= \Sigma EA_{\text{CHANNEL ENDS}} \\ &= (1.047) \times 10^6 \end{aligned}$$

The ratio $EA_T/E_0 = 1.047 \times 10^6 / 7.56 \times 10^6 = 13.8\%$

It is estimated that 13.8% of the initial potential energy of F-294 package subjected to 30-ft free drop test, is absorbed in the 1st stage.

4.2.2.2 Energy Absorption by one I-beam

This energy absorption is an approximation. Each flange of the I-beam member is treated as a discrete fin - 2 flange fins

A Two Flange Fins

See Figure 2.10.9-F19

- Effective height, $h = 4$ in.
- Thickness, $t = 0.375$ in.
- Loaded length, $b = 63$ in.
- material = ASTM A-36
- % of crush* = 22.5%
- loading angle = 0° (angle of inclination to the unyielding surface)

* This implies only bending (single hinge failure mode) of fin only.

$$\begin{aligned}
 M_p &= \sigma_y b t^2 / 4 \\
 &= 36,000 \times 63 \times (0.375)^2 / 4 \\
 &= 79,734 \text{ in.-lb.} \\
 N &= 9 \text{ (Figures 2.10.9-F6.1 and 6.2 22.5\%, 10 in. height)} \\
 EA_{\text{FLANGE FIN}} &= N \times M_p \\
 &= 9 \times 79,734 \\
 &= 717,609 \text{ in.-lb. per flange per I-beam}
 \end{aligned}$$

As there are two flange fins per I-beam,

$$EA_{\text{FLANGE}} = 2 \times 717,609 = 1.435 \times 10^6 \text{ in.-lb.}$$

Therefore per I-beam end, the energy absorption is

$$\begin{aligned}
 EA_{\text{I-BEAM}} &= EA_{\text{FLANGE}} \\
 &= 1.435 \times 10^6 \text{ in.-lb.}
 \end{aligned}$$

4.2.3 Energy Absorbed by Two Structural Elements: 1st Stage

The total energy absorbed by four channel ends and one I-beam is

$$\begin{aligned}
 EA_{\text{T,1st stage}} &= \Sigma EA_{\text{CHANNEL ENDS}} + EA_{\text{I-BEAM}} \\
 &= (1.047 + 1.435) \times 10^6 \text{ in.-lb.} \\
 &= 2.482 \times 10^6 \text{ in.-lb.}
 \end{aligned}$$

Ratio of 1st stage energy Absorbed/Initial Potential Energy

$$\begin{aligned}
 EA_{\text{T,1st stage}}/E_0 &= 2.482 \times 10^6 / 7.56 \times 10^6 \\
 &= 32.8\%
 \end{aligned}$$

It is estimated that 32.8% of the initial potential energy of F-294 package subjected to 30-ft free drop is absorbed in the first stage of the drop. In the 2nd and 3rd stage, the energy absorbed has been computed as per sections 4.1.2 to 4.1.5

4.2.4 Summary of Energy Absorbed in Side Drop #2

In the side drop #2, the energy of 30-ft drop is absorbed as per Table 2.10.9-T6.

Table 2.10.9-T6
Energy Balance in Side Drop #2

Stage	Structural Element	Energy Absorbed x 10 ⁶ in.-lb.	% of 30-Ft Drop Energy
1st	Shipping skid	2.488	32.8%
2nd	Crush shield fins	1.37	18.1%
2nd	Container fins	0.63	8.3%
3rd	Cylindrical fireshield	0.339	4.4%
3rd	container fins	1.63	21.5%
3rd	cask shell and lead	2.721	36.0%
Total		8.875	121.1%

4.2.5 Peak Force and G-loads

4.2.5.1 Channel Ends

$$[\text{Height of fin/thickness of fin}] = 10/0.5 = 20$$

From Figure 2.10.9-F7.1, Unit Peak force, $P_1 = 12,000$ lb. per in of loaded length per fin

$$\begin{aligned} \text{Loaded length per channel end} &= 2 \times \text{flange length} + \text{web} \\ &= 2 \times 3.5 + 8 \\ &= 15 \text{ in.} \end{aligned}$$

$$\text{Number of channel ends} = 4$$

$$\text{Total loaded length} = 4 \times 15 = 60 \text{ in.}$$

Peak force, $FP_1 = \text{unit peak force} \times \text{loaded length} \times \text{no. of fins}$

$$\begin{aligned} &= 12,000 \times 60 \\ FP_1 &= 720,000 \text{ lb.} \end{aligned}$$

4.2.5.2 I-beam

$$[\text{Height of fin/thickness of fin}] = 4/0.375 = 10.7$$

From Fig 2.10.9-F7.1, Unit Peak force, $P_2 = 60,000$ lb. per in. of loaded length per fin.

The container weight is acting over 44 in. length. The bottom shipping skid length is 78 in. It is assumed the loaded length of the I-beam is average i.e., $(48 + 78/2 = 63$ in. approximately.

$$\text{Number of flanges on one I-beam} = 2$$

$$\begin{aligned} \text{Peak force } FP_2 &= \text{unit peak force} \times \text{loaded length} \times \text{no. of fins} \\ &= 60,000 \times 63 \times 2 \\ &= 7.56 \times 10^6 \text{ lb.} \end{aligned}$$

4.2.5.4 Total Peak Force, ΣFP and G-loads in First Stage

The cumulative peak force ΣFP is:

$$\begin{aligned} \Sigma FP &= FP_1 + FP_2 \\ &= (0.72 + 7.56) \times 10^6 \\ &= 8.28 \times 10^6 \text{ lb.} \end{aligned}$$

Therefore the G-load, based on 1st Stage drop is

$$\begin{aligned} \text{G-load}_{\text{stage 1}} &= \Sigma FP_{\text{stage 1}} / W_{F-294} \\ &= 8.28 \times 10^6 \text{ lb.} / 21,000 \text{ lb.} \\ &= 394 \text{ g's.} \end{aligned}$$

Therefore the shipping skid is subject to: 394 g's in the first stage of side drop #2.

Peak force and G-loads

$$\begin{aligned} \text{1st stage: Peak force} &= 8.28 \times 10^6 \text{ lb., G-load} = 394 \text{ g's.} \\ \text{2nd stage: Peak force} &= 2.1 \times 10^6 \text{ lb., G-load} = 100 \text{ g's.} \\ \text{3rd stage: Peak force} &= 9.991 \times 10^6 \text{ lb., G-load} = 500 \text{ g's} \end{aligned}$$

4.3 IMPLICATIONS OF PEAK FORCE AND G-LOAD ON THE INTEGRITY OF CONTAINER AND INTERNALS

4.3.1 Integrity of SS304L Shell Around Lead Shielding

Let us assume that the pairs of fins, 5 and 6, 4 and 7, and 3 and 8 impact at the following times:

Fins #5 and #6 t millisecond

Fins #4 and #7 t + 0.1 milliseconds

Fins #3 and #8 t + 0.2 milliseconds

There are three major issues to consider in order to examine the dynamic fracture of the stainless steel shell under the cooling fin:

1. duration of impact
 2. critical impact velocity
 3. stress level
1. Duration of impact: see Figure 2.10.9-F20 extracted from Ref. [34]. Based on this data, it takes about 20 milliseconds loading period before the ss jacket is considered to be even yielded (plasticized). The duration of the impact of fins #5 and #6 before fins #4 and #7 and fins #3 and #8 come to impact is of the order of 0.1 millisecond.
 2. Critical impact velocity: fracture of the fin is not likely as the critical impact velocities are in the range of 200 ft/sec while the initial impact velocities are 44 ft/sec and less. See Figure 2.10.9-F21, the critical impact velocities for metals, material appended from Refs. [41] and [43].
 3. Stress level: Peak force on the cooling fins #5 and #6, based on Davis's data,

$$FP_{\text{FIN\#5\&6}} = 55,000 \times 32 \times 2$$

$$= 3.52 \times 10^6 \text{ lb.}$$

The average compressive stress on the shell due to peak force $FP_{\text{FIN\#5\&6}}$.

The effective shell area $A = 2 \times 32 \times 3.142 = 201 \text{ in}^2$.

The average compressive stress $\sigma_C = FP_{\text{FIN\#5\&6}}/A = 3,520,000/201 = 17,512 \text{ psi}$.

The static UTS of ss304L is 70,000 psi.

Therefore, the container stainless steel shell is not likely to fracture in the zone around the fin #5 and #6 and the shell. The safety factor = Static UTS/Applied Stress = $70,000/17,512 = 4$.

Overall, based on three arguments (duration of time of impact, velocity of impact, and the resulting compressive stress in the shell < static UTS), the fins or the ss shell will not *fracture*.

Figure 2.10.9-F9
F-294 - Side Drop #1

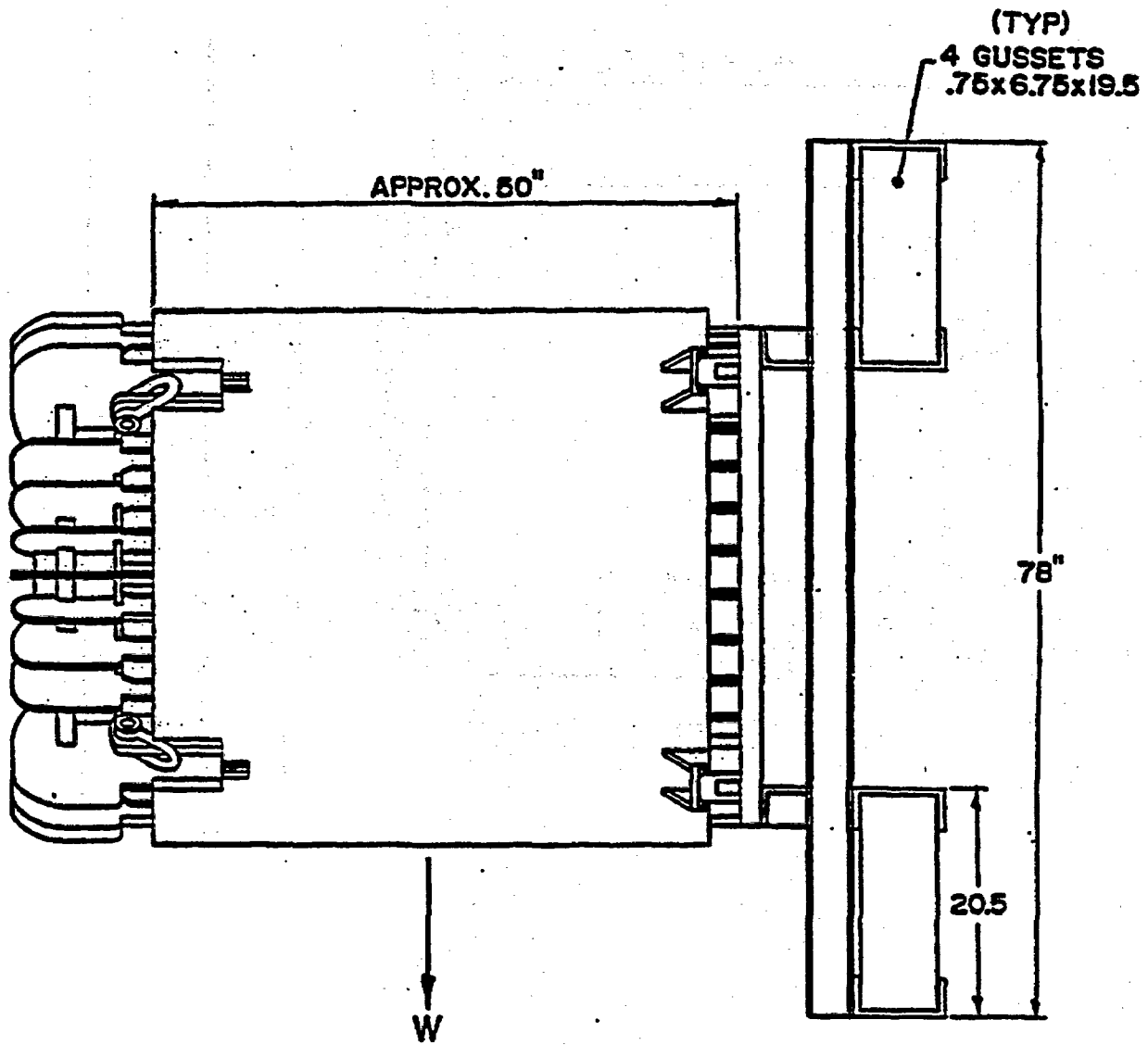


Figure 2.10.9-F10
F-294 - Side Drop #2

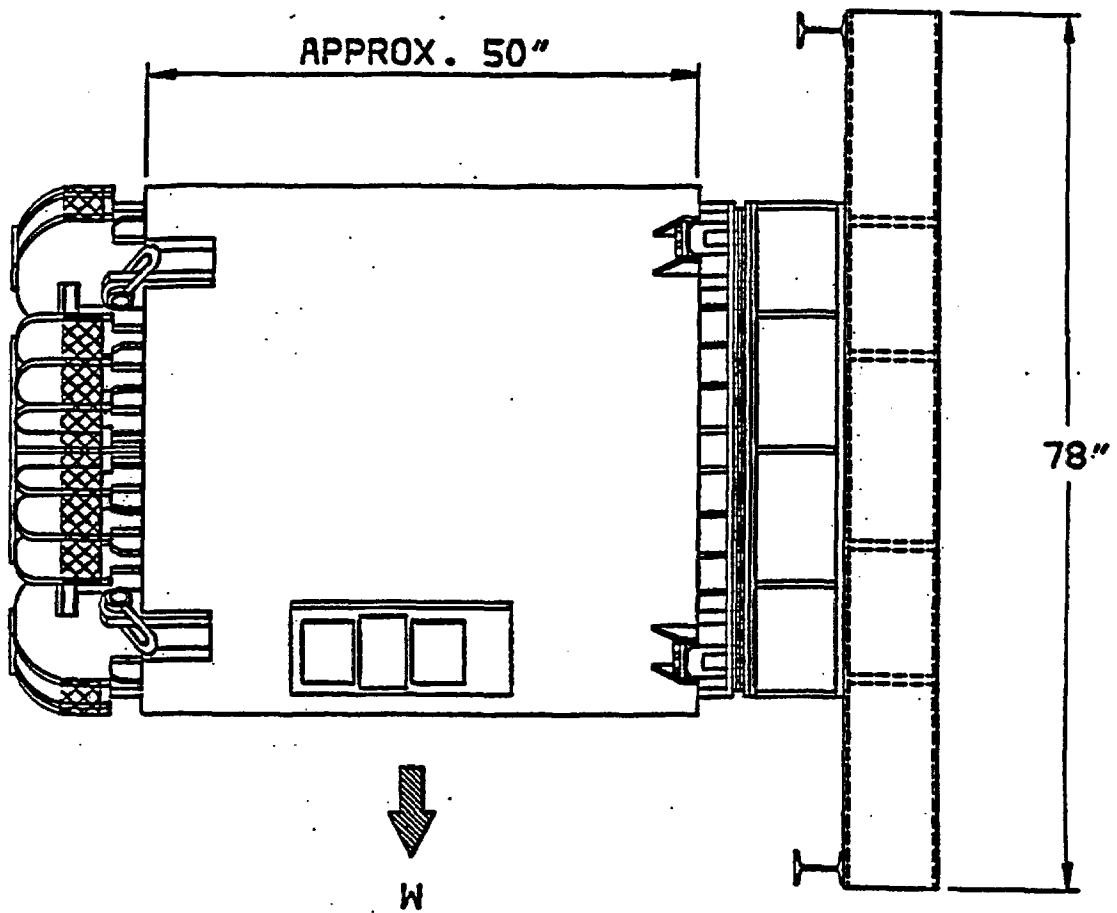


Figure 2.10.9-F11
Mode of Impact - Side Drop #1

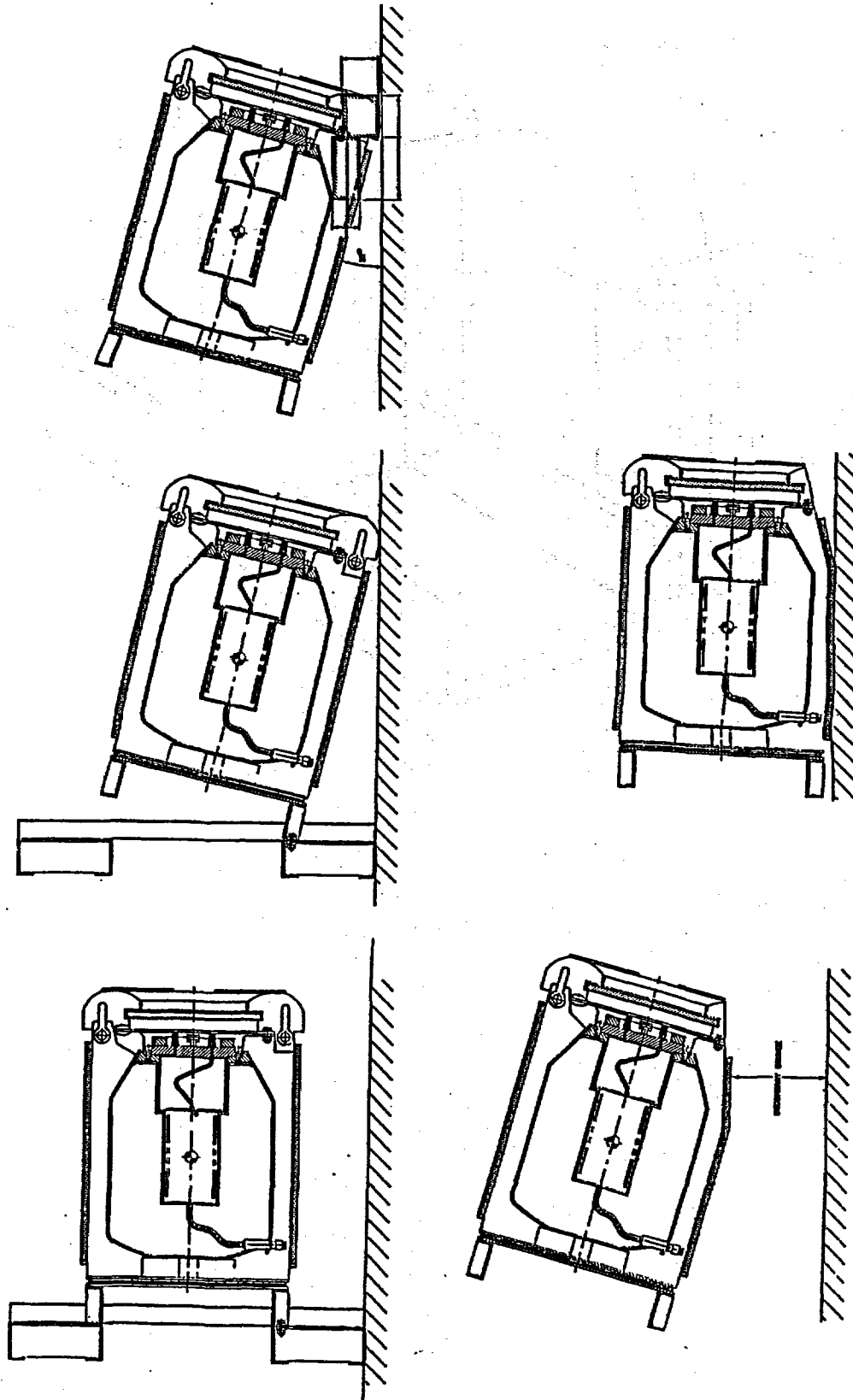


Figure 2.10.9-F12
Impact of Shipping Skid

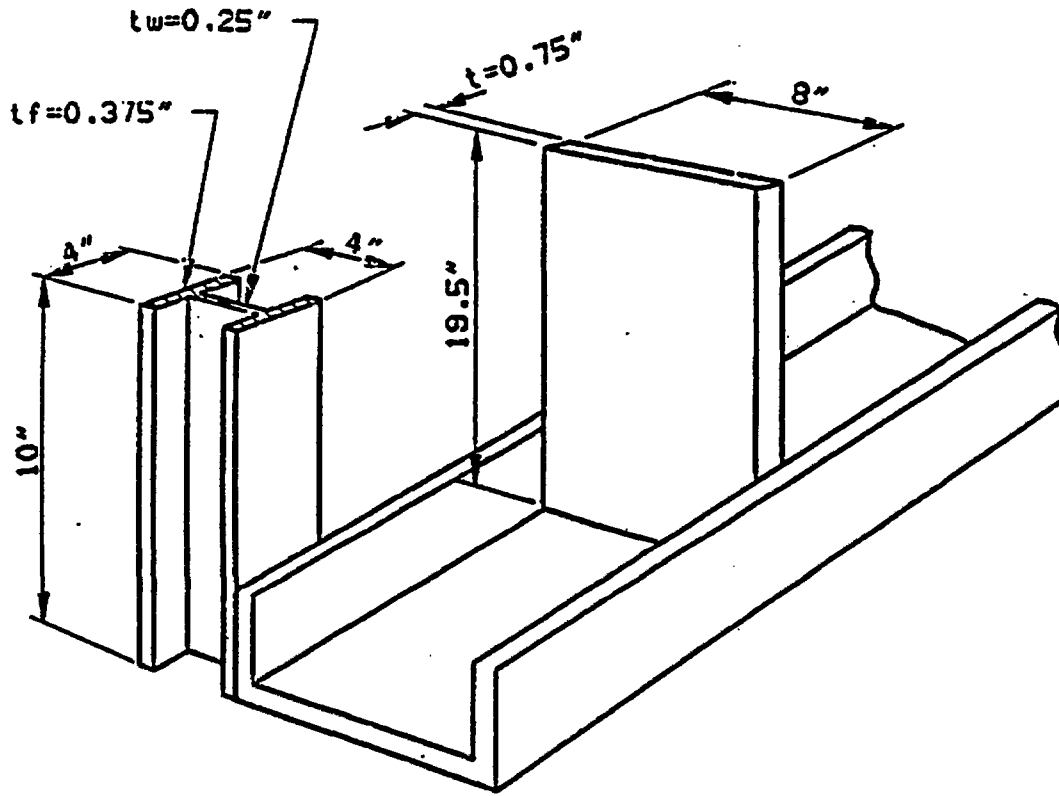


Figure 2.10.9-F13
Layout and Numbering of Fins - Side Drop #1: 2nd Stage

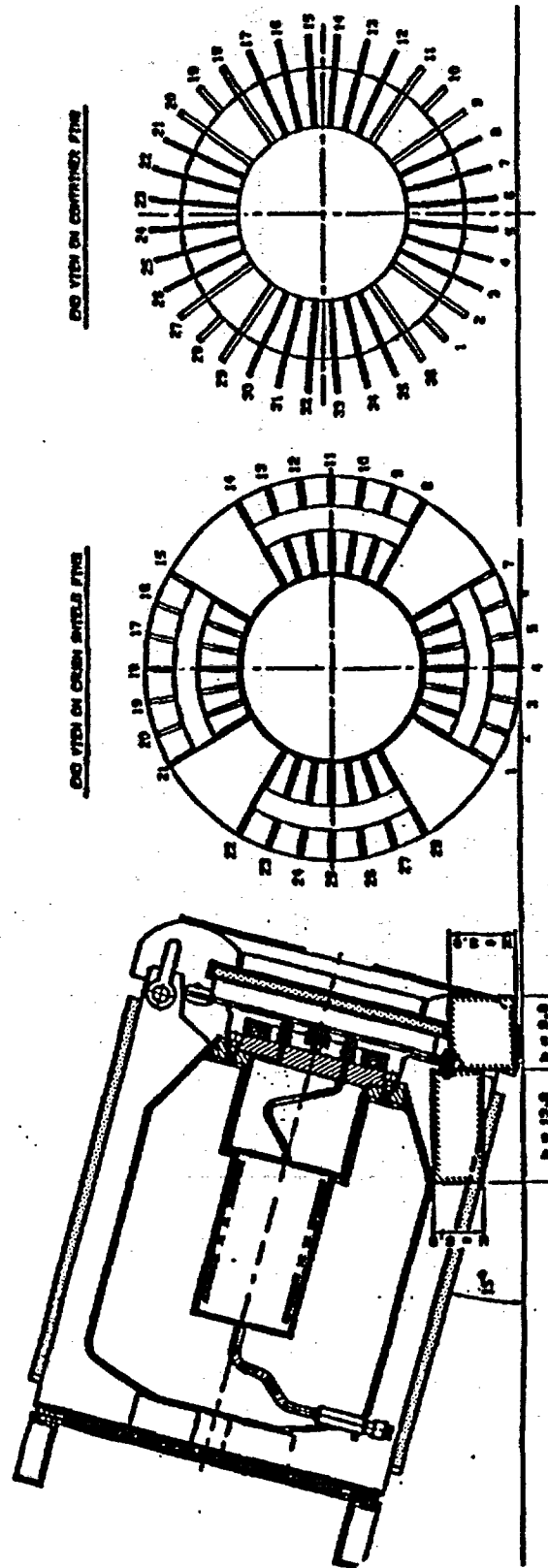


Figure 2.10.9-F14
Zone of Impact - Side Drop #1: 3rd Stage

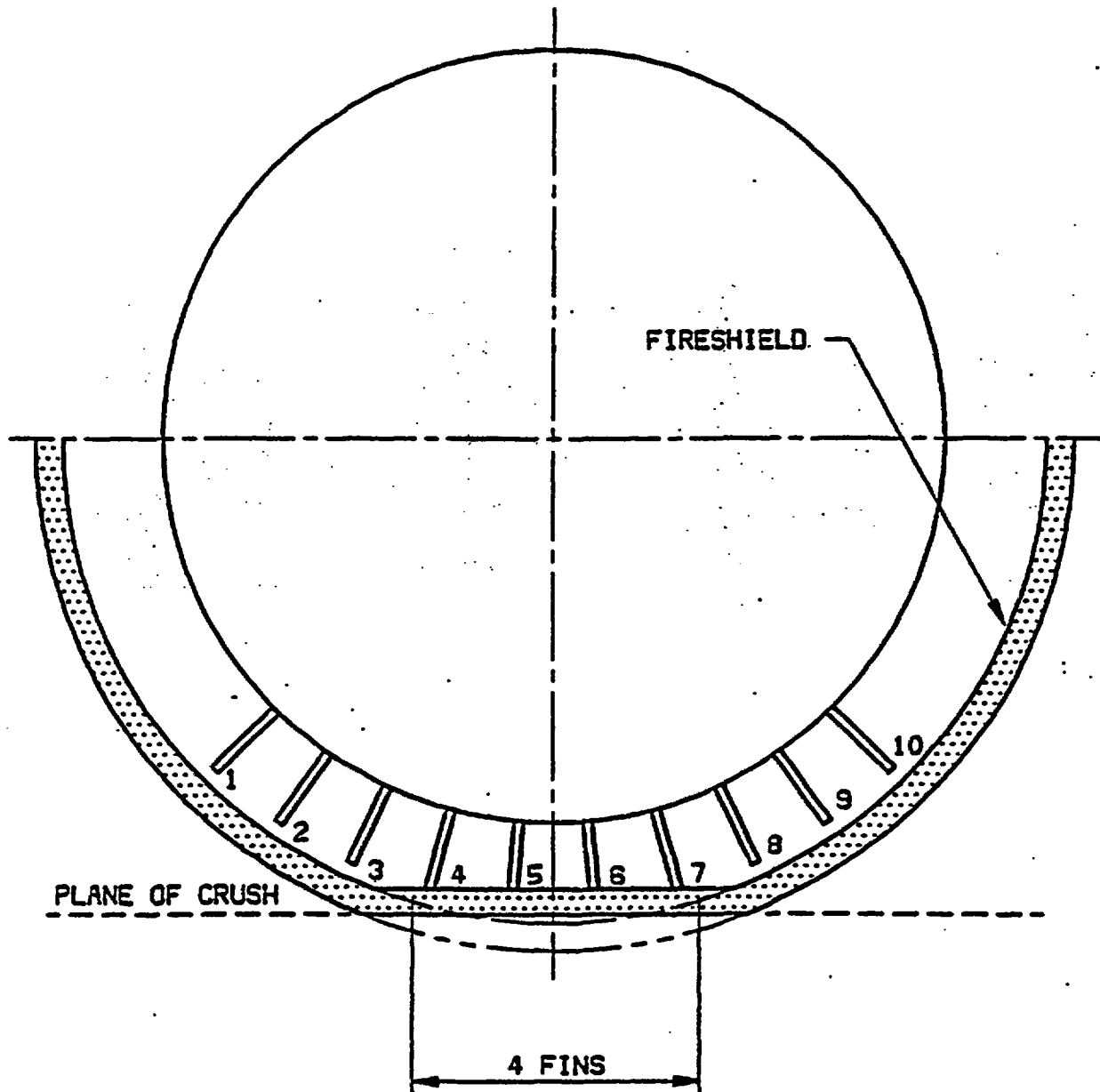


Figure 2.10.9-F15
Cylindrical Fireshield - Side Drop #1

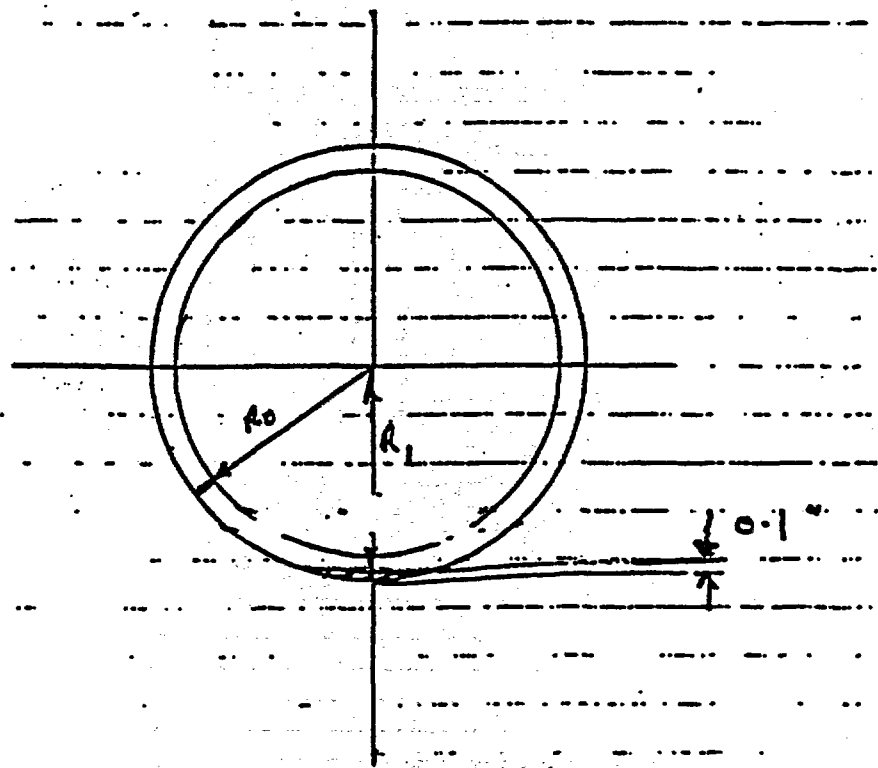


Figure 2.10.9-F16
Container Model for Estimating Lead Slump or Displacement in Side Drop

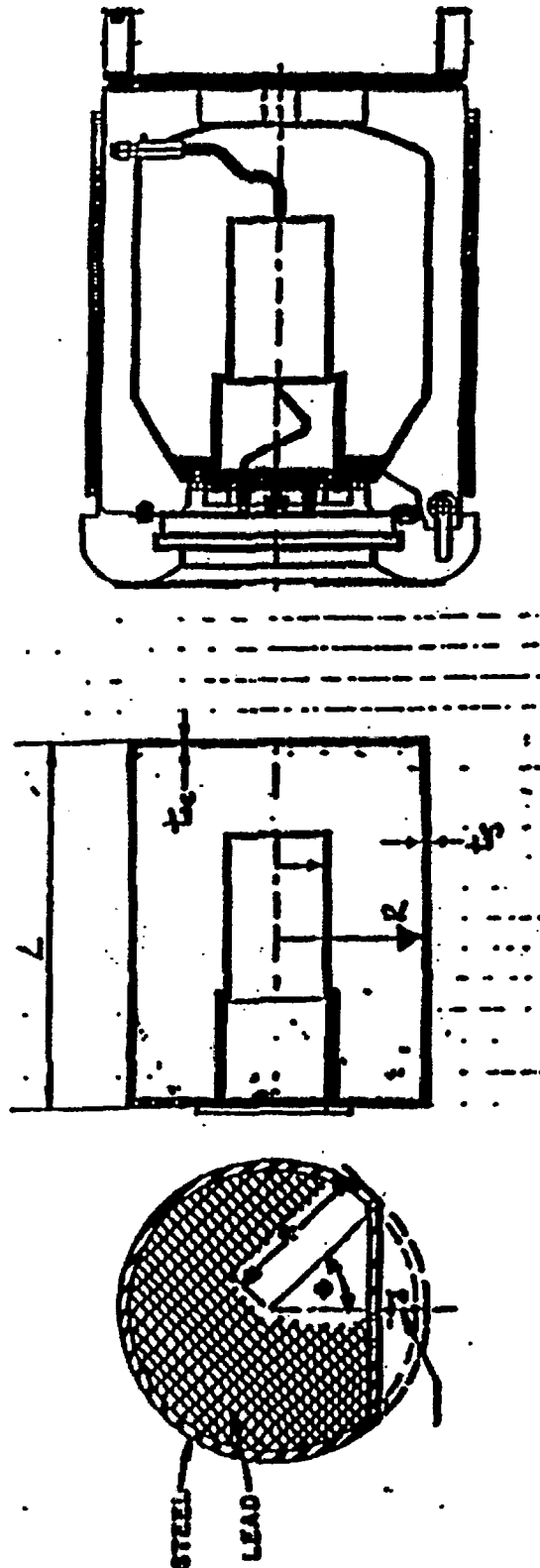


Figure 2.10.9-F17
Nomograph for Determining Half Angle of Flat Developed (θ) due to
Impact of a Cylindrical Cask with Axis Horizontal
 (from Ref. [8], p 61)

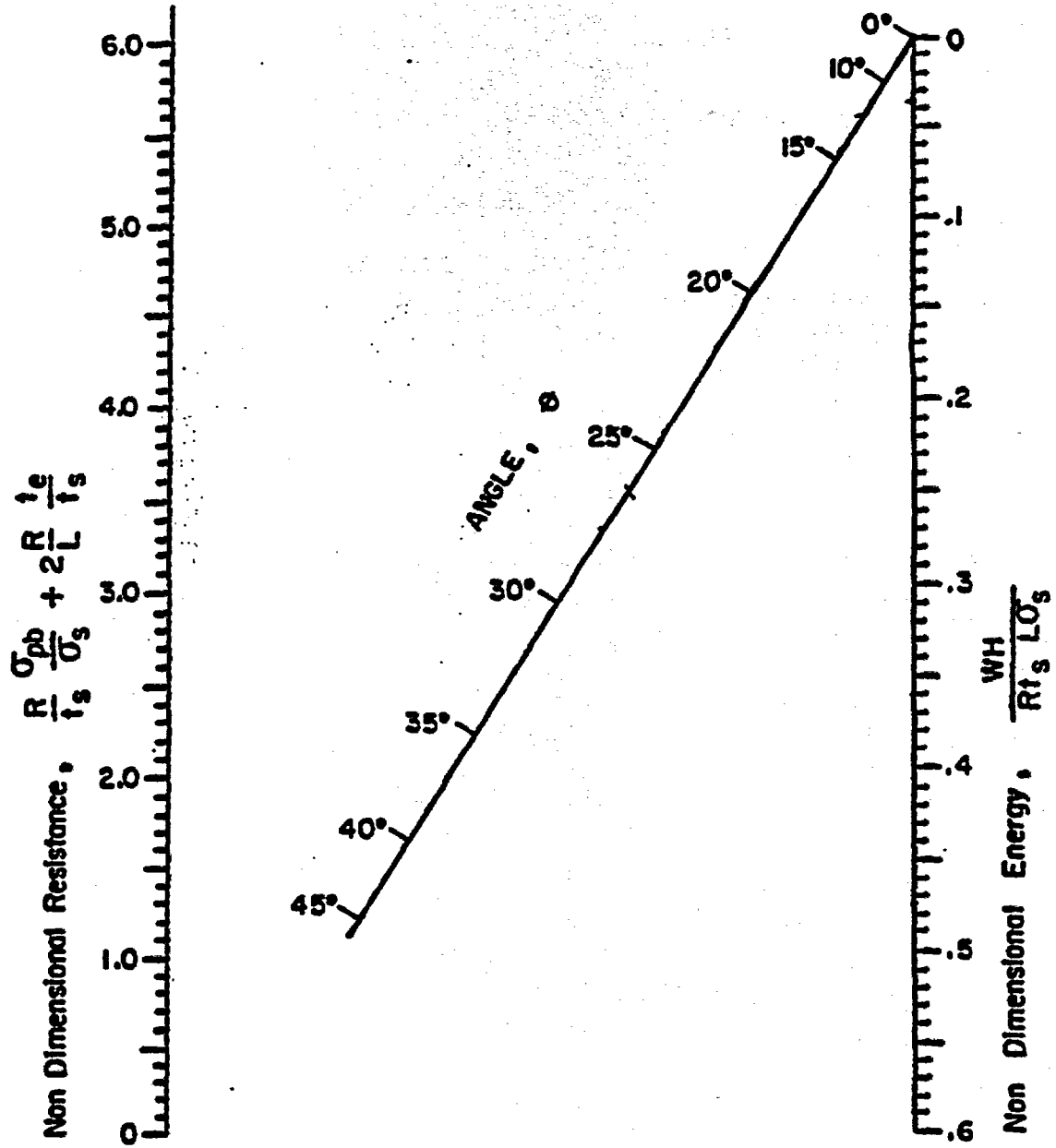


Figure 2.10.9-F18
End View of the Deformation in a Steel-encased Solid Lead Cylinder

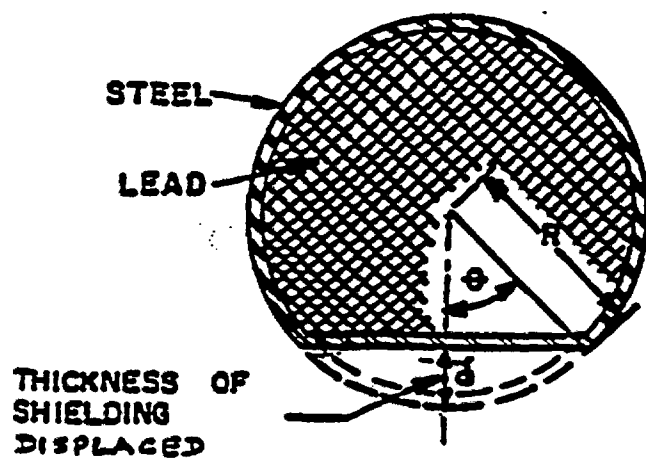


Figure 2.10.9-F19
Impact of Shipping Skid - Side Drop #2, 1st Stage

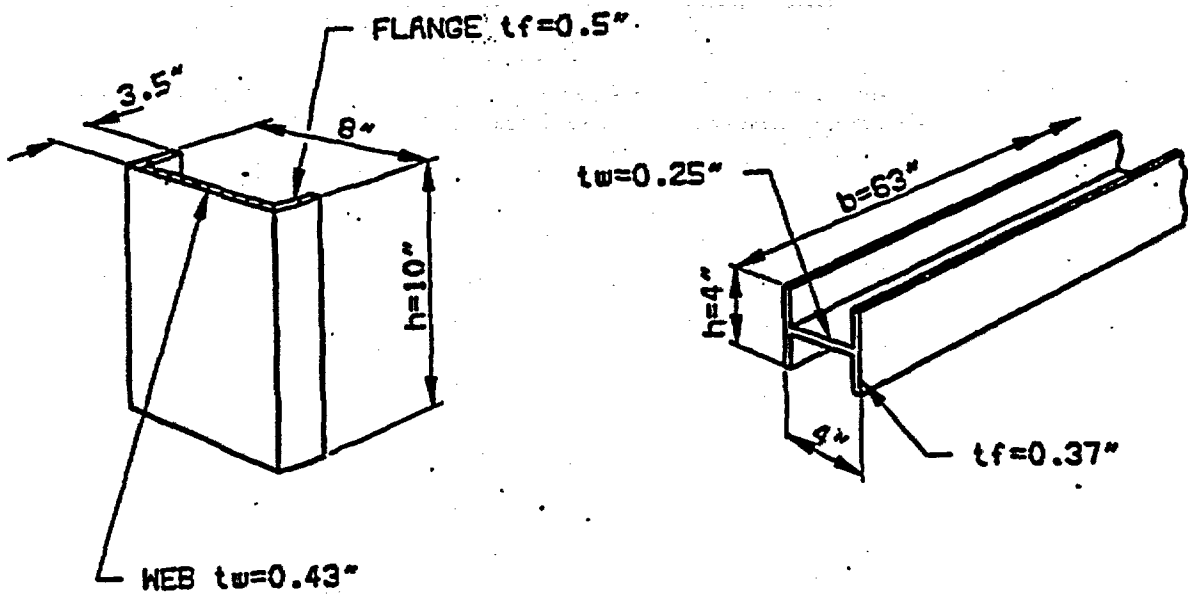
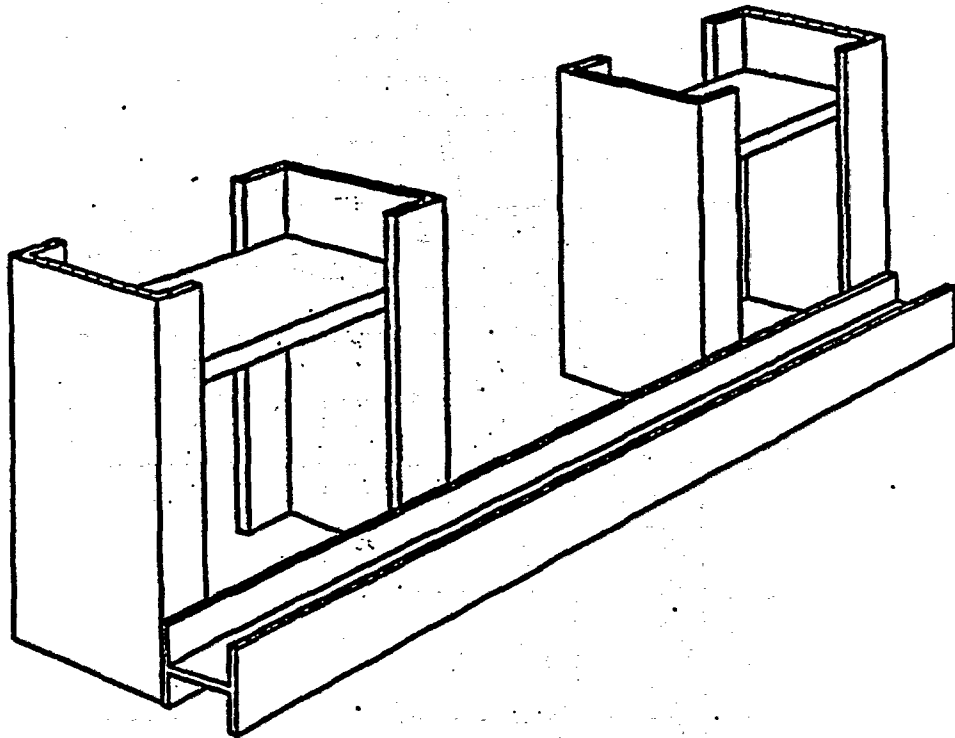


Figure 2.10.9-F20
Stress versus Strain for Three Rapid Load Tests on Type 302 Stainless Steel
 (Data appended from Ref. [34])

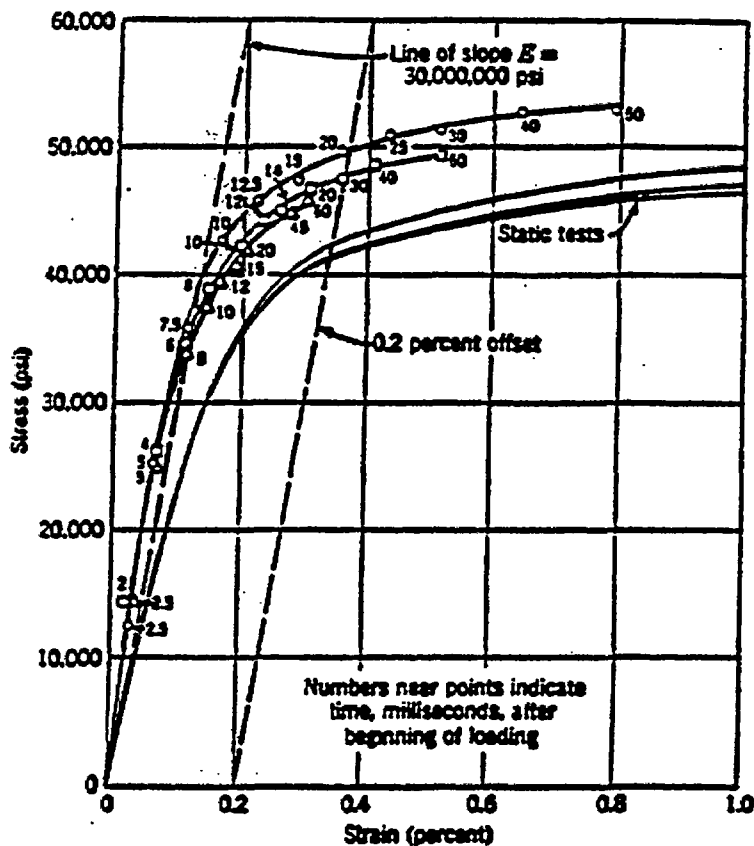


Fig. 10.9 Stress versus strain for three rapid load tests on type 302 stainless steel. [After Clark and Wood (19), courtesy of The American Society for Testing and Materials.]

Figure 2.10.9-F21
Critical Impact Velocities of Metals
(Data appended from Refs. [41] and [43])

PROPERTIES OF MATERIALS

17

$$v_1 = \int_0^{\epsilon_n} \sqrt{\frac{d\sigma}{d\epsilon}} d\epsilon \quad \text{Equation (2-4)}$$

When the strain reaches the value ϵ_n corresponding to the ultimate strength of the material, the slope of the engineering tensile stress-strain curve, $d\sigma/d\epsilon$, becomes zero. Theory, therefore, predicts that rupture will occur at the instant of impact at the impacted end of the bar when the impact velocity is

$$v_2 \geq v_c = \int_0^{\epsilon_n} \sqrt{\frac{d\sigma}{d\epsilon}} d\epsilon \quad \text{Equation (2-5)}$$

It has been experimentally found (2) that for $v_1 \geq v_c$ the bar ruptures near the impacted end and that the plastic strain propagated along the bar is very much less than for impact velocities slightly below the critical velocity. Thus, in a very long specimen, any impact velocity below the critical impact velocity may cause deformation but will not cause fracture at least until reflection at the far end has taken place. At velocities above the critical impact velocity, fracturing would be expected to occur in the neighborhood of the point of impact.

The critical impact velocities of several metals are listed in Table 2-1. Those critical impact velocities listed lie roughly

Table 2-1
Critical Impact Velocities of Several Metals
(After Clark and Wood Ref. 3)

Metal	Condition	Critical Impact Velocity (ft/sec)	
		Experimental	Theoretical ^a
Aluminum alloys			
23	Annealed	>200	178
25	1/2H		38
24S	Annealed	>200	174
26ST	As-received	>200	250
Magnesium alloys			
Dow F	As-received	>200	233
Dow J	As-received	>200	203
Copper	Annealed	>200	231
Copper	Cold-rolled	50	43
Cast iron	Annealed	100	•
Steels			
SAE 1022	Annealed	180	•
SAE 1022	Cold-rolled	100	95
SAE 1095	Normalized	>200	233
SAE 1095	Annealed (HT)	180	231
Stainless 302	As-received	>200	450

• Existence of yield point prevents computation of critical velocity.
^a Computed from static engineering stress-strain curve.

5. TOP CORNER DROP

5.1 MODE OF IMPACT

See Figure 2.10.9-F22

During a top corner drop test, the following impact scenario is depicted:

1st Stage 1st phase:

The top crush shield impacts the unyielding surface. The crush shield is normally restrained by the top container fins. The impact forces are therefore transmitted through the crush shield fins into the container top fins. The crush shield fins will crush until they have absorbed as much energy as they are capable of before "bottoming".

2nd phase:

Next, the container top fins (3/8 in., 0.5 in. thick) will crush until they have absorbed as much energy as they are capable of before "bottoming". The container lift lug fin (1.25 in. thick) will crush until "bottomed out" (i.e., 30% crush or less).

3rd phase:

Next, the top sector of the cylindrical fireshield will impact.

4th phase:

Next, the top corner of the cask will impact and start absorbing impact energy.

2nd Stage

The container will bounce; the height depends upon the elastic energy stored in the 1st stage.

3rd Stage

The container will be subjected to rotation and drop again (secondary drop) and come to rest on its side.

5.2 ENERGY ABSORPTION, G-LOADS FOR 1ST STAGE

There are energy absorption structural elements that can be analyzed. These are

1. crush shield fins
2. container fins
3. cylindrical fireshield top sector
4. cask top corner.

The energy absorbed by 1., 2., and 4. shall be presented here.

5.2.1 Energy Absorbed by the Fins of the Crush Shield

Refer to Figure 2.10.9-F23 for layout and numbering of crush shield fins.

How many fins are in the zone of impact? See Figure 2.10.9-F23. It is estimated from the graphical data, that 10 fins (0.5 in. thick) come into play. Refer to Figure 2.10.9-F25 for representative fin parameters.

What is the loading angle for each fin?

$$\theta = \beta \times \cos \alpha$$

where

θ = fin loading angle (°)

β = angle between fin 1 and fin n

α = angle between impact pad and the longitudinal axis of the package = 57°

Table 2.10.9-T7 lists the appropriate θ , loading angles for all the fins of the crush shield, as calculated in the following example; e.g.,

For Fins #1 and #28 (i.e., 0.5 in. thick fin)

$$\begin{aligned}\theta &= \beta \times \cos \alpha \\ \theta &= 15 \times \cos 57^\circ \\ \theta &= 8.2^\circ\end{aligned}$$

For Fins #2 and #27 (i.e., 0.5 in. thick fin)

$$\begin{aligned}\theta &= \beta \times \cos \alpha \\ \theta &= 25 \times \cos 57^\circ \\ \theta &= 13.6^\circ\end{aligned}$$

For Fins #3 and #26 (i.e., 0.5 in. thick fin)

$$\begin{aligned}\theta &= \beta \times \cos \alpha \\ \theta &= 35 \times \cos 57^\circ \\ \theta &= 19^\circ\end{aligned}$$

For Fins #4 and #25 (i.e., 0.5 in. thick fin)

$$\begin{aligned}\theta &= \beta \times \cos \alpha \\ \theta &= 45 \times \cos 57^\circ \\ \theta &= 24.5^\circ\end{aligned}$$

For Fins #5 and #24 (i.e., 0.5 in. thick fin)

$$\begin{aligned}\theta &= \beta \times \cos \alpha \\ \theta &= 55 \times \cos 57^\circ \\ \theta &= 30^\circ\end{aligned}$$

Table 2.10.9-T7
Fin Data for the Crush Shield Fins in Top Corner Drop Orientation

Type of Fins	Designated Fin #	No. of Fins	Loading Angle, q	Parameter N	Fin Factor, N/N_0
0.5 in.	1, 28	2	8.2°	18	18/20 = 0.9
0.5 in.	2, 27	2	13.6°	14	14/20 = 0.7
0.5 in.	3, 26	2	19.0°	4.5	4.5/20 = 0.225
0.5 in.	4, 25	2	24.5°	3.5	3.5/20 = 0.175
0.5 in.	5, 24	2	30.0°	3.0	3/20 = 0.15

- i) Fins #1 and #28
- Effective height, $h = 6$ in.
 - Thickness, $t = 0.5$ in.
 - Loaded length, $b = 11$ in.
 - material = ASTM A-36
 - % of crush = 45%
 - loading angle = 8.2° (angle of inclination to the unyielding surface)

Therefore, at crush of 45%, for fin height of 5 in., fin inclination angle of 8.2°, from Figure 2.10.9-F6.2, the parameter [absorbed energy/plastic moment], $N = 18$.

Note: for 0° fin loading angle, at 45% crush, 5 in. fin, from Figure 2.10.9-F6.1, the parameter [absorbed energy/plastic moment], $N_0 = 20$.

$$\begin{aligned} EA_{\text{FINS \#1,\#28}} &= 2 \times N \times \sigma_Y \times b \times t^2 / 4 \\ &= 2 \times 18 \times 46,000 \times 11 \times (0.5)^2 / 4 \\ &= 2 \times 0.569 \times 10^6 \\ &= 1.138 \times 10^6 \text{ in.-lb.} \end{aligned}$$

ii) Fins #2 and #27

- Effective height, $h = 6$ in.
- Thickness, $t = 0.5$ in.
- Loaded length, $b = 11$ in.
- material = ASTM A-36
- % of crush = 45%
- loading angle = 13.6° (angle of inclination to the unyielding surface)

Therefore, at crush of 45%, for fin height of 6 in., fin inclination angle of 13.6°, from Figures 2.10.9-F6.2 and 2.10.9-F6.3, the parameter [absorbed energy/plastic moment], $N = 14.0$

$$\begin{aligned} EA_{\text{FINS \#2,\#27}} &= 2 \times 14. \times \sigma_Y \times b \times t^2 / 4 \\ &= 2 \times 14. \times 46,000 \times 11 \times (0.5)^2 / 4 \\ &= 2 \times 0.443 \times 10^6 \\ &= 0.886 \times 10^6 \text{ in.-lb.} \end{aligned}$$

iii) Fins #3 and #26

- Effective height, $h = 6$ in.
- Thickness, $t = 0.5$ in.
- Loaded length, $b = 11$ in.
- material = ASTM A-36
- % of crush = 45%
- loading angle = 19° (angle of inclination to the unyielding surface)

Therefore, at crush of 45%, for fin height of 6 in., fin inclination angle of 19°, from Figure 2.10.9-F6.3, the parameter [absorbed energy/plastic moment], $N = 4.5$

$$\begin{aligned} EA_{\text{FINS \#3,\#26}} &= 2 \times N \times \sigma_Y \times b \times t^2 / 4 \\ &= 2 \times 4.5 \times 46,000 \times 11 \times (0.5)^2 / 4 \\ &= 2 \times 0.142 \times 10^6 \\ &= 0.284 \times 10^6 \text{ in.-lb.} \end{aligned}$$

iv) Fins #4 and #25

- Effective height, $h = 6$ in.
- Thickness, $t = 0.5$ in.
- Loaded length, $b = 11$ in.
- material = ASTM A-36
- % of crush = 45%
- loading angle = 24.5° (angle of inclination to the unyielding surface)

Therefore, at crush of 45%, for fin height of 6 in., fin inclination angle of 24.5°, from Figures 2.10.9-F6.3 and 2.10.9-F6.4, the parameter [absorbed energy/plastic moment], $N = 3.5$

$$\begin{aligned} EA_{\text{FINS \#4,\#25}} &= 2 \times N \times \sigma_Y \times b \times t^2 / 4 \\ &= 2 \times 3.5 \times 46,000 \times 11 \times (0.5)^2 / 4 \\ &= 2 \times 0.110 \times 10^6 \\ &= 0.220 \times 10^6 \text{ in.-lb.} \end{aligned}$$

v) Fins #5 and #24

- Effective height, $h = 6$ in.
- Thickness, $t = 0.5$ in.
- Loaded length, $b = 11$ in.
- material = ASTM A-36
- % of crush = 45%
- loading angle = 30° (angle of inclination to the unyielding surface)

Therefore, at crush of 45%, for fin height of 6 in., fin inclination angle of 30°, from Figure 2.10.9-F6.4, the parameter [absorbed energy/plastic moment], $N = 3$.

$$\begin{aligned} EA_{\text{FINS \#5,\#24}} &= 2 \times N \times \sigma_Y \times b \times t^2 / 4 \\ &= 2 \times 3 \times 46,000 \times 11 \times (0.5)^2 / 4 \\ &= 2 \times 0.0948 \times 10^6 \\ &= 0.189 \times 10^6 \text{ in.-lb.} \end{aligned}$$

Therefore the sum of energy absorbed by all the fins is

$$\begin{aligned} EA_{\text{crush shield fins}} &= [EA_{\text{FINS \#1,\#28}} + EA_{\text{FINS \#2,\#27}} + EA_{\text{FINS \#3,\#26}} \\ &\quad + EA_{\text{FINS \#4,\#25}} + EA_{\text{FINS \#5,\#24}}] \\ &= [1.138 + 0.886 + 0.284 + 0.220 + 0.189] \times 10^6 \text{ in.-lb.} \\ &= 2.717 \times 10^6 \text{ in.-lb.} \end{aligned}$$

5.2.2 Energy Absorbed by Top Fins of the Container

Refer to Figure 2.10.9-F24 for layout and numbering of container fins.

There are three types of fins on the top of the container

- 1.25 in. thick
- 0.5 in. thick
- 0.375 in. thick

Refer to Figure 2.10.9-F25 for depiction of representative fin parameters etc.

How many fins are in the zone of impact? See Figure 2.10.9-F24. It is estimated from the graphical data, that only one lift lug fin (1.25 in. thick) and two fins (1/2 in. thick) and 10 fins (3/8 in. thick) come into play. Lift lug fin (1.25 in. thick) is designated fin #1; two 0.5 in. thick fins adjacent to the lift lug fin are designated fin #2 and fin #36.

What is the loading angle for each fin?

$$\theta = \beta \times \cos \alpha$$

where

θ = fin loading angle (°)

β = angle between fin 1 and fin n

α = angle between impact pad and the longitudinal axis of the package.

Table 2.10.9-T8 lists the appropriate θ , loading angles for all the fins of the container, as calculated in the following example;

For Fin #1 (i.e., 1.25 in. thick lift lug fin)

$$\theta = \beta \times \cos \alpha$$

$$\theta = 0 \times \cos 57^\circ$$

$$\theta = 0^\circ$$

For Fins #2 and #36 (i.e., 0.5 in. thick fin)

$$\theta = \beta \times \cos \alpha$$

$$\theta = 10 \times \cos 57^\circ$$

$$\theta = 5.4^\circ$$

For Fins #3 and #35 (i.e., 0.375 in. thick fin)

$$\theta = \beta \times \cos \alpha$$

$$\theta = 20 \times \cos 57^\circ$$

$$\theta = 10.9^\circ$$

For Fins #4 and #34 (i.e., 0.375 in. thick fin)

$$\theta = \beta \times \cos \alpha$$

$$\theta = 30 \times \cos 57^\circ$$

$$\theta = 16.4^\circ$$

For Fins #5 and #33 (i.e., 0.375 in. thick fin)

$$\theta = \beta \times \cos \alpha$$

$$\theta = 40 \times \cos 57^\circ$$

$$\theta = 21.7^\circ$$

and so on.

Table 2.10.9-T8
Container Fin Data for Top Corner Drop Orientation

Type of Fins	Designated # Fin Number	No. of Fins	Loading Angle, θ	Parameter N
1.25 in. Lift Lug fin	1	1	0°	16.
0.5 in. fin	2, 36	2	5°	19.5
0.375 in. fin	3, 35	2	10.9°	18.0
0.375 in. fin	4, 34	2	16.4°	10.0
0.375 in. fin	5, 33	2	21.7°	4.0
0.375 in. fin	6, 32	2	27.2°	3.25
0.375 in. fin	7, 31	2	32.7°	3.

i) 1.25 in. thick fin parameters

- Effective original height, $h = 4$ in.
- Thickness, $t = 1.25$ in.
- Loaded length, $b = 5$ in.
- material = ss304L
- % of crush* = 30%
- loading angle = 0° (angle of inclination to the unyielding surface)

Therefore, at crush of 30%, for fin height of 4 in., from Figure 2.10.9-F6.1, the parameter [absorbed energy/plastic moment], $N = 16$

$$\begin{aligned} EA_{FIN\#1} &= N \times M_P \\ &= N \times [\sigma_Y \times b \times t^2 / 4] \\ &= 16 \times [25,000 \times 5 \times (1.25)^2 / 4] \\ &= 0.781 \times 10^6 \text{ in.-lb.} \end{aligned}$$

ii) Fins #2 and #36

- Effective height, $h = 5$ in.
- Thickness, $t = 0.5$ in.
- Loaded length, $b = 10$ in.
- material = ss304L
- % of crush = 45%
- loading angle = 5.4° (angle of inclination to the unyielding surface)

Therefore, at crush of 45%, for fin height of 5 in., fin inclination angle of 5.4° rounded up to 10° , from Figure 2.10.9-F6.2, the parameter [absorbed energy/plastic moment], $N = 19.5$

$$\begin{aligned} EA_{FINS\#2,\#36} &= 2 \times N \times \sigma_Y \times b \times t^2 / 4 \\ &= 2 \times 19.5 \times 25,000 \times 10 \times (0.5)^2 / 4 \\ &= 2 \times 0.304 \times 10^6 \\ &= 0.608 \times 10^6 \text{ in.-lb.} \end{aligned}$$

iii) Fins #3 and #35

- Effective height, $h = 5$ in.
- Thickness, $t = 0.375$ in.
- Loaded length, $b = 10$ in.
- material = ss304L
- % of crush = 45%
- loading angle = 10.9° (angle of inclination to the unyielding surface)

Therefore, at crush of 45%, for fin height of 5 in., fin inclination angle of 10.9° rounded down to 10° , from Figure 2.10.9-F6.2, the parameter [absorbed energy/plastic moment], $N = 18$.

$$\begin{aligned} EA_{FINS\#3,\#35} &= 2 \times N \times \sigma_Y \times b \times t^2 / 4 \\ &= 2 \times 18 \times 25,000 \times 10 \times (0.375)^2 / 4 \\ &= 2 \times 0.158 \times 10^6 \\ &= 0.316 \times 10^6 \text{ in.-lb.} \end{aligned}$$

iv) Fins #4 and #34

- Effective height, $h = 5$ in.
- Thickness, $t = 0.375$ in.
- Loaded length, $b = 10$ in.
- material = ss304L
- % of crush = 45%
- loading angle = 16.4° (angle of inclination to the unyielding surface)

Therefore, at crush of 45%, for fin height of 5 in., fin inclination angle of 16.4° , from Figures 2.10.9-F6.2 and 2.10.9-F6.3, the parameter [absorbed energy/plastic moment], $N = 10$.

$$\begin{aligned} EA_{\text{FINS \#4,\#34}} &= 2 \times N \times \sigma_Y \times b \times t^2 / 4 \\ &= 2 \times 10 \times 25,000 \times 10 \times (0.375)^2 / 4 \\ &= 2 \times 0.088 \times 10^6 \\ &= 0.176 \times 10^6 \text{ in.-lb.} \end{aligned}$$

v) Fins #5 and #33

- Effective height, $h = 5$ in.
- Thickness, $t = 0.375$ in.
- Loaded length, $b = 10$ in.
- material = ss304L
- % of crush = 45%
- loading angle = 21.7° (angle of inclination to the unyielding surface)

Therefore, at crush of 45%, for fin height of 5 in., fin inclination angle of 21.7° , from Figures 2.10.9-F6.3 and 2.10.9-F6.4, the parameter [absorbed energy/plastic moment], $N = 4$.

$$\begin{aligned} EA_{\text{FINS \#5,\#33}} &= 2 \times N \times \sigma_Y \times b \times t^2 / 4 \\ &= 2 \times 4 \times 25,000 \times 10 \times (0.375)^2 / 4 \\ &= 2 \times 0.0351 \times 10^6 \\ &= 0.0703 \times 10^6 \text{ in.-lb.} \end{aligned}$$

vi) Fins #6 and #32

- Effective height, $h = 5$ in.
- Thickness, $t = 0.375$ in.
- Loaded length, $b = 10$ in.
- material = ss304L
- % of crush = 45%
- loading angle = 27.2° (angle of inclination to the unyielding surface)

Therefore, at crush of 45%, for fin height of 5 in., fin inclination angle of 27.2° rounded up to 30° , from Figure 2.10.9-F6.4, the parameter [absorbed energy/plastic moment], $N = 3.25$

$$\begin{aligned} EA_{\text{FINS \#6,\#32}} &= 2 \times N \times \sigma_Y \times b \times t^2 / 4 \\ &= 2 \times 3.25 \times 25,000 \times 10 \times (0.375)^2 / 4 \\ &= 2 \times 0.028 \times 10^6 \\ &= 0.056 \times 10^6 \text{ in.-lb.} \end{aligned}$$

vii) Fins #7 and #31

- Effective height, $h = 5$ in.
- Thickness, $t = 0.375$ in.
- Loaded length, $b = 10$ in.
- material = ss304L
- % of crush = 45%
- loading angle = 32.7° (angle of inclination to the unyielding surface)

Therefore, at crush of 45%, for fin height of 5 in., fin inclination angle of 32.7° rounded down to 30° , from Figures 2.10.9-F6.4 and 2.10.9-F6.5, the parameter [absorbed energy/plastic moment], $N = 3$.

$$\begin{aligned} EA_{\text{FINS \#7, \#31}} &= 2 \times N \times \sigma_y \times b \times t^2 / 4 \\ &= 2 \times 3 \times 25,000 \times 10 \times (0.375)^2 / 4 \\ &= 2 \times 0.0264 \times 10^6 \\ &= 0.0528 \times 10^6 \text{ in.-lb.} \end{aligned}$$

Therefore the sum of energy absorbed by all the fins is

$$\begin{aligned} EA_{\text{container fins}} &= [EA_{\text{FINS \#1}} + EA_{\text{FINS \#2, \#36}} + EA_{\text{FINS \#3, \#35}} + EA_{\text{FINS \#4, \#34}} \\ &\quad + EA_{\text{FINS \#5, \#33}} + EA_{\text{FINS \#6, \#32}} + EA_{\text{FINS \#7, \#31}}] \\ &= [0.781 + 0.608 + 0.316 + 0.176 + 0.070 + 0.056 + 0.0528] \times 10^6 \text{ in.-lb.} \\ &= 2.06 \times 10^6 \text{ in.-lb.} \end{aligned}$$

5.3 TOTAL ENERGY ABSORBED, EXCLUSIVE OF EFFECTS OF REINFORCING STRUCTURAL MEMBERS

Table 2.10.9-T9 lists the total energy absorbed.

Table 2.10.9-T9
Breakdown of the Energy Absorbed in the Top Corner Drop Orientation

Item	Energy Absorbing Element	Energy Absorbed In-Lb.
1	Container top cooling fins (0.5 in. and 0.375 in.)	1.279×10^6
2	Container lift lug fin	0.781×10^6
3	Crush shield	2.717×10^6
$\Sigma 1, 2, 3$		$\Sigma EA = 4.777 \times 10^6$

Without taking credit of the reinforcing structural members and other energy-absorbing elements (top corner of the cylindrical fireshield, top fireshield, extensions of the crush shield fins), the total energy absorption capability, assuming 45% crush of all fins except 30% crush for the lift lug fin, is 4.777×10^6 in.-lb. In summary, it is computed that 63% ($4.777 \times 10^6 / 7.56 \times 10^6$) of the 30-ft drop energy will be absorbed by the energy-absorbing elements in the impact in the top corner orientation. The total crush distance is estimated to be 5 in. (i.e., $0.45 \times 6 + 0.45 \times 5$).

5.4 EFFECT OF REINFORCING MEMBERS ON THE IMPACT RESISTANCE

Calculations are presented here to arrive at a "modification factor" to account for the stiffness of a composite section vis-à-vis the stiffness of a non-composite section of the crush shield structural members. It is assumed that the stiffness of a structural member is proportional to its 2nd moment of area.

5.4.1 Load Spreading Structural Members

See Figure 2.10.9-F26. The structural members are:

- Top load spreader plate (Area A1) (sometimes designated upper donut ring)
- Ring collar (Area A2)
- Top fireshield (Areas A3, A4, A5)
- Donut ring (Area A6) (sometimes designated lower donut ring)

As far as the crush shield is concerned, all of the above provide additional stiffness. However to simplify the problem, only the top load spreader plate (Area A1) is considered to provide the additional stiffness.

5.4.2 2nd Moment of Area of Fin Area A0 About XX

See Figure 2.10.9-F27.

$$I_{XX} = [0.5 \times 6^3/12] = 9 \text{ in}^4$$

2nd moment of area of load spreader plate of area A1 about xx

$$I_{XX} = A1 \times l^2 = [0.5 \times 3 \times (3.25)^2] = 15.8 \text{ in}^4$$

The fin area A0 is defined as the NON-COMPOSITE section of the unit cell of the crush shield. The fin area A0 plus A1 together is defined as the COMPOSITE section of the unit cell of the crush shield.

K1, Ratio of $[I_{\text{COMPOSITE SECTION}}/I_{\text{NON-COMPOSITE SECTION}}]$

$$K1 = [(9 + 15.8)/9] = 2.75$$

This ratio, K1 is designated as the stiffening factor for one composite fin at 0° loading angle. As there are 10 nominal fins in the zone of impact, and as they are impacting at various loading angles, it is computed that out of 10 fins, only 4.3 fins (see Table 2.10.9-T7 last column: $[0.9 + 0.7 + 0.225 + 0.175 + 0.150] \times 2$) are considered as the fins effectively impacting at 0° loading angle. Consequently, the stiffening factor K1, as applied to a group of fins, is modified as follows

$$KG = K1 \times 4.3/10 = 2.75 \times 4.3/10 = 1.182$$

where

KG = stiffening factor for a group of fins

K1 = stiffening factor for one composite fin.

The impact absorption of the "NON-COMPOSITE" crush shield fin can be modified to the impact absorption of "COMPOSITE" crush shield fin by use of stiffening factor KG (= 1.182). The stiffening factor KG is an estimate of the contribution to the energy absorbing capability, due to these extra load-spreading, reinforcing structural elements.

5.5 TOTAL ENERGY ABSORBED, INCLUSIVE OF LOAD SPREADING EFFECTS

Table 2.10.9-T10 is developed from a modification of Table 2.10.9-T9 to take into account the contribution, in terms of energy absorption, made by the structural members other than the crush shield fins. Taking credit of the load spreading structural member of the crush shield, the combined total energy absorption capability is 5.27×10^6 in.-lb. In summary, it is estimated that 69.7% ($5.27 \times 10^6/7.56 \times 10^6$) of the initial potential energy, in a 30-ft free drop, is absorbed by the crush shield and other impact absorbing elements.

Table 2.10.9-T10
Energy Absorbed in the Top Corner Drop Orientation, Inclusive of Effects of
Stiffening Structural Members of the Crush Shield

Item	Energy absorbing element	Energy absorbed, E_{TA} , (in.-lb.) $\times 10^6$	Modification factor	Energy absorbed Modified, E_{TAM} , (in.-lb.) $\times 10^6$
1	Container top fins	1.279	1	1.279
2	Crush shield fins	2.717	1.182	3.211
3	Lift lug fin	0.781	1.	0.781
Σ				5.271

5.6 ESTIMATE OF PEAK FORCES AND EFFECT OF PEAK FORCE ON THE CONTAINER SHELL

5.6.1 Estimate of Peak Force

Peak forces are evaluated using Ref. [18]. It should be noted during impact, this "peak" force is only experienced by the F-294 package for an extremely short time (in order of less than 100 milliseconds).

a) For crush shield fins (0.5 in. thick)

1. [height of fin/thickness of fin] = $6/0.5 = 12$

2. fin loading angle = $8.2^\circ, 13.6^\circ, 19^\circ, 24.5^\circ, 30^\circ$

3.1 Unit peak force $P_1 = 52,000$ lb. per in of loaded length per fin
(See Figure 2.10.9-F7.2). (10°)

3.2 Unit peak force $P_2 = 41,000$ lb. per in of loaded length per fin
(See Figures 2.10.9-F7.2 and 2.10.9-F7.3). (13.6°)

3.3 Unit peak force $P_3 = 20,000$ lb. per in of loaded length per fin
(See Figures 2.10.9-F7.2 and 2.10.9-F7.3). (19°)

3.4 Unit peak force $P_4 = 11,000$ lb. per in of loaded length per fin
(See Figures 2.10.9-F7.3 and 2.10.9-F7.4). (24.5°)

3.5 Unit peak force $P_5 = 4,000$ lb. per in of loaded length per fin
(See Figure 2.10.9-F7.4). (30°)

4. Loaded length of the fin = 11 in.

5. Total peak force experienced by the package due to impact of the crush shield;

$$\begin{aligned} \Sigma F_{\text{CRUSH SHIELD}} &= \text{loaded length} \times \Sigma[\text{unit peak force} \times \text{number of fins}] \\ &= 11 \times [P_1 \times 2 + P_2 \times 2 + P_3 \times 2 + P_4 \times 2 + P_5 \times 2] \\ &= 11 \times 2 [52,000 + 41,000 + 20,000 + 11,000 + 4,000] \\ &= 22 \times [128,000] \\ &= 2.816 \times 10^6 \text{ lb.} \end{aligned}$$

b) For container fins (0.375 in. thick)

1. [height of fin/thickness of fin]= $5/0.375 = 13.3$
2. Fin loading angle = $10.9^\circ, 16.4^\circ, 21.7^\circ, 27.2^\circ, 32.7^\circ$
- 3.1 Unit peak force $P_1 = 49,000$ lb. per in of loaded length per fin (see Figure 2.10.9-F7.2). (10°)
- 3.2 Unit peak force $P_2 = 27,000$ lb. per in of loaded length per fin (See Figures 2.10.9-F7.2 and 2.10.9-F7.3).(16.4°)
- 3.3 Unit peak force $P_3 = 12,000$ lb. per in of loaded length per fin (See Figures 2.10.9-F7.2 and 2.10.9-F7.3).(21.7°)
- 3.4 Unit peak force $P_4 = 7,000$ lb. per in of loaded length per fin (See Figures 2.10.9-F7.3 and 2.10.9-F7.4).(27.2°)
- 3.5 Unit peak force $P_5 = 3,000$ lb. per in of loaded length per fin (See Figures 2.10.9-F7.4 and 2.10.9-F7.5).(32.7°)
4. Loaded length of the fin = 10 in.
5. Total peak force experienced by the package due to impact of the 0.375 in. thick top fins of the container ;

$$\begin{aligned}
 \Sigma FP_{0.375 \text{ FINS, CONTAINER}} &= \text{loaded length} \times \Sigma[\text{unit peak force} \times \text{number of fins}] \\
 &= 10 \times [P_1 \times 2 + P_2 \times 2 + P_3 \times 2 + P_4 \times 2 + P_5 \times 2] \\
 &= 10 \times 2 [49,000 + 27,000 + 12,000 + 7,000 + 3,000] \\
 &= 20 \times [98,000] \\
 &= 1.96 \times 10^6 \text{ lb.}
 \end{aligned}$$

c) For container fins (0.5 in. thick)

1. [height of fin/ thickness of fin]= $5/0.5 = 10$.
2. fin loading angle = 5°
- 3.1 Unit peak force $P_1 = 66,000$ lb. per in of loaded length per fin (see Figures 2.10.9-F7.1 and 2.10.9-F7.2) (5°)

$$\begin{aligned}
 \Sigma FP_{0.5 \text{ FINS, CONTAINER}} &= \text{loaded length} \times [\text{unit peak force} \times \text{number of fins}] \\
 &= 10 \times [P_1 \times 2] \\
 &= 10 \times 2 [66,000] \\
 &= 20 \times [66,000] \\
 &= 1.32 \times 10^6 \text{ lb.}
 \end{aligned}$$

d) For lift lug fin (1.25 in. thick)

1. [height of fin/thickness of fin]= $5/1.25 = 4$
2. fin loading angle = 0°
- 3.1 Unit peak force $P_1 = 200,000$ lb. per in of loaded length per fin (See Figure 2.10.9-F7.1) (0°)

$$\begin{aligned}
 \Sigma FP_{\text{LIFT LUG FIN CONTAINER}} &= \text{loaded length} \times [\text{unit peak force} \times \text{number of fins}] \\
 &= 5 \times [P_1 \times 1] \\
 &= 5 \times [200,000] \\
 &= 5 \times [200,000] \\
 &= 1.00 \times 10^6 \text{ lb.}
 \end{aligned}$$

The total peak force, ΣFP

$$\begin{aligned}\Sigma FP &= FP_{\text{CRUSH SHIELD}} + FP_{0.375 \text{ FIN CONTAINER}} + FP_{0.5 \text{ FIN CONTAINER}} + FP_{\text{LIFT LUG FIN CONTAINER}} \\ &= [2.816 + 1.96 + 1.32 + 1.000] \times 10^6 \text{ lb.} \\ &= 7.096 \times 10^6 \text{ lb.}\end{aligned}$$

5.6.2 Estimate G-Load During Peak Force Duration

Based on Davis's method (Ref. [18]) of estimating peak force, the G-load is

$$\begin{aligned}G &= \Sigma FP / W_{F-294} \\ &= 7.096 \times 10^6 / 21,000 \\ &= 338 \text{ g's.}\end{aligned}$$

Estimate of G-load (Ref. [33]) by linear method, assuming no "bottoming":

$$G = 2 \times H / s$$

where

$$\begin{aligned}H &= \text{drop test height} = 30 \text{ feet} = 360 \text{ in.} \\ s &= \text{total crush distance} = 5.0 \text{ in.} \\ G &= 2 \times 360 / 5 \\ &= 144 \text{ g's.}\end{aligned}$$

In the top corner drop orientation, the F-294 package is subjected to a G-load range of $144 \leq G\text{-load} \leq 338$ g's at the impact zone.

5.6.3 Effect of Peak Force on the SS Shell Directly Under the Foot of the Lift Lug Fin

For the lift lug fin/container shell, see Figure 2.10.9-F28.

The 0.5 in. thick ss shell is reinforced with a pad approximately 0.5 in. thick x 10.5 in. wide x 11 in. long. The compressive (bearing) load on the container shell at the foot of the lift lug fin is

$$\begin{aligned}\sigma_c &= \text{Peak force/area under compression} \\ &= [FP_{0.5 \text{ FIN CONTAINER}} + FP_{\text{LIFT LUG FIN CONTAINER}}] / A \\ &= [(1.32 + 1.0) \times 10^6] / (10.5 \times 11) \\ &= [2.32 \times 10^6] / 115.7 \\ &= 20,051 \text{ psi.}\end{aligned}$$

The shear stress across 1.0 in. thick wall:

$$\begin{aligned}\tau &= \text{peak force/area under shear} \\ &= [FP_{0.5 \text{ FIN CONTAINER}} + FP_{\text{LIFT LUG FIN CONTAINER}}] / A_{\text{SHEAR}} \\ &= [(1.32 + 1.0) \times 10^6] / [(1.0 \times \{(11 + 10.52) \times 2\})] \\ &= [2.32 \times 10^6] / 43 \\ &= 53,488 \text{ psi.}\end{aligned}$$

The principal stress across the wall of the container in the lift lug footprint zone is:

$$\begin{aligned}\sigma_1 &= \sigma_c / 2 + \sqrt{[(\sigma_c / 2)^2 + \tau^2]} \\ &= 20,051 / 2 + \sqrt{[(20,051 / 2)^2 + 53,488^2]} \\ &= 10,026 + 54,420 \\ &= 64,446 \text{ psi}\end{aligned}$$

Since the maximum stress $\sigma_1 = 64,446$ psi in the container wall is less than the static ultimate compressive stress of the conical dished head (material ss304L UTS = 70,000 psi), the container reinforced wall will not fracture (dynamic). Also, the dynamic compressive strength of ss304L data as per Ref. [12] is used to arrive at the estimated strain. The container wall at the foot of the lift lug fin, will be deformed plastically by about 0.150 to 0.20 in. It must be noted that the estimated stress and the deformation of the container wall are based on instantaneous "peak force" and therefore they are fairly conservative.

5.7 SUMMARY OF RESULTS SO FAR

1. 63% of the 30-ft drop energy is absorbed by basically three energy absorbing elements (the container top fins, crush shield fins, lift lug fin). The estimated deformation is 5.0 in.
2. 69.7% of the 30-ft drop energy is absorbed, inclusive of reinforcing member effects of the top ring of the crush shield.
3. The estimated peak force is 7.1×10^6 lb. at the impact zone.
4. The estimated peak G-load is 338 g's at the impact zone.
5. The reinforcing pad under the foot of lift lug fin serves to prevent shear of the container wall, thereby maintaining the structural integrity of the ss outer shell around the lead shield.
6. The energy absorption by top fire shield, cylindrical fireshield (top zone), the container body, the plug and the crack shield is not taken into account.

5.8 ENERGY ABSORBED BY THE CASK

So far we have shown that 63% of the 30-ft drop energy is absorbed by two impact limiting devices (crush shield and the container fins) on the basis of excluding the effect of reinforcing members of the crush shield. If we include the effects of the reinforcing members of the crush shield the energy absorbed moves from 63% to 69.7% of the 30-ft drop energy. Essentially, it has yet to be shown how the remaining 31% to 37% of the 30-ft drop energy is absorbed. Discounting energy absorption contribution from the cylindrical fireshield, additional crushing of fins etc., it will be shown here that the cask in the top corner sector absorbs up to 37% of the 30-ft drop energy.

5.8.1 Impact Areas and Volumes

See Figure 2.10.9-F29 for the layout of the F-294 cask showing the impact front progression in the top corner drop orientation. There are a number of sub-components that come into play as the impact front progresses.

- At section 00, the crack shield (solid stainless steel) is the first component to impact.
- At section 22, the plug flange (ss), plug bolts, container female flange come into play.
- At section 33, the conical shell (ss) comes into play
- Between sections 55 and 66, the lead shielding and the conical shell etc. (ss) come into play.

Using this Figure 2.10.9-F29 we can estimate the impact area and the volume of stainless steel and lead, for every increment ($y = 0.25$ in.) of the impact front. The areas are calculated and depicted on the drawing using AUTOTROL Series 5000 release 8.2 Program and recaptured in Figure 2.10.9-F29. Figure 2.10.9-F30 shows the areas and the volumes as a function of y , impact progression.

The volume of the prism, pyramid or frustum of a pyramid is found by using the prismoidal formula.

A_n = area at one end of the body;

A_{n+1} = area of the middle section between the two end surfaces;

A_{n+2} = area at other end of the body;

Δy = $[y_{n+2} - y_n]$ = height of the body

then, the volume of the body is

$$V = \Delta y/6 [A_n + 4A_{n+1} + A_{n+2}]$$

(Ref. to *Machinery Handbook*, 18th edition, Pg. 164).

Table 2.10.9-T11
Cask in Top Corner Drop: Estimate of Stainless Steel Area and Volume Crushed

Section	y, (in.)	A _{SS} (in ²)	V _{SS} (in ³)
00	0	0	0
11	0.25	6.48	0.27
22	0.50	23.34	4.12
33	0.75	79.52	15.22
44	1.00	156.07	45.57
55	1.25	197.98	90.39
66	1.50	241.39	144.56

5.8.2 Dynamic Properties of Material

(Ref. Shappert: *Cask Designers Handbook*)

Lead:

F_d = dynamic compressive strength - 10,000 psi max., 5,000 psi min.

E_{sp} = specific energy - 5,000 in.-lb./in³

Stainless Steel:

F_d = dynamic strength = 39,000 psi at 200°F

E_{sp} = specific energy = 3,840 ft.-lb./in³
= 46,080 in.-lb./in³

5.8.3 Energy Absorbed by Cask Top Plug/Container Corner

See Table 2.10.9-T11 for tabulation of areas, volumes as a function of y, impact progression.

At Section 44 (y = 1.0 in.): We are in the stainless steel material zone only.

Energy absorbed by ss:

$$\begin{aligned} E_{\text{cask}} &= E_{\text{SP-SS}} \times V_{\text{SS-44}} \\ &= 46,080 \times 45.57 \\ &= 2.1 \times 10^6 \text{ in.-lb. (27.7\% of 30-ft drop)} \end{aligned}$$

At Section 55 (y = 1.25 in.): we are in the stainless steel material zone only.

Energy absorbed by ss:

$$\begin{aligned} E_{\text{cask}} &= E_{\text{SP-SS}} \times V_{\text{SS-55}} \\ &= 46,080 \times 90.39 \\ &= 4.165 \times 10^6 \text{ in.-lb. (55\% of 30-ft drop)} \end{aligned}$$

By interpolation between sections 44 and 55, at y = 1.125 in., the crush area = 170 in² and the crush volume 68 in³.

At mid Section 55 and 44 (y = 1.125 in.): We are in the stainless steel material zone only.

Energy absorbed by ss:

$$\begin{aligned} E_{\text{cask}} &= E_{\text{SP-SS}} \times V_{\text{SS-(44+55)/2}} \\ &= 46,080 \times 68 \\ &= 3.13 \times 10^6 \text{ in.-lb. (41.4\% of 30-ft drop)} \end{aligned}$$

Therefore 3.13×10^6 in.-lb. of energy is absorbed, by crushing of stainless steel cask material only between sections 44 and 55 at displacement = 1.125 in. deformation of stainless steel. As the stainless steel is deformed 1.125 in., the maximum amount of lead displaced is 1.125 in. in a radial direction (radial 33° from the F-294 original C of G).

5.8.4 Footprint G-Loads

The G-loads at section 44 are estimated as follows:

Impact load, P:

$$\begin{aligned} P &= [\sigma \times A]_{SS} \\ &= [39,000 \text{ psi} \times 156.07 \text{ in}^2] \\ &= 6.086 \times 10^6 \text{ lb.} \end{aligned}$$

$$\begin{aligned} \text{G-load SECTION-44} &= \text{Impact load, } P/W_{F-294} \\ &= 6.086 \times 10^6 / 21,000 \\ &= 290 \text{ g's.} \end{aligned}$$

The G-loads at section 55 are estimated as follows:

Impact load, P:

$$\begin{aligned} P &= [\sigma \times A]_{SS} \\ &= [39,000 \text{ psi} \times 197.98 \text{ in}^2] \\ &= 7.72 \times 10^6 \text{ lb.} \end{aligned}$$

$$\begin{aligned} \text{G-load SECTION-55} &= \text{Impact load, } P/W_{F-294} \\ &= 7.72 \times 10^6 / 21,000 \\ &= 368 \text{ g's.} \end{aligned}$$

The G-loads at mid section between section 44 and 55 are estimated as follows:

Impact load, P:

$$\begin{aligned} P &= [\sigma \times A]_{SS} \\ &= [39,000 \text{ psi} \times 170 \text{ in}^2] \\ &= 6.63 \times 10^6 \text{ lb.} \end{aligned}$$

$$\begin{aligned} \text{G-load MID-SECTION OF [44+55]} &= \text{Impact load, } P/ W_{F-294} \\ &= 6.63 \times 10^6 / 21,000 \\ &= 315 \text{ g's.} \end{aligned}$$

Conclude:

When the 2.8×10^6 in.-lb. of remaining energy is absorbed by the cask in the top corner, the resulting G-load is 315 g's and the displacement of lead is 1.125 in. along the vector 33° from CG from vertical axis.

5.9 SUMMARY OF ENERGY BREAKDOWN, PEAK FORCE, G-LOADS AT EACH STAGE

5.9.1 Energy Balance

Energy balance (with no credit of stiffening of crush shield due to reinforcements):

1st Stage	1st phase:	
	$E_{A_{\text{crush shield fins}}}$	$= 2.717 \times 10^6$ in.-lb. (35.9% of 30-ft drop)
	2nd phase:	
	$E_{A_{\text{container fins}}}$	$q = 2.06 \times 10^6$ in.-lb. (27.2% of 30-ft drop)
	4th phase:	
	E_{cask}	$= 3.13 \times 10^6$ in.-lb. (41.4% of 30-ft drop)
	E_{TOTAL}	$= 7.907 \times 10^6$ in.-lb. (104.5% of 30-ft drop)

5.9.2 Peak Force and G-loads

1st Stage 1st and 2nd phases:

$$\begin{aligned} FP_{\text{crush shield fins}} &= 2.82 \times 10^6 \text{ lb.} \\ FP_{\text{container fins}} &= 4.28 \times 10^6 \text{ lb.} \end{aligned}$$

After the crush shield fins and the container fins bottom out, the G-load = 338 g's

4th phase:

$$FP_{\text{cask}} = 6.63 \times 10^6 \text{ lb. G-load} = 315 \text{ g's}$$

The G-load on the cask at the impact point is 315 g's.

At locations away from the impact point but within the container, the G-loads are reduced (see section 8). The magnitude of the reduction in G-load is justified as per Ref. [37] Transnucleaire: to Dupont 15 ton flask. See Appendix 2.10.10. At 120 cm. from the impact zone of 25 cm., the G-loads were 50% or lower. Based on this, the G-loads on F-294 the cavity end plate, a distance of 80 cm. from the impact point, are in the range of $0.66 \times 338 \text{ g's} = 223 \text{ g's}$. This G-load data shall be used to evaluate stresses on the cavity end plate.

5.9.3 Displacements

Crush shield deforms by approximately: 45% of 6-inch height of fin = 2.7 in.

Container fins deform by approximately: 45% of 5-inch height of fin = 2.25 in.

Top corner of cask (stainless steel) is disclosed approximately: 1.125 in.

As the stainless steel is deformed 1.125 in., the maximum amount of lead displaced is 1.125 in. in a radial direction (radial 33° from the F-294 original C of G). This is depicted in Figure 2.10.9-F3. This amount of lead displacement is used for the basis of shielding calculation for post-accident conditions.

Figure 2.10.9-F22
F-294 in Top Corner Drop Orientation

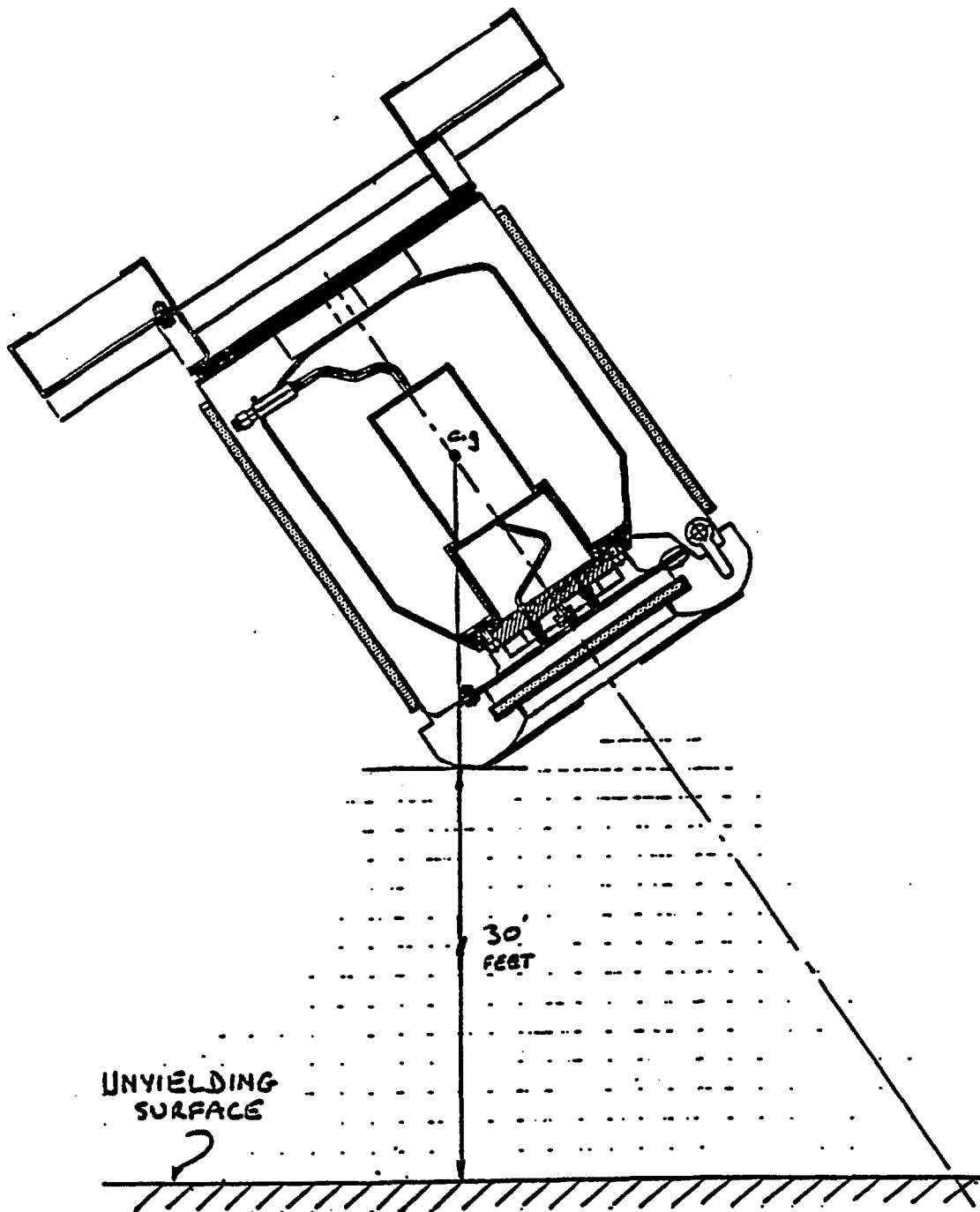


Figure 2.10.9-F23
Crush Shield Fins in Top Corner Drop: Zone of Impact and Identification of Fins

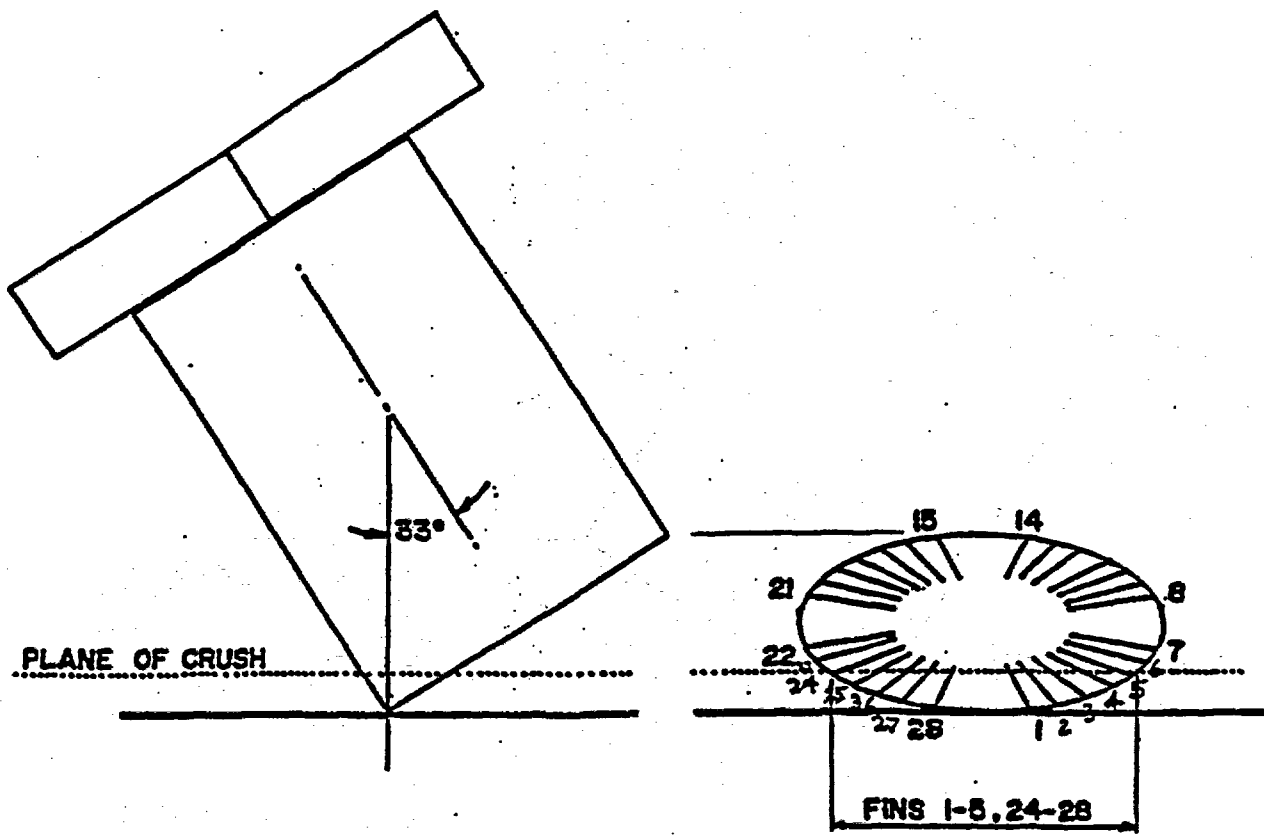


Figure 2.10.9-F24
Container Fins in Top Corner Drop Orientation: Zone of Impact and Identification of Fins

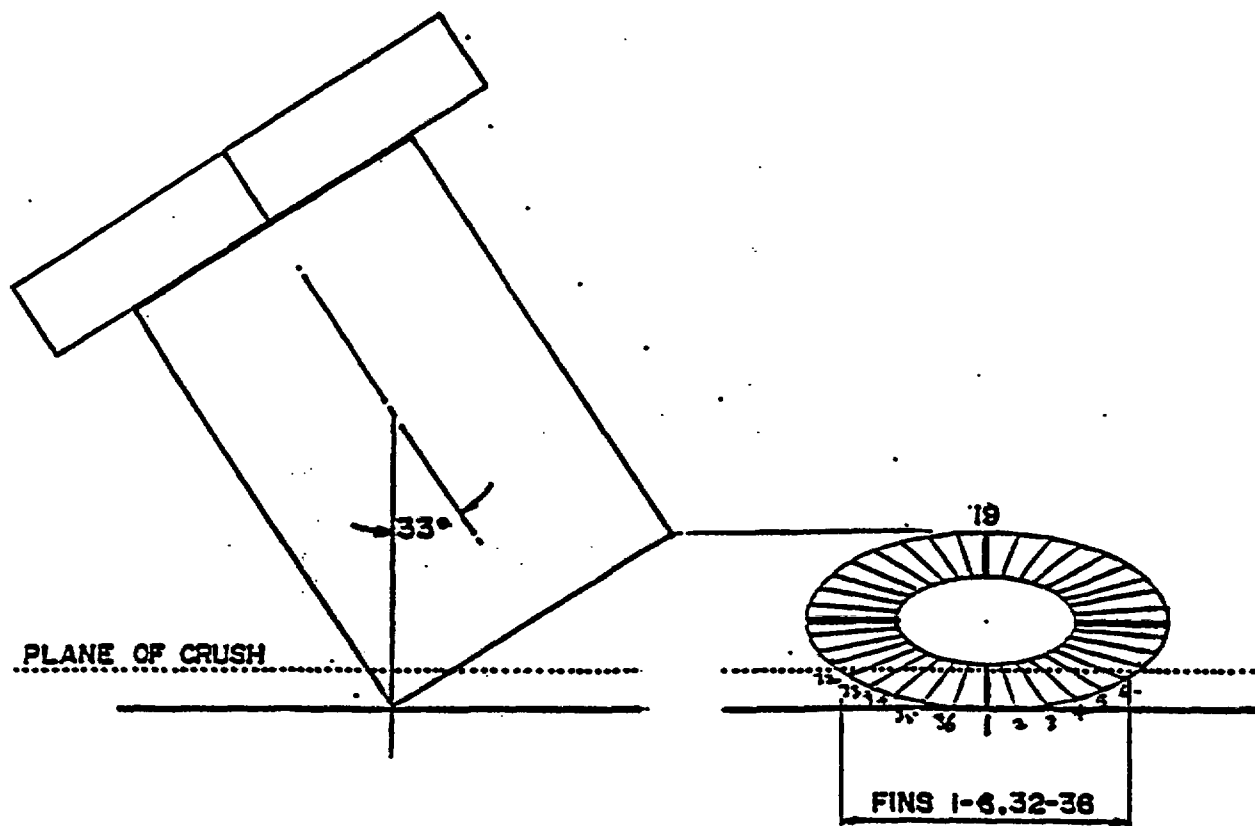


Figure 2.10.9-F25
F-294 in Top Corner Drop Orientation: Geometrical Data of the Impact Absorbing Fins

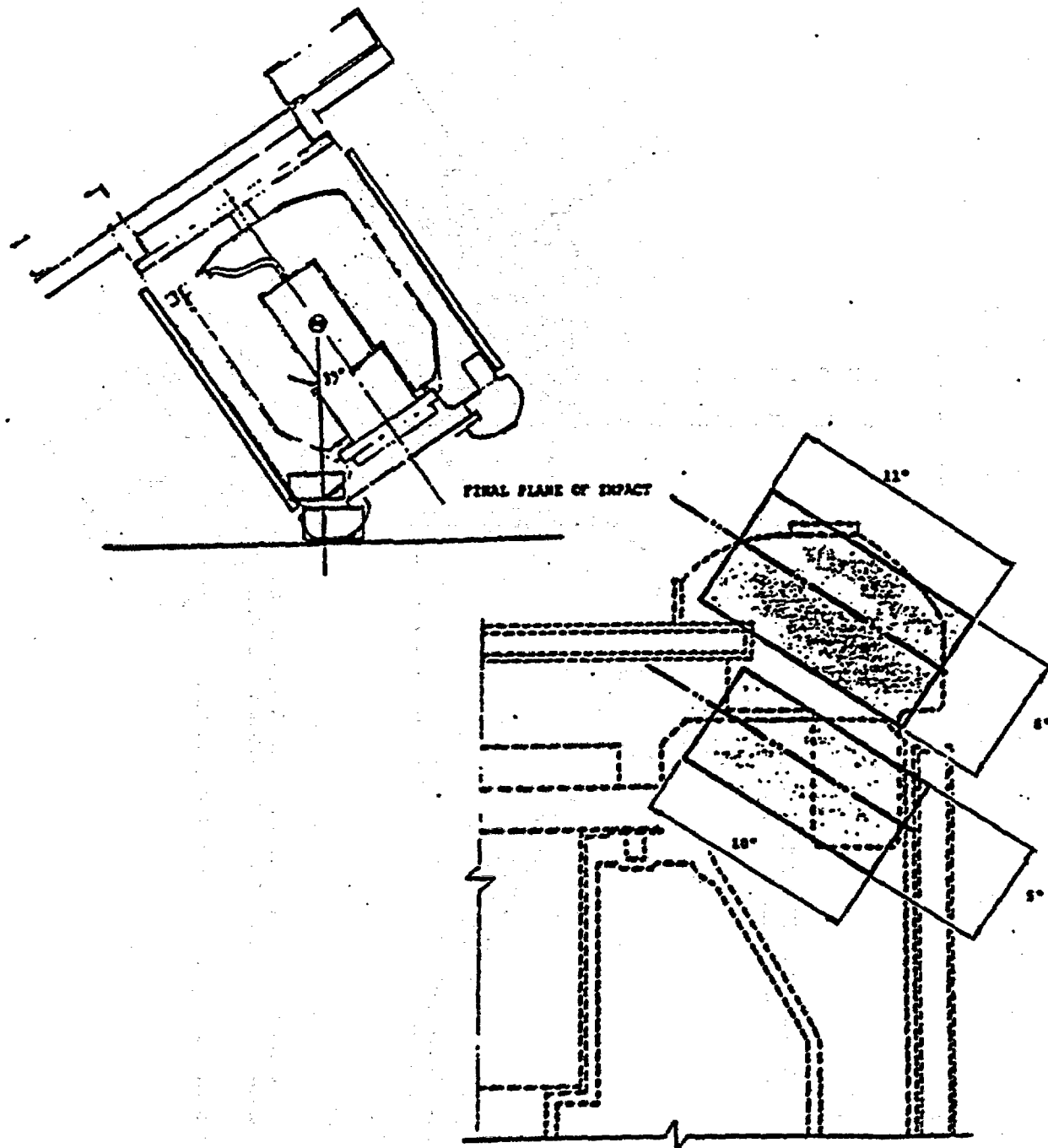


Figure 2.10.9-F26
Crush Shield Impact Absorbing Fin
Geometrical Data with respect to Stiffness Factor Calculation

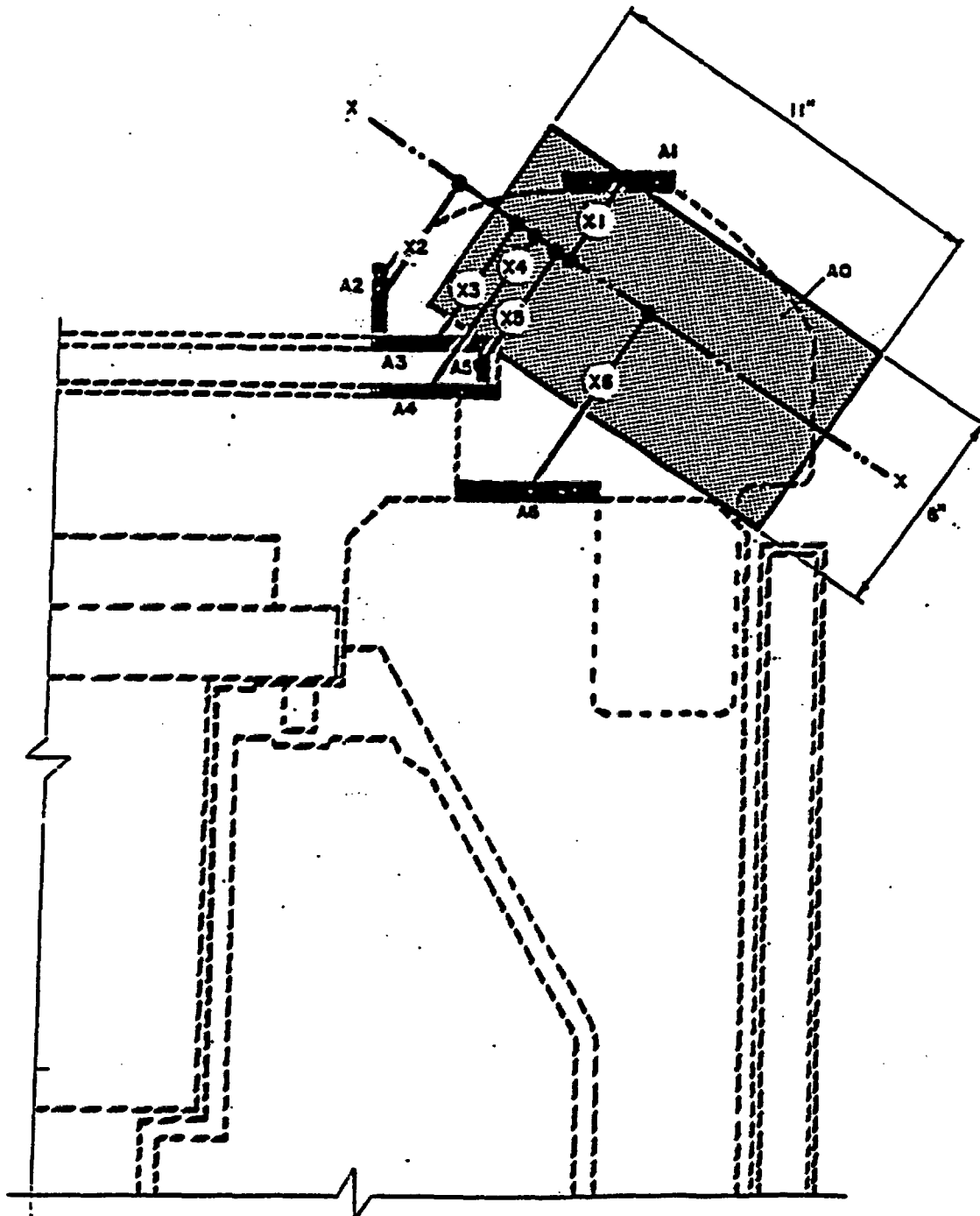


Figure 2.10.9-F27
Definition of Unit Cell - Crush Shield

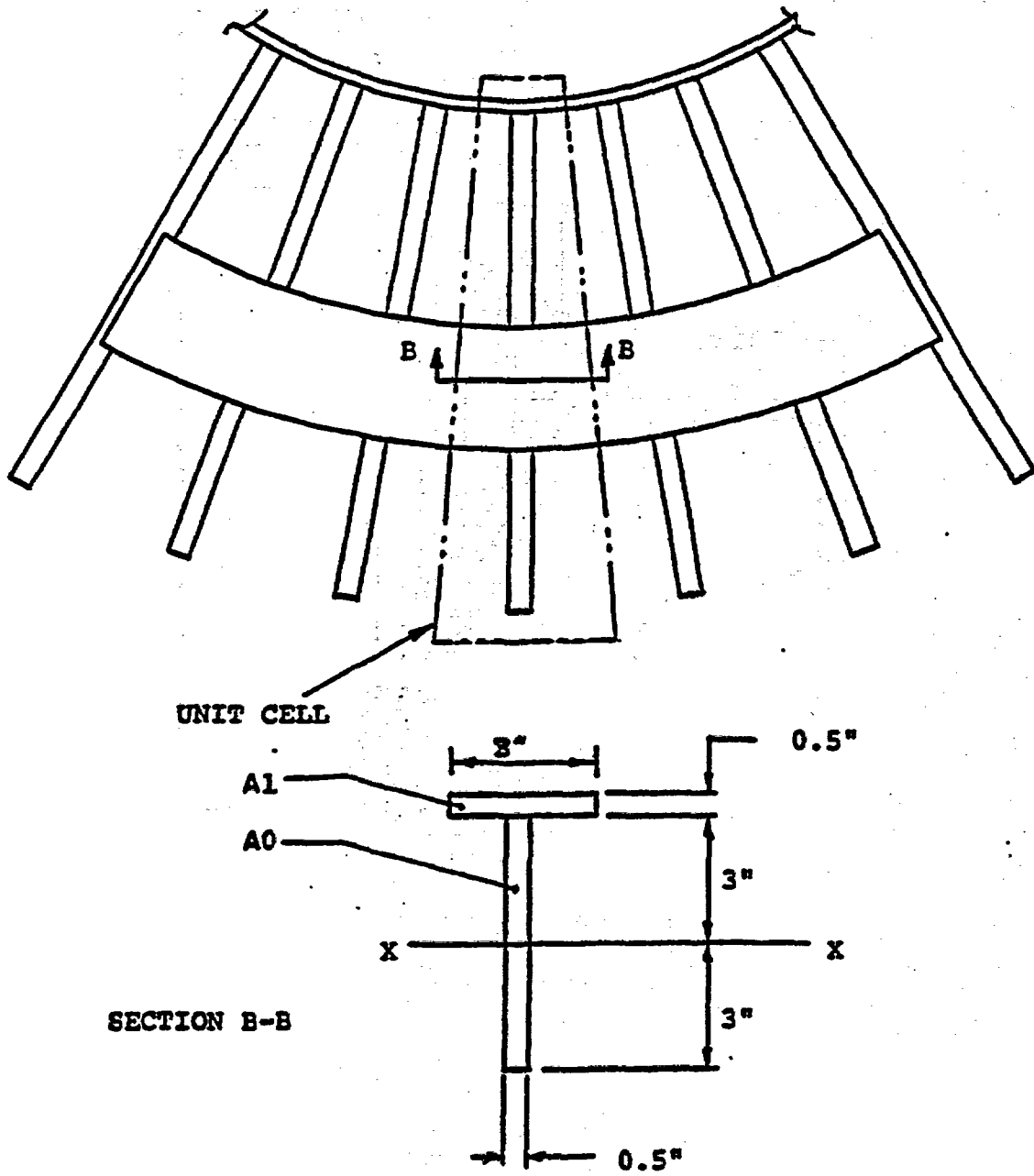


Figure 2.10.9-F28
Container Lift Lug Fin/Shell Area

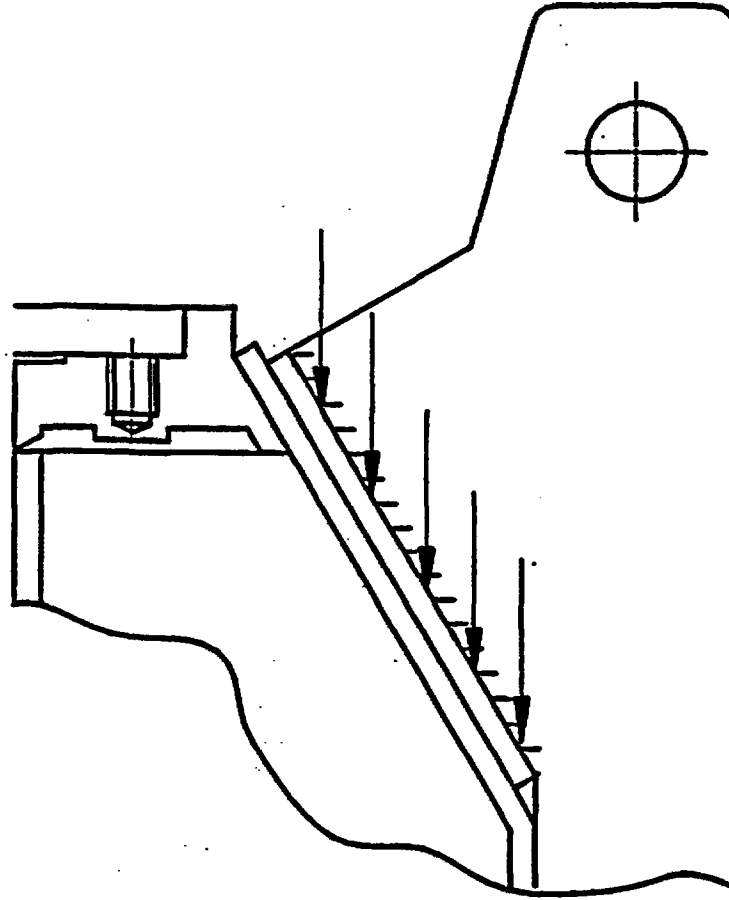
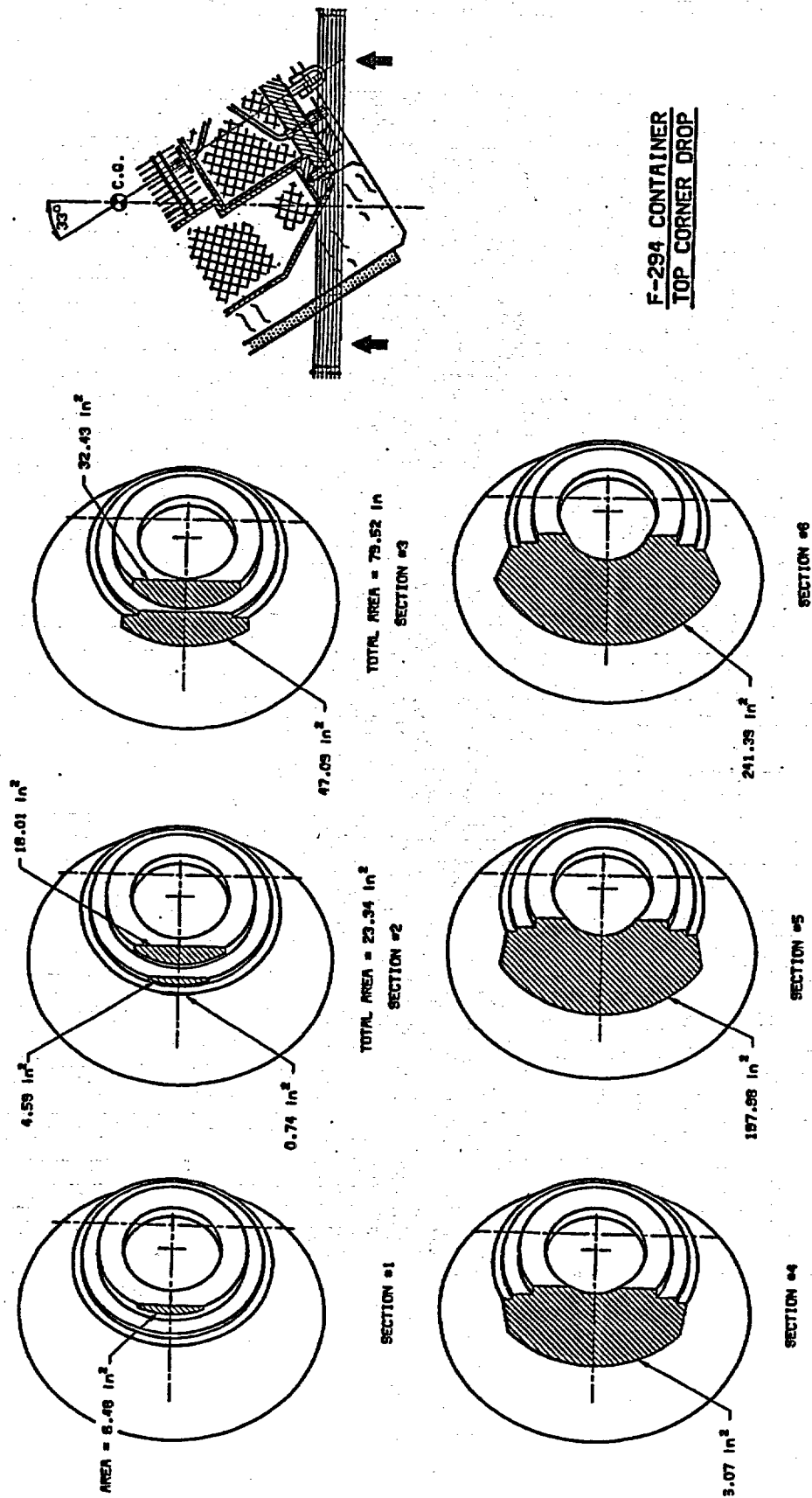


Figure 2.10.9-F29
 Top Corner Drop Orientation: Impact Progression in the Top Corner of the Cask

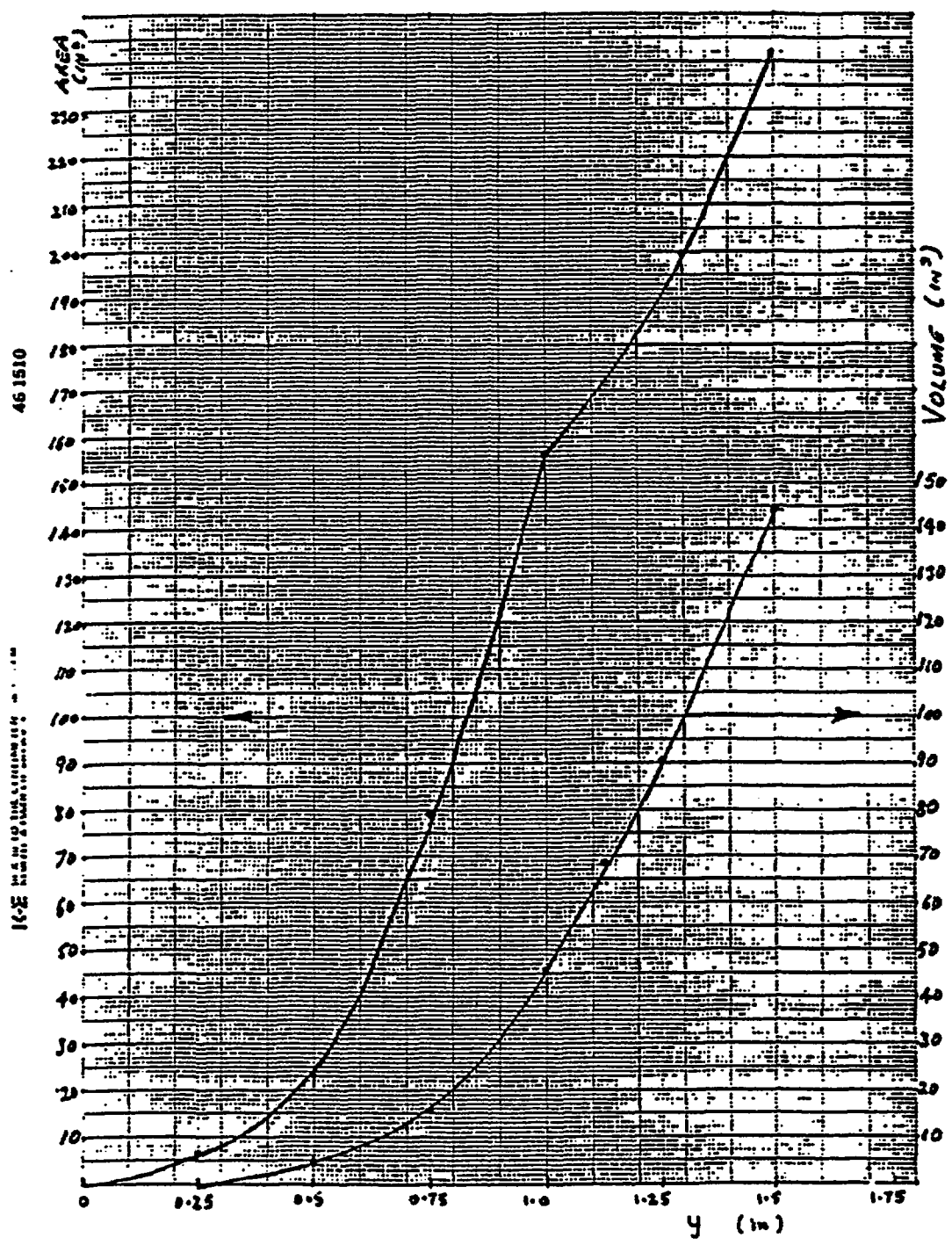


Rev. A, Dec'93

-2.10.9.107-

TR-9301-F294

Figure 2.10.9-F30
 Top Corner of the Cask, Area and Volume as a Function of Impact Progression, y



6. BOTTOM CORNER DROP

6.1 MODE OF IMPACT

See Figure 2.10.9-F31

During a bottom corner drop test, the following impact scenario is depicted:

1st Stage 1st phase:

The channel of the shipping skid impacts the unyielding surface. The impact forces are therefore transmitted through the shipping skid into the container fixed skid. The channel of the shipping skid and the container fixed skid and some container bottom fins will crush until they have absorbed as much energy as they are capable before "bottoming".

2nd Stage 1st phase:

Next, the fasteners connecting the shipping skid to the container fixed skid will snap. Also the container and the shipping skid shall be subject to secondary bounce. After the secondary bounce, the container shall rotate one side and the shipping skid rotate the opposite side.

3rd Stage 1st phase:

Next, the top sector of the container (the crush shield, the container fins & the cylindrical fire shield) will impact the unyielding surface.

2nd phase:

Next, the bottom corner of the cask will impact and start absorbing impact energy until it comes to rest on its side.

6.2 ENERGY ABSORPTION, G-LOADS FOR 1ST STAGE

There are three energy absorption structural elements that can be analyzed. These are:

1. shipping skid channel, gusset
2. fixed skid channel, gusset, sandwiched plate
3. cylindrical bottom fins

The energy absorbed by 1, 2, and 3 shall be presented here.

6.2.1 Energy Absorption Contribution by one Channel of the Shipping Skid

6.2.1.1 Fin: Web of the Shipping Skid Channel

Fin parameters.

See Figure 2.10.9-F32.

- Effective original height, $h = 8$ in. (8 in. web of the 8 x 3 channel)
- Thickness, $t = 0.43$ in.
- Loaded length, $b = 78$ in.
- material = ASTM A-36
- % of crush = 30%
- loading angle = 48.5° (angle of inclination to the unyielding surface)

Energy Absorbed EA at 40° Fin loading angle

$$EA = N \times M_p$$

where

$$\begin{aligned}
 N &= [(Absorbed\ Energy)/(Plastic\ Moment)] \\
 &= 1.5 \text{ (Figure 2.10.9-F6.5, at 8 in., 30\%)} \\
 M_p &= \text{plastic moment} \\
 &= \sigma_Y * bt^2 / 4 \\
 &= 36,000 * 78 * (0.43)^2 / 4 \\
 &= 129,800 \text{ in.-lb.}
 \end{aligned}$$

where

$$\begin{aligned}
 \sigma_Y &= \text{yield stress of A-36} = 36,000 \text{ psi} \\
 b &= \text{loaded length of the fin} \\
 t &= \text{fin thickness}
 \end{aligned}$$

Therefore

$$\begin{aligned}
 EA &= 1.5 * 129,800 \text{ in.-lb.} \\
 &= 194,700 \text{ in.-lb. per fin.}
 \end{aligned}$$

As there is one channel out of four impacting, therefore there is one 0.43 in. thick fin to consider. Therefore energy absorbed by 1, 0.43 in. thick fin is

$$\begin{aligned}
 EA_{WEB, CHANNEL} &= 194,700 \text{ in.-lb.} \\
 &= 0.195 * 10^6 \text{ in.-lb.}
 \end{aligned}$$

6.2.1.2 Fin: Flange of the Shipping Skid Channel

Fin parameters.

See Figure 2.10.9-F32.

- Effective original height, $h = 3.5$ in. (3.5 in. web of the 8x3.5 channel)
- Thickness, $t = 0.5$ in.
- Loaded length, $b = 78$ in.
- material = ASTM A-36
- % of crush = 30%
- loading angle = 41.5° (angle of inclination to the unyielding surface)

Energy Absorbed EA at 40° Fin loading angle

$$EA = N * M_p$$

where

$$\begin{aligned}
 N &= [(Absorbed\ Energy)/(Plastic\ Moment)] \\
 &= 2 \text{ (Figure 2.10.9-F6.5, at 4 in., 30\%)} \\
 M_p &= \text{plastic moment} \\
 &= \sigma_Y * bt^2 / 4 \\
 &= 36,000 * 78 * (0.5)^2 / 4 \\
 &= 177,500 \text{ in.-lb.}
 \end{aligned}$$

where

$$\begin{aligned}
 \sigma_Y &= \text{yield stress of A-36} = 36,000 \text{ psi} \\
 b &= \text{loaded length of the fin} \\
 t &= \text{fin thickness}
 \end{aligned}$$

Therefore

$$\begin{aligned}
 EA &= 2 * 177,500 \text{ in.-lb.} \\
 &= 351,000 \text{ in.-lb. per fin.}
 \end{aligned}$$

As there is one channel impacting, therefore there is one 0.5 in. thick fin. Therefore, energy absorbed by 1, 0.5 in. thick fin is

$$\begin{aligned}
 EA_{FLANGE, CHANNEL} &= 351,000 \text{ in.-lb.} \\
 &= 0.351 * 10^6 \text{ in.-lb.}
 \end{aligned}$$

6.2.1.3 Energy Absorption by Four Gusset Plates of the Shipping Skid

See Figure 2.10.9-F32.

i) Representative Fin Parameters

- Effective height, $h = 4$ in.
- Thickness, $t = 0.75$ in.
- Loaded length, $b = 4$ in.
- material = ASTM A-36
- % of crush = 30%
- fin loading angle = 0°

ii) Energy absorbed by one fin at 0° loading angle.

$$\begin{aligned} E_A &= N * M_P \\ &= N * \sigma_Y * bt^2 / 4 \\ &= 16 * 36,000 * 4 * (0.75)^2 / 4 \\ &= 324,000 \text{ in.-lb. per fin} \end{aligned}$$

where

$$\begin{aligned} E_A &= \text{Energy absorbed per fin in.-lb.} \\ N &= \text{Empirical parameter relating [absorbed energy/plastic moment] to} \\ &\quad \text{[deformation/original height] for a mild steel fin.} \\ &= \text{From Figure 2.10.9-F6.1, for 4-inch fin height, 30\% crush, } N = 16. \\ M_P &= \text{Plastic Moment in.-lb.} \\ &= \sigma_Y * bt^2 / 4 \\ \sigma_Y &= \text{yield stress of ASTM A-36 steel} = 36000 \text{ psi.} \end{aligned}$$

iii) Energy absorbed by 4, 0.75 in. thick gusset fins

$$\begin{aligned} EA_{\text{GUSSET}} &= 4 * 324,000 \\ &= 1.296 \times 10^6 \text{ in.-lb.} \end{aligned}$$

6.2.1.4 Energy Absorbed by Shipping Skid

Total energy absorbed by the shipping skid is:

$$\begin{aligned} EA_{\text{SHIPPING SKID}} &= EA_{\text{WEB, CHANNEL}} + EA_{\text{FLANGE, CHANNEL}} + EA_{\text{GUSSET}} \\ &= 0.195 \times 10^6 + 0.351 \times 10^6 + 1.296 \times 10^6 \\ &= 1.842 \times 10^6 \text{ in.-lb.} \end{aligned}$$

6.2.2 Peak Forces in the Shipping Skid

Peak forces in the shipping skid are evaluated using Ref. [18].

a) For channel web (0.43 in. thick)

1. [height of fin/thickness of fin] = $8/0.43 = 18.6$
2. Fin loading angle = 48.5° ; approximate to 40°
3. Unit peak force $P_1 = 2,000$ lb. per in of loaded length per fin
(see Figure 2.10.9-F7.5) (40°)
4. $FP_1 =$ loaded length x unit peak force
 $= b \times P_1$
 $= 78 \text{ in.} \times 2,000 \text{ lb./in.}$
 $= 156,000 \text{ lb.}$

b) For channel flange (0.5 in. thick)

1. [height of fin/thickness of fin] = $3.5/0.5 = 7$
2. Fin loading angle = 48.5° ; approximate to 40°
3. Unit peak force $P_2 = 8,000$ lb. per in of loaded length per fin (see Figure 2.10.9-F7.5) (40°)
4. $FP_2 =$ loaded length x unit peak force
 $= b \times P_1$
 $= 78 \text{ in.} \times 8,000 \text{ lb./in.}$
 $= 624,000 \text{ lb.}$

c) For channel gusset (0.75 in. thick)

1. [height of fin/thickness of fin] = $4/0.75 = 5.3$
2. Fin loading angle = 0°
3. Unit peak force $P_3 = 100,000$ lb. per in of loaded length per fin (see Figure 2.10.9-F7.1) (0°)
4. $FP_3 =$ loaded length x unit peak force
 $= b \times P_3$
 $= 4 \text{ in.} \times 100,000 \text{ lb./in.}$
 $= 400,000 \text{ lb.}$
5. $FP_{\text{GUSSETS}} = 4 \times FP_3$
 $= 4 \times 400,000$
 $= 1.6 \times 10^6 \text{ lb.}$

Peak force in the shipping skid

$$\begin{aligned}
 FP_{\text{SHIPPING SKID}} &= FP_1 + FP_2 + FP_{\text{GUSSETS}} \\
 &= [0.156 + 0.624 + 1.6] \times 10^6 \text{ lb.} \\
 &= 2.38 \times 10^6 \text{ lb.}
 \end{aligned}$$

6.2.3 Energy Absorption Contribution by One Channel of the Fixed Skid

6.2.3.1 *Fin: Web of the Shipping Skid Channel*

Representative Fin parameters.

See Figure 2.10.9-F32.

- Effective original height, $h = 8$ in. (8-inch web of the 8 x 3 channel)
- Thickness, $t = 0.43$ in.
- Loaded length, $b = 44$ in.
- material = ASTM A-36
- % of crush = 30%
- loading angle = 48.5° (angle of inclination to the unyielding surface)
- = 40° approximation

Energy Absorbed EA at 40° Fin loading angle

$$EA = N \times M_p$$

where

$$N = \frac{[(\text{Absorbed Energy})/(\text{Plastic Moment})]}{= 1.5 \text{ (Figure 2.10.9-F6.1, at 8 in., 30\%)}$$

$$\begin{aligned} M_p &= \text{plastic moment} \\ &= \sigma_y \times bt^2 / 4 \\ &= 36,000 \times 44 \times (0.43)^2 / 4 \\ &= 73,220 \text{ in.-lb.} \end{aligned}$$

where

$$\begin{aligned} \sigma_y &= \text{yield stress of A-36} = 36,000 \text{ psi} \\ b &= \text{loaded length of the fin} \\ t &= \text{fin thickness} \end{aligned}$$

Therefore

$$\begin{aligned} EA &= 1.5 \times 73,220 \text{ in.-lb.} \\ &= 109,800 \text{ in.-lb. per fin.} \end{aligned}$$

As there is one channel impacting, therefore there is one 0.43 in. thick fin. Therefore, energy absorbed by one, 0.43 in. thick fin is

$$\begin{aligned} EA_{\text{WEB, CHANNEL}} &= 109,800 \text{ in.-lb.} \\ &= 0.109 \times 10^6 \text{ in.-lb.} \end{aligned}$$

6.2.3.2 Fin: Flange of the Fixed Skid Channel

Representative Fin parameters.

See Figure 2.10.9-F32.

- Effective original height, h = 3.5 in. (3.5 in. web of the 8x3.5 channel)
- Thickness, t = 0.5 in.
- Loaded length, b = 44 in.
- material = ASTM A-36
- % of crush = 30%
- loading angle = 41.5° (angle of inclination to the unyielding surface)

Energy Absorbed EA at 40° Fin loading angle

$$EA = N \times M_p$$

where

$$N = \frac{[(\text{Absorbed Energy})/(\text{Plastic Moment})]}{= 2 \text{ (Figure 2.10.9-F6.1, at 4 in., 30\%)}$$

$$\begin{aligned} M_p &= \text{plastic moment} \\ &= \sigma_y \times bt^2 / 4 \\ &= 36,000 \times 44 \times (0.5)^2 / 4 \\ &= 99,000 \text{ in.-lb.} \end{aligned}$$

where

$$\begin{aligned} \sigma_y &= \text{yield stress of A-36} = 36,000 \text{ psi} \\ b &= \text{loaded length of the fin} \\ t &= \text{fin thickness} \end{aligned}$$

Therefore

$$\begin{aligned} EA &= 2 \times 99,000 \text{ in.-lb.} \\ &= 198,000 \text{ in.-lb. per fin.} \end{aligned}$$

As there is one channel impacting, therefore there is one 0.5 in. thick fin. Therefore, energy absorbed by one, 0.5 in. thick fin is

$$\begin{aligned} EA_{\text{FLANGE, CHANNEL}} &= 198,000 \text{ in.-lb.} \\ &= 0.198 \times 10^6 \text{ in.-lb.} \end{aligned}$$

6.2.3.3 Energy Absorption by Gussets

Gusset fins

Representative gusset fin parameters

- Effective height, $h = 4$ in.
- Thickness, $t = 0.5$ in.
- Loaded length, $b = 3$ in.
- material = ASTM A-36
- % of crush* = 30%
- loading angle = 0° (angle of inclination to the unyielding surface)

* This implies only bending (single hinge failure mode) of fin only.

$$\begin{aligned} N &= 16 \text{ (Figures 2.10.9-F6.1 at 30\%, 4 in. fin height)} \\ EA_{\text{GUSSET}} &= N \times M_p \\ &= N \times \sigma_y \frac{bt^2}{4} \\ &= 16 \times 36,000 \times 3 \times (0.5)^2 / 4 \\ &= 16 \times 6,750 \\ &= 108,000 \text{ in.-lb.} \\ \text{Number of gussets} &= 5 \\ EA_{\text{GUSSETS}} &= 5 \times EA_{\text{GUSSET}} \\ &= 5 \times 108,000 \\ &= 540,000 \text{ in.-lb.} \end{aligned}$$

6.2.3.4 Energy Absorbed by the Flexure of the Sandwiched Plate

Not accounted for.

6.2.3.5 Total Energy Absorbed by the Fixed Skid

$$\begin{aligned} EA_{\text{FIXED SKID}} &= EA_{\text{WEB, CHANNEL}} + EA_{\text{FLANGE, CHANNEL}} + EA_{\text{GUSSETS}} \\ &= 109,000 + 198,000 + 540,000 \\ &= 847,000 \text{ in.-lb.} \\ &= 0.847 \times 10^6 \text{ in.-lb.} \end{aligned}$$

Sandwiched plates have been ignored.

6.2.4 Peak Forces in the Fixed Skid

6.2.4.1 Peak Forces in the Fixed Skid

Peak forces in the fixed skid are evaluated using Ref. [18].

- a) For channel web (0.43 in. thick)
 1. [height of fin/thickness of fin] = $8/0.43 = 18.6$
 2. Fin loading angle = 48.5° ; approximate to 40°
 3. Unit peak force $P_1 = 2,000$ lb. per in of loaded length per fin (See Figure 2.10.9-F7.5). (40°)

4. $FP_1 = \text{loaded length} \times \text{unit peak force}$
 $= b \times P_1$
 $= 44 \text{ in.} \times 2,000 \text{ lb./in.}$
 $= 88,000 \text{ lb.}$
- b) For channel flange (0.5 in. thick)
1. [height of fin/thickness of fin] = $3.5/0.5 = 7$
 2. Fin loading angle = 48.5° ; approximate to 40°
 3. Unit peak force $P_2 = 8,000 \text{ lb. per in of loaded length per fin}$
(see Figure 2.10.9-F7.5) (40°)
 4. $FP_2 = \text{loaded length} \times \text{unit peak force}$
 $= b \times P_1$
 $= 44 \text{ in.} \times 8,000 \text{ lb./in.}$
 $= 352,000 \text{ lb.}$
- c) For channel gusset (0.75 in. thick)
1. [height of fin/thickness of fin] = $3/0.5 = 6$
 2. Fin loading angle = 0°
 3. Unit peak force $P_3 = 100,000 \text{ lb. per in of loaded length per fin}$
(see Figure 2.10.9-F7.1) (0°)
 4. $FP_3 = \text{loaded length} \times \text{unit peak force}$
 $= b \times P_3$
 $= 3 \text{ in.} \times 100,000 \text{ lb./in.}$
 $= 300,000 \text{ lb.}$
 5. $FP_{\text{GUSSETS}} = 5 \times FP_3$
 $= 5 \times 300,000$
 $= 1.5 \times 10^6 \text{ lb.}$

6.2.4.2 Peak Force in the Shipping Skid

$$FP_{\text{SHIPPING SKID}} = FP_1 + FP_2 + FP_{\text{GUSSETS}}$$

$$= [0.088 + 0.352 + 1.5] \times 10^6 \text{ lb.}$$

$$= 1.94 \times 10^6 \text{ lb.}$$

6.2.5 Energy Absorbed, G-loads for the Container Bottom Fins

6.2.5.1 Energy Absorbed by Bottom Fins of the Container

Refer to Figure 2.10.9-F32 for layout and numbering of container fins.

There is only one type of cooling fin at the bottom of the container 1) 0.375 in. thick. Refer to Figure 2.10.9-F32 for depiction of effective fin parameters etc.

How many fins are in the zone of impact? See Figure 2.10.9-F32. It is estimated from the graphical data, that 12 fins (3/8 in. thick) come into play.

What is the loading angle for each fin?

$$\theta = \beta \times \cos \alpha$$

where

θ = fin loading angle (°)

β = angle between fin 1 and fin n

α = angle between impact pad and the longitudinal axis of the package = 48.5°

Table 2.10.9-T12 lists the appropriate θ , loading angles for all the fins of the container, as calculated in the following example;

For Fin #5 and #6 (i.e., 0.375 in. thick fin)

$$\theta = \beta \times \cos \alpha$$

$$\theta = 5 \times \cos 48.5^\circ$$

$$\theta = 3.4^\circ$$

For Fin #4 and #7 (i.e., 0.375 in. thick fin)

$$\theta = \beta \times \cos \alpha$$

$$\theta = 15 \times \cos 48.5^\circ$$

$$\theta = 10.1^\circ$$

For Fin #3 and #8 (i.e., 0.375 in. thick fin)

$$\theta = \beta \times \cos \alpha$$

$$\theta = 25 \times \cos 48.5^\circ$$

$$\theta = 16.8^\circ$$

For Fin #2 and #9 (i.e., 0.375 in. thick fin)

$$\theta = \beta \times \cos \alpha$$

$$\theta = 35 \times \cos 48.5^\circ$$

$$\theta = 23.5^\circ$$

For Fin #1 and #10 (i.e., 0.375 in. thick fin)

$$\theta = \beta \times \cos \alpha$$

$$\theta = 45 \times \cos 48.5^\circ$$

$$\theta = 30^\circ$$

For Fin #36 and #11 (i.e., 0.375 in. thick fin)

$$\theta = \beta \times \cos \alpha$$

$$\theta = 55 \times \cos 48.5^\circ$$

$$\theta = 36.9^\circ$$

**Table 2.10.9-T12
Container Fin Data for Bottom Corner Drop Orientation**

Type of fins	Designated # Fin Number	No. of fins	Loading Angle, θ	Parameter N
0.375 in. fin	5,6	2	3.4°	14
0.375 in. fin	4,7	2	10.1°	14
0.375 in. fin	3,8	2	16.8°	7
0.375 in. fin	2,9	2	23.5°	2.5
0.375 in. fin	1,10	2	30°	2
0.375 in. fin	36,11	2	37°	1.5

i) Fins #5 and #6

- Effective original height, $h = 6$ in.
- Thickness, $t = 0.375$ in.
- Loaded length, $b = 9$ in.
- material = ss304L
- % of crush* = 30%
- loading angle = 3.4° (angle of inclination to the unyielding surface)

Therefore, at crush of 30%, for fin height of 6 in., from Figure 2.10.9-F6.1, the parameter [absorbed energy/plastic moment], $N = 14$

$$\begin{aligned} EA_{\text{FIN}\#5, \#6} &= N \times M_p \\ &= N \times [\sigma_y \times b \times t^2 / 4] \\ &= 14 \times [25,000 \times 9 \times (.375)^2 / 4] \\ &= 0.110 \times 10^6 \text{ in.-lb.} \end{aligned}$$

ii) Fins #4 and #7

- Effective height, $h = 6$ in.
- Thickness, $t = 0.375$ in.
- Loaded length, $b = 9$ in.
- material = ss304L
- % of crush = 30%
- loading angle = 10.1° (angle of inclination to the unyielding surface)

Therefore, at crush of 30%, for fin height of 10 in., fin inclination angle of 10° Figure 2.10.9-F6.2, the parameter [absorbed energy/plastic moment], $N = 14$

$$\begin{aligned} EA_{\text{FINS}\#4, \#7} &= 2 \times N \times \sigma_y \times b \times t^2 / 4 \\ &= 2 \times 14 \times 25,000 \times 9 \times (0.375)^2 / 4 \\ &= 2 \times 0.110 \times 10^6 \\ &= 0.220 \times 10^6 \text{ in.-lb.} \end{aligned}$$

iii) Fins #3 and #8

- Effective height, $h = 6$ in.
- Thickness, $t = 0.375$ in.
- Loaded length, $b = 9$ in.
- material = ss304L
- % of crush = 30%
- loading angle = 16.8° (angle of inclination to the unyielding surface)

Therefore, at crush of 30%, for fin height of 6 in., fin inclination angle of 20° from Figures 2.10.9-F6.2 and 2.10.9-F6.3, the parameter [absorbed energy/plastic moment], $N = 7$.

$$\begin{aligned} EA_{\text{FINS}\#3, \#8} &= 2 \times N \times \sigma_y \times b \times t^2 / 4 \\ &= 2 \times 7 \times 25,000 \times 9 \times (0.375)^2 / 4 \\ &= 0.110 \times 10^6 \text{ in.-lb.} \end{aligned}$$

iv) Fins #2 and #9

- Effective height, $h = 6$ in.
- Thickness, $t = 0.375$ in.
- Loaded length, $b = 9$ in.
- material = ss304L
- % of crush = 30%
- loading angle = 23.5° (angle of inclination to the unyielding surface)

Therefore, at crush of 30%, for fin height of 6 in., fin inclination angle of 23.5° , from Figures 2.10.9-F6.3 and 2.10.9-F6.4, the parameter [absorbed energy/plastic moment], $N = 2$

$$\begin{aligned} EA_{\text{FINS \#2,\#9}} &= 2 \times N \times \sigma_Y \times b \times t^2 / 4 \\ &= 2 \times 2 \times 25,000 \times 9 \times (0.375)^2 / 4 \\ &= 0.031 \times 10^6 \text{ in.-lb.} \end{aligned}$$

v) Fins #1 and #10

- Effective height, $h = 6$ in.
- Thickness, $t = 0.375$ in.
- Loaded length, $b = 9$ in.
- material = ss304L
- % of crush = 30%
- loading angle = 30° (angle of inclination to the unyielding surface)

Therefore, at crush of 30%, for fin height of 6 in., fin inclination angle of 30° , from Figure 2.10.9-F6.4, the parameter [absorbed energy/plastic moment], $N = 1.5$

$$\begin{aligned} EA_{\text{FINS \#1,\#10}} &= 2 \times N \times \sigma_Y \times b \times t^2 / 4 \\ &= 2 \times 1.5 \times 25,000 \times 9 \times (0.375)^2 / 4 \\ &= 0.023 \times 10^6 \text{ in.-lb.} \end{aligned}$$

vi) Fins #36 and #11

- Effective height, $h = 6$ in.
- Thickness, $t = 0.375$ in.
- Loaded length, $b = 9$ in.
- material = ss304L
- % of crush = 30%
- loading angle = 37° (angle of inclination to the unyielding surface)

Therefore, at crush of 30%, for fin height of 6 in., fin inclination angle of 23.5° , from Figure 2.10.9-F6.4, the parameter [absorbed energy/plastic moment], $N = 1$

$$\begin{aligned} EA_{\text{FINS \#36,\#11}} &= 2 \times N \times \sigma_Y \times b \times t^2 / 4 \\ &= 2 \times 1 \times 25,000 \times 9 \times (0.375)^2 / 4 \\ &= 0.015 \times 10^6 \text{ in.-lb.} \end{aligned}$$

Therefore, the sum of energy absorbed by all the fins is

$$\begin{aligned} EA_{\text{container fins}} &= [EA_{\text{FINS \#5,\#6}} + EA_{\text{FINS \#4,\#7}} + EA_{\text{FINS \#3,\#8}} + EA_{\text{FINS \#2,\#9}} \\ &\quad + EA_{\text{FINS \#1,\#10}} + EA_{\text{FINS \#36,\#11}}] \\ &= [0.110 + 0.220 + 0.110 + 0.031 + 0.023 + 0.015] \times 10^6 \text{ in.-lb.} \\ &= 0.509 \times 10^6 \text{ in.-lb.} \end{aligned}$$

6.2.6 PEAK FORCES IN THE BOTTOM CONTAINER FINS

- a) For container fins (0.375 in. thick)
1. [height of fin/thickness of fin] = $6/0.375 = 16$
 2. fin loading angle = $3.4^\circ, 10.1^\circ, 16.8^\circ, 23.5^\circ, 30^\circ, 37^\circ$
 - 3.1 unit peak force $P_1 = 25,000$ lb. per in of loaded length per fin
(see Figures 2.10.9-F7.1 and 2.10.9-F7.2) (3.4°)
 - 3.2 Unit peak force $P_2 = 37,500$ lb. per in of loaded length per fin
(see Figure 2.10.9-F7.2) (10.1°)
 - 3.3 Unit peak force $P_3 = 25,000$ lb. per in of loaded length per fin
(see Figures 2.10.9-F7.2 and 2.10.9-F7.3) (16.8°)
 - 3.4 Unit peak force $P_4 = 7,000$ lb. per in of loaded length per fin
(see Figures 2.10.9-F7.3 and 2.10.9-F7.4) (23.5°)
 - 3.5 Unit peak force $P_5 = 2,000$ lb. per in of loaded length per fin
(see Figure 2.10.9-F7.4) (30°)
 - 3.6 Unit peak force $P_6 = 2,000$ lb. per in of loaded length per fin
(see Figure 2.10.9-F7.5) (37°)
 4. Loaded length of the fin = 9 in.
 5. Total peak force experienced by the package due to impact of the 0.375 in. thick top fins of the container;

$$\begin{aligned} \Sigma FP_{0.375 \text{ FINS, CONTAINER}} &= \text{loaded length} \times \Sigma[\text{unit peak force} \times \text{number of fins}] \\ &= 9 \times [P_1 \times 2 + P_2 \times 2 + P_3 \times 2 + P_4 \times 2 + P_5 \times 2 + P_6 \times 2] \\ &= 9 \times 2 [25,000 + 37,500 + 25,000 + 7,000 + 2,000 + 2,000] \\ &= 18 \times [98,500] \\ &= 1.773 \times 10^6 \text{ lb.} \end{aligned}$$

6.3 ENERGY, PEAK FORCES, G-LOADS SUMMARY AT END OF 1ST STAGE

Energy summary at the end of first stage:

$EA_{\text{SHIPPING SKID}}$	$= 1.842 \times 10^6$
$EA_{\text{FIXED SKID}}$	$= 0.847 \times 10^6 \text{ in.-lb.}$
sandwiched plates	= not available
$EA_{\text{container fins}}$	$= 0.509 \times 10^6 \text{ in.-lb.}$
Total	$= 3.198 \times 10^6 \text{ in.-lb. (42.3\% of 30-ft drop)}$

Peak forces summary at the end of first stage:

$FP_{\text{SHIPPING SKID}}$	$2.38 \times 10^6 \text{ lb.}$
$FP_{\text{FIXED SKID}}$	$= 1.94 \times 10^6 \text{ lb.}$
$FP_{\text{CONTAINER BOTTOM FINS}}$	$= 1.77 \times 10^6 \text{ lb.}$
Total FP_{TOTAL}	$= 6.09 \times 10^6 \text{ lb.}$

G-load at end of 1st stage:

$$\begin{aligned} \text{G-load} &= FP_{\text{TOTAL}}/W_{F-294} \\ &= 6.09 \times 10^6 \text{ lb.}/21,000 \text{ lb.} \\ &= 290 \text{ g's.} \end{aligned}$$

6.4 2ND STAGE: SECONDARY BOUNCE

The amount of secondary bounce will be proportional to the amount of elastic energy absorbed in the 1st phase.

6.5 3RD STAGE: TOP SIDE CORNER OF CONTAINER IMPACT

There are three (3) energy absorption structural elements that can be analyzed. These are

1. A top/side sector of the crush shield
2. A top/side sector of the cylindrical fireshield
3. A top/side sector of the container external cooling fins

6.5.1 Energy Absorption by Fins of Crush Shield

Refer to Figure 2.10.9-F33 for layout and numbering of crush shield fins.

How many fins are in the zone of impact? See Figure 2.10.9-F33. It is estimated from the graphical data, that 7 fins (0.5 in. thick) come into play.

What is the loading angle for each fin?

$$\theta = \beta \times \cos \alpha$$

where

$$\theta = \text{fin loading angle (}^\circ\text{)}$$

$$\beta = \text{angle between vertical axis and fin } n$$

$$\alpha = \text{angle between impact pad and the longitudinal axis of the package} = 7^\circ$$

Table 2.10.9-T13 lists the appropriate θ , loading angles for all the fins of the crush shield, as calculated in the following example:

For Fin #4 (i.e., 0.5 in. thick fin)

$$\theta = \beta \times \cos \alpha$$

$$\theta = 0 \times \cos 7^\circ$$

$$\theta = 0^\circ$$

For Fins #3 and #5 (i.e., 0.5 in. thick fin)

$$\theta = \beta \times \cos \alpha$$

$$\theta = 10 \times \cos 7^\circ$$

$$\theta = 10^\circ$$

For Fins #2 and #6 (i.e., 0.5 in. thick fin)

$$\theta = \beta \times \cos \alpha$$

$$\theta = 20 \times \cos 7^\circ$$

$$\theta = 20^\circ$$

For Fins #1 & #7 (i.e., 0.5 in. thick fin)

$$\theta = \beta \times \cos \alpha$$

$$\theta = 30 \times \cos 7^\circ$$

$$\theta = 30^\circ$$

Table 2.10.9-T13

Fin Data for the Crush Shield Fins in Bottom Corner Drop: 3rd Stage

Type of Fins	Designated #	No. of Fins	Loading Angle θ	Parameter N
0.5 in.	#4	1	0°	12
0.5 in.	#3, #5	2	10°	12
0.5 in.	#2, #6	2	20°	3
0.5 in.	#1, #7	2	30°	1.7

i) Fin #4

- Effective height, $h = 8$ in.
- Thickness, $t = 0.5$ in.
- Loaded length, $b = 9$ in.
- material = C-1020
- % of crush = 30%
- loading angle = 0° (angle of inclination to the unyielding surface)

Therefore, at crush of 30%, for fin height of 8 in., fin inclination angle of 0°, from Figure 2.10.9-F6.1, the parameter [absorbed energy/plastic moment], $N = 12$.

$$\begin{aligned}
 EA_{\text{FINS \#4}} &= N \times \sigma_Y \times b \times t^2 / 4 \\
 &= 12 \times 46,000 \times 9 \times (0.5)^2 / 4 \\
 &= 0.3105 \times 10^6 \text{ in.-lb.}
 \end{aligned}$$

ii) Fins #3 and #5

For Fin #3 and #5 (i.e., 0.5 in. thick fin)

$$\begin{aligned}
 \theta &= \beta \times \cos \alpha \\
 \theta &= 10 \times \cos 7^\circ \\
 \theta &= 10^\circ
 \end{aligned}$$

- Effective height, $h = 8$ in.
- Thickness, $t = 0.5$ in.
- Loaded length, $b = 9$ in.
- material = C-1020
- % of crush = 30%
- loading angle = 10° (angle of inclination to the unyielding surface)

Therefore, at crush of 30%, for fin height of 8 in., fin inclination angle of 10°, from Figure 2.10.9-F6.2, the parameter [absorbed energy/plastic moment], $N = 12$

$$\begin{aligned}
 EA_{\text{FINS \#3,\#5}} &= 2 \times N \times \sigma_Y \times b \times t^2 / 4 \\
 &= 2 \times 12 \times 46,000 \times 9 \times (0.5)^2 / 4 \\
 &= 2 \times 0.3105 \times 10^6 \\
 &= 0.621 \times 10^6 \text{ in.-lb.}
 \end{aligned}$$

iii) Fins #2, #6

For Fin #2 and #6 (i.e., 0.5 in. thick fin)

$$\theta = \beta \times \cos \alpha$$

$$\theta = 20 \times \cos 7^\circ$$

$$\theta = 20^\circ$$

- Effective height, $h = 8$ in.
- Thickness, $t = 0.5$ in.
- Loaded length, $b = 9$ in.
- material = C-1020
- % of crush = 30%
- loading angle = 20° (angle of inclination to the unyielding surface)

Therefore, at crush of 30%, for fin height of 8 in., fin inclination angle of 34° , from Figure 2.10.9-F6.3, the parameter [absorbed energy/plastic moment], $N = 3$

$$\begin{aligned} EA_{\text{FINS \#2,\#6}} &= 2 \times N \times \sigma_Y \times b \times t^2 / 4 \\ &= 2 \times 3 \times 46,000 \times 9 \times (0.5)^2 / 4 \\ &= 2 \times 77,625 \\ &= 0.155 \times 10^6 \text{ in.-lb.} \end{aligned}$$

iv) Fins #1, #7

For Fin #1 and #7 (i.e., 0.5 in. thick fin)

$$\theta = \beta \times \cos \alpha$$

$$\theta = 30 \times \cos 7^\circ$$

$$\theta = 30^\circ$$

- Effective height, $h = 8$ in.
- Thickness, $t = 0.5$ in.
- Loaded length, $b = 9$ in.
- material = C-1020
- % of crush = 30%
- loading angle = 30° (angle of inclination to the unyielding surface)

Therefore, at crush of 30%, for fin height of 8 in., fin inclination angle of 30° , from Figures 2.10.9-F6.4, the parameter [absorbed energy/plastic moment], $N = 1.7$

$$\begin{aligned} EA_{\text{FINS \#1,\#7}} &= 2 \times N \times \sigma_Y \times b \times t^2 / 4 \\ &= 2 \times 1.7 \times 46,000 \times 9 \times (0.5)^2 / 4 \\ &= 2 \times 44,000 \times 10^6 \\ &= 0.088 \times 10^6 \text{ in.-lb.} \end{aligned}$$

Therefore the sum of energy absorbed by all the fins is

$$\begin{aligned} EA_{\text{crush shield fins}} &= [EA_{\text{FINS \#4}} + EA_{\text{FINS \#3,\#5}} + EA_{\text{FINS \#2,\#6}} + EA_{\text{FINS \#1,\#7}}] \\ &= [0.310 + 0.621 + 0.155 + 0.088] \times 10^6 \text{ in.-lb.} \\ &= 1.174 \times 10^6 \text{ in.-lb.} \end{aligned}$$

6.5.2 Peak Force for Crush Shield

Peak forces are evaluated using Ref. [18]. It should be noted that, during impact, this "peak" force is only experienced by the F-294 package for an extremely short time (in the order of less than 100 milliseconds).

a) For crush shield fins (0.5 in. thick)

1. [height of fin/ thickness of fin]= $8/0.5 = 16$
2. Fin loading angle = $0^\circ, 10^\circ, 20^\circ, 30^\circ$
- 3.1 Unit peak force $P_1 = 12,500$ lb. per in of loaded length per fin
(See Figure 2.10.9-F7.1). (0°)
- 3.2 Unit peak force $P_2 = 37,500$ lb. per in of loaded length per fin
(See Figures 2.10.9-F7.2 and 2.10.9-F7.3). (10°)
- 3.3 Unit peak force $P_3 = 12,000$ lb. per in of loaded length per fin
(See Figures 2.10.9-F7.2 and 2.10.9-F7.3). (20°)
- 3.4 Unit peak force $P_4 = 3,000$ lb. per in of loaded length per fin
(See Figures 2.10.9-F7.3 and 2.10.9-F7.4). (30°)
4. Loaded length of the fin = 9 in.
5. Total peak force experienced by the package due to impact of the crush shield;

$$\begin{aligned} \Sigma F_{\text{CRUSH SHIELD}} &= \text{loaded length} \times \Sigma[\text{unit peak force} \times \text{number of fins}] \\ &= 9 \times [P_1 \times 1 + P_2 \times 2 + P_3 \times 2 + P_4 \times 2] \\ &= 9 \times [12,500 \times 1 + 37,500 \times 2 + 12,000 \times 2 + 3,000 \times 2] \\ &= 9 \times [117,500] \\ &= 1.057 \times 10^6 \text{ lb.} \end{aligned}$$

6.5.3 Energy Absorbed by Top/Side Fins of the Container

Refer to Figure 2.10.9-F33 for layout and numbering of container fins.

There are three types of fins on the top of the container:

- 1.25 in. thick
- 0.5 in. thick
- 0.375 in. thick

The container lift lug fin and the 0.5 in. thick fin adjacent to the lift lug fin do not come into play as they are just outside the zone of impact. Lift lug fin is at 45° to the shipping skid. Refer to Figure 2.10.9-F33 for depiction of effective fin parameters etc.

How many fins are in the zone of impact? See Figure 2.10.9-F33. It is estimated from the graphical data, that 6 fins (3/8 in. thick) come into play.

What is the loading angle for each fin?

$$\theta = \beta \times \cos \alpha$$

where

θ = fin loading angle ($^\circ$)

β = angle between fin 1 and fin n

α = angle between impact pad and the longitudinal axis of the package = 7°

Table 2.10.9-T14 list the appropriate θ , loading angles for all the fins of the container, as calculated in the following example;

For Fins #5 and #6 (i.e., 0.375 inch fin)

$$\begin{aligned}\theta &= \beta \times \cos \alpha \\ \theta &= 5 \times \cos 7^\circ \\ \theta &= 5^\circ\end{aligned}$$

For Fins #4 and #7 (i.e., 0.375 in. thick fin)

$$\begin{aligned}\theta &= \beta \times \cos \alpha \\ \theta &= 15 \times \cos 7^\circ \\ \theta &= 15^\circ\end{aligned}$$

For Fins #3 and #8 (i.e., 0.375 in. thick fin)

$$\begin{aligned}\theta &= \beta \times \cos \alpha \\ \theta &= 25 \times \cos 7^\circ \\ \theta &= 25^\circ\end{aligned}$$

Table 2.10.9-T14
Bottom Corner Drop, 3rd Stage: Container Fin Data

Type of Fins	Designated # Fin Number	No. of Fins	Loading Angle, θ	Parameter N
0.375 in. fin	#5, #6	2	5°	16.
0.375 in. fin	#4, #7	2	15°	8.5
0.375 in. fin	#3, #8	2	25°	2.5

i) Fins #5 and #6

- Effective height, $h = 6$ in.
- Thickness, $t = 0.375$ in.
- Loaded length, $b = 13.8$ in.
- material = ss304L
- % of crush = 30%
- loading angle = 5° (angle of inclination to the unyielding surface)

Therefore, at crush of 30%, for fin height of 6 in., fin inclination angle of 5°, from Figures 2.10.9-F6.1 and 2.10.9-F6.2, the parameter [absorbed energy/plastic moment], $N = 16$.

$$\begin{aligned}EA_{\text{FINS \#5,\#6}} &= 2 \times N \times \sigma_Y \times b \times t^2 / 4 \\ &= 2 \times 16 \times 25,000 \times 13.8 \times (0.375)^2 / 4 \\ &= 2 \times 194,000 \\ &= 0.388 \times 10^6 \text{ in.-lb.}\end{aligned}$$

ii) Fins #4 and #7

- Effective height, $h = 6$ in.
- Thickness, $t = 0.375$ in.
- Loaded length, $b = 13.8$ in.
- material = ss304L
- % of crush = 30%
- loading angle = 15° (angle of inclination to the unyielding surface)

Therefore, at crush of 30%, for fin height of 6 in., fin inclination angle of 15° , from Figures 2.10.9-F6.2 and 2.10.9-F6.3, the parameter [absorbed energy/plastic moment], $N = 8.5$.

$$\begin{aligned} EA_{\text{FINS \#4,\#7}} &= 2 \times N \times \sigma_Y \times b \times t^2 / 4 \\ &= 2 \times 8.5 \times 25,000 \times 13.8 \times (0.375)^2 / 4 \\ &= 2 \times 103,000 \\ &= 0.206 \times 10^6 \text{ in.-lb.} \end{aligned}$$

iii) Fins #3 and #8

- Effective height, $h = 6$ in.
- Thickness, $t = 0.375$ in.
- Loaded length, $b = 13.8$ in.
- material = ss304L
- % of crush = 30%
- loading angle = 25° (angle of inclination to the unyielding surface)

Therefore, at crush of 30%, for fin height of 6 in., fin inclination angle of 25° , from Figures 2.10.9-F6.3 and 2.10.9-F6.4, the parameter [absorbed energy/plastic moment], $N = 2.5$

$$\begin{aligned} EA_{\text{FINS \#3,\#8}} &= 2 \times N \times \sigma_Y \times b \times t^2 / 4 \\ &= 2 \times 2.5 \times 25,000 \times 13.8 \times (0.375)^2 / 4 \\ &= 2 \times 30,000 \\ &= 0.060 \times 10^6 \text{ in.-lb.} \end{aligned}$$

Therefore the sum of energy absorbed by all the fins is

$$\begin{aligned} EA_{\text{container fins}} &= [EA_{\text{FINS \#5,\#6}} + EA_{\text{FINS \#4,\#7}} + EA_{\text{FINS \#3,\#8}}] \\ &= [0.388 + 0.206 + 0.060] \times 10^6 \text{ in.-lb.} \\ &= 0.654 \times 10^6 \text{ in.-lb.} \end{aligned}$$

6.5.4 Peak forces for Top Container Fins

a) For container fins (0.375 in. thick)

1. [height of fin/thickness of fin] = $6/0.375 = 16$
2. Fin loading angle = $5^\circ, 15^\circ, 25^\circ$

- 3.1 For fins 5,6 with Fin loading angle = 5°, Unit peak force $P_1 = 25,000$ lb. per in of loaded length per fin (see Figure 2.10.9-F7.3). (5°)
- 3.2 For fins 4,7 with Fin loading angle = 15°, Unit peak force $P_2 = 25,000$ lb. per in of loaded length per fin (see Figures 2.10.9-F7.2 and 2.10.9-F7.3).(15°)
- 3.3 For fins 3,8 with Fin loading angle = 25°, Unit peak force $P_3 = 8,000$ lb. per in of loaded length per fin (see Figures 2.10.9-F7.2 and 2.10.9-F7.3).(25°)
4. Loaded length of the fin = 13.8 in.
5. Total peak force experienced by the package due to impact of the 0.375 in. thick top fins of the container;

$$\begin{aligned}
 \Sigma FP_{0.375 \text{ FINS, CONTAINER}} &= \text{loaded length} \times \Sigma [\text{unit peak force} \times \text{number of fins}] \\
 &= 13.8 \times [2 \times P_1 + 2 \times P_2 + 2 \times P_3] \\
 &= 13.8 \times [2 \times 25,000 + 2 \times 25,000 + 2 \times 8,000] \\
 &= 13.8 \times [116,000] \\
 &= 1.6 \times 10^6 \text{ lb.}
 \end{aligned}$$

6.5.5 Summarize 3rd Stage

Energy absorbed:

$$\begin{aligned}
 EA_{\text{crush shield fins}} &= 1.174 \times 10^6 \text{ in.-lb.} \\
 EA_{\text{container fins}} &= 0.654 \times 10^6 \text{ in.-lb.} \\
 EA_{\text{3rd stage}} &= 1.828 \times 10^6 \text{ in.-lb.}
 \end{aligned}$$

Peak forces:

$$\begin{aligned}
 \Sigma FP_{\text{CRUSH SHIELD}} &= 1.057 \times 10^6 \text{ lb.} \\
 \Sigma FP_{0.375 \text{ FINS, CONTAINER}} &= 1.6 \times 10^6 \text{ lb.} \\
 \Sigma FP_{\text{3rd stage}} &= 2.657 \times 10^6 \text{ lb.}
 \end{aligned}$$

6.6 ENERGY ABSORPTION, G-LOADS FOR 4TH STAGE

There are two (2) energy absorption structural elements. These are:

1. A bottom/side sector of the cylindrical fireshield
2. A bottom/side sector of the container external cooling fins.

Both shall be considered herein.

6.6.1 Energy Absorption by External Cooling Fins on the Container

See Figure 2.10.9-F34.

i) Fins #5 and #6 Parameters

- Effective height, $h = 4$ in.
- Thickness, $t = 0.375$ in.
- Loaded length, $b = 32$ in.
- material = ss304L
- % of crush = 30%
- loading angle = 5° (angle of inclination to the unyielding surface)

Therefore, at crush of 30%, for fin height of 4 in., from Figures 2.10.9-F6.1 and 2.10.9-F6.2, the parameter [absorbed energy/plastic moment], $N = 16$

$$\begin{aligned}
 EA_{\text{FINS}\#5,6} &= 2 \times N \times M_p \\
 &= 2 \times 16 \times [\sigma_Y \times b \times t^2 / 4] \\
 &= 2 \times 16 \times [25,000 \times 32 \times (0.375)^2 / 4] \\
 &= 0.9 \times 10^6 \text{ in.-lb.}
 \end{aligned}$$

ii) Fins #4 and #7

- Effective height, $h = 4$ in.
- Thickness, $t = 0.375$ in.
- Loaded length, $b = 32$ in.
- material = ss304L
- % of crush = 30%
- loading angle = 15° (angle of inclination to the unyielding surface)

Therefore, at crush of 30%, for fin height of 4 in., fin inclination angle of 15° , from Figures 2.10.9-F6.2 and 2.10.9-F6.3, the parameter [absorbed energy/plastic moment], $N = 10$

$$\begin{aligned}
 EA_{\text{FINS}\#4,7} &= 2 \times N \times \sigma_Y \times b \times t^2 / 4 \\
 &= 2 \times 10 \times 25,000 \times 32 \times (0.375)^2 / 4 \\
 &= 2 \times 0.281 \times 10^6 \\
 &= 0.562 \times 10^6 \text{ in.-lb.}
 \end{aligned}$$

iii) Fins #3 and #8

- Effective height, $h = 4$ in.
- Thickness, $t = 0.375$ in.
- Loaded length, $b = 32$ in.
- material = ss304L
- % of crush = 30%
- loading angle = 25° (angle of inclination to the unyielding surface)

Therefore, at crush of 30%, for fin height of 4 in., fin inclination angle of 25° , from Figures 2.10.9-F6.2 and 2.10.9-F6.3, the parameter [absorbed energy/plastic moment], $N = 3.5$

$$\begin{aligned}
 EA_{\text{FINS}\#3,8} &= 2 \times N \times \sigma_Y \times b \times t^2 / 4 \\
 &= 2 \times 3.5 \times 25,000 \times 32 \times (0.375)^2 / 4 \\
 &= 2 \times 0.098 \times 10^6 \\
 &= 0.196 \times 10^6 \text{ in.-lb.}
 \end{aligned}$$

Cumulative energy absorbed by external cooling fins

$$\begin{aligned}
 \Sigma EA_{\text{FINS}} &= EA_{\text{FINS}\#5,6} + EA_{\text{FINS}\#4,7} + EA_{\text{FINS}\#3,8} \\
 &= (0.900 + 0.562 + 0.196) \times 10^6 \text{ in.-lb.} \\
 &= 1.658 \times 10^6 \text{ in.-lb.}
 \end{aligned}$$

6.6.2 Peak forces for Side Container Fins

a) For container fins (0.375 in. thick)

1. [height of fin/thickness of fin] = $4/0.375 = 10.7$
2. Fin loading angle = $5^\circ, 15^\circ, 25^\circ$
- 3.1 For fins 5,6 with Fin loading angle = 5° , Unit peak force $P_1 = 60,000$ lb. per in of loaded length per fin (see Figures 2.10.9-F7.1 and 2.10.9-F7.2) (5°)
- 3.2 For fins 4,7 with Fin loading angle = 15° , Unit peak force $P_2 = 40,000$ lb. per in of loaded length per fin (see Figures 2.10.9-F7.2 and 2.10.9-F7.3) (15°)

- 3.3 For fins 3,8 with Fin loading angle = 24.5°, Unit peak force $P_3 = 13,000$ lb. per inch of loaded length per fin (see Figures 2.10.9-F7.2 and 2.10.9-F7.3) (25°)
4. Loaded length of the fin = 32 in.
5. Total peak force experienced by the package due to impact of the 0.375 in. thick top fins of the container.

$$\begin{aligned}\Sigma FP_{0.375 \text{ FINS, CONTAINER}} &= \text{loaded length} \times \Sigma[\text{unit peak force} \times \text{number of fins}] \\ &= 32 \times [2 \times P_1 + 2 \times P_2 + 2 \times P_3] \\ &= 32 \times [2 \times 60,000 + 2 \times 40,000 + 2 \times 13,000] \\ &= 32 \times [226,000] \\ &= 7.232 \times 10^6 \text{ lb.}\end{aligned}$$

6.6.3 Energy Absorbed by the Cylindrical Fireshield

In the third stage of the impact we had neglected to estimate the energy absorbed by the cylindrical fireshield. In the fourth stage, the cylindrical fireshield side is impacted. 3rd and 4th stage impacts of the fireshield shall be combined and analyzed here (see Figure 2.10.9-F35). A cylindrical fireshield is a cylindrical shell which is deformed by some amount in the side impact. A simple model is given here:

Step 1

The radius R_0 decreases to R_i .

$$\begin{aligned}\text{the strain is } \epsilon &= [R_0 - R_i] / R_0 \\ &= \Delta / R_0\end{aligned}$$

Step 2

The stress, σ = function (ϵ)

Step 3

The compressive stress $\sigma_c = 1.6 \times \sigma$

Step 4

The crushed area $A_{\text{crush}} = L \times c$

$$c = 2 [\Delta (2R_0 - \Delta)]^{0.5}$$

Therefore

$$\begin{aligned}A_{\text{crush}} &= L \times c \\ A_{\text{crush}} &= L \times 2 [\Delta (2R_0 - \Delta)]^{0.5}\end{aligned}$$

Step 5

Mean crushed area $A_{\text{mean crush}} = A_{\text{crush}} / 2$

Step 6

Mean Impact force, $F_c = \sigma_c \times A_{\text{mean crush}}$

Step 7

Work done, $U = F_c \times \Delta$

Step 8

$$G\text{-load} = F_c / W_{F-294 \text{ LESS SKID}}$$

Plugging in the data:

$$\begin{aligned}\Delta &= 0.1 \text{ in.} \\ R_0 &= 23.75 \text{ in.} \\ L &= 30.0 \text{ in.} \\ \sigma &= 32,000 + [23,000/20] \times \epsilon(\%) \end{aligned}$$

we find

$$\begin{aligned}\epsilon &= 0.1/23.75 = 0.00421 \\ \sigma &= 32,000 + [23,000/20] \times \epsilon(\%) \\ &= 32,000 + [23,000/20] \times 0.421 \\ &= 32,000 + 484 \\ &= 32,484 \text{ psi} \\ \sigma_c &= 1.6 \times \sigma \\ &= 1.6 \times 32,484 \text{ psi} \\ &= 51,974 \text{ psi} \\ c &= 2 [\Delta (2R_0 - \Delta)]^{0.5} \\ &= 2 [0.1 (2 \times 23.75 - 0.1)]^{0.5} \\ &= 4.35 \text{ in.} \\ L &= 30 \text{ in.} \\ A_{\text{crush}} &= L \times c \\ &= 30. \times 4.35 \\ &= 130.5 \text{ in}^2 \\ A_{\text{mean crush}} &= A_{\text{crush}} / 2 \\ &= 130.5/2 \\ &= 65.35 \text{ in}^2 \end{aligned}$$

Mean Impact force

$$\begin{aligned}F_c &= \sigma_c \times A_{\text{mean crush}} \\ &= 51,974 \text{ psi} \times 65.25 \\ &= 3.391 \times 10^6 \text{ lb.} \end{aligned}$$

Work done

$$\begin{aligned}U &= F_c \times \Delta \\ &= 3.391 \times 10^6 \text{ lb.} \times 0.1 \text{ in.} \\ &= 0.339 \times 10^6 \text{ in.-lb.} \end{aligned}$$

Hence, it is estimated that for a small deformation of 0.1 in. over a length of 30 in., the energy absorbed by the cylinder is 0.339×10^6 in.-lb.

6.6.4 Summarize 4th Stage

Energy absorbed:

$$\begin{aligned} EA_{\text{container side fins}} &= 1.658 \times 10^6 \text{ in.-lb.} \\ EA_{\text{cylindrical fireshield}} &= 0.339 \times 10^6 \text{ in.-lb.} \\ EA_{\text{4th stage}} &= 1.997 \times 10^6 \text{ in.-lb.} \end{aligned}$$

Peak forces:

$$\begin{aligned} FP_{\text{container side fins}} &= 7.232 \times 10^6 \text{ lb.} \\ \Sigma FP_{\text{cylindrical fireshield}} &= 3.391 \times 10^6 \text{ lb.} \\ \Sigma FP_{\text{4th stage}} &= 10.623 \times 10^6 \text{ lb.} \end{aligned}$$

6.7 ENERGY ABSORBED BY CASK SHELL AND LEAD ESTIMATE OF LEAD MOVEMENT OR SLUMP

When the container without the fins is approximated to a cylindrical cask with flat end plates dropped in side drop orientation, the container will absorb energy upon impact in three ways:

1. by deformation of end plates
2. by movement of lead
3. by deformation of cylindrical outer shell.

A relatively small amount of energy is absorbed in bending the steel shell at the point of impact and is therefore neglected in this analysis. Such a model is presented in Figure 2.10.9-F16.

Shappert [Ref. [8], page 59] has provided a method of estimating the amount of lead movement for such a cask. We shall apply formula as per Ref. [8], page 59 to estimate lead movement in the F-294 container. It should be noted that 92.8% of the energy absorption has been accounted for (see section 6.10); consequently, it is required to consider only the remaining 7.2% of the potential energy due to 30-ft height of the package. However, for 7.2% factor shall be increased to say 10% of 30-ft drop height energy to provide a conservative estimate of the lead slump.

The formula is:

$$WH/t_s R L \sigma_s = [F_1(\theta)][R/t_s(\sigma_{pb}/\sigma_s) + 2(R/L)(t_e/t_s)] + F_2(\theta)$$

where

$$\begin{aligned} W &= \text{effective cask weight} = 21,000 \text{ lb.} - W_{\text{skid}} = 21,000 - 980 = 20,020 \text{ lb.} \\ H &= \text{effective drop height} = 10\% \text{ of } 30 \text{ feet} = 36 \text{ in.} \\ F_1(\theta) &= \theta - 1/2(\sin 2\theta) \\ F_2(\theta) &= \sin \theta (2 - \cos \theta) - \theta \\ R &= \text{the outer shell radius} = 18 \text{ in.} \\ t_s &= \text{the outer shell thickness} = 0.5 \text{ in.} \\ L &= \text{length of the shell} = 50.25 - 6.0 = 44.25 \text{ in.} \\ \sigma_s &= \text{the dynamic flow stress of ss304 shell, psi} = 50,000 \text{ psi} \\ \sigma_{pb} &= \text{the dynamic flow stress in lead} = 5000 \text{ psi} \\ t_e &= \text{thickness of ss304 end plate} = 0.5 \text{ in.} \\ \theta &= \text{the angle defined in Figure 2.7.1.2-ii)-F12, degrees} \end{aligned}$$

The above formula is based on assumptions that the yield point stress of the ss304 end piece is the same as that of the ss304 shell and that the end pieces are of equal thickness. In order to use the above formula, the angle θ and the cask geometry must be known. The angle θ may be determined from Figure 2.10.9-F17 (reproduced from Ref. [8], Shappert, Page 61), which is based on the above formula. The maximum displacement of shielding represented by the outer shell flattening, δ , may be calculated by $\delta = R(1 - \cos \theta)$

Calculate Non-dimensional Resistance Parameter #1.

$$\begin{aligned} & [R/t_s(\sigma_{Pt}/\sigma_s) + 2(R/L)(t_s/t_s)] \\ & [18/0.5(5,000/5,000) + 2(18/44.25)(0.5/0.5)] \\ & [3.6 + 0.8135] \\ & [4.4135] \end{aligned}$$

Calculate Non-dimensional Energy Parameter #2.

$$\begin{aligned} & [WH/t_sRL\sigma_s] \\ & [20020 \times 36 / (0.5 \times 18 \times 44.25 \times 50000)] \\ & [0.0362] \end{aligned}$$

Use nomograph as per Figure 2.10.9-F17, with parameter #1 = 4.4135 and parameter #2 = 0.0362. Connect the line between the two parameters and read the value of $\theta = 13^\circ$

See Figure 2.10.9-F18.

$$\begin{aligned} \delta &= R(1 - \cos\theta) \\ \delta &= 18(1 - \cos(13^\circ)) \\ \delta &= 18(1 - 0.974) \\ \delta &= .461 \text{ in.} \end{aligned}$$

Now $\delta = t_s + \Delta_{\text{lead}}$

where

$$\begin{aligned} t_s &= \text{thickness of flattened ss304 shell} = 0.5 \\ \Delta_{\text{lead}} &= \text{amount of lead shielding displaced} \\ \Delta_{\text{lead}} &= \delta - t_s \\ &= 0.461 - 0.5 \\ &= -0.039 \text{ in.} \end{aligned}$$

To summarize, in the bottom corner drop orientation, it is estimated that the amount of lead shielding displaced in the F-294 container is zero in.

6.8 SUMMARY OF ENERGY BALANCE AND PEAK FORCES IN BOTTOM CORNER DROP

Energy balance.

1st Stage

$$EA_{\text{1st stage}} = 3.198 \times 10^6 \text{ in.-lb.} = 42.3\%$$

3rd Stage

$$\begin{aligned} EA_{\text{crush shield fins}} &= 1.174 \times 10^6 \text{ in.-lb.} = 15.5\% \\ EA_{\text{container fins}} &= 0.654 \times 10^6 \text{ in.-lb.} = 8.6\% \\ EA_{\text{cyl. fireshield}} &= \text{not accounted for} \end{aligned}$$

4th Stage

$$\begin{aligned} EA_{\text{container fins}} &= 1.658 \times 10^6 \text{ in.-lb.} = 21.9\% \\ EA_{\text{cyl. fireshield}} &= 0.339 \times 10^6 \text{ in.-lb.} = 4.4\% \end{aligned}$$

Total energy absorbed so far = 7.02×10^6 in.-lb. = 92.8%
% absorbed = $7.02 \times 10^6 / 7.56 \times 10^6 = 92.8\%$
% not absorbed = 7.2%

The 7.2% of 30-ft drop energy shall be taken up by the cask shell and lead. 10% of 30-ft drop energy is shown to be absorbed by the cask shell and lead. This is presented in section 6.9.

Peak forces and G-loads

1st stage: Peak force = 6.09×10^6 lb., G-load = 290 g's.
3rd stage: Peak force = 2.08×10^6 lb., G-load = 104 g's.
4th stage: Peak force = 10.623×10^6 lb., G-load = 530 g's

Displacements

In the 4th stage, the cask absorbs some energy ; however there is no lead slump as most of the energy appears to be absorbed in the cask stainless steel shell.

**Figure 2.10.9-F31
Bottom Corner Drop: Mode of Impact**

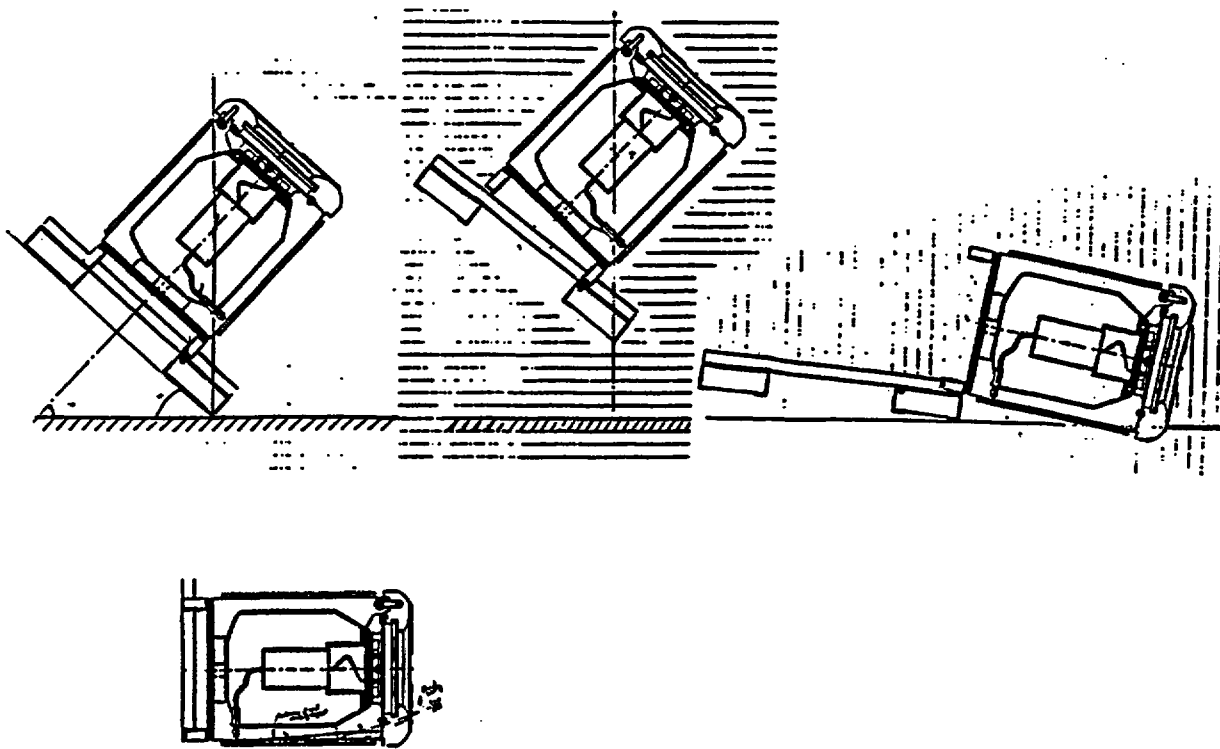


Figure 2.10.9-F32
Bottom Corner Drop: Representative Fin Parameters

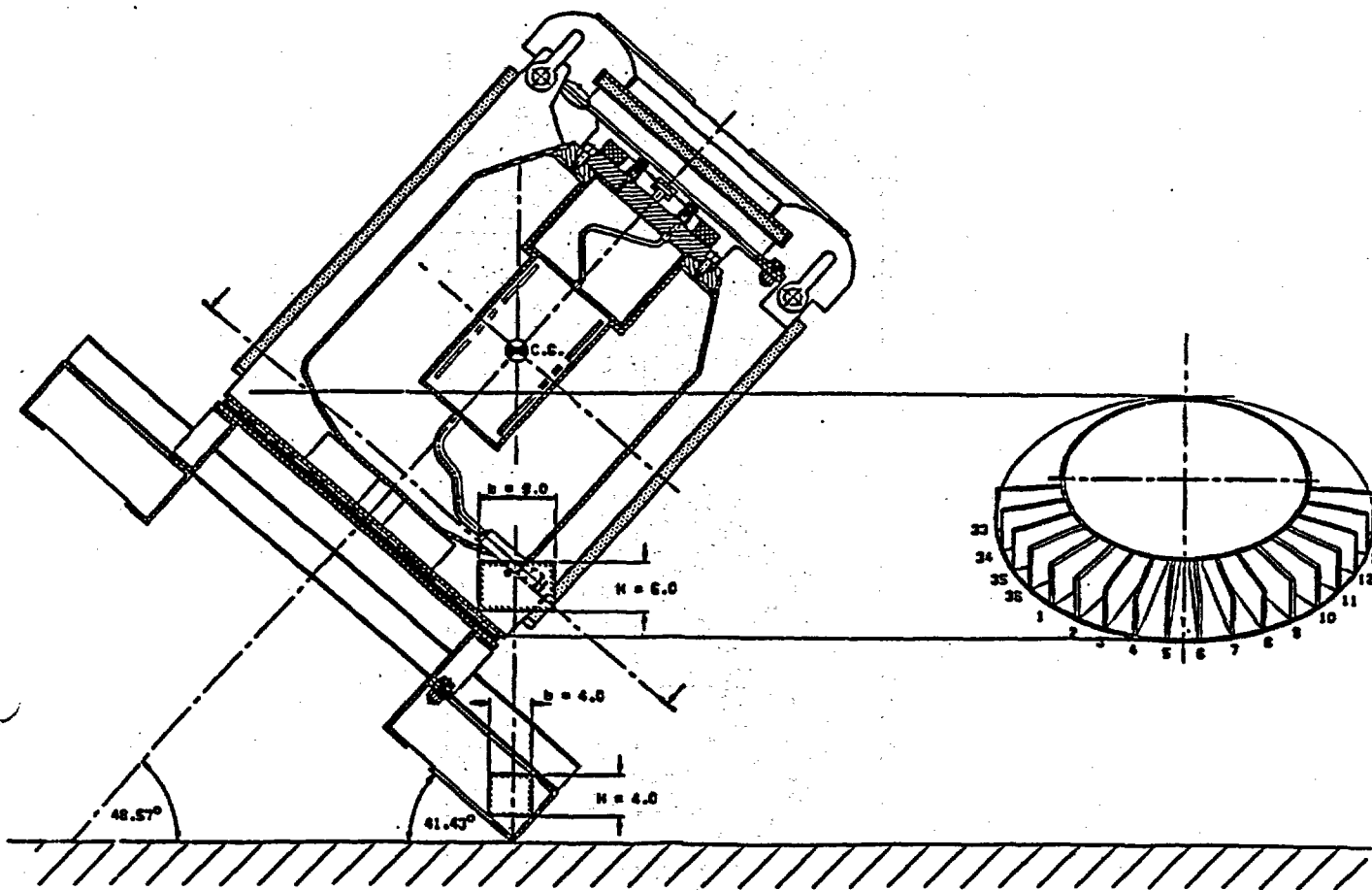


Figure 2.10.9-F33
Bottom Corner Drop: 3rd Stage Impact: Representative Fin Parameters

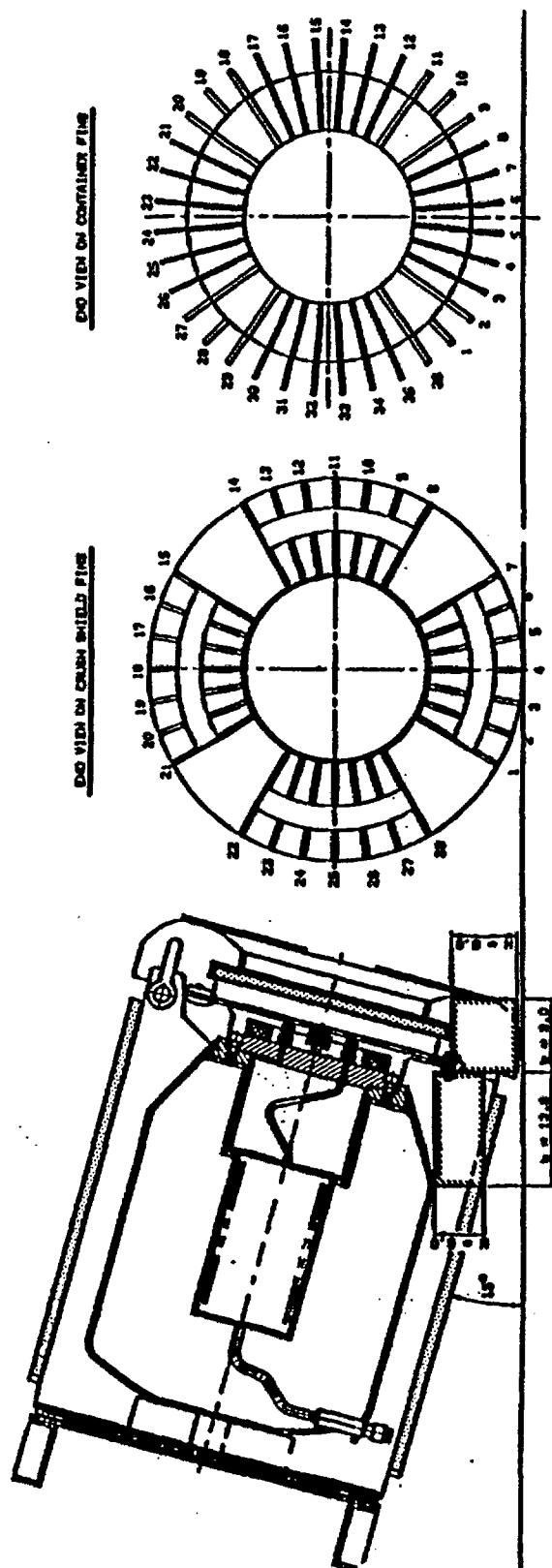


Figure 2.10.9-F34
Bottom Corner Drop: 4th Stage Impact: Container Side Fins

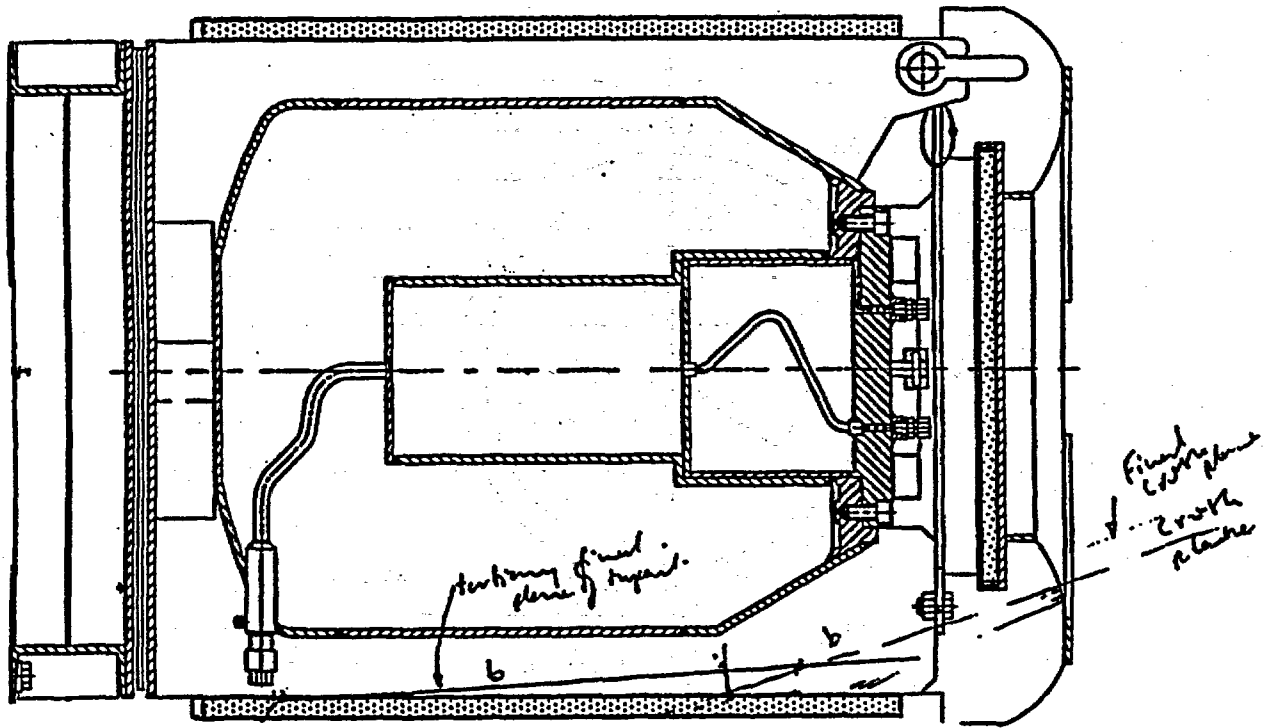
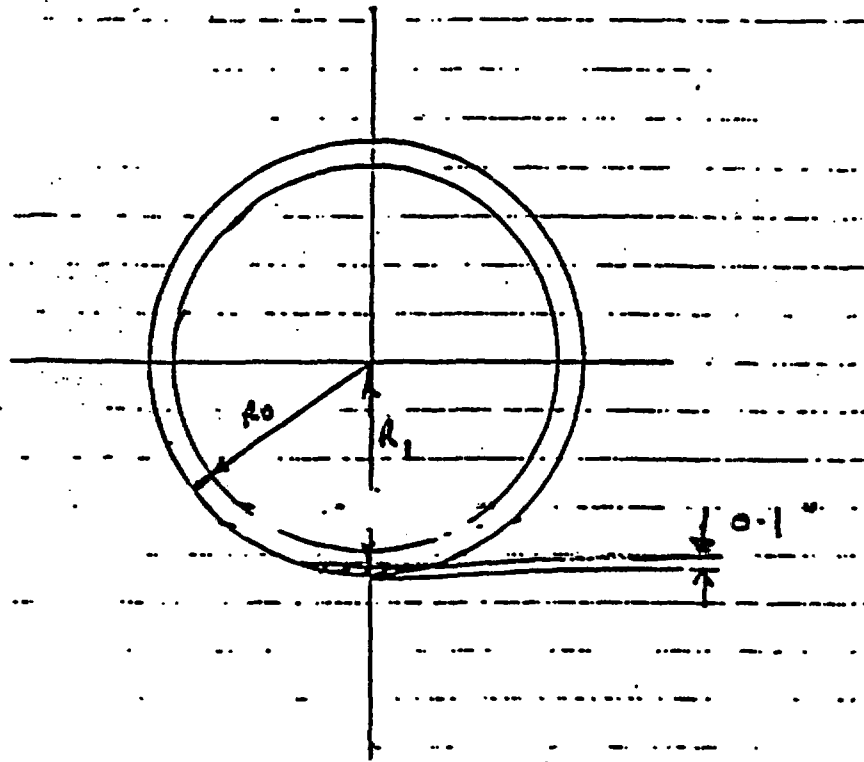


Figure 2.10.9-F35
Bottom Corner Drop: 4th Stage Impact: Cylindrical Fireshield Impact



7. BOTTOM END DROP

7.1 MODE OF IMPACT

See Figure 2.10.9-F36

The shipping skid will impact the unyielding surface first. The four 8 x 3 channels will crush. The shipping skid will also deform like a dish.

7.2 ENERGY ABSORPTION CONTRIBUTION BY FOUR CHANNELS OF THE SHIPPING SKID

7.2.1 Energy Absorbed by the Webs of the Channels

Fin Parameters (see Figure 2.10.9-F37).

- Effective original height, $h = 8$ in. (8-inch web of the 8 x 3 channel)
- Thickness, $t = 0.43$ in.
- Loaded length, $b = 78$ in.
- material = ASTM A-36
- % of crush = 22.5%
- loading angle = 0° (angle of inclination to the unyielding surface)

$$EA = N \times M_p$$

where

$$N = \frac{[(\text{Absorbed Energy})/(\text{Plastic Moment})]}{= 11 \text{ (Figure 2.10.9-F6.1, at 8 in., 22.5\%)}}$$

$$M_p = \text{plastic moment}$$

$$= \sigma_y * bt^2 / 4$$

$$= 36,000 \times 78 \times (0.43)^2 / 4$$

$$= 129,800 \text{ in.-lb.}$$

where

$$\sigma_y = \text{yield stress of A-36} = 36,000 \text{ psi}$$

$$b = \text{loaded length of the fin}$$

$$t = \text{fin thickness}$$

Therefore

$$EA = 11 \times 129,800 \text{ in.-lb.}$$

$$= 1.427 \times 10^6 \text{ in.-lb. per fin.}$$

As there are four channels, therefore there are 4, 0.43 in. thick fins. Therefore, energy absorbed by 4, 0.43 in. thick fins is

$$EA_{\text{channels}} = 4 \times 1.427 \text{ in.-lb.}$$

$$= 5.7 \times 10^6 \text{ in.-lb.}$$

7.3 ENERGY ABSORPTION CONTRIBUTION BY EIGHT GUSSETS OF THE SHIPPING SKID

7.3.1 Energy Absorbed by the Gussets of the Shipping Skid

Fin Parameters (see Figure 2.10.9-F37).

- Effective original height, $h = 8$ in. (8 in. web of the 8 x 3 channel)
- Thickness, $t = 0.75$ in.
- Loaded length, $b = 3 + 3 = 6$ in. per gusset
- material = ASTM A-36
- % of crush = 10%
- loading angle = 0° (angle of inclination to the unyielding surface)

$$EA = N \times M_p$$

where

$$N = \frac{[(\text{Absorbed Energy})/(\text{Plastic Moment})]}{= 9 \text{ (Figure 2.10.9-F6.1, at 8 in., 10\%)}}$$

$$M_p = \text{plastic moment}$$

$$= \sigma_y * bt^2 / 4$$

$$= 36,000 \times 6 \times (0.75)^2 / 4$$

$$= 30,375 \text{ in.-lb.}$$

where

$$\sigma_y = \text{yield stress of A-36} = 36,000 \text{ psi}$$

$$b = \text{loaded length of the fin}$$

$$t = \text{fin thickness}$$

Therefore

$$EA = 9 \times 30,375 \text{ in.-lb.}$$

$$= 273 \times 10^6 \text{ in.-lb. per gusset fin.}$$

As there are eight gussets, therefore, there are 8, 0.75 in. thick fins. Therefore, energy absorbed by eight, 0.75 in. thick fins is

$$EA_{\text{gussets}} = 8 \times 0.273 \times 10^6 \text{ in.-lb.}$$

$$= 2.187 \times 10^6 \text{ in.-lb.}$$

7.4 ENERGY ABSORBED BY THE SHIPPING SKID ALONE

$$EA_{\text{channels}} = 5.7 \times 10^6 \text{ in.-lb.}$$

$$EA_{\text{gussets}} = 2.187 \times 10^6 \text{ in.-lb.}$$

$$EA_{\text{shipping skid}} = 7.887 \times 10^6 \text{ in.-lb.}$$

Hence, the shipping skid, by itself, is capable of absorbing 7.887×10^6 in.-lb./ 7.56×10^6 in.-lb. = 104% of the 30-ft drop energy in the bottom end drop orientation. The skid channels, 8 x 3 will crush by a distance of 22.5% x 8 in. = 1.8 in.

7.5 ESTIMATE OF PEAK FORCES AND G-LOADS

Peak forces evaluated using DAVIS method (Ref. [18])

- a) for shipping skid fins (channel web) (0.5 in. thick)
1. [height of fin/thickness of fin] = $8/0.5 = 16$
 2. Unit peak force $P_1 = 12,500$ lb. per in of loaded length per fin (see Figure 2.10.9-F7.1).
 3. $FP_1 = \text{Unit peak force} \times \text{loaded length per fin} \times \text{number of fins loaded at } 0^\circ$
 $= 12,500 \times 78 \times 4$
 $= 3.9 \times 10^6$ lb.
- b) for shipping skid fins (gusset) (0.75 in. thick)
1. [height of fin/thickness of fin] = $8/0.75 = 10.6$
 2. Unit peak force $P_1 = 75,000$ lb. per in of loaded length per fin (see Figure 2.10.9-F7.1).
 3. $FP_2 = \text{Unit peak force} \times \text{loaded length per fin} \times \text{number of fins loaded at } 0^\circ$
 $= 75,000 \times 6 \times 8$
 $= 3.6 \times 10^6$ lb.

Total Peak force

$$\begin{aligned} FP_{\text{shipping skid}} &= FP_1 + FP_2 \\ &= 3.9 \times 10^6 + 3.6 \times 10^6 \text{ lb.} \\ &= 7.5 \times 10^6 \text{ lb.} \end{aligned}$$

Estimated G-load

$$\begin{aligned} \text{G-load} &= FP_{\text{shipping skid}} / W_{F-294} \\ &= 7.5 \times 10^6 / 21,000 \\ &= 357 \text{ g's} \end{aligned}$$

Therefore in the bottom end drop, the G-load is 357 g's.

7.6 SUMMARY FOR BOTTOM END DROP

1. Hence the shipping skid, by itself, is capable of absorbing 7.887×10^6 in.-lb./ 7.56×10^6 in.-lb. = 104% of the 30-ft drop energy in the bottom end drop orientation.
2. The skid channels, 8 x 3 will crush by a distance of 22.5% x 8 in. = 1.8 in.
3. In the bottom end drop, the G-load 357 g's at the impact point.

Figure 2.10.9-F36
F-294: Bottom End Drop Orientation

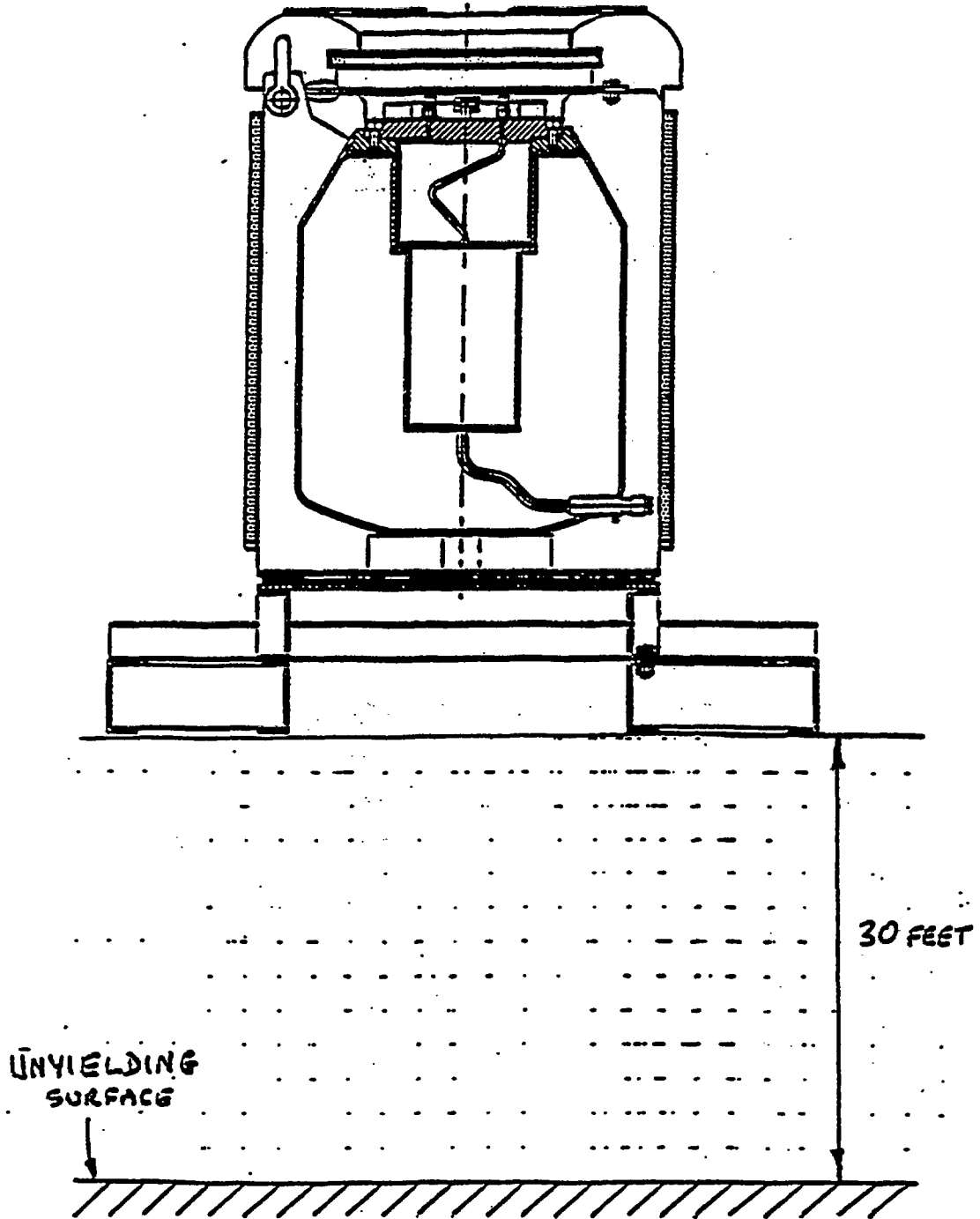
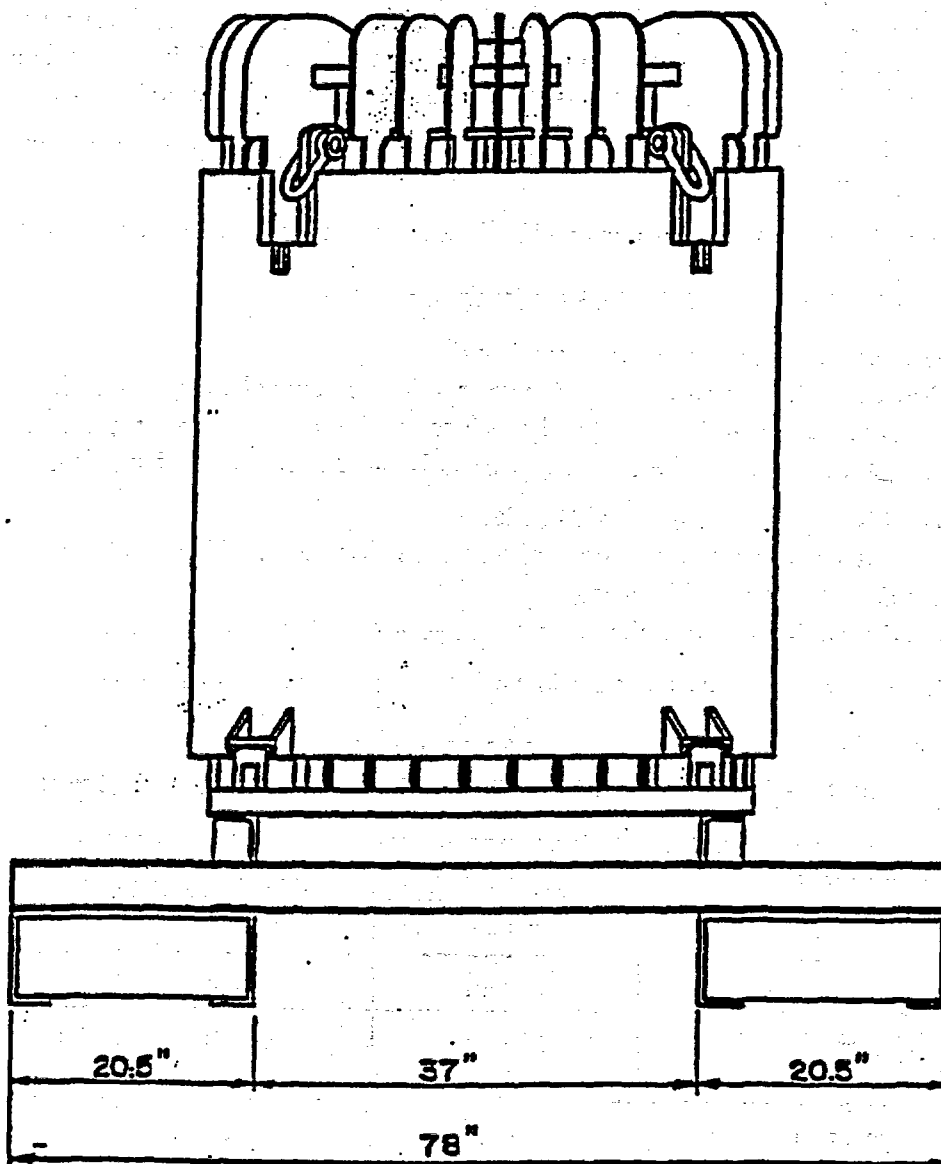


Figure 2.10.9-F37
Bottom End Drop Orientation: Geometrical Data for Fins



8. TRANSNUCLEAIRE DATA FROM REF. [37] WITH REFERENCE TO 15-TON DUPONT CASK DROP DATA

8.1 MEASUREMENTS MADE ON A 15-TON PACKAGING

The packaging used was a 15-ton Dupont de Nemours packaging which has been the subject of a large number of drop tests. Table 15 is reproduced from a Table contained in Ref. [39] summarizing the measurements of deceleration at various points in the packaging, for various drop heights.

These results clearly show that, during an impact, deceleration varies according to the height of the point considered in the packaging.

They also show that the deceleration varies roughly linearly as a function of the height of the drop.

8.2 APPLICATION OF THIS TEST DATA TO F-294

Based on this data, the following two inferences are drawn.

1. The G-loads at locations away from the impact face are considerably reduced.
2. For the same weight of the package, the G-load resulting from a free drop is a function of drop height. For example the G-load at 1 m. is 10%-12.5% of G-load at 9.1m.

For application of this drop test data to the F-294 package.

1. At distances 100 cm. from the impact face, a reduction factor of 0.66 x G-loads at the impact face shall be used for F-294 package.
2. For free drop at 3-foot drop, the $G\text{-load}_{3\text{-FOOT DROP}} = 20\% \times G\text{-load}_{30\text{-ft DROP}}$.

The factor of 20% is far more conservative than the test data factor of 10% - 12.5%.

Table 2.10.9-T15
Drop Test Data for 15-Ton Dupont Packaging from Transnucleaire Ref. [37]

Test number	1	2	3
Drop height	2.30m	4.50 m	9.10 m
Impact surface	bottom	bottom	bottom
Deceleration on bottom (25 cm from impact face)	320 g's	750 g's	1200 g's - 1500 g's
Deceleration at upper part (120 cm from the impact face)	140 g's	250 g's	?

9. SPECIAL ISSUES

9.1 CRUSH SHIELD RETENTION DURING 30-FT DROP

Step 1

The crush shield is fastened to the container as follows:

1. Quantity = 8, fasteners at top, connecting crush shield to the container top fins bracket.
The size of the fasteners is: 1 in. dia. x 2.5 in. long, SAE Gr. 8.
2. Quantity = 8, fasteners at side, connecting crush shield fins to the container side fins.
The size of the fasteners is: 1 in. dia. x 2.5 in. long, SAE Gr. 8.

Step 2

The weight of the crush shield is $W_{\text{CRUSH SHIELD}} = 730 \text{ lb.}$

Step 3

Static load-carrying capability of the fasteners.

Step 3.1

For top end, top corner, bottom end drop orientations, out of 16 fasteners, 8 are in tension and the remaining 8 are in shear.

#1. 8 bolts in tension:

$$\begin{aligned} P_1 &= \text{No. of bolts} \times \text{UTS} \times \text{Stress Area} \\ &= 8 \times 150,000 \text{ psi} \times 0.551 \text{ in}^2 \\ &= 661,200 \text{ lb.} \end{aligned}$$

#2. 8 bolts in shear:

$$\begin{aligned} P_2 &= \text{No. of bolts} \times \text{UTS in shear} \times \text{Stress Area} \\ &= 8 \times 0.6 \times 150,000 \text{ psi} \times 0.551 \text{ in}^2 \\ &= 396,720 \text{ lb.} \end{aligned}$$

Total load capability static based, $P_{\text{STATIC-BASED}}$

$$\begin{aligned} &= P_1 + P_2 \\ &= 661,200 + 396,720 \text{ lb.} \\ &= 1,057,920 \text{ lb.} \end{aligned}$$

Step 3.2

For side drop #1, side drop #2, bottom corner drop orientations, out of 16 fasteners, all 16 are in shear.

#2. 16, bolts in shear:

$$\begin{aligned} P_1 &= \text{No. of bolts} \times \text{UTS in shear} \times \text{Stress Area} \\ &= 16 \times 0.6 \times 150,000 \text{ psi} \times 0.551 \text{ in}^2 \\ &= 396,720 \text{ lb.} \\ &= 793,440 \text{ lb.} \end{aligned}$$

Total load capability static based, $P_{\text{STATIC-BASED}}$

$$\begin{aligned} &= P_1 \\ &= 793,440 \text{ lb.} \end{aligned}$$

Step 4

G-load carrying capability based on static UTS consideration.

Step 4.1

For top end, top corner, bottom end drop orientations,

$$\begin{aligned} \text{G-load}_{\text{STATIC-BASED}} &= P_{\text{STATIC-BASED}} / W_{\text{CRUSH SHIELD}} \\ &= 1,057,920 / 730 \\ &= 1,449 \text{ g's} \end{aligned}$$

Step 4.2

For side drop #1, side drop #2, bottom corner drop orientations,

$$\begin{aligned} \text{G-load}_{\text{STATIC-BASED}} &= P_{\text{STATIC-BASED}} / W_{\text{CRUSH SHIELD}} \\ &= 793,440 / 730 \\ &= 1,086 \text{ g's} \end{aligned}$$

Step 5

What G-loads are estimated for various drop test orientations?

At the impact point,

top end drop	G-load = 200 g's
side drop #1	G-load = 520 g's
side drop #2	G-load = 500 g's
top corner drop	G-load = 338 g's
bottom corner drop	G-load = 530 g's
bottom end drop	G-load = 334 g's

Step 6

Compare the G-load capability of fasteners, on static basis to the G-loads calculated at the impact point for various drop test orientations.

Step 6.1

For *top end, top corner, and bottom end drop* orientations,

$$G\text{-load}_{\text{STATIC-BASED}} = 1,449 \text{ g's}$$

The maximum G-load sustained in above drop test orientations is 338 g's.

Safety factor: $G\text{-load capability}/G\text{-load sustained} = 1,449/338 = 4.28$

Therefore, all of the fasteners connecting the crush shield to the container shall not fail.

Step 6.2

For *side drop #1, side drop #2, bottom corner drop* orientations,

$$G\text{-load}_{\text{STATIC-BASED}} = 1,086 \text{ g's}$$

The maximum G-load sustained in above drop test orientations is 530 g's.

Safety factor: $G\text{-load capability}/G\text{-load sustained} = 1,086/530 = 2.04$

Therefore, all of the fasteners connecting the crush shield to the container shall not fail.

Step 7

As the dynamic UTS is 1.5 to 2 times the static UTS, there is additional factor of safety due to this consideration. Therefore it is concluded that the crush shield fasteners shall have the capability to retain the crushshield during the 30-ft drop in any orientation.

9.2 CYLINDRICAL FIRESHIELD RETENTION DURING 30-FT DROP TEST

See Figure 2.10.9.F38 illustrating how the cylindrical fireshield is fastened.

Step 1

The cylindrical fireshield is fastened to the container base plate as follows:

1. Quantity = 8, fasteners at bottom, connecting cylindrical fireshield bracket to the container skid top plate bracket. The size of the fasteners is: 1 in. dia. x 2.5 in. long, SAE Gr. 8.

Step 2

The weight of the fireshield is $W_{\text{CYLINDRICAL FIRESHIELD}} = 1,125 \text{ lb.}$

Step 3

Static Load carrying capability of the fasteners.

Step 3.1

For top end, top corner, bottom end drop orientations, all eight fasteners are in tension.

#1. 8, bolts in tension:

$$\begin{aligned} P_1 &= \text{No. of bolts} \times \text{UTS} \times \text{Stress Area} \\ &= 8 \times 150,000 \text{ psi} \times 0.551 \text{ in}^2 \\ &= 661,200 \text{ lb.} \end{aligned}$$

Total load capability static based, $P_{\text{STATIC-BASED}}$

$$\begin{aligned} &= P_1 \\ &= 661,200 \text{ lb.} \end{aligned}$$

Step 3.2

For side drop #1, side drop #2, bottom corner drop orientations, all 8 fasteners are in shear.

#2. 8, bolts in shear:

$$\begin{aligned} P_1 &= \text{No. of bolts} \times \text{UTS in shear} \times \text{Stress Area} \\ &= 8 \times 0.6 \times 150,000 \text{ psi} \times 0.551 \text{ in}^2 \\ &= 396,720 \text{ lb.} \end{aligned}$$

Total load capability static based, $P_{\text{STATIC-BASED}}$

$$\begin{aligned} &= P_1 \\ &= 396,720 \text{ lb.} \end{aligned}$$

Step 4

G-load carrying capability based on static UTS consideration.

Step 4.1

For top end, top corner, bottom end drop orientations,

$$\begin{aligned} \text{G-load}_{\text{STATIC-BASED}} &= P_{\text{STATIC-BASED}} / W_{\text{CRUSH SHIELD}} \\ &= 661,200 \text{ lb.} / 1,125 \\ &= 587 \text{ g's} \end{aligned}$$

Step 4.2

For side drop #1, side drop #2, bottom corner drop orientations,

$$\begin{aligned} \text{G-load}_{\text{STATIC-BASED}} &= P_{\text{STATIC-BASED}} / W_{\text{CRUSH SHIELD}} \\ &= 396,720 / 1,125 \\ &= 352 \text{ g's} \end{aligned}$$

Step 5

What G-loads are estimated for various drop test orientations?

At the impact point,

- top end drop G-load = 200 g's
- side drop #1 G-load = 520 g's
- side drop #2 G-load = 500 g's
- top corner drop G-load = 338 g's
- bottom corner drop G-load = 530 g's
- bottom end drop G-load = 334 g's

Step 6

Compare the G-load capability of fasteners, on static basis to the G-loads calculated at the impact point for various drop test orientations.

Step 6.1

For top end, top corner, bottom end drop orientations,

$$\text{G-load}_{\text{STATIC-BASED}} = 586 \text{ g's}$$

The maximum G-load sustained in above drop test orientations is 338 g's.

$$\text{Safety factor: G-load capability/G-load sustained} = 586/338 = 1.73$$

Therefore, all of the fasteners connecting the cylindrical fireshield to the container shall not fail.

Step 6.2

For side drop #1, side drop #2, bottom corner drop orientations,

$$\text{G-load}_{\text{STATIC-BASED}} = 330 \text{ g's}$$

The maximum G-load sustained in above drop test orientations is 530 g's.

$$\text{Safety factor: G-load capability/ G-load sustained} = 352/530 = 0.664$$

Therefore, some of the fasteners connecting the cylindrical fireshield to the container may appear to fail on static considerations alone.

The integrity of fasteners and cylindrical fireshield retention is further examined:

In the bottom corner drop, the fireshield shall be retained in position by any one of the four brackets on which the fireshield is mounted to the bottom fixed skid (see Figure 2.9.10-F38)

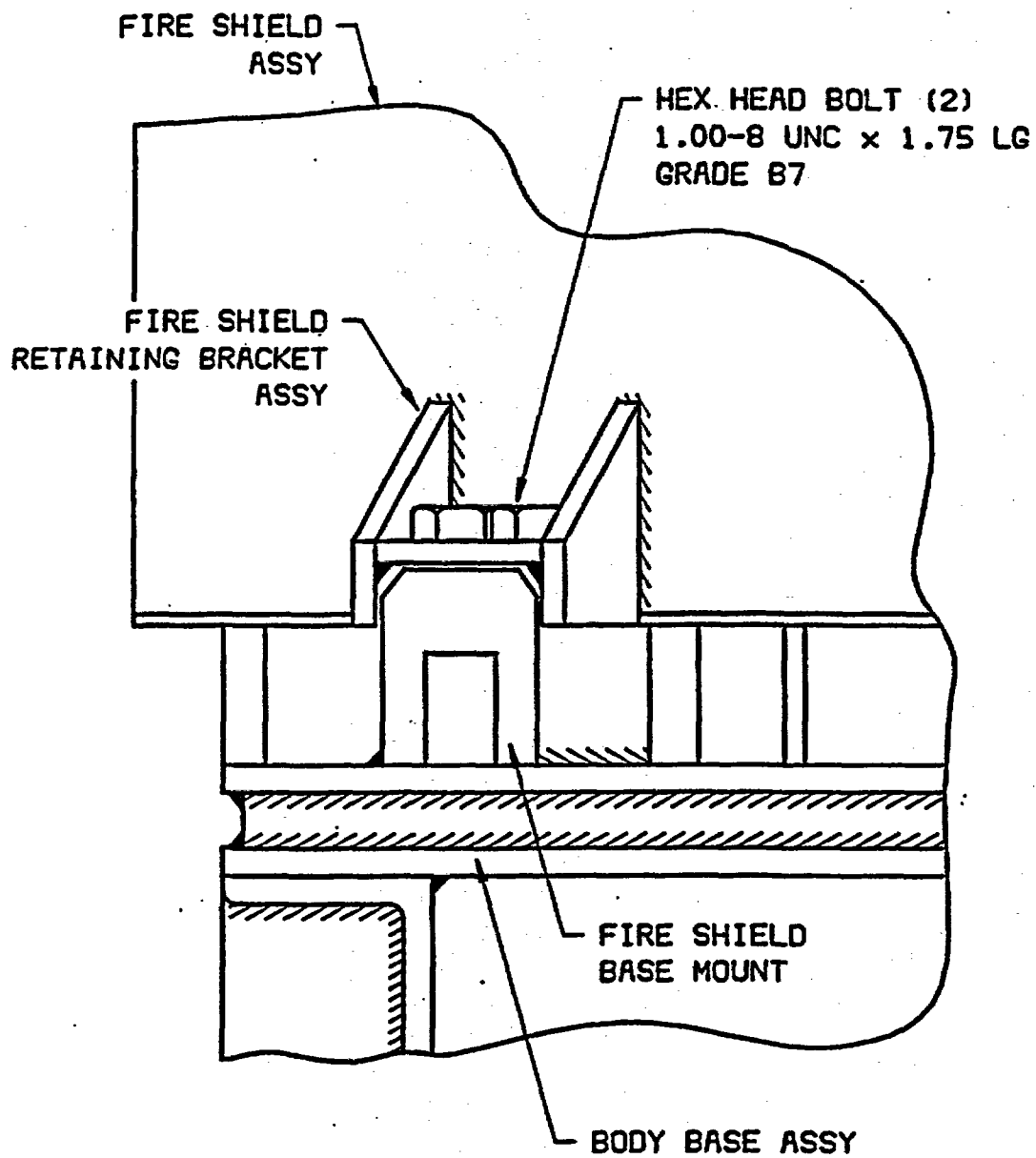
In the side drop, the fasteners may fail but the fireshield by virtue of its cylindrical shape is restrained in top (by the crush shield); in the bottom (by the fixed skid brackets) and around the circumference (by the container fins). Consequently the fireshield is trapped.

In addition, the fasteners share the impact load with the welds of the bracket. Consequently the impact load on the fasteners is marginally reduced. Also, out of four brackets, only two brackets are in the zone of impact, the remaining two brackets are outside the zone of impact.

Step 7

As the dynamic UTS is 1.5 to 2 times the static UTS, there is an additional factor of safety due to this consideration. Therefore, it is concluded that the fireshield fasteners shall have the capability to retain the fireshield during the 30-ft drop in top, top corner and bottom drop orientations. In the side drop # 1, side drop #2 and bottom corner drop orientations, some or all of the fireshield fasteners may fail; despite that, the cylindrical fireshield shall be retained due to the fact that it is trapped and redundancy (four separate connecting brackets).

Figure 2.10.9-F38
Fastening of the Cylindrical Fireshield to the Container Base



APPENDIX 2.10.10

CONTENTS

1. "UNBRAKO" BOLTING MATERIAL 3

2. "NEOPRENE" GASKET..... 5

3. TRANSNUCLEAIRE SELECTED REFERENCE PAGES..... 7

4. MDS NORDION METALLURGICAL REPORT NUMBER 9724 TYPE 316L STAINLESS STEEL
TIME/TEMPERATURE SENSITIZATION TESTING REPORT, JUNE 1998 (REFERENCE [59]) 9

5. IN/QA 1368 F294: TEST PLAN FOR F-294 REGULATORY TESTS (REFERENCE [48]) 11

6. IN/QA 1369 F294: QUALITY PLAN FOR F-294 REGULATORY TESTS (REFERENCE [49]) 13

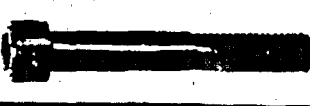
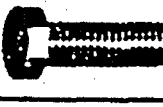
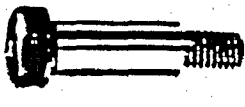
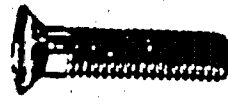
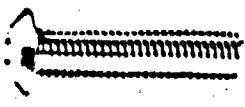
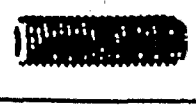
7. A-16485-TN-1 DECELERATION MEASUREMENTS DURING DROP TESTS OF AN
F-294 PACKAGING (REFERENCE [55]) 15

8. MDS NORDION F-294 TRANSPORT PACKAGING TESTING (REFERENCE [56])..... 17

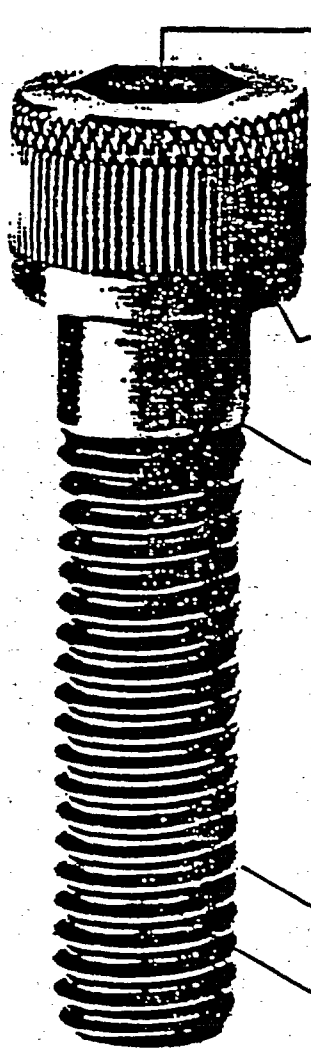
This page left blank intentionally.

1. "UNBRAKO" BOLTING MATERIAL

This page left blank intentionally.

TYPE	APPEARANCE	PERFORMANCE (See Note 1)			CAPABILITY (See Note 3)				STANDARDS (See Note 2)					
		tensile psi	10 ⁷ cycle dynamic fatigue (psi)	operating temperatures (imprated)	material	corrosion resistance	magnetic non-magnetic	UNRC diameter	UNRC length	SAE	NAS/AN			
Socket Head Cap Screws 1960 Series Alloy Steel		190,000 180,000	20,000	550°F	heat treated alloy steel	plating optional	magnetic	#1 to 5/8" 3/4" to 3"	1/16" to 3/8"	#0 to 5/8" 3/4" to 3"	1/16" to 3/8"	MS16997 and MS16998 MS24675 thru MS24678	NAS 1351 NAS 1352	
Socket Head Cap Screws 1960 Series Stainless Steel		80,000	30,000	800°F	austenitic stainless steel	excellent	non-magnetic	#1 to 5/8"	1/16" to 3/8"	#0 to 5/8"	1/16" to 3/8"	MS16995 MS16996 MS24673 MS24674	NAS 1351 NAS 1352	
Socket Head Cap Screws KS 812 Series		125,000	40,000	800°F	austenitic stainless steel	excellent	non-magnetic	#3 to 3/8"	1/8" to 3-1/4"	#3 to 3/8"	1/8" to 3-1/4"	-	-	
Socket Head Cap Screws KS 1216 Series		160,000	30,000	1200°F	precipitation hardened corrosion resistant steel	excellent	non-magnetic	#3 to 1"	1/8" to 1/2"	#3 to 1"	3/32" to 1/2"	-	-	
Socket Head Cap Screws M 25A Series		180,000	20,000	1,000°F	chrome-moly-vanadium steel	plating optional	magnetic	#10 to 1"	to order	#10 to 1"	to order	-	-	
Socket Head Cap Screws Low Head Series		170,000	20,000	550°F	heat treated alloy steel	fair	magnetic	#3 to 1/2"	3/8" to 1-1/2"	#3 to 1/2"	3/8" to 1-1/2"	-	-	
Shoulder Screws		heat treat level psi 160,000	shear strength in psi 96,000	550°F	heat treated alloy steel	fair	magnetic	UNRC thread #10 to 1-1/2"	shoulder		MSS1975		-	
Flat Head Socket Screws Alloy/ Stainless		Uniform, controlled 82° under-head angle for maximum flushness and side wall contact; non-slip hex socket feature reduces marring of material	180,000	96,000	550°F	heat treated alloy steel	plating optional	magnetic	#1 to 1"	1/8" to 10"	#0 to 1"	1/8" to 10"	MS24667 thru MS24671	-
			56,000	45,000	800°F	austenitic stainless steel	excellent	non-magnetic						
Button Head Cap Screws Alloy/ Stainless		Low heads streamline design, use in materials too thin to countersink; also for non-critical loading requiring heat treated screws	160,000	96,000	550°F	heat treated alloy steel	plating optional	magnetic	#1 to 5/8"	1/16" to 4"	#0 to 5/8"	1/16" to 4"	-	-
			56,000	45,000	800°F	austenitic stainless steel	excellent	non-magnetic						
Socket Set Screws Alloy Steel		Fasten collars, sheaves, gears, knobs on shafts. Locate machine parts. Cone, half-dog, flat, oval, cup and self-locking cup points standard	hardness Rc 45-53	450°F	heat treated alloy steel	plating optional	magnetic	#1 to 1-1/2"	1/16" to 6"	#0 to 1-1/2"	1/16" to 6"	MSS1963-66 MSS1973-77 MSS1981-82	AN565	
Socket Set Screws Stainless Steel		Use stainless for corrosive, cryogenic or elevated temperature environments. Plain cup point standard. Other styles on special order	-	800°F	austenitic stainless steel	excellent	non-magnetic	#1 to 1-1/2"	1/16" to 6"	#0 to 1-1/2"	1/16" to 6"	MSS1021-.23-.24 MSS1031-.38 MSS1045-.47	-	

Performance data listed are general guidelines only. Due to variables in materials and manufacturing, actual performance may vary. Standards referenced are general guidelines only. UNBRAKO is a registered trademark of UNBRAKO, INC. All rights reserved. UNBRAKO, INC. is not responsible for the use of this information in any application. Parts can be supplied to these standards.



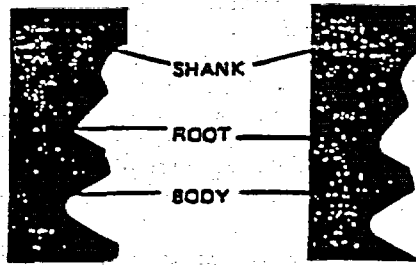
Deep, accurate socket for high torque wrenching. Double knurls for easier handling, quick identification.

Head with increased bearing area for greater load-carrying capacity. An UNBRAKO socket screw "original".

Precision forged for symmetrical grain flow, maximum strength.

Elliptical fillet doubles fatigue life at critical head-shank juncture. An UNBRAKO socket screw development.

"J-R" (radiused-root runout) increases fatigue life as much as 300% in this critical area. An UNBRAKO socket screw "original".



CONVENTIONAL THREAD RUNOUT - Note sharp angle at root where high stress concentration soon develops crack which penetrates into body of screw.

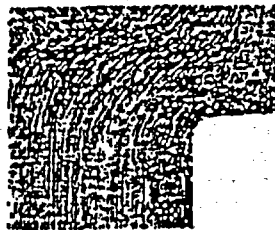
UNBRAKO "J-R" (RADIUSED-ROOT RUNOUT) THREAD - Controlled radius of runout root provides a smooth form that distributes stress and increases fatigue life of fastener as much as 300% in certain sizes.

Fully formed radiused thread increases fatigue life 100% over other thread forms. An UNBRAKO socket screw development.

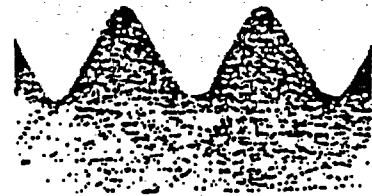
Controlled heat treatment produces maximum strength without brittleness or decarburization.



Accurate control of socket depth gives more wrench engagement than other screws, permits full tightening without cracking or reaming the socket, yet provides ample metal in the crucial fillet area for maximum head strength.



Controlled head forging forms uniform grain flow with unbroken flow lines; makes heads stronger; prevents failure in vital fillet area; adds to fatigue strength of the screw.



Cross-section of radiused fully formed threads. Contour-following flow lines provide extra shear strength in threads, resist stripping and provide high fatigue resistance. Note the large root radius.

Data Pages appended from UNBRAKO Catalogue

UNBRAKO socket screw development doubles fatigue life of the

SOCKET HEAD CAP SCREWS...Why socket screws? why UNBRAKO?

If you use fasteners, you know their importance in today's technology. Higher pressures, higher stresses and higher speeds demand stronger, more reliable joints, and stronger, more reliable fasteners to hold them together.

For parts must stay together. A single failure can destroy a satellite or stop an assembly line. Reliability must be total.

That's why industry is using more and more socket head cap screws, the strongest threaded fasteners you can buy "off-the-shelf". They have the extra strength and fatigue resistance required for total reliability in high strength fastening.

tensile and fatigue strength
UNBRAKO socket head cap screws have the highest levels of strength and fatigue resistance in the industry. They exceed both government and industry standards by as much as 20%. Instead of the usual range of 160,000 psi, minimum strength levels of UNBRAKO screws are consistently 180,000 or 190,000 psi, depending on size. At the same time ductility and fatigue resistance are not sacrificed.

When you buy tension fasteners (which is what socket head cap screws basically are) you're buying clamping force — the ability to hold things together. The 20% additional strength offered by UNBRAKO screws can save dollars, if you use the screws correctly.

That extra 20% lets you use (a) fewer fasteners of the same size, or (b) the same number of smaller screws to achieve the same clamping force. With fewer fasteners you save on drilling and tapping, have fewer screws to buy and install. If you go the other way, smaller screws cost less and permit reduced assembly size, saving space, material and weight.

And if you have dynamic stress or varying load conditions, the phenomenal fatigue resistance of UNBRAKO screws gives you an additional bonus of built-in protection against fatigue failure.

design

One of three major factors in the superiority of UNBRAKO socket head screws is design. For example, socket

depth is carefully controlled. The socket is deep enough for full tightening without reaming or cracking, but not deep enough to weaken the head area and cause failure.

Another design exclusive, inspired by SPS research in aerospace fasteners, is the radiused root thread form of UNBRAKO socket screws. Fatigue life is increased by as much as 100% (depending on size) over screws with other threads. A scientifically designed radius at the thread root is responsible, adding both fatigue resistance and strength in the area of the screw most prone to failure. It adds metal where it is needed to provide maximum strength.

A recent further refinement of this thread profile is the "3-R" thread runout ("Radiused-Root-Runout"). The root of the runout is also radiused to eliminate the usual sharp "V" — a major point of weakness in other threads. Fatigue life in this critical area is increased as much as 300% in certain sizes.

Class 3A tolerances are standard, the closest without selective assembly. They combine maximum cross-section with smooth assembly, and assure better mating of parts.

The elliptical fillet at the juncture of head and shank is another aerospace-inspired SPS development. This compound curve more than doubles fatigue life in the head area without reduction of critical bearing area. Discontinuity is minimized and stress concentrations are reduced, providing an added margin of safety. Heads are correctly proportioned to screw size, assuring full clamping force without indentation and loss of preload.

properties

Second major factor in UNBRAKO socket screw superiority is their physical properties. These are no accident. Consistently higher stress levels are a direct result of customized heat treatment. Despite the most exacting material selection, variations in steel from lot to lot require that each "heat" of UNBRAKO socket screws be heat treated in accordance with its specific chemistry. Carbon content of furnace atmospheres is closely controlled, since carburization (too much carbon) makes screws brittle, while decarburization

(too little carbon) results in soft surface with poor strength and resistance to wear. Every lot of steel is therefore pre-tested and its treatment tailored to produce a uniform product.

manufacturing control

Closely controlled manufacturing is the third factor. Rigid control of every operation of a socket screw is necessary in order to guarantee performance.

Heads of standard UNBRAKO socket screws are forged, not machined. Machining cuts metal fibers, breaks flow lines, creates planes of weakness at stress points. Forging, on the other hand, forms metal, produces uniform grain flow, makes heads stronger by compressing the metal. Head bearing area is strictly perpendicular to screw body to avoid strains and misalignment. Fillet areas are precisely controlled, with fillets made glass smooth to eliminate surface irregularities where cracks can start.

Radiused threads of standard UNBRAKO screws are rolled, not ground or cut. Rolled threads are more uniform and closer tolerances can be maintained because SPS thread roll dies and rolling techniques produce smoother surfaces and more accurate size control. High points and planes of weakness are avoided.

plating

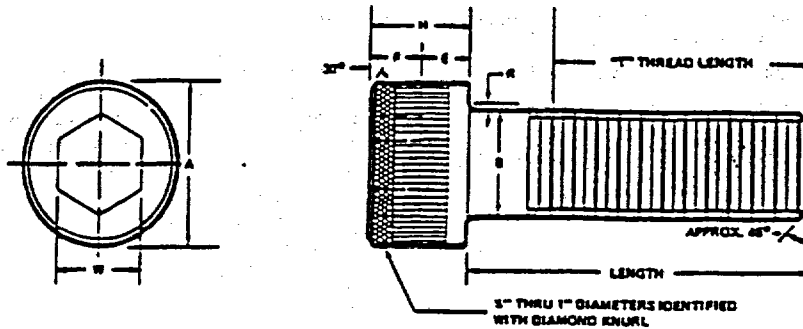
Plating becomes more critical as the demand for plated screws increases. UNBRAKO socket screws that are to be plated are accurately controlled to be within tolerance after plating. Precision plating thickness brings screws to correct dimensions, while rigid control of the plating process guards against screw failure from hydrogen embrittlement. This is a brittle condition caused by hydrogen diffusing into the base material during cleaning and electroplating. It can cause screw failure long after the screw is tightened, but can be avoided by the extreme care in processing given every plated UNBRAKO socket screw.

UNBRAKO socket screws pay off in savings

You get extra safety and reliability in UNBRAKO socket screws, plus significant economies, both in the cost of the fasteners and the cost of their installation. Furthermore, they protect the reputation of your product, which can well depend on the fasteners that hold it together.

These are considerations too important to overlook as production costs continue to rise and reliability requirements become more exacting.

SOCKET HEAD CAP SCREWS 1960 Series Dimensions/mechanical properties



DIMENSIONS

nom. size	basic screw diameter	threads per inch		A		B		E	F	H		W	R		T		
		UNRC	UNRF	head diameter		body diameter				max.	min.		max.	min.		max.	min.
				max.	min.	max.	min.										
#6	.060	-	80	.096	.091	.060	.0568	.020	.025	.060	.057	.050	.007	.003	.500		
	.073	64	72	.118	.112	.073	.0695	.025	.031	.073	.070	.0625	.007	.003	.625		
	.086	56	64	.140	.134	.086	.0822	.029	.038	.086	.083	.0781	.008	.004	.625		
#8	.099	48	56	.161	.154	.099	.0949	.034	.044	.099	.095	.0781	.008	.004	.625		
	.112	40	48	.183	.176	.112	.1075	.038	.051	.112	.108	.0937	.009	.005	.750		
	.125	40	44	.205	.198	.125	.1202	.043	.057	.125	.121	.0937	.010	.006	.750		
#10	.138	32	40	.226	.218	.138	.1329	.047	.064	.138	.134	.1093	.010	.006	.750		
	.164	32	36	.270	.262	.164	.1585	.056	.077	.164	.159	.1406	.012	.007	.875		
	.190	24	32	.312	.303	.190	.1840	.065	.090	.190	.185	.1562	.014	.009	.875		
1/4	.250	20	28	.375	.365	.250	.2435	.095	.120	.250	.244	.1875	.014	.009	1.000		
5/16	.312	18	24	.468	.457	.3125	.3053	.119	.151	.312	.306	.2500	.017	.012	1.125		
3/8	.375	16	24	.562	.550	.375	.3678	.143	.182	.375	.368	.3125	.020	.015	1.250		
7/16	.437	14	20	.656	.642	.4375	.4294	.166	.213	.437	.430	.3750	.023	.018	1.375		
1/2	.500	13	20	.750	.735	.500	.4919	.190	.245	.500	.492	.3750	.026	.020	1.500		
9/16	.562	12	18	.843	.827	.5625	.5538	.214	.265	.562	.554	.4375	.028	.022	1.625		
5/8	.625	11	18	.937	.921	.625	.6163	.238	.307	.625	.616	.5000	.032	.024	1.750		
3/4	.750	10	16	1.125	1.107	.750	.7406	.285	.370	.750	.740	.6250	.039	.030	2.000		
7/8	.875	9	14	1.312	1.293	.875	.8647	.333	.432	.875	.864	.7500	.044	.034	2.250		
1	1.000	8	12	1.500	1.479	1.000	.9886	.380	.495	1.000	.988	.7500	.050	.040	2.500		
1 1/8	1.125	7	12	1.687	1.665	1.125	1.1086	.428	.557	1.125	1.111	.8750	.055	.045	2.812		
1 1/4	1.250	7	12	1.875	1.852	1.250	1.2336	.475	.620	1.250	1.236	.8750	.060	.050	3.125		
1 3/8	1.375	6	12	2.062	2.038	1.375	1.3568	.523	.682	1.375	1.360	1.0000	.065	.055	3.437		
1 1/2	1.500	6	12	2.250	2.224	1.500	1.4818	.570	.745	1.500	1.485	1.0000	.070	.060	3.750		
1 3/4	1.750	5	12	2.625	2.597	1.750	1.7295	.665	.870	1.750	1.734	1.2500	.080	.070	4.375		
2	2.000	4 1/2	12	3.000	2.970	2.000	1.9780	.760	.995	2.000	1.983	1.5000	.090	.075	5.000		
2 1/4	2.250	4 1/2	12	3.375	3.344	2.250	2.2280	.855	1.120	2.250	2.232	1.7500	.100	.085	5.625		
2 1/2	2.500	4	12	3.750	3.717	2.500	2.4762	.950	1.245	2.500	2.481	1.7500	.110	.095	6.250		
2 3/4	2.750	4	12	4.125	4.090	2.750	2.7262	1.045	1.370	2.750	2.730	2.0000	.120	.105	6.875		
3	3.000	4	12	4.500	4.464	3.000	2.9762	1.140	1.495	3.000	2.979	2.2500	.130	.115	7.500		

NOTES

Material: "UNBRAKO" high grade alloy steel or austenitic stainless steel.

Heat Treatment: Alloy steel - Rc 38-45.

Concentricity: Body to head O.D.—within 2% of body diameter T.I.R. or .006 T.I.R. whichever is greater. Body to hex socket—(sizes up to 1/2")—within 3% of body diameter T.I.R. or .006 T.I.R. whichever is greater; (sizes over 1/2")—within 6% of body diameter.

The plane of the bearing surface shall be perpendicular to the axis of the screw within a maximum deviation of 1°.

For body and grip lengths see pages 10 and 11.

See page 14 for stainless steel mechanical properties and seating torques.

Thread class: #0 through 1" dia.—3A; over 1" dia.—2A

Note: Performance data listed are for standard production items only. Non-stock items may vary due to variables in methods of manufacture. It is suggested that the user verify performance on any non-standard parts for critical applications.

MECHANICAL PROPERTIES

APPLICATION DATA

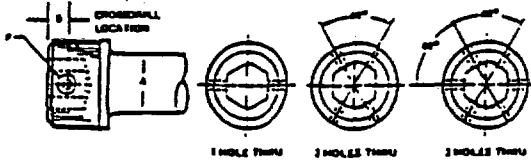
nom. size	tensile strength (pounds)		tensile strength psi min.	yield strength psi min.	double shear strength of body lb. min.	recommended seating torque* inch-lbs.				hole dimensions			
	UNRC	UNRF				UNRC		UNRF		tap drill size †		body drill size	counter-bore size
			plain	cadmium plated	plain	cadmium plated	UNRC	UNRF					
2	-	342	190,000	170,000	640	-	-	2	1	-	3/64	#51	.115
2 1/4	499	528	190,000	170,000	950	4	3	4	3	1.5mm	#53	#48	.140
2 1/2	702	749	190,000	170,000	1,320	6	4	7	5	#50	#50	3/32	.172
2 3/4	925	994	190,000	170,000	1,750	10	7	11	8	#47	#45	#36	.194
3	1,150	1,260	190,000	170,000	2,240	15	11	16	12	#43	#42	#31	.219
3 1/4	1,510	1,580	190,000	170,000	2,800	20	15	21	16	#38	#38	9/64	.250
3 1/2	1,730	1,930	190,000	170,000	3,400	28	21	30	23	#36	#33	#23	.272
3 3/4	2,560	2,800	190,000	170,000	4,800	49	35	50	38	#29	#29	#15	.316
4	3,330	3,800	190,000	170,000	6,450	64	50	76	57	#25	#21	#5	.359
1/4	6,050	6,910	190,000	170,000	11,200	150	112	170	128	#7	#7	17/64	.422
5/16	9,960	11,000	190,000	170,000	17,500	305	230	325	245	F	I	21/64	.515
3/8	14,700	16,700	190,000	170,000	25,200	545	410	570	430	5/16	Q	25/64	.609
7/16	20,200	22,600	190,000	170,000	34,200	840	630	900	680	U	-25/64	29/64	.703
1/2	27,000	30,400	190,000	170,000	44,700	1,300	970	1,370	1,030	27/64	29/64	33/64	.797
9/16	34,600	38,600	190,000	170,000	56,600	1,860	1,400	1,970	1,480	31/64	13 mm	37/64	.890
5/8	42,900	48,600	190,000	170,000	69,900	2,530	1,900	2,660	2,000	35/64	14.5 mm	41/64	1.000
3/4	60,200	67,100	180,000	155,000	95,400	4,400	3,300	4,800	3,600	21/32	11/16	49/64	1.187
7/8	83,100	91,700	180,000	155,000	129,800	7,000	5,300	7,600	5,700	49/64	20.5 mm	57/64	1.375
1	109,000	119,000	180,000	155,000	169,600	10,400	7,800	11,000	8,300	7/8	59/64	1 1/64	1.562
1 1/8	137,000	154,000	180,000	155,000	214,000	14,900	11,200	16,600	12,500	25mm	1 3/64	1 5/32	1.750
1 1/4	175,000	193,000	180,000	155,000	265,000	21,000	15,800	22,600	17,000	1 7/64	1 11/64	1 9/32	1.969
1 3/8	208,000	237,000	180,000	155,000	320,000	27,800	20,800	29,300	22,000	1 7/32	1 19/64	1 13/32	2.158
1 1/2	253,000	285,000	180,000	155,000	381,000	38,500	27,500	39,300	29,500	34mm	36mm	1 17/32	2.344
1 3/4	342,000	394,000	180,000	155,000	519,000	59,400	44,800	59,400	51,600	1 35/64	1 21/32	1 25/32	2.750
2	450,000	521,000	180,000	155,000	678,000	89,900	67,400	103,000	78,000	1 25/32	48.5mm	2 1/32	3.125
1/4	585,000	664,000	180,000	155,000	858,000	131,000	98,200	150,000	112,000	2 1/32	55.0mm	2 9/32	3.500
2 1/2	720,000	828,000	180,000	155,000	1,060,000	164,000	135,000	164,000	155,000	2 1/4	2 13/32	2 17/32	3.875
2 3/4	888,000	1,006,000	180,000	155,000	1,282,000	228,000	183,000	228,000	208,000	2 1/2	2 21/32	2 25/32	4.250
3	1,074,000	1,204,000	180,000	155,000	1,528,000	322,000	242,000	361,000	271,000	2 3/4	2 29/32	3 1/32	4.625

*Torques calculated to induce 100,000 psi tensile stress in the screw threads

†C. and H. Head on screw with 70% thread height.

SOCKET HEAD CAP SCREWS 1960 Series (Continued)

Cross-Drilled Type



Any UNBRAKO socket head cap screw (alloy, stainless steel or other material) may be ordered with standard cross-drilling of the head for safety wiring. Such screws are considered specials and price and delivery for each order will be quoted individually. Standard types of cross-drilling are shown on this page.

APPLICABLE STANDARDS – MS 24673 thru 24678; NAS 1351, 1352; Fed. Spec. FF-S-86, ASTM A574, ANSI B18.3-1969

DETAILS

A Screw Size Nom.	B Cross-Drill Location		P Hole Diameter		Alignment Plug Ret.
	Max.	Min.	Max.	Min.	
#2	.035	.025	.032	.026	.0210
#3	.035	.025	.032	.026	.0210
#4	.040	.026	.039	.033	.0280
#5	.045	.030	.039	.033	.0280
#6	.050	.035	.039	.033	.0280
#8	.060	.040	.050	.044	.0390
#10	.065	.045	.050	.044	.0390
1/4	.085	.065	.050	.044	.0340
5/16	.104	.084	.050	.044	.0340
3/8	.123	.103	.067	.061	.0510
7/16	.141	.121	.067	.061	.0510
1/2	.160	.140	.067	.061	.0510
9/16	.179	.159	.067	.061	.0510
5/8	.198	.178	.067	.061	.0510
3/4	.235	.215	.097	.091	.0810
7/8	.273	.253	.097	.091	.0810
1	.310	.290	.097	.091	.0810
1 1/8	.348	.328	.127	.119	.1040
1 1/4	.385	.365	.127	.119	.1040
1 3/8	.423	.403	.127	.119	.1040
1 1/2	.460	.440	.127	.119	.1040
1 5/8	.498	.478	.127	.119	.1040
1 3/4	.535	.515	.127	.119	.1040
1 7/8	.573	.553	.127	.119	.1040
2	.610	.590	.127	.119	.1040

PART NUMBERING – 1960 SERIES – Socket Head Cap Screws

The part number of a socket head cap screw consists of: (1) a basic part number describing item and material and followed by suffix letters noting optional features (i.e. LOC-WEL self-locking); (2) a dash number for the diameter, with one suffix

letter to indicate type of thread (UNRC or UNRF); (3) a second dash number for length (in 16ths), followed by a suffix letter for type of finish. The diagram below shows a typical part number and interprets each component number and letter.

FINISH

B – Chemical Black Oxide	S – Silver Plate – P23
C – Cadmium Plate – P1	U – Clear Zinc Plate – P6
D – Cadmium Plate – P4	Z – Zinc Plate – P8

No letter indicates standard black finish (Thermal Oxide) for alloy steel and passivation for stainless steel.
See page 77 for plating specifications.

LENGTH in 16ths

THREAD TYPE C-coarse, F-fine

DIAMETER

BIA.	1	2	3	4	5	6	8	10	12	14	16	18	20		
CASH NO.	90	91	92	93	94	95	96	98	1	4	5	6	7	8	9

BIA.	1	2	3	4	5	6	8	10	12	14	16	18	20	22	24	28	32	36	40	44	48
CASH NO.	110	112	114	116	118	120	122	124	128	132	136	140	144	148	152	156	160	164	168	172	176

OPTIONAL FEATURES

Cross Drilled Heads:	Self-Locking:
H1 – 1 Hole Thru	E – Loc-Wel to Mil-F-18240
H2 – 2 Holes Thru	K – Nylok to Mil-F-18240
H3 – 3 Holes Thru	L – Loc-Wel (Commercial)
	N – Nylok (Commercial)
	TF – Tru-Flex

BASIC PART NUMBER

20097 – socket head cap screw-alloy steel
20098 – socket head cap screw-corrosion resistant steel

Example Part Number: 20097 H3L -94 C -24 C

20097: Alloy Steel (Alloy Steel), Drilled Head (3) and LOC-WEL (H3L), -94: Diameter #4 (UNRC), -24: Length 1 1/2" (Cadmium Plate), C: Finish (Cadmium Plate)

2. "NEOPRENE" GASKET

This page left blank intentionally.

the chromassure system

CHROMASSURE... COLOR ASSURANCE O-RINGS

Error resulting from a mixup in basic polymer is potentially the greatest quality problem a seal user can experience. Basic polymer differences can result in a seal swelling to lock up a unit, shrinking away — providing a leak path or complete degradation resulting from fluid and/or temperature incompatibility. With today's product liability claims on the rise, a seal user can't afford to take unnecessary chances.

Parker Sea' CHROMASSURE materials offer you high-performance color seals comparable to or exceeding their black rubber counterparts. Parker CHROMASSURE O-rings are available in the most commonly required elastomers and compounds meeting the most popular specifications.

THE CHROMASSURE SYSTEM

The CHROMASSURE plan is simple. A single color represents each of the different major polymer families. CHROMASSURE color identification is integral, throughout the entire seal, not just a superficial coating that will wear away. CHROMASSURE color remains for the life of the seal.

CHROMASSURE seals offer you superior performance in the most demanding service and in addition have four specific benefits not available with traditional "Basic Black" polymers. These important benefits help you:

- **ELIMINATE ASSEMBLY ERRORS OF INCORRECT ELASTOMER.**

CHROMASSURE will vividly identify the proper elastomer on your assembly line and virtually assure that correct seal material is used.

- **UPGRADE PRODUCT QUALITY AND RELIABILITY**

Installation of the proper elastomer means improved reliability of your product; consequently fewer quality headaches.

- **MINIMIZE WARRANTY AND LIABILITY PROBLEMS**

CHROMASSURE offers an added margin of safety by strengthening internal quality controls. If non-black seals are installed in your product, customer repair with unauthorized replacement seals will be more evident... giving you added warranty protection.

- **PROTECT AND INSURE YOUR AFTERMARKET**

Where "non-black" seals are utilized, the end user is more likely to come back to you for his "special" colored replacement seal needs.

For additional information, contact your Parker Seal Distributor, Territory Manager or Parker Seal direct at (606) 269-2351.

THE CHROMASSURE SYSTEM

POLYMER	COLOR	TYPICAL PARKER COMPOUND	SPECIFICATION
Ethylene Propylene	Purple	E893-80	2AA 815 A 13 F17 L14
Fluorocarbon	Brown	V884-75 / V894-90	MII-R-83248 CL.1 CL.2
Fluorosilicone	Blue	L1120-70	MII-R-25985 CL.1, GR.70
Neoprene	Red	C944-70	AMS 3205
Nitrile	Black	N674-70	3CH 720 A25 B14 E16 E35
Silicone	Rust	S604-70	AMS 2304



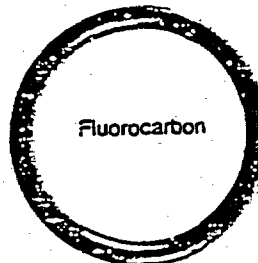
Fluorosilicone

L1120-70



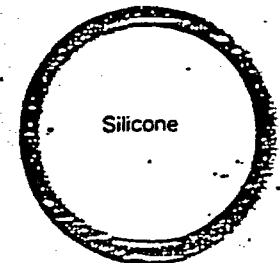
Nitrile

N674-70



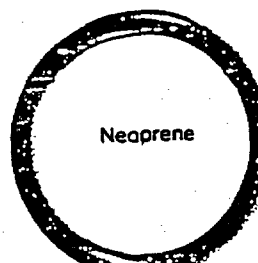
Fluorocarbon

V884-75/V894-90



Silicone

S604-70



Neoprene

C944-70

Ethylene
Propylene

E893-80

basic elastomers

Following is a review of the various elastomers available for use in seals. Typical trade names are listed. However, it is not intended as a complete list of elastomer manufacturers. If any of the rubber terms used in the descriptions are confusing, turn to the "Glossary of Seal and Rubber Terms" at the end of Section A1 for explanation. Service recommendations mentioned in this section are necessarily abbreviated. For more comprehensive information on this important subject see the fluid compatibility table, (Table B5.)

BUTADIENE RUBBER (BR)

Typical Trade Names:

Ameripol CB B.F. Goodrich
 Budene Goodyear Tire & Rubber Co.
 Diene Firestone Synthetic Rubber Latex Co.
 Trans 4 or Cis 4 Philips Chemical Co.
 Polybutadiene is an elastomer with properties very similar to natural rubber. Its physical properties are not quite up to natural rubber. However, in some cases its low temperature characteristics are better. Butadiene is primarily a tire polymer.

BUTYL RUBBER (IIR)

Typical Trade Names:

Bucar Butyl Columbian Chemicals Co.
 Exxon Butyl Exxon Chemical Co. USA
 Polysar Butyl Polysar, Ltd.
 Butyl rubber is an all petroleum product made by co-polymerizing isobutylene and just enough isoprene to obtain the desired degree of unsaturation necessary for vulcanization. Brominated and chlorinated butyl rubber are also available and are prepared by select replacement of hydrogen with bromine or chlorine.

Until the introduction of ethylene propylene rubber, butyl was the only elastomer which was satisfactory for Skydrol 500 service over a temperature range of -65 to $+225^{\circ}\text{F}$ (-54 to $+107^{\circ}\text{C}$).

In addition, butyl has excellent resistance to gas permeation which makes it particularly useful for vacuum applications, and accounts for its wide use in the manufacture of inner tubes and the inside layer of tubeless tires.

Butyl is recommended for

Phosphate ester type hydraulic fluids (Skydrol, Fyrquel, Pydraul).

Ketones (MEK, Acetone)

Silicone fluids and greases.

Butyl is not recommended for:

Petroleum oils.

Di-ester base lubricants.

CHLORINATED POLYETHYLENE (CM)

Trade Name:

CPE Dow Chemical Co.
 Chlorinated polyethylene is made from a high density polyethylene. Its saturated backbone and its chlorine content give it limited resistance to petroleum oils and good resistance to oxidation. Unlike neoprene, the chlorination of CPE is random and can be varied. As the chlorine content is increased, resistance to petroleum oils improves but low temperature flexibility becomes poorer. CPE can be blended with other polymers to improve their flame and impact resistance. In fact, it is seldom used alone, the bulk of the product being used for blending purposes.

CHLOROSULFONATED POLYETHYLENE (CSM)

Trade Name:

Hypalon E. I. duPont de Nemours
 The ethylene monomer with some of the hydrogen replaced by chlorine and sulphur groups is the main constituent of this elastomer.

It is useful over a temperature range of -65 to $+250^{\circ}\text{F}$ (-54 to $+121^{\circ}\text{C}$) but its mechanical properties, compression and permanent set characteristics are less than is desired for both dynamic and static sealing applications.

Chlorosulfonated Polyethylene has good acid resistance.

EPICHLOROHYDRIN RUBBER (CO, ECO)

Typical Trade Names:

Hercior Hercules Inc.
 Hydrin B. F. Goodrich Co.
 Epichlorohydrin is a recent addition to the oil resistant polymer class. Compounds of this type are aliphatic polyethers with chlorofunctional side chains. Two basic classes, homopolymers (CO) and copolymers (ECO) are available. Both have excellent resistance to hydrocarbon oils, fuels, and ozone. High temperature resistance is good, but compression set at 300°F is only fair. This property, plus the corrosive nature of epichlorohydrin, are limiting factors in some applications.

Copolymers give very good low temperature properties, providing a temperature range of -65°F to $+275^{\circ}\text{F}$ (-54°C to $+135^{\circ}\text{C}$) where corrosion is not likely to be encountered and where compression set is not a problem. The homopolymers are useful thru a temperature range of approximately -40°F to $+275^{\circ}\text{F}$ (-40°C to $+135^{\circ}\text{C}$) under the same conditions.

ETHYLENE ACRYLIC

Trade Name:

VAMAC E. I. duPont de Nemours

Ethylene acrylic compounds are considered "medium performance elastomers," having a useful temperature range extending from approximately -30 to $+350^{\circ}\text{F}$. Resistance to weathering, ozone, and air aging is very good, and they have sufficient resistance to petroleum oils and automatic transmission fluids to make them look attractive for automotive applications.

ETHYLENE PROPYLENE RUBBER (EPM, EPDM)

Typical Trade Names:

Nordel E. I. duPont de Nemours Co.
 Royalene Uniroyal
 Vistalon Exxon Chemical Co. USA
 Epsyn Copolymer Rubber & Chemical Corp.
 Epcar B. F. Goodrich Co.

Ethylene propylene rubber is an elastomer prepared from ethylene and propylene monomers (ethylene propylene copolymer) and at times with a small amount of a third monomer (ethylene propylene terpolymers). It was introduced to the rubber industry in 1951 and quickly won broad acceptance in the sealing world because of its excellent resistance to Skydrol and other phosphate ester type hydraulic fluids.

Ethylene propylene has a temperature range of -65 to $+300^{\circ}\text{F}$ (-54 to $+149^{\circ}\text{C}$) for most applications.

EP is recommended for:

Phosphate ester base hydraulic fluids (Skydrol, Pydraul, Pydraul).

Steam (to 400°F) (204°C).

Water.

Silicone oils and greases.

Dilute acids.

Dilute alkalis.

Ketones (MEK, acetone).

Alcohols.

Automotive brake fluids.

EP is not recommended for:

Petroleum oils.

Di-ester base lubricants.

FLUOROCARBON RUBBER (FKM)

Typical Trade Names:

Fuorel 3M
 Kalrez (high temp) E.I. duPont de Nemours Company
 Kel-F 3M (formerly Kellogg)
 Viton E.I. duPont de Nemours Company

Fluorocarbon elastomers were first introduced in the mid 1950's. Since then they have grown to major importance in the seal industry. Due to its wide spectrum chemical compatibility and temperature range and its low compression set, fluorocarbon rubber is the most significant single elastomer development in recent history.

Its working temperature range is considered to be -15 to $+400^{\circ}\text{F}$ (-29 to $+204^{\circ}\text{C}$), but it will take temperatures up to 600°F (316°C) for short periods of time, and Du Pont's Kalrez is normally recommended up to 500°F (260°C). On the low temperature end, Parker's compound V835-75 will seal down to -40°F (-40°C) in a static seal. Though the standard compounds have been known to seal at -65°F (-54°C) in some special static applications, the normal low temperature limit is -15°F (-26°C).

Special formulations having extra chemical resistance are also available, and new types are being developed constantly.

Fluorocarbon O-rings should be considered for seal use in aircraft, automobile and other mechanical devices requiring maximum resistance to elevated temperature and to many functional fluids.

FKM is recommended for:

Petroleum oils.

Di-ester base lubricants (MIL-L-7808, MIL-L-6085).

Silicate ester base lubricants (MLO 8200, MLO 85 OS-45.)

Silicone fluids and greases.

Halogenated hydrocarbons (carbon tetrachloride, trichloroethylene).

Selected phosphate ester fluids.

Acids.

FKM is not recommended for:

Ketones (MEK, acetone).

Skydrol fluids.

Amines (UDMH), anhydrous ammonia.

Low molecular weight esters and ethers.

Hot hydrofluoric or chlorosulfonic acids.

FLUOROSILICONE (FSi)

Typical Trade Name:

Silastic LS. Dow Corning Co

Fluorosilicone combines the good high- and low-temperature properties of silicone with basic fuel and oil resistance. The primary uses of fluorosilicones are in fuel systems where the dry-heat resistance of silicone is required, but a seal may be exposed to petroleum oils and/or hydrocarbon fuels. In some fuels and oils, however, the high temperature limit is more conservative because temperatures approaching 350°F may degrade the fluid, producing acids which attack fluorosilicone elastomers.

On the other end of the temperature scale, fluorosilicones typically seal at temperatures as low as -100°F (-73°C). High strength type fluorosilicones are available. Certain these exhibit much improved resistance to compression set.

ISOPRENE RUBBER-SYNTHETIC (IR)

Typical Trade Names:

Natsyn Goodyear Tire & Rubber Co

Polyisoprene has the distinction of being a synthetic elastomer which has the same chemical composition as natural rubber. For a guide to its chemical and physical properties refer to Natural Rubber below.

NATURAL RUBBER—NATURAL POLYISOPRENE (NR)

Crude natural rubber is found in the juices of many plants including the shrub guayule, Russian dandelion, goldenrod and dozens of other shrubs, vines and trees. The principal source is the tree Hevea Brasiliensis which is native to Brazil. Petroleum oils are the greatest enemy of natural rubber compounds. The synthetics have all but completely replaced natural rubber for seal use.

NR is recommended for:

Automotive brake fluid.

NR is not recommended for:

Petroleum products.

NEOPRENE RUBBER (CHLOROPRENE, CR)**Trade Name:**

Neoprene (formerly E. I. duPont de Nemours Company)
 Butaclor Distugil
 Denka Denka Chem. Co.
 Neoprenes are homopolymers of chloroprene (chlorobutadiene) and were among the earliest of the synthetic rubbers available to the seal manufacturers. Neoprene can be compounded for service at temperatures of -65 to $+300^{\circ}\text{F}$ (-54 to $+149^{\circ}\text{C}$). Most elastomers are either resistant to deterioration from exposure to petroleum lubricants or oxygen. Neoprene is unusual in having limited resistance to both. This, combined with broad temperature range and moderate cost accounts for its desirability in many seal applications.

Chloroprene is recommended for:

Refrigerants (Freons, ammonia)
 High aniline point petroleum oils.
 Mild acid resistance.
 Silicate ester lubricants.

Chloroprene is not recommended for:

Phosphate ester fluids.
 Ketones (MEK, acetone).

NITRILE OR BUNA N (NBR)**Typical Trade Names:**

Chemigum Goodyear Tire & Rubber Co.
 Paracril Uniroyal
 Hycar Goodrich Chemical Co.
 Krynac Polysar, Ltd.
 Ny Syn Copolymer Rubber & Chem. Corp.

Nitrile, chemically, is a copolymer of butadiene and acrylonitrile. Acrylonitrile content is varied in commercial products from 18% to 42%. As the nitrile content increases, resistance to petroleum base oils and hydrocarbon fuels increases, but low temperature flexibility decreases.

Due to its excellent resistance to petroleum products, and its ability to be compounded for service over a temperature range of -65 to $+275^{\circ}\text{F}$ (-54 to $+135^{\circ}\text{C}$), nitrile is the most widely used elastomer in the seal industry today. Most military rubber specifications for fuel and oil resistant MS and AN O-rings require nitrile base compounds. It should be mentioned, however, that to obtain good resistance to low temperature with nitrile compounding, it is almost always necessary to sacrifice some high temperature fuel and oil resistance.

Nitrile compounds are superior to most elastomers with regard to compression set or cold flow, tear and abrasion resistance. Inherently, they do not possess good resistance to ozone, sunlight or weather but this can be substantially improved through compounding. However, since ozone and weather resistance are not always built in, seals from nitrile bases should not be stored near electric motors or other equipment which may generate ozone, or in direct sunlight.

Nitrile is recommended for:

General purpose sealing.
 Petroleum oils and fluids.
 Cold Water.

Silicone greases and oils.

Di-ester base lubricants (MIL-L-7808).
 Ethylene glycol base fluids (Hydrolubes).

Nitrile is not recommended for:

Halogenated hydrocarbons (carbon tetrachloride, trichloroethylene).
 Nitro hydrocarbons (nitrobenzene, aniline).
 Phosphate ester hydraulic fluids (Skydrol, Fyrquel, Pydraul).
 Ketones (MEK, acetone).
 Strong acids.
 Ozone.
 Automotive brake fluid.

POLYPHOSPHAZENE FLUOROELASTOMER (FZ)**Trade Name:**

EYPEL-F Ethyl Corp.
 EYPEL-F elastomer should effectively solve many difficult sealing problems due to its combination of physical properties, fluid resistance and temperature range. The base polymer was developed for the U.S. Army by Firestone Tire and Rubber Company, and it has much the same temperature range (-85 to $+325/350^{\circ}\text{F}$) and fluid resistance (especially petroleum products) as fluorosilicone elastomers but physical properties are definitely better — enough so that polyphosphazene compounds have performed adequately in dynamic and extrusion tests. Major disadvantage is its resistance to water which is only fair to poor.

POLYACRYLATE RUBBER (ACM)**Typical Trade Names:**

Cyanacryl American Cyanamid Co.
 Hycar B. F. Goodrich Chemical Co.

This material has outstanding resistance to petroleum fuel and oil. In addition, it possesses complete resistance to oxidation, ozone, and sunlight, combined with an ability to resist flex cracking. Compounds from this base polymer have been developed which are adaptable for continuous service in hot oil over the temperature range 0° to $+350^{\circ}\text{F}$ (-18° to $+177^{\circ}\text{C}$). Resistance to hot air is slightly superior to nitrile polymers, but strength, compression set and water resistance are inferior to many of the other polymers. There are several polyacrylate types available commercially, but all are polymerization products of acrylic acid esters.

Greatest usage of polyacrylate is by the automotive industry in automatic transmissions and power steering gears using Type A fluid.

POLYSULFIDE RUBBER (T)

Typical Trade Names:

Polysulfide Rubber Thiokol Chemical Corp.

Polysulfide Rubber was one of the earliest commercial synthetic polymers and is prepared from dichlorides and sodium polysulfide. It has a remarkable combination of solvent resistance, low temperature flexibility, flex-crack resistance, and oxygen and ozone resistance. However, heat resistance, mechanical strength and compression set are not outstanding. Other seal compounds are more versatile from the performance standpoint, hence polysulfide rubber is recommended by Parker only for specific applications which cannot be satisfied by any other elastomer. Temperature range is -25 to +225°F (-34 to +107°C). Seals of polysulfide are recommended for service involving contact with solutions of petroleum solvents, ketones and ethers.

POLYURETHANE RUBBER (AU, EU)

Trade Names:

Texin Mobay Chemical Co.
 Adiprene E.I. duPont de Nemours Company
 Cyanaprene American Cyanamid Co.
 Pellethane Union Carbide
 Roylar Uniroyal

Polyurethanes exhibit outstanding mechanical and physical properties in comparison with other elastomers. Over a temperature range of -65 to 200°F resistance to petroleum oils, hydrocarbon fuels, oxygen, ozone and weathering is good. However, polyurethanes quickly deteriorate when exposed to acids, ketones and chlorinated hydrocarbons. Certain types of polyurethane are also sensitive to water and humidity.

The inherent toughness and abrasion resistance of polyurethane seals is particularly desirable in hydraulic systems where high pressures, shock loads, wide metal tolerances, or abrasive contamination is anticipated.

SBR RUBBER (BUNA S OR GRS) Typical Trade Names:
 Too numerous to list.

SBR rubber is probably best known under its old designation Buna S or GRS (Government Rubber Styrene), which refers to the rubber originally made during World War II in United States Government-owned plants as a substitute for natural rubber.

However, when the manufacture of this elastomer was turned over to private industry its designation was changed to indicate the chemical composition: styrene and butadiene rubber. Tires account for most of its usage.

Together SBR and natural rubber account for approximately 90% of total world rubber consumption. Very little of these two materials is used in seals.

SBR is recommended for:

- Automotive brake fluid.
- Alcohols (low molecular weight).
- Water.

SBR is not recommended for:

- Ozone.
- Petroleum Oils.
- Sunlight.

SILICONE RUBBER (SI)

Typical Trade Names:

Phosiz Rhone
 Silastic Dow Corning
 No trade name General
 No trade name Stauffer Chemical Co.

The silicones are a group of elastomeric material from silicone, oxygen, hydrogen and carbon. As the silicones have poor tensile strength, tear resistance, abrasion resistance. Special compounds have been which have exceptional heat and compression set and high strength compounds have also been developed but their strength does not compare to conventional. Silicones possess excellent resistance to temperature extremes. Flexibility below -175°F (-114°C) has been demonstrated and Parker has compounded silicone in which will resist temperatures to 700°F (371°C) for periods. The maximum temperature at which silicone recommended for continuous service in dry air is (200°C). Silicone's retention of properties at the temperatures is superior to other elastic materials. Silicones compounds are not normally recommended for dynamic sealing applications due to their relatively low and high coefficient of friction.

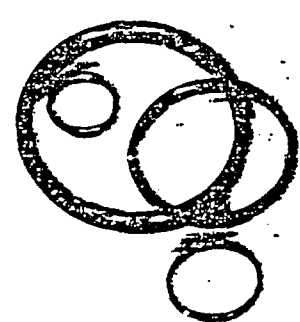
Many silicone compounds have a higher than normal shrinkage that results in finished parts being not when produced in standard molds. Consult chapter more information about the effects of mold shrinkage seal compounds.

Silicones are recommended for:

- Dry heat.
- High-amine point oils.
- Chlorinated di-phenyls.

Silicones are not recommended for:

- Most petroleum fluids.
- Ketones (MSEK, acetone).
- Water and steam.



AS-4

physical and chemical characteristics

In addition to the elastomer descriptions, it is necessary to present more details about the important physical and chemical properties of compounds. These are needed to provide a clearer picture of how they fit together and enter into selection of a seal compound.

RESISTANCE TO FLUID As used throughout this manual, the term "fluid" denotes the substance retained by the seal. It may be a liquid, a gas, or a mixture of both. We intend that it shall even include powders or solids as well, if such should enter the seal picture. The term "medium" — plural "media" — is often used with the same meaning.)

The chemical effect of the fluid on the seal is of prime importance. The fluid must not alter the operational characteristics or reduce the life expectancy of the seal significantly. That is, excessive deterioration of the seal must be avoided. It is easy, however, to be misled on this point. A significant amount of volume shrinkage usually results in premature leakage of any O-ring seal, whether static or dynamic. On the other hand, a compound that swells excessively in a fluid, or develops a large increase or decrease in hardness, tensile strength, or elongation, will often continue to serve well for a long time as a static seal in spite of such undesirable test results.

HARDNESS Throughout the seal industry, the Type A durometer, manufactured by the Shore Instrument Company, is the standard instrument used to measure the hardness of most rubber compounds. (The Type D durometer is recommended where the Type A reading is over 90.)

The durometer has a calibrated spring which forces an indenter point into the test specimen against the resistance of the rubber. There is an indicating scale on which the hardness is read directly. It is calibrated to read 100 if there is no penetration, as on a flat glass or steel surface. (For specimens that are too thin or provide too small an area for accurate durometer readings, the Wallace Micro Hardness Tester is recommended.)

The softer materials, those with lower hardness readings, will flow more easily into the microline grooves of the mating part. This is particularly important in low pressure seals because they are not activated by fluid pressure. Conversely, the harder materials offer greater resistance to flow. Referring back to the O-ring seal diagram, figure A1-5, it can be seen that a harder ring will have greater resistance to extrusion into the narrow gap beyond the groove.

There are applications in which the compressive load available for assembly is limited. In these situations, figures A4-11 through A4-13 are helpful, providing compressor load requirements for O-rings of several degrees of hardness for each of the five standard cross sections.

In dynamic applications, the hardness of the O-ring is doubly important because it also affects friction. Although a harder compound will, in general, have a lower coefficient of friction than a softer material, the actual running and breakout friction values are higher because the load required to squeeze the harder material into a given O-ring cavity is so much greater.

For most applications, compounds having a Type A durometer hardness of 70 to 80 is the most suitable compromise. This is particularly true of dynamic applications where 90 durometer compounds or harder often allow a few drops of fluid to pass with each cycle, and soft stocks tend to erode, wear, and extrude.

Normally durometer hardness is referred to in increments of five or ten, as 60 durometer, 75 durometer, etc. — not as 62 durometer, 66 durometer or 73 durometer. This practice is based on (1), the fact that durometer is generally called out in specifications with a tolerance of ± 5 (i.e., 65 ± 5 , 70 ± 5 , 90 ± 5), (2), the inherent variance from batch to batch of a given rubber compound due to slight differences in raw materials and processing techniques and (3), the variance encountered in reading durometers. On a 70 durometer stock, for example, one person might read 69 and another 71. This small difference is to be expected and is considered to be within experimental error.

TOUGHNESS is not a measured property or parameter but a general term frequently used to summarize the combination of resistance to physical forces rather than chemical action. It is used as a relative term in practice. The next sections are major indications of, and contribute to the "toughness" picture of a compound.

TENSILE STRENGTH Measured in psi (pounds per square inch) required to rupture a specimen of a rubber material, tensile strength is a fair production control measurement used to insure uniformity of compound, and also useful as an indication of deterioration of the compound after it has been in contact with a fluid for long periods. If such contact results in a small reduction in tensile strength, life may be relatively long. If a large reduction of tensile strength occurs, life may be relatively short. Exceptions to this rule do occur. Tensile strength is not a proper indication of resistance to extrusion, nor is it ordinarily used in design calculations. However, in dynamic applications a minimum of 1000 psi is normally necessary to assure good strength characteristics.

TABLE A3-10
COMPARISON OF PROPERTIES OF COMMONLY USED ELASTOMERS

ELASTOMER TYPE (POLYMER)	PROPERTIES														
	PARKER CONDUIT PREFIX LETTER	OXIDATION RESISTANCE	ACID RESISTANCE	ALKALI RESISTANCE	TEMPERATURE RANGE	DYNAMIC FRICTION	ELECTRICAL PROPERTIES	FLAME RESISTANCE	HEAT RESISTANCE	WATER RESISTANCE	UV RESISTANCE	WEAR RESISTANCE	TEAR RESISTANCE	AGEING RESISTANCE	LOW TEMPERATURE RESISTANCE
Butadiene	C	B	FG	FG	G	B	G	B	B	B	B	B	B	B	FG
Butyl	B	FG	G	B	G	B	G	B	G	B	B	B	B	B	G
Chlorinated Polyethylene	N	G	B	FG	FG	G	G	GE	G	B	B	B	B	B	B
Chlorosulfonated Polyethylene	H	G	G	B	FG	B	B	G	G	G	B	B	B	G	B
Epichlorohydrin	V	G	FG	G	GE	G	B	FG	FG	GE	B	B	B	G	B
Ethylene Acrylic	A	F	F	FG	G	F	B	P	B	B	B	B	B	G	B
Ethylene Propylene	B	GE	G	B	GE	GE	G	B	B	G	B	B	B	GE	B
Fluorocarbon	V	G	B	B	FG	GE	B	B	B	G	B	B	B	GE	FG
Fluorosilicone	L	B	FG	B	GE	V	B	C	B	B	G	B	GE	B	B
Isoprene	I	B	FG	FG	G	B	G	B	B	B	B	B	G	GE	B
Natural Rubber	R	B	FG	FG	G	B	G	B	B	B	B	B	G	GE	B
Neoprene	C	G	FG	FG	FG	B	B	G	G	G	FG	GE	B	FG	B
Nitrile or Buna N	N	G	F	FG	G	GE	F	B	G	G	B	B	B	GE	FG
Perfluorinated Fluoroelastomer	F	F	B	G	B	B	FG	G	B	B	B	B	B	B	B
Polyacrylate	A	C	B	F	B	B	B	B	B	B	B	B	B	FG	B
Polysulfide	T	B	B	G	G	B	B	B	B	B	B	B	B	B	B
Polyurethane	P	B	B	B	G	B	FG	B	B	G	G	B	B	GE	B
SBR or Buna S	G	G	B	FG	G	G	G	F	FG	F	B	B	B	FG	GE
Silicone	S	P	FG	GE	B	B	B	B	B	B	B	B	B	B	B

P - POOR F - FAIR G - GOOD E - EXCELLENT

t of the preceding portions of this handbook have dealt with selecting the best rubber compound for a given application. Here will be found background information to help understanding better the factors involved in the process. This chapter will provide some guidance when recommended limits should be exceeded, or when unlisted fluids are encountered. Compound selection may be classified in two categories: — pioneering type and the non-pioneering type. If no pioneering were ever encountered it would be possible to skip the other sections of this handbook and select the proper compound for an application from the tables. Since non-pioneering applications will include the greater part of all design work normally encountered, this category will be discussed first.

NON-PIONEERING DESIGN The term "non-pioneering design" refers to reapplication of proven design. Three cases come to mind immediately:

When using the same fluid, gland design practices, and operating conditions, the same compounds as utilized in the previous design may be trusted to give successful results.

When military service or other customer requires the use of some specific compound by citing a formulation, compound designation, or specification, the designer must select the compound that meets such criteria and no options exist as to compound choice. By use of such specifications, the problem becomes "non-pioneering" in that known successful solutions are relied on. FOR SUCH DESIGN CONDITIONS, TABLES BC, BS, and B- LIST THE MOST USED SPECIFICATIONS AND INDICATE APPLICABLE PARKER COMPOUNDS.

There is a third case of "non-pioneering design" in which the designer can use past successes of others as a basis for a design foreign to his own experience. Chapters AE and AF provide gland design data based on "average" operating conditions, established by wide-spread field conditions developed from years of experience with O-rings in similar fashion, many stock compounds have proved to be satisfactory in certain fluids when used in gland design. Provided operating conditions are within specified limits, gland design presents nothing new, and problems should arise. THE FLUID COMPATIBILITY TABLE, TABLE BE, PROVIDES SPECIFIC SEAL COMPOUND RECOMMENDATIONS FOR SERVICE WITH A VARIETY OF FLUIDS. Each foregoing category is based on successful practice under similar service conditions. This is the heart of the non-pioneering approach.

MINOR PIONEERING DESIGN This implies that there is something new and therefore unknown or at least unproved out in the design. There are at least two recognizable levels in this area which we elect to call "minor pioneering" and "major pioneering."

Minor Pioneering applies when only a slight departure from previous practice is involved. If new operating conditions apply or some change in gland design is made but either is radically different from the past design conditions, the previous design data will certainly apply as a starting point. If a fluid is new to the user, but is listed in the fluid

compatibility table, influence of the fluid retains "minor pioneering" status. (If the new fluid is foreign to the user's experience and not listed in the table, the problem has suddenly become "major pioneering.") Each designer makes his own choice of how to test a new design and his decision should be based on how far the application deviates from known successful usage.

Major Pioneering applies when there is radical departure from previous practice. The most likely example is the use of a new fluid, foreign to anyone's past experience. If the fluid's chemical nature can be related to another fluid of known effect on a compound, this may reduce the problem to "minor pioneering."

For example, if the fluid is a silicate ester, it can be surmised that its effect on the seal will be similar to MLO-8200, MLC-2515, or OS 45 type III and IV, since these also have a silicate ester base. In the case of petroleum base fluids, comparison of the aniline point of the fluid with that of standard test fluids gives a fair estimate of the fluid's effect on a seal.

It is fortunate that major engineering problems constitute only a very small percentage of the total work, for they do not normally offer a direct and immediate answer. However, by using table B1 or B5 it should be relatively simple to select one or two compounds for trial. The most likely compound should then be put on simulated service test. If performance is satisfactory, the answer is at hand—if not, a more accurate analysis and a better compound selection may be made based on test results.

In summary, selecting an applicable compound is a matter of finding a "reasonable" starting point and proving the adequacy of such a selection by functional testing.

RAPID METHODS FOR PREDICTING THE COMPATIBILITY OF ELASTOMERS WITH MINERAL BASED OILS

In view of the ever increasing number of operating oils and sealing materials, it is desirable that a means be established to enable interested parties to employ suitable combinations of oil and rubber without the need for carrying out lengthy immersion tests on each combination.

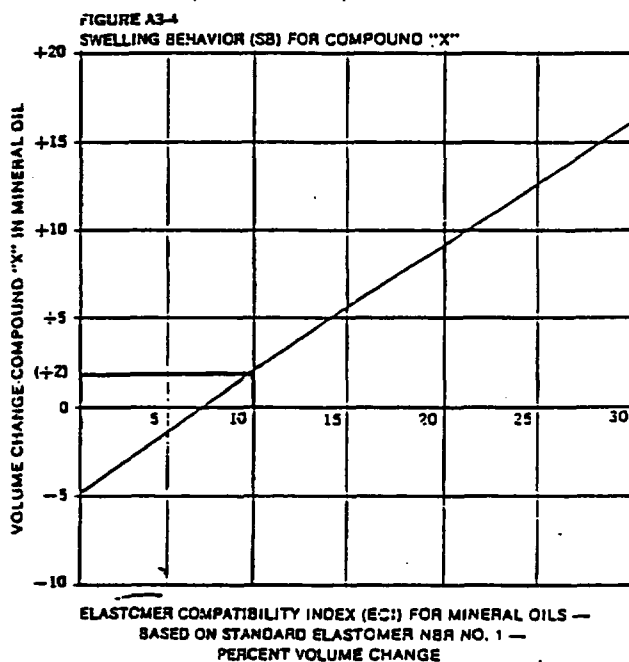
A well known rapid method for material selection is based on the aniline point of the oil, which is the lowest temperature at which a given amount of fresh aniline mixes with an equal volume of the particular oil. Oils with the same aniline point usually have similar effect on rubber. The lower the aniline point, the more severe is the swelling action. The ASTM reference oils cover a range of aniline points found in lubricating oils. Oil No. 1 has a high aniline point (225°F/124°C) and causes slight swelling or shrinkage. Oil No. 2 has a medium aniline point (200°F/93°C) and causes intermediate swelling, while Oil No. 3 has a low aniline point (157°F/70°C) and causes high or extreme swelling of seal compounds. Any other commercial oil with the same or similar aniline point can be expected to have a similar effect on a particular sealing material as the corresponding ASTM oil. However, it has been found that the aniline point method is not always reliable. Some commercial oils of the same

aniline point can differ significantly in their swelling power because they contain different sorts and amounts of additives.

A new, rapid, and more accurate method for predicting the compatibility of commercial rubbers in mineral based oils involves the use of a representative reference compound called standard NBR 1. The action of mineral oils can be evaluated against this standard rubber in terms of the elastomer compatibility index or ECI. Previous work has shown that there is an approximate linear relationship between the equilibrium percentage volume changes of NBR 1 in a range of mineral oils and those of any commercial nitrile in the same oils. In other words if equilibrium percentage changes in volume of different commercial nitrile rubbers in different mineral oils are plotted against those of standard elastomer NBR 1, a straight line can be obtained for each nitrile compound. This enables interested parties to predict the volume change of a particular rubber material in any mineral oil if the compatibility index of this oil (i.e. the percentage volume change of NBR 1) is known.

The straight line graph for a particular compound is called the swelling behavior, or SB of the compound. Figure A3-4 gives an example of such a graph.

Further details on elastomer compatibility index and swelling behavior can be provided on request.



Example: To find the volume change of Compound "X" in a mineral oil having an ECI of +10 for volume, follow the 10% vertical ECI line until it intersects the slanted line. Follow the horizontal line from that point to the vertical axis. Compound "X" will have a volume swell of approximately 2% in that oil.

OPERATING CONDITIONS The practical selection of a specific Parker compound number depends on adequate definition of the operating conditions for the seal. In approximate order of application, these are:

FLUID The first thing to be considered when selecting a compound is its resistance to the fluids with which it will

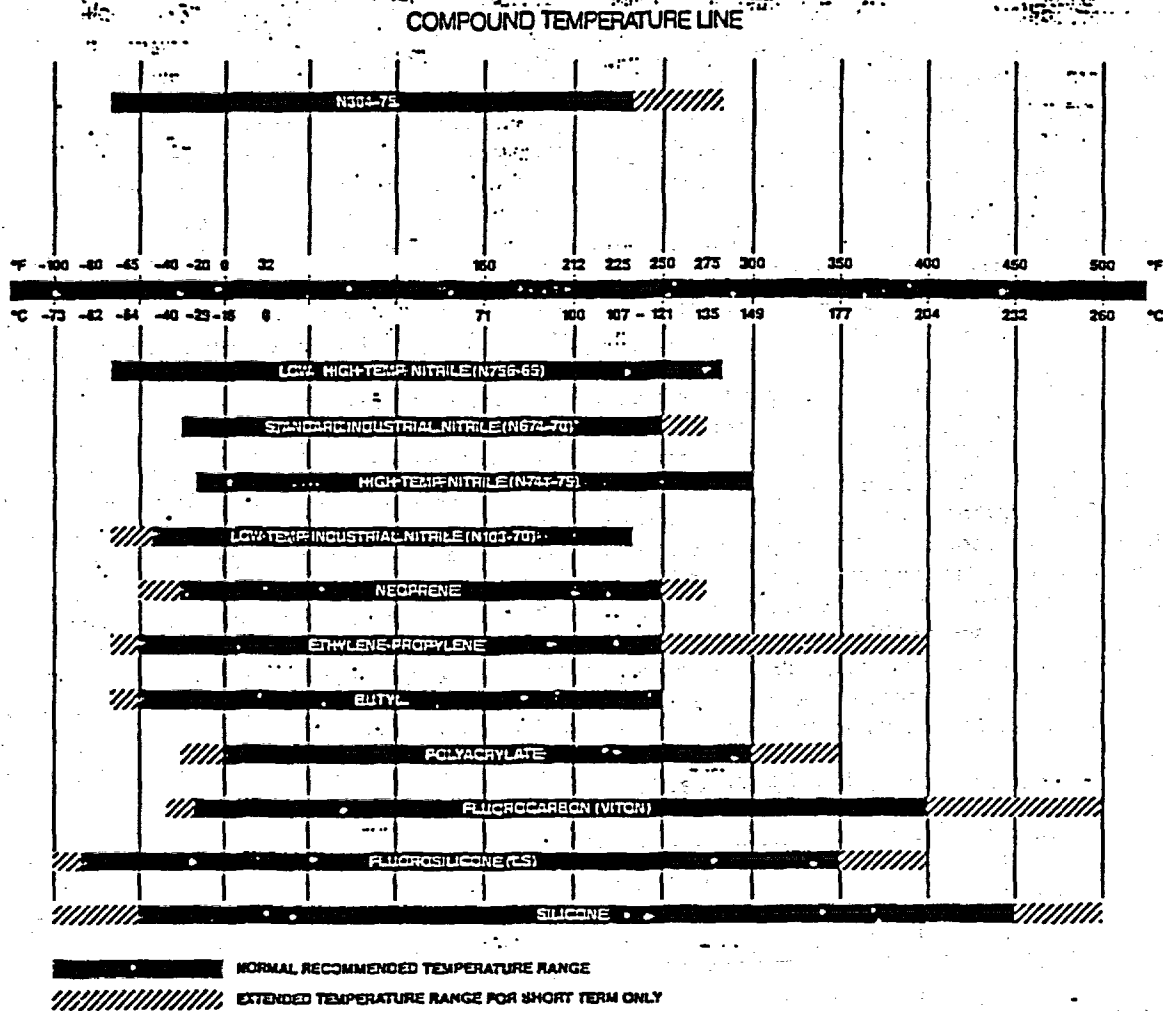
come in contact. This means all fluids, including the oil to be sealed, outside air, any lubricant, or an occasional cleaning or purging agent to be used in the system. For example, in pipe lines, it is common practice to pump a variety of fluids in sequence through a line with a pig (floating piug) separating each charge. In a crankcase, raw gasoline, diesel fuel, gaseous products of combustion, acids formed in service, and water from condensation, can be expected to contaminate the engine oil. In both these cases, the seal compound must be resistant to all fluids involved including any lubricant to be used on the seal. Therefore, whenever possible, it is a good practice to use the fluid being sealed as the lubricant, eliminating one variable.

Thus far only the effects of fluids on seal compounds have been discussed. Consideration must also be given to the effect of the compound on system fluids. For example:

- (1) There are some ingredients used in compounds which cause chemical deterioration of Freon refrigerants. When choosing a compound for use with Freon, it should not contain any of the ingredients which cause this breakdown.
- (2) Compounds containing large amounts of free sulfur for vulcanization should not be used in contact with certain metals or fluids, because the sulfur will promote corrosion of the metal or cause chemical change of the fluid.
- (3) Compounds for food and breathing applications should contain only non-toxic ingredients.
- (4) Seals used in meters or other devices which must be read through glass, a liquid, or plastic, must not discolor these materials and hinder vision. Sound judgment, then, dictates that all fluids involved in an application be considered. Once this is done, it is a simple matter to check the tables to find a compound suitable for use with all the media.

TEMPERATURE Temperature ranges are often over specified. For example, a torch or burner might reach temperatures of 750° to 1,000°F. However, the tanks of gas being sealed may be located a good distance from this heat source and the actual ambient temperature at the seal might be as low as 250° to 300°F (121° to 149°C). Or, a specification for aircraft landing gear bearing seals might call out -65° to +400°F (-54° to 205°C). Yet the bearing grease to be sealed becomes so viscous at -65°F (-54°C) it cannot possibly leak out. At the high end, there is a time-temperature relationship in the landing roll-out which allows rapid heat dissipation through the magnesium wheel housing on which the seals are mounted. This, combined with low thermal conductivity of the seal, limits heat input to the seal so that temperature may never exceed 160°F (71°C). As a result, a more realistic temperature range would be -30° to +180°F (-34° to +82°C). This can be handled by a good, industrial type nitrile compound as N674-70. Parker has applied a realistic temperature range with a margin of safety when setting the general operating temperature range for seal compounds. The maximum temperature recommendation for a compound is based on long term functional service. If it is subjected to this temperature continuously, it should perform reliably for 1000 hours. Time at less than maximum temperature will extend life. Similarly, higher temperature will reduce it.

FIGURE A3-5 TEMPERATURE CAPABILITIES OF PRINCIPAL ELASTOMERS EMPLOYED IN SEALS



Elastomers

TABLE A3-11 TYPES OF ELASTOMERS USED IN AIRPLANE AND AUTOMOBILE APPLICATIONS

Molding Dies
EPDM, SBR, or SBR/NATURAL RUBBER Blend
Ozone and Weather Resistant.

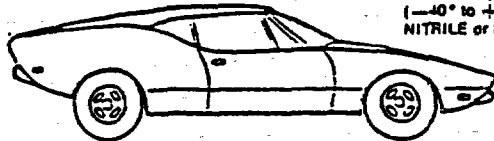
Transmission Fluid
-40° to +300°F
(-40° to +149°C)
NITRILE or POLYACRYLATE
Petroleum Oil Resistant

Instrument Fluid, Silicone Fluids
-65° to +275°F
(-54° to +149°C)
BUTYL or FLUROSILICONE

Thermal De-icing (Hot Air)
-65° to +500°F
(-54° to +260°C)
SILICONE

Windshield Wipers
NATURAL RUBBER
Abrasion, Water, Weather Resistant

Engine
-40° to +300°F
(-40° to +150°C)
NITRILE or POLYACRYLATE



Gasoline
-40° to +180°F
(-40° to +82°C)
NITRILE
Fuel Resistant

Inner Tubes
BUTYL
Permeability Resistant

Brake Fluid
-40° to +250°F (-40 to +121°C)
ETHYLENE PROPYLENE or SBR

Fuel (JP5), Access Doors
-65° to +160°F
(-54° to +71°C)
NITRILE

Lubricating System
Lubricating Oils (Diester Base)
-65° to +275°F
(-54° to +135°C)
FLUOROELASTOMERS

Tires
NATURAL RUBBER/SBR or SBR/BR Blends
Abrasion Resistant.

Landing Gear Brake Systems (Phosphate Esters)
-65° to +300°F
(-54° to +149°C)
ETHYLENE PROPYLENE

The high temperature limits assigned to compounds in this handbook are conservative estimates of the maximum temperature for 1000 hours of continuous service in the media the compounds are most often called on to seal. Since the top limit for any compound varies with the medium, the high temperature limit for many compounds is shown as a range rather than a single figure. This range may be reduced or extended in unusual fluids.

Since some fluids decompose at a temperature lower than the maximum temperature limit of the elastomer, the temperature limits of both the seal and the fluid must be considered in determining limits for a system.

Low temperature service ratings in the past have been based on values obtained by ASTM test methods D736 and D746. The present ASTM D2000/SAE 200 specification still calls for the ASTM D746 low temperature test (ASTM D736 is obsolete). For O-rings and other compression seals, however, the TR-10 value per ASTM D1414 provides a better means of approximating the low temperature capability of an elastomer compression seal, the low temperature sealing limit being generally about 15°F below the TR-10 value. This is the formula that has been used, with a few exceptions, to establish the recommended low temperature limits for Parker Seal Group compounds in tables A3-13, B5, and B10.

This is the lowest temperature normally recommended for

static seals. In dynamic use, or static applications with pulsing pressure, sealing may not be accomplished below the TR10 temperature, or 15°F higher than the low limit recommendation in the Handbook.

These recommendations are based on Parker tests. Some manufacturers use a less conservative method to arrive at low temperature recommendations, but similar compounds with the same TR10 temperature would be expected to have the same actual low temperature limit regardless of catalog recommendations.

A few degrees may sometimes be gained by increasing the squeeze on the O-ring section, while insufficient squeeze may cause O-ring leakage before the recommended low temperature limit is reached.

The low temperature limit on an O-ring seal may be compromised if the seal is previously exposed to extra high temperature or a fluid that causes it to take a set, or is a fluid that causes the seal compound to shrink. Conversely, the limit may be lowered significantly if the fluid swells the compound.

With decreasing temperature, elastomers shrink approximately ten times as much as surrounding metal parts. In a rod type assembly, whether static or dynamic, this effect causes the sealing element to hug the rod more firmly as the temperature goes down. Therefore, an O-ring may seal below the recommended low temperature limit when used as a rod type seal.

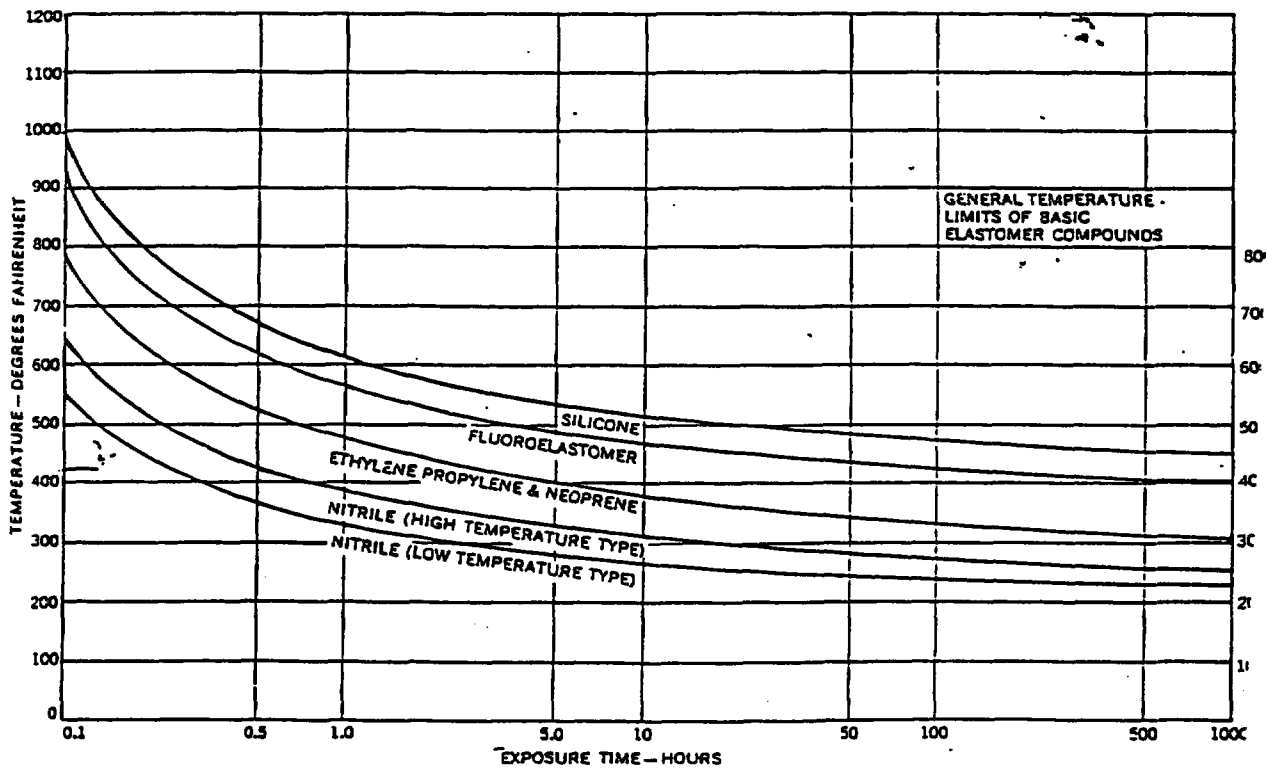


FIGURE A3-6 SEAL LIFE AT TEMPERATURE

This chart is intended only as a rough guide. It cannot be used for precise predictions of seal life. Results will vary with compound and fluid medium.

When excessive side loads are encountered on maximum tolerance rods or glands, and the pressure is in the low range, leakage may occur at temperatures 10 or 15°F (5 or 8°C) above the TR-10 value. It may be necessary, therefore, to add as much as +40°F (+22°C) to the low temperature shown in the tables for this type of service.

TIME The three obvious "dimensions" in sealing are fluid, temperature, and pressure. The fourth dimension, equally important, but easily overlooked, is time.

Heretofore temperature limits, both high and low, have been published at conventional short term test temperatures. These have little bearing on actual long term service of the seal in either static or dynamic applications. A comparison of the temperature limits of individual compounds in this handbook with previous literature will reveal that for comparable materials the upper temperature limit is more conservatively expressed. The narrower temperature range does not imply that the compounds discussed are inferior to others. Rather, that high temperature values based on continuous seal reliability for 1,000 hours are being recommended. As illustrated by graph (Fig. A3-6), short term or intermittent service at higher temperatures can be handled by these materials.

For example, an industrial nitrile (buna N) compound, N674-70, is recommended to only 250°F, yet it is known to seal satisfactorily for five minutes at 1000°F (538°C) and at 300°F (149°C) for 300 hours. Therefore, when the application requires a temperature higher than that recommended in the compound and fluid tables, check the temperature curve to determine if the total accumulated time at high temperature is within the maximum allowable limit. The sealing ability of a compound deteriorates with total accumulated time at temperature. The curves show the safe, cumulative time at a given temperature for specific elastomers used as static seals. For dynamic seal applications, temperatures as much as 25°F (14°C) below those indicated may be more realistic.

MECHANICAL REQUIREMENTS An important consideration in selecting the proper seal material should be the nature of its mechanical operation, i.e. reciprocating, oscillating, rotating, or static. How the seal functions will influence the limitations on each of the parameters (fluids, temperature, pressure, and time) previously discussed.

Static applications require little additional compound consideration. The prime requisite of a static seal compound is good compression set resistance.

Dynamic applications, due to movement, are more involved.

All properties must approach the optimum in a dynamic seal compound, resilience to assure that the seal will remain in contact with the sealing surface, low temperature flexibility, to compensate for thermal contraction of the seal, extrusion resistance to compensate for wider gaps which are encountered in dynamic glands, and abrasion resistance, to hold to a minimum the wearing away or eroding of the seal due to rubbing.

COMPOUND PREFERENCE If a choice of more than one compound exists after following all specified steps the deciding factor will probably be cost or availability. Use table A3-12 as a guide, or contact your Parker representative for this information.

TABLE A3-12 ORDER OF POLYMER PREFERENCE

ORDER OF PREFERENCE	COMPOUND	ORDER OF PREFERENCE	COMPOUND
1	Nitrile (N)	7	SBR (G)
2	EP (E)	8	Polyacrylate (A)
3	Fluorocarbon (V)	9	Fluorosilicone (L)
4	Neoprene (C)	10	Butyl (B)
5	Silicone (S)	11	Epichlorohydrin (Y)
6	Polyurethane (F)	12	Polysulfide (T)

SELECTING A COMPOUND Having discussed the major aspects of seal design that affect compound selection, here is a summary of the necessary steps to follow, always keeping in mind that standard compounds should be used wherever possible for availability and minimum cost.

1. If military fluid or rubber specifications apply, select the compound from table B1 or B2.
2. For all other applications, locate all fluids that will come in contact with the seal in the fluid compatibility table, table B5.
3. Select a compound suitable for service in all fluids, considering the mechanical (pressure, dynamic, static) and temperature-time requirements of the application.
4. If a compound of different durometer from that listed in the fluid compatibility tables must be used, find a harder or softer compound in the same base polymer in table A3-13*.

*NOTE: The Parker Seal compound designations have a definite purpose. In addition to being catalog numbers, they denote the base polymer by prefix letter and the durometer hardness by suffix number. However, there is one exception, compound 47-071, which was shown on military QPL lists before Parker Seal initiated their latest numbering system. Once approved by the Military, a compound designation cannot be changed.

TABLE A3-13 COMPOUND SIMILARITY

General purpose O-ring compounds are listed by polymer and type A durometer hardness for ease of selection. Note that the last two digits of Parker O-ring compound numbers indicate this type A hardness. For example, compound E540-80 is an 80 durometer material. The one exception is compound 47-071, which is a 70 durometer compound.

Butadiene, chlorosulfonated polyethylene, isoprene, natural rubber, and a few other elastomers do not generally perform as well as the listed polymers in seal applications, and Parker does not offer O-rings in these materials. See the fluid compatibility table for alternates in the desired fluid medium.

POLYMER	COMPOUND	TEMPERATURE RANGE(1)	
		DEGREES FAHRENHEIT	DEGREES CELSIUS
Polyacrylate	A1107-70	-5 to 350	(-20 to 177)
Butyl	B612-70	-75 to 250	(-60 to 120)
Neoprene	C356-45	-70 to 250/300	(-60 to 120/150)
	C267-50	-60 to 250/300	(-50 to 120/150)
	C518-60	-60 to 250/300	(-50 to 120/150)
	C557-70	-45 to 250/300	(-43 to 120/150)
	C873-70	-45 to 250/300	(-43 to 120/150)
	C944-70	-45 to 250/300	(-43 to 120/150)
	C147-70	-55 to 250/300	(-48 to 120/150)
Ethylene Propylene	E529-60	-75 to 250/400	(-60 to 120/205)
	E603-70	-70 to 250/400	(-57 to 120/205)
	E692-75	-70 to 250/400	(-57 to 120/205)
	E540-80	-70 to 250/400	(-57 to 120/205)
	E893-80	-70 to 250/400	(-57 to 120/205)
	E1080-80	-70 to 250/400	(-57 to 120/205)
Polyphosphazene	F953-70	-85 to 350	(-65 to 177)
	G244-70	-70 to 225	(-57 to 107)
SBR (Buna S)	L999-40	-100 to 350	(-73 to 177)
Fluorosilicone	L449-65	-100 to 350/400	(-73 to 177/205)
	L1120-70	-100 to 350	(-73 to 177)
Nitrile	N545-40	-45 to 225/250	(-43 to 107/120)
	N299-50	-55 to 225/250	(-48 to 107/120)
	N406-60	-40 to 225/250	(-40 to 107/120)
	N525-50	-25 to 250	(-32 to 120)
	N506-65	-70 to 180/225	(-57 to 82/107)
	N674-70	-30 to 250	(-35 to 120)
	N497-70	-35 to 212	(-37 to 100)
	N163-70	-45 to 250	(-43 to 120)
	47-071 (2)	-60 to 180/225	(-51 to 82/107)
	N103-70	-55 to 225	(-48 to 107)
	N602-70	-70 to 180/225	(-57 to 82/107)
	N741-75	-20 to 250/300	(-29 to 120/150)
	N304-75	-65 to 225/250	(-55 to 107/120)
	N756-75	-65 to 250/275	(-55 to 120/135)
	N256-85	-15 to 212	(-25 to 100)
	N552-90	-30 to 250	(-35 to 120)
	N507-90	-65 to 180/250	(-55 to 82/120)
Polyurethane	P642-70	-40 to 180/225	(-40 to 82/107)
Silicone	S469-40	-75 to 400/450	(-60 to 205/232)
	S595-50	-70 to 400/450	(-57 to 205/232)
	S613-60	-60 to 450	(-50 to 232)
	S604-70	-65 to 450	(-55 to 232)
	S455-70	-65 to 450/500	(-55 to 232/260)
	S614-80	-60 to 400	(-50 to 205)
Fluorocarbon	V747-75	-15 to 400/500	(-25 to 205/260)
	V835-75	-40 to 400	(-40 to 205)
	V884-75	-15 to 400	(-25 to 205)
	V709-90	-15 to 400	(-25 to 205)

(1) The low temperature limits shown here are 15°F below the JF10 values. Actual limits in use will vary with the fluid medium. See Figure A3-6 for effect of time at varied temperature.

(2) 47-071 is a 70 durometer nitrile compound.

testing

An elastomer is seldom under the same confinement conditions when laboratory physical property tests are made as when installed as a seal. The usual compression, lack of tension, and limited room for expansion as installed, all result in a different physical response from that measured on an identical but unconfined part.

Example: A silicone compound tested in hydrocarbon fuel in the free state may exhibit 150% swell. Yet, seals of such a compound confined in a gland having volume only 10% larger than the seal, will likely perform satisfactorily. Complete immersion may be much more severe than an actual application where fluid contact with the seal is limited through design. Or, the service might involve only occasional splash or fume contact with the fluid being sealed. Different parts made from the same batch of compound under identical conditions will give varying results when tested in exactly the same way because of their difference in shape, thickness, and surface to volume relationship (see figure A3-7). Humidity alone has been found to affect the tensile strength of some compounds.

Correlation between test data and service conditions is not a simple problem, it is an industry-wide problem. Until improvement can be made, manufacturers and users must use the available data to the best of their ability. In essence, it is the misapplication of data, not the measurements, that causes difficulty. However, with data in some other form, such misapplication might well be reduced greatly.

ASTM Designation D471 (Standard Method of Test for Change in Properties of Elastomeric Vulcanizates Resulting from Immersion in Liquids) states: "In view of the wide variations often present in service conditions, this accelerated test may not give any direct correlation with service performance. However, the method yields comparative data on which to base judgment as to expected service quality and is especially useful in research and development work."

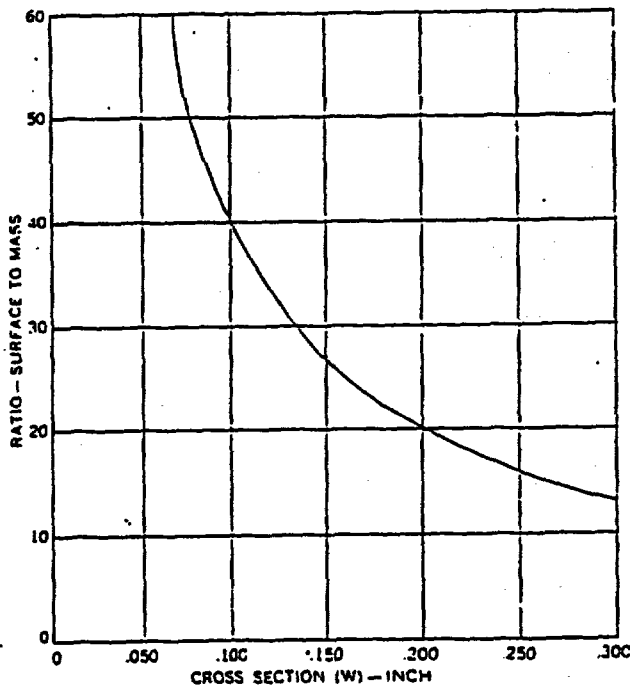


FIGURE A3-7 RELATIVE EFFECT OF O-RING CROSS SECTION ON AREA EXPOSED TO FLUID ATTACK (TOTAL IMMERSION).

3. TRANSNUCLEAIRE SELECTED REFERENCE PAGES

3. TRANSNUCLEAIRE SELECTED REFERENCE PAGES

This page left blank intentionally.

This page left blank intentionally.

REPORT ON THE IMPLICATIONS OF THE
TESTS REQUIREMENTS FOR TYPE B
PACKAGINGS AND A STUDY OF
PRACTICAL SOLUTIONS

EURATOM CONTRACT N° 024 - 65 - E.C.I.C.



TRANSNUCLEAIRE

11 & 11 Bis Rue Christophe Colomb.

Paris 8^e

Tel. 225 14 77

225 08 86

Telex 28.992

7 West 57th Street

New York, NY 10019

355 7320

" REPORT ON THE IMPLICATIONS OF THE TESTS REQUIREMENTS FOR
TYPE B PACKAGINGS AND A STUDY OF PRATICAL SOLUTIONS "

- CONTENTS -

<u>INTRODUCTION</u>	7
<u>PART I - THERMAL TEST -</u>	13
<u>- CHAPTER I -</u>	
<u>GENERAL -</u>	
<u>- CHAPTER II -</u>	
<u>HEAT EXCHANGE BETWEEN FIRE AND PACKAGING -</u>	21
<u>CASE OF A CONVEX SURFACE -</u>	
1 - Heat exchange by radiation	22
2 - Heat exchange by convection	24
3 - Overall value of heat exchange	24
4 - Specific case of the theoretical test data	25
<u>- CHAPTER III -</u>	
<u>STUDY AND INFLUENCE OF THE VARIOUS PARAMETERS OF HEAT EXCHANGE -</u>	29
1 - Radiation temperatures	31
2 - Emissivity of the radiation environment	32
3 - Absorption coefficient of the surface of the packaging	34
3.1 - Tests on mild steel specimens	34
3.2 - Tests on stainless steel specimens	39
4 - Emissivity coefficient of the packaging surface	40
5 - Estimation of heat exchange by convection	40
5.1 - Fire parameters	40
5.2 - Surface parameters	42
5.3 - Order magnitude of heat exchange	42
6 - Specific case of the regulatory open-fire	46
6.1 - Flame temperature	46
6.2 - Flame emissivity	48
6.3 - Incident radiated flux	48
6.4 - Absorption coefficient of the external surface	48
6.5 - Amount of convection	49

- CHAPTER IV -HEAT EXCHANGE BETWEEN FIRE AND PACKAGING -
CASE OF AN EXTERNAL FINNED SURFACE -

1 - Theoretical study	83
1.1 - Absorption of the quantity of incident heat radiated by the fire	83
1.2 - Quantity of heat emitted by the packaging	83
1.3 - Quantity of heat absorbed by convection	83
1.4 - Complete formulation	83
2 - Experimental study	81
2.1 - Test program	82
2.2 - Results	81
3 - Conclusion	81

- CHAPTER V -CALCULATION OF HEAT DIFFUSION IN THE PACKAGING -

1 - Graphical method	87
1.1 - Plane surfaces	87
1.2 - Cylinder of revolution	94
1.3 - Spherical packaging	99
2 - Iterative numerical calculative method	103
2.1 - Applications in common with the graphical method	103
2.2 - Application to a parallelepiped packaging	104
3 - Analytical method	109
3.1 - Application to lead-steel packagings-plane wall	111
3.2 - Application to lead-steel packagings-cylindrical walls	116
4 - Melting of lead	122
4.1 - Heat transmission through liquid lead	123
4.2 - Progression of the melting face	123
4.3 - Calculation in the case of total melting of the lead	123
4.4 - Calculation in the case of partial melting of the lead	125
5 - Steel packagings	127
6 - Packagings without γ shielding	130

- CHAPTER VI -CONSEQUENCES OF THE THERMAL TEST

1 - Temperatures reached in the shielding material	131
2 - Temperatures reached by the contents	133
2.1 - Lead-steel packagings	136
2.2 - Steel packagings	139
2.3 - Packagings without shielding	139
3 - Temperatures reached by the gaskets	140
4 - Temperature gradients in packaging	140
5 - Conclusion	141

- <u>CHAPITRE VII</u> -	
<u>THERMAL PROTECTION METHODS</u>	143
- <u>ANNEX I</u> -	
<u>THERMAL CHARACTERISTICS OF STEEL AND LEAD LEAD-STEEL JUNCTIONS -</u>	157
- <u>ANNEX II</u> -	
<u>TEST METHOD USING SCALE MODEL -</u>	175
- <u>ANNEX III</u> -	
<u>REMARKS ON THE THERMAL TEST DEFINITIONS -</u>	193
<u>PART II - MECHANICAL TEST -</u>	185
- <u>CHAPTER I</u> -	
<u>GENERAL -</u>	187
- <u>CHAPTER II</u> -	
<u>MECHANICAL CHARACTERISTICS OF MATERIALS IN THE ENVIRONMENTAL CONDITIONS OF THE MECHANICAL TEST -</u>	193
1 - Steel	194
1.1 - Deformation and fracture of steel	194
1.2 - Method of calculating the resistance of a Packaging	196
1.3 - Parameters encouraging the appearance of brittle fracture	198
2 - Lead	208
- <u>CHAPTER III</u> -	
<u>NINE METER DROP - STEROMECHANICAL ASPECTS OF THE IMPACT -</u>	209
1 - Velocity and energy	209
1.1 - General relationships	209
1.2 - Order of magnitude of	211
1.3 - Maximum rebound velocity	212
1.4 - Vibrating energy released on impact	213
2 - Decelerations and velocities during a drop onto a side	214
2.1 - Theoretical study	215
2.2 - Experimental results	224
3 - Edge or corner drop	230
3.1 - Mechanism of the impact	230
3.2 - Decelerations and deformations	232

- INTRODUCTION -

This report covers the studies we have carried out and the results obtained, in accordance with the tasks attributed to our Company as part of the Study Contract cited in reference.

By this contract, the EUROPEAN ATOMIC ENERGY COMMUNITY entrusted a group of five organizations and societies, acting jointly and severally (BELGONUCLEAIRE - Belgium, COMMISSARIAT A L'ENERGIE ATOMIQUE - France, NUKEM - Federal Republic of Germany, PHILIPS DUPHAR - Holland, TRANSNUCLEAIRE - France) with an overall set of studies the object of which may be briefly summarized : the technical requirements relating to packagings for radioactive materials.

The technical requirements in question were drawn up by the International Atomic Energy Agency in its "Regulations for the Safe Transport of Radioactive Materials, 1964 Revised Edition" (amended in 1966 and taking into account the approved results of the work of a Group of Experts in February, 1966), which we shall hereafter refer to in this report as : the Regulations.

Within the overall set of studies, the specific tasks allotted to our Company are summarized in the title of this report :

"REPORT ON THE IMPLICATIONS OF THE TESTS REQUIREMENTS FOR
TYPE B PACKAGINGS AND A STUDY OF PRACTICAL SOLUTIONS"

The tests in question are primarily those described in Annex IV.1.4 of the Regulations, representing conventional accident conditions. These tests comprise, cumulatively, a mechanical test (a 9 meter drop onto a rigid flat surface, a 1.20 meter drop onto a steel bar), and a thermal test.

- CHAPTER IV -

OVERALL AND LOCAL DAMAGE

I - 1 METER DROP

II - 9 METER DROP

1 - Overall damage -

2 - Local damage -

ANNEX IV.1 -

Description of the one-ton model packaging

- CHAPTER V -

STUDY OF THE DIMENSIONING OF THE CLOSURE DEVICE

I - CALCULATION IN THE ELASTIC RANGE -

- 1 - Calculation method using certain simple assumptions
- 2 - Extension of the calculation method to the general case

II - FRACTURE CALCULATIONS -

III - SHEARING -

IV - EXPERIMENTAL STUDY -

V - SIMILARITY -

- CHAPTER VI -

STUDY OF SHOCK- ABSORBING COVERS

CONCLUSION

BIBLIOGRAPHY

A type B packaging must meet the following requirements after these tests : retain sufficient of its radiation shielding, prevent loss or dispersal of the radioactive contents (with certain tolerances in the case of large sources).

How should packagings be studied, designed, planned and fabricated to meet these requirements and how should it be decided and proved that the requirements are met ? Anybody who has been concerned with these problems has been aware of the difficulties and the economic consequences.

The difficulties arise mainly from the fact that the problems arising are in general outside the scope of the conventional work of a constructor's design office and that, for a number of these problems, the physical, mathematical or experimental basis for solving them are poorly defined or possibly even non-existent.

It is therefore most often appropriate, as the Regulations say, to carry out drop and thermal tests on models or prototypes of the packaging in question.

However, in a number of cases this leads to a very considerable expenditure because, while a large number of tests have to be carried out in order to be certain of producing the maximum amount of damage, several prototypes have sometimes to be fabricated and tested before evidence is obtained that the packaging meets the Regulations. Moreover, such tests become virtually impossible to perform for very large packagings.

However, for some years, a number of studies have been undertaken in this field by various countries (notably the United States, England and France) : pure theoretical studies, theoretical and experimental studies on scale models, and systematic experimental studies.

Substantial results have been obtained. They now make it possible to dispense with a number of tests, and it is even possible to show directly that some packagings conform by calculative methods or other appropriate evidence, as contained in the Regulations.

Because of the obvious value of such results, not only from the economic standpoint but also from the technical standpoint (since they can lead to methods of proving which are of wider scope than isolated tests), we were requested to proceed with the work undertaken.

The guidelines laid down were as follows :

- To establish practical calculative methods, with numerical examples, for the largest possible number of the problems to be solved.

When calculation is not possible, to establish test methods on scale models or partial assemblies. Where applicable, to justify methods by comparison.

- Starting from the general results of calculations and tests carried out during the study, and from the whole set of results (tests and calculations) published in the literature, to formulate general recommendations for the design and construction of packagings.
- To give a few examples of practical ways of meeting the requirements of the Regulations.

We were also asked to go beyond general recommendations and to try to establish technical specifications. This, we were unable to do, partially because of the great variety of cases to be dealt with, and also because we could make no claim to provide definitive solutions.

This report summarizes the basic features of the studies which we have carried out within the general framework explained above.

Although most of the examples chosen and the related tests concern lead-steel packagings, the methods explained and recommendations made are generally applicable to a very large number of types of packaging .

3 - LEAD-STEEL JUNCTION -

a) No bond -

When fabrication is made without trying to obtain bonding between lead and outer shell, shrinkage occurs during cooling after casting due to the difference of dilatation coefficients of lead and steel.

The importance of shrinkage depends on casting methods and outer shell dimensions and materials.

With a stainless steel outer shell and adequate casting method, shrinkage is on the order of 4°/oo, i.e. for instance 2 mm at the radius for a packaging of 1 m diameter.

With a mild steel outer shell, whose dilatation coefficient is lower than for stainless steel, shrinkage may be greater.

b) Lead bonded -

Bonding can be obtained by various processes, which we will not explain here.

Let us say only that bonding can be easily achieved on an open steel wall it is much more difficult inside a steel vessel practically closed. It is also more difficult with stainless steel than with mild steel.

If bonding is perfect, which can be checked by ultra-sonic inspection, thermal bond should also be perfect.

This is actually obtained for instance with a plane steel wall and a certain thickness of lead bonded, the outer surface of the lead being bare.

On the other hand, our experience shows us that in the case of packagings and in spite of a perfect bonding to the outer shell, ultra-sonic checked, there is always some discrepancy between thermal test and calculations for the heat transmission through the inner shell/lead/outer shell assembly.

Compared with calculations based on a perfect thermal bonding, tests show that in fact there is a certain extra resistance to the passage of heat.

Thus, on a series of six identical cylindrical 20 ton packagings (constructed by the Soci t  Lyonnaise de Plomberie Industrielle), an extra resistance to the passage of heat compared with calculations is found equivalent to an air gap of 25mm varying slightly around this value according to the packaging. Ultrasonic inspection, however, showed perfect outer shell/lead bonding.

There are a number of possible explanations :

- The calculation cannot be very accurate particularly when there is a great difference between the outer shell surface area and the inner cavity surface area. This was the case for the six packagings mentioned above.

If the heat flux introduced in the calculation is the flux on the inner cavity, there is then good agreement between tests and calculation.

- Bonding to the outer shell has a tendency to work against hooping on the inner shell.
- Lack of homogeneity in the lead mass which is being drawn both towards the outer shell and towards the inner shell.
- Traces of oxide over a varying surface area at the outside shell/lead interface (which does not show up with ultra-sonic controls).

We have no knowledge of the results obtained by other constructors.

c) Behavior in the thermal test -

In the case of not bonded lead, an air gap of say, 2 mm, corresponds to a temperature drop of several hundred degrees, for the initial heat fluxes involved in the thermal test.

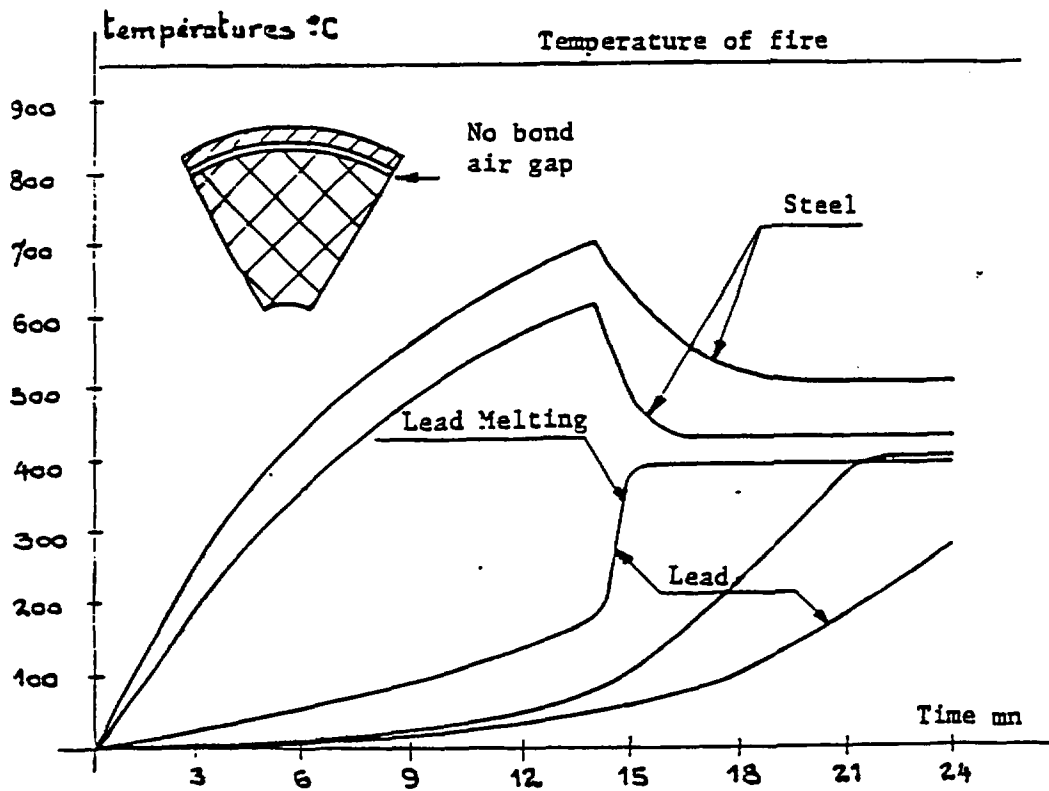
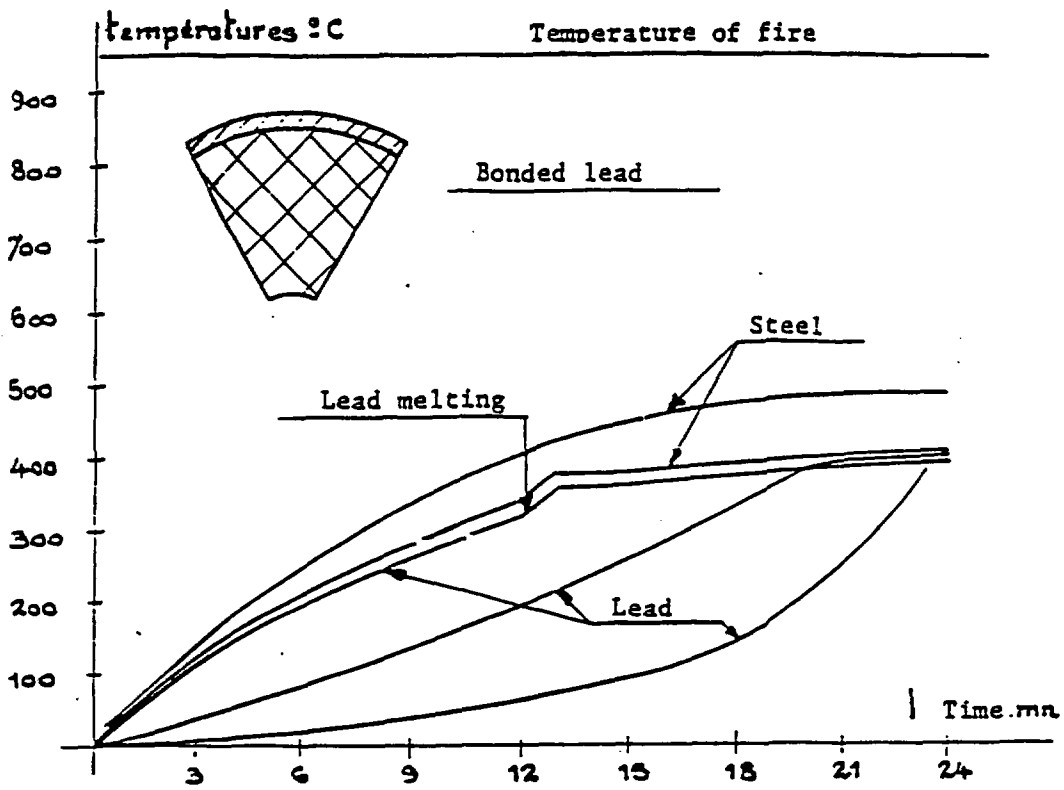


FIG. A.2

The temperature of the outer shell will thus rise very quickly, enlarging still further the air gap because of the differential expansion compared with the relatively cold lead.

The shell will then transmit heat to the lead by radiation.

In reality, the process will often be less accentuated, because the air gap is not uniformly distributed and its overall effect will be substantially reduced.

In the case of bonded lead, there will be little or no temperature drop (perfect thermal bonding) between the outer shell and the lead.

The French Commissariat à l'Energie Atomique has carried out a number of very interesting tests in this field.

Models of the sort shown schematically in figure A 2 have been produced and tested either in a furnace or in an open air fire.

In figure A 2, we give the comparative results for two similar models, one with bonded lead and the other with a uniformly distributed air gap.

In spite of the very considerable difference between the curve showing the temperature rise in the outside layer of lead, there is only a difference of 2 to 3 minutes for the beginning of melting and the same temperature ceiling is reached in the molten lead.

For this reason, we feel that when calculations are carried out, it is necessary to make the assumption of perfect thermal contact between the outer shell and the lead, whether or not the lead is bonded.

These tests show that the temperature ceiling is at about 375°C. This would appear anomalous although explanations for it can be found (see chapter V, paragraph 4).

2.2.1 - Measurements made on a 15 ton packaging

The packaging used was a 15 ton Dupont de Nemours packaging which has been the subject of a large number of drop tests. Shown below is an extract from the table contained in reference 11, summarizing the measurements of deceleration at various points in the packaging, for various drop height :

Test n°	1	2	3
Drop height	2.30 m	4.50 m	9.10 m
Impact surface	bottom	bottom	bottom
Deceleration on bottom (25cm from the impact face)	320 g	750 g	1200 to 1500 g
Deceleration at upper part (1.20 m from the impact face)	140 g	250 g	?

These results clearly show that during an impact, deceleration varies according to the height of the point considered in the packaging.

They confirm that in real cases decelerations are lower at low levels and higher at high levels than in the theoretical picture obtained above.

They also show that deceleration varies roughly linearly as a function of the height of drop.

- BIBLIOGRAPHY -

- 1 - Williams H. Mac Adams - "Heat Transmission".
(Mac Graw-Hill - New York - 1964 - 3rd edition)
- 2 - Minutes of the Albuquerque Symposium - 12/15 January 1965.
- 3 - G.P. Wachtell and J.W. Langhaar
Fire test and thermal behaviour of 15 ton lead shielded cask.
(AEC Research and development report - doc. DP 1070 - October 1966).
- 4 - Aktiebolaget Atomenergi
Doc. T PM/SK - 190 - 195 - 199 - and 223
M.R. Blomquist : "Thermal test on finned transport containers".
- 5 - CEA document n° TS/O2934 dated 19.7.1965
"Compte rendu provisoire de l'essai au feu effectué à
Moronvilliers dated 15th April 1965"
- 6 - L.B. Shappert : "A guide to the design of shipping casks for
the transportation of radioactive material".
- 7 - CEA document N-536 - "Essai au feu des emballages pour le transport
des produits radioactifs : définition des conditions d'essai".
- 8 - CEA document TS/O 36626 dated 16th February 1966
"Compte rendu des essais au feu effectués à Moronvilliers
dated 20th October 1965".
- 9 - F.E. Dixon : "The design of shielded containers to IAEA standards"
Doc. UKAEA - TCAP/P 64 - August 1962.
- 10 - L.H. Horn : "Fire tests of shipping containers and Cobalt 60
teletherapy head" - Underwriters, laboratories - doc. 000274
category n° UC 23 - I I T - TID 4500 - 31st March 1963.
- 11 - W.I. Thisell and J.W. Langhaar : "Static and Impact tests on 15 ton
cask for shipping irradiated fuel" issued by Savannah River Laboratory
Doc. DP 843.
- 12 - Timoshenko : "Strength of Materials", Part I and Part II.
- 13 - Werner Goldsmith "Impact - The theory and physical behaviour
of colliding solids". (Publisher : Arnold - London).

4. **MDS NORDION METALLURGICAL REPORT NUMBER 9724
TYPE 316L STAINLESS STEEL TIME/TEMPERATURE SENSITIZATION TESTING
REPORT, JUNE 1998
(REFERENCE [59])**

This page left blank intentionally.

MDS NORDION METALLURGICAL REPORT NUMBER 9724

TYPE 316L STAINLESS STEEL
TIME/TEMPERATURE SENSITIZATION TESTING
REPORT

J CULBERTSON
June 5, 1998

TABLE OF CONTENTS

1.....INTRODUCTION

2.....SUMMARY

3.....CHART 1

4.....DISCUSSION

5.....PHOTOGRAPHS

1.....INTRODUCTION

Type 316L Stainless Steel, commonly used for radioisotope encapsulation, has been tested for formation of chromium carbide precipitation. The precipitation, referred to as sensitization, is of primary concern when formed in the grain boundaries. The grain boundary carbide is an indication that the stainless steel has lost some of its resistance to corrosion. The low carbon grade of stainless steel (316L) is selected for use largely because of its lower probability of sensitization. This brief study is focused on the amount of grain boundary sensitization. The tests performed in this study included selected temperature soaks (900, 1000 and 1200⁰F) for various lengths of time.

2.....SUMMARY

Exposure times of up to 1000 hours at 900⁰F have resulted in no formation of sensitized material. There is, however, some sensitized material after 10 hours exposure at 1000⁰F. There is sensitized material formed after 1 hour at 1200⁰F. Chart 1 relates the extent of sensitization of the test samples. Figures 1 to 5 illustrate the effect on the microstructure from some exposures.

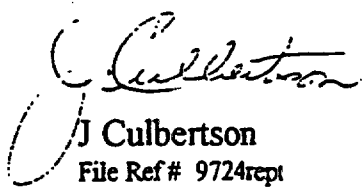
3.....CHART 1.

Relative Amount of Carbide Formation
(% of linear transformation of grain envelope)

SOAK TIME (Hours)	900 ⁰ F	1000 ⁰ F	1200 ⁰ F
<i>1</i>	0	0	10-30
<i>3</i>	0	0	30-40
<i>8</i>	0	0	40-50
<i>10</i>	0	2-4	50-60
<i>30</i>	0	4-8	60-65
<i>80</i>	0	20-30	85
<i>100</i>	0	50-60	95
<i>300</i>	0	70-80	100
<i>1000</i>	0	Not req'd	Not req'd

4.....DISCUSSION

The 316L stainless steel used for this testing was in the form of tubing. The tubing was inserted into the furnace in an air environment, which is most representative of the conditions encountered during the lifetime of finished capsules. The percentage of carbide precipitation within the grain boundaries, as presented in chart 1, is a linear measure of the formation of the precipitate as a ratio of the overall linear grain boundary total. The results of this test program illustrate the advantage of using the low Carbon grade type 316 stainless steel. While sensitization can occur within the temperature range of 800^oF and 1500^oF it appears as though the low carbon grade will resist sensitization at 900^oF for an indefinite time and above 900^oF for shorter times. Even the low carbon grade, however, will suffer sensitization quite rapidly at 1200^oF.


J Culbertson
File Ref # 9724rept

5....PHOTOGRAPHS

Figure 1 Typical austenitic grain structure with no sensitization
Exposure: 100 hours at 900°F

400X
9724A

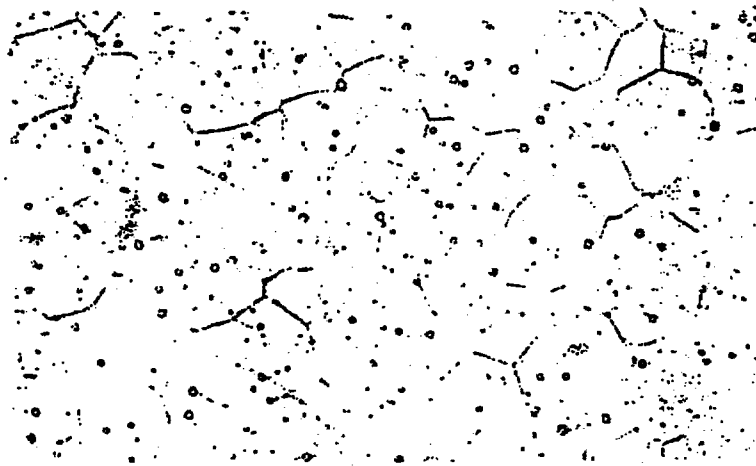


Figure 2 Austenitic grain structure with some sensitization
Exposure: 3 hours at 1200°F

400X
9724B

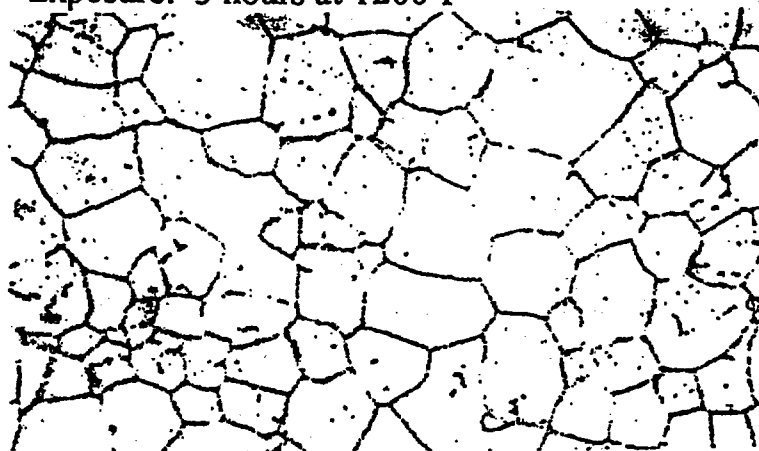


Figure 3 Austenitic grains enveloped by carbide precipitation
Exposure: 300 hours at 1200°F

400X
9724C

5....PHOTOGRAPHS



Figure 4 Austenitic grain structure of control sample. Material with no elevated temperature exposure. Note: No sensitization
9724D 200X

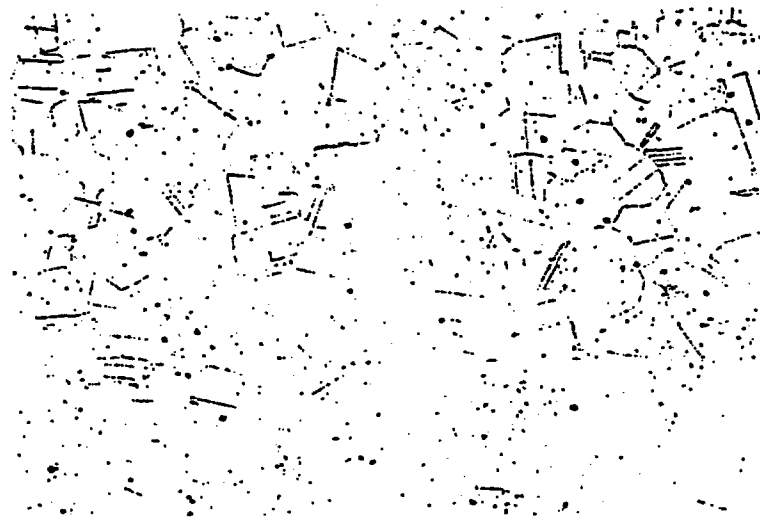


Figure 5 Austenitic grain structure of sample material exposed for 1000 hrs at 900°F. Note: no sensitization
9724E 200X

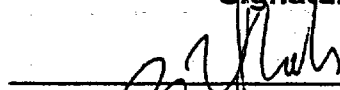
5. **IN/QA 1368 F294: TEST PLAN FOR F-294 REGULATORY TESTS**
(REFERENCE [48])

This page left blank intentionally.

Test Plan for F-294 Regulatory Tests

Signatures

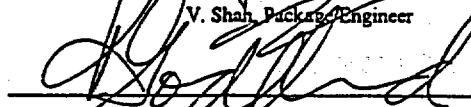
Prepared by:



V. Shah, Package Engineer

Date: 98-07-12

Reviewed by:



R. Goddard, Manager, Industrial Source Production

Date: 98/1/12

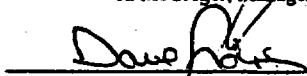
Reviewed by:



R. McGregor, Manager, Regulatory Affairs

Date: 98/6/13

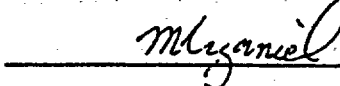
Approved by:



D. Sidney, Manager, Quality Assurance

Date: 98-01-15

Approved by:



M. Krzaniak, Manager, Package & Facility Engineering

Date: 98/6/14

Document History

Date	Version	Comments	Prepared by	Reviewed by	Approved by
	1	CCF: A1232-C-00A			

TABLE OF CONTENTS

1. INTRODUCTION..... 3

2. QUALITY ASSURANCE REQUIREMENTS..... 3

2.1 TESTING BY MDS NORDION INTERNATIONAL 3

2.2 INDEPENDENT TESTING..... 3

2.3 MEASURING EQUIPMENT..... 3

3. DESCRIPTION OF THE DROP TEST FACILITY 4

4. F-294 TEST SPECIMEN 4

5. OVERALL TEST PLAN..... 4

5.1 PHASE 1: TESTS DONE PRIOR TO DROP TESTS. 4

5.2 PHASE 2: DROP TESTS AT CRL, AECL-RESEARCH CO. 7

5.3 PHASE 3: POST -DROP TASKS AND TESTS ON TESTED F-294 SPECIMEN 8

6. DOCUMENTATION REQUIREMENTS: 10

7. OVERALL TEST PROGRAM ACCEPTANCE CRITERIA 10

8. SCHEDULE 10

9. REFERENCES..... 11

List of Tables

1 F-294 OVERALL TEST PROGRAM 12

List of Figures

1 F-294 TEST FLOWSHEET 13

List of Attachments

1. CO-QC/TP-0001 (2): RADIATION INTEGRITY FOR NEW TRANSPORT PACKAGES PROCEDURE
2. IN/OP 0019 Z000 (G): RADIOACTIVE MATERIAL TRANSPORT PACKAGING INSPECTION AND MAINTENANCE PROCEDURE
3. IN/OP 0597 F294 (A): PROCEDURE FOR F-294 STEADY STATE THERMAL TEST
4. IN/OP 0598 F294 (A): PROCEDURE FOR HELIUM LEAK TEST OF CAVITY
5. CO-C5/IT-0002 (3): IN-CELL HELIUM LEAK DETECTION FOR INDUSTRIAL RADIOACTIVE SOURCES

1. INTRODUCTION

MDS-Nordion is committed to providing a capability for our USA customers for domestic shipment of C-188 cobalt-60. The F-294 transport package is designed to be used for this purpose. In December 1993, MDS Nordion submitted a Safety Analysis Report (SAR) Rev. A (MDS Nordion Report: TR-9301-F294 Rev. A)[1] in support of Certificate of Compliance for the F-294 transport package. A first response was received from the USNRC on Dec. 8 1994 [2]. Subsequently MDS-Nordion responded to USNRC 's concerns and revised the SAR and submitted SAR Rev. B (Nordion report: TR-9301-F294 Rev. B)[3] to USNRC. A second response was received from USNRC on March 18 1997 [4]. A further meeting was held between USNRC and MDS-Nordion in Spring of 1997. At this stage of the licensing process, it appears that the resolution of the USNRC's concerns can best be addressed by tests on F-294 rather than analysis. Consequently, MDS-Nordion has decided to proceed with the prescribed regulatory tests to be conducted on a full scale F-294 test specimen to address structural concerns. To address the thermal concerns, MDS-Nordion is proposing to de-rate the contents from the original flask license limit of 450 kilocuries of cobalt-60 to 360 kilocuries of cobalt -60 and carry out the appropriate thermal analysis. This report outlines the overall test plan and provides details to conduct appropriate regulatory tests on the full scale F-294 test specimen to meet 10CFR 71 [5] requirements. Where applicable, a description of tests and detailed test procedures are included herein.

2. QUALITY ASSURANCE REQUIREMENTS

The F-294 regulatory tests shall be managed as per this document and the quality plan document [6].

2.1 Testing by MDS Nordion International

Where testing is performed by MDS Nordion Inc., it will be thoroughly documented by the person using sketches, photographs, videotapes and appropriate data sheets. All test results shall be reviewed by a Quality Control representative.

2.2 Independent testing

Where tests are performed by an organization independent from MDS-Nordion, this organization shall follow an MDS Nordion approved test plan. As a minimum, the organization shall have written procedures, check sheets, etc. to verify that the tests were conducted as specified in a test plan. The test results shall be documented by this organization in a form of an approved test report.

2.3 Measuring equipment

Calibrated instruments shall be used for measurements. The type of instrument the serial number, when the instrument was last calibrated should be recorded on the test data sheet.

Calibration data provided by a manufacturer (or a supplier) for thermocouples, accelerometers (transducers) is considered acceptable, provided the calibration interval has not lapsed.

Where calibrated instruments are not used to measure the test data, it should be duly noted and the deviation explained, and approved by Quality Assurance.

3. DESCRIPTION OF THE DROP TEST FACILITY

Chalk River Laboratory of AECL-Research Co have been contracted by MDS-Nordion to carry out the drop tests on the F-294 test specimen. The drop tests shall be carried out at the drop test facility located at AECL-Research Co., Chalk River, Ontario, Canada. The drop test facility consists of an impact pad and a hoisting tower (Ref. CRL Drawing E -4511-2001). The base pad is fabricated from reinforced concrete (of size approximately 10 ft. x 10 ft. x 10 ft.) resting on a solid bedrock. The upper surface of the pad is covered with a 4-inch thick alloy steel plate (Specification ASTM A-203 Grade E; YS = 56.7 ksi) secured to the reinforced concrete (CRL drawing E-4511-2002). The top steel plate has a provision for mounting a target pin for puncture tests.

4. F-294 TEST SPECIMEN

The F-294 test packaging has been fabricated as per Dwg. F029401-001 Issue C and Technical Specification DS 0757 F294 Issue A. This F-294 packaging is designated the full scale F-294 test specimen. The F-294 test specimen has been demonstrated to meet the quality standard specified in the technical specification DS 0757 F294 Issue A.

The full scale F-294 test specimen consists of the assembly of the following components:

- 1) A container (flask) assembly.
- 2) The cylindrical fireshield.
- 3) The top integral crushshield and fireshield
- 4) The removable shipping skid.
- 5) F-313 source cage, inclusive of 8 dummy C-188's.
- 6) Dummy weights (up to 1000 lb.) evenly distributed.
- 7) Accelerometer instrumentation.

5. OVERALL TEST PLAN.

The details of the overall test plan are given in Table 1. Figure 1 outlines the test flowsheet. There are 3 phases of the test plan: 1) Phase 1 addresses the tests to be done prior to the drop tests. 2) Phase 2 addresses the actual drop tests. 3) Phase 3 addresses the post-drop tests.

5.1 Phase 1: Tests done prior to drop tests.

Note: Appropriate photographs shall be taken to provide visual record of the test.

5.1.1 Inspect F-294 Test specimen for fit test.

As fabricated F-294 packaging shall be inspected for fit test to ensure that the components fit. Where the components do not fit, the deviations should be noted on the inspection/fit-test report. Subsequently appropriate repairs can be carried out based on this report.

Test Plan for F-294 Regulatory Tests

5.1.2 Weigh F-294 test specimen.

Each component and the assembly of the F-294 test specimen shall be weighed. The following items are to be weighed separately:

- 1) Dummy weights
- 2) Source carrier (cage)
- 3) Dummy C-188's shall be weighed.

5.1.3 Dimensional measurement of F-294 test specimen.

The F-294 container assembly shall be measured for dimensions to provide a baseline of the status of the shape of F-294 prior to the drop tests.

The dimensional measurement requirements shall be specified by the project engineer.

5.1.4 Air pressure test of the F-294 cavity.

The cavity of the F-294 shall be air pressure leak tested as per procedure outlined in Appendix 1 of IN/OP 0019 Z000. The torque for the plug closure bolts, drainline plug and the ventline plug shall be specified by the project engineer.

5.1.5 Helium Leak test of the F-294 cavity.

The cavity of the F-294 shall be helium leak tested as per procedure outlined in IN/OP 0598 F294. The torque for the plug closure bolts, drainline plug and the ventline plug shall be specified by the project engineer.

5.1.6 Inspect and dimensional measurements of Dummy C-188's

The dummy C-188's shall be inspected as per guidelines of standard capsule inspection procedure CO-QC/IT-0001. The dimensional measurements of the dummy C-188's shall be carried out. The dimensional measurement requirements shall be specified by the project engineer.

5.1.7 Helium Leak test of dummy C-188's.

The dummy C-188's shall be helium leak tested as per guidelines of procedure CO-C5/IT-0002 or appropriate instructions as per manufacturer's leak testing equipment.

5.1.8 Inspection of F-313 source carrier.

The dimensional measurements and the inspection of the F-313 shall be carried out. The dimensional measurement requirements and appropriate instructions shall be specified by the project engineer.

5.1.9 Radiation Survey

In cell #6, the F-294 test specimen shall be loaded with active C-188 sources in F-313 carrier with approx. 360 kCi of cobalt-60. Source loading diagrams are to be reviewed by the project engineer prior to actual source loading. Prior to source loading, appropriate consideration shall be given to temperature instrumentation, on the C-188's and the cavity wall of F-294.

Radiation survey of the flask and the package shall be carried out separately as per procedure CO-QC/TP-0001. In the radiation survey report, it shall be duly noted that the procedure CO-QC/TP-0001 supersedes DS 0726 Z00, which has been specified in the F-294 technical specification DS 0757 F294.

The cavity of the F-294 shall be purged with Argon.

The torque for the plug closure bolts shall be specified by the project engineer. The ventline and drainline plugs shall be sealed to allow for retention of argon gas in the F-294 cavity but permit the thermocouples wires to pass.

5.1.10 Normal thermal test.

The F-294 temperature data requirements shall be provided by the project engineer. Prior to C-188 source loading, the F-294 shall be instrumented with thermo-couples in the F-294 cavity and provisions shall be made to measure temperatures of C-188's sources. The balance of the thermocouples shall be mounted either prior to source loading or after source loading at the discretion of Manager, Cobalt Source Production.

5.1.10.1 Case 1: F-294 Without extra Insulation.

The normal thermal test shall be carried out as per procedure IN/OP 0597 F294 and other written instructions from project engineer.

5.1.10.2 Case 2: F-294 With extra Insulation.

Extra thermal insulation, as specified by the project engineer, shall be temporarily installed on the F-294 test specimen.

The normal thermal test shall be carried out as per procedure IN/OP 0597 F294 and other written instructions from project engineer.

Note: After Radiation survey and normal thermal tests have been carried out, the F-294 shall be unloaded in Cell #6.

5.1.11 Mounting Dummy weights to F-294 test specimen.

F-294 test specimen shall be modified by welders qualified to CSA W47.1 to provide brackets etc. for mounting dummy weights. Dummy weights shall be weighed and identified. A check shall be conducted to ensure that the dummy weights fit on the F-294. Location of the dummy weights for all test orientations will be documented and justified by the project engineer and reviewed by Quality Assurance.

Test Plan for F-294 Regulatory Tests

5.1.12 Modifications to F-294 test specimen.

The plug bottom and the cavity bottom of the F-294 shall be modified to provide mounting for the accelerometers. The F-294 test specimen shall be modified to provide attachment points for hoisting the slings for the drop test. Any other appropriate modification shall be carried out to ensure that the F-294 components fit. Modifications shall be recorded on the engineering drawings (markups, photographs and or sketches are acceptable) and initialed by the project engineer and reviewed by Quality Assurance.

5.1.13 Ship F-294 test specimen to CRL, AECL-Research Co.

The F-294 test specimen inclusive of the dummy C-188's, F-313 carrier and the dummy weights shall be shipped to CRL, AECL Research Co.

5.2 Phase 2: Drop tests at CRL, AECL-Research Co.

5.2.1 Order of the tests.

Normal free drop test shall be done first followed by the Hypothetical Accident drop tests. 30-foot free drop test shall be done second; the puncture tests shall be done third. (i.e. 40 in. pin drop test). This will be in compliance with Para 71.73 (a) of Ref. [5].

5.2.2 Mounting accelerometers.

CRL shall mount up to 4 accelerometers on the F-294 test specimen. The location of the accelerometers are as follows.

- G1: Top of the plug.
- G2: Bottom of the plug (i.e. container cavity side).
- G3: Bottom of the container cavity.
- G4: Bottom of the container skid (fixed skid).

Note: Prior to the drop tests, the status of the container shall be recorded by CRL. The torques on the fasteners shall be recorded and verified.

5.2.3 Test #1: Normal Free Drop test, top end drop orientation

Note: Where required, repairs may be completed in the field to ensure F-294 configuration of 21,500 lbs. test weight is maintained.

5.2.4 Test #2: 30-foot free drop test, side oblique drop orientation (15° to horizontal)

5.2.5 Test #3A or Test #3B : Puncture test, drop orientation to detach crush shield

After Test#2, the container will be evaluated. The project engineer, in conjunction with Quality Assurance (QA), will decide the drop test orientation.

Test Plan for F-294 Regulatory Tests

- 5.2.6 Test #4: Puncture test, impact cylindrical fireshield
- 5.2.7 Test #5: Puncture test, impact on fixed skid lower plate
- 5.2.8 Test #6: 30-foot free drop test, top end drop orientation.
- 5.2.9 Test #7: Puncture test, impact on the crush shield upper plate
- 5.2.10 Ship the tested F-294 specimen to MDS-Nordion, Kanata.

5.3 Phase 3: Post -drop tasks and tests on tested F-294 specimen**5.3.1 Receipt of tested F-294 specimen.**

Photograph appropriately under the direction of the project engineer. Remove dummy weights.

5.3.2 Damage Assessment #1 of tested F-294 specimen

Photograph appropriately under the direction of the project engineer. Repeat dimensional measurements as per 5.1.3 and complete additional measurements as instructed by the project engineer. Do not un-torque the plug closure bolts. Assess damage.

5.3.3 Air pressure test of the F-294 cavity.

The cavity of the F-294 shall be air pressure leak tested as per procedure outlined in Appendix 1 of IN/OP 0019 Z000. Do not use water in the cavity. Do not un-torque the plug closure bolts. Push the accelerometer cables as far as possible in the drainline and the ventline. Torque the drainline plug and the ventline plug to the same values that were present following the final drop test.

5.3.4 Helium Leak test of the F-294 cavity.

The cavity of the F-294 shall be helium leak tested as per procedure outlined in IN/OP 0598 F294 . Do not un-torque the plug closure bolts. Push the accelerometer cables as far as possible in the drainline and the ventline. Torque the drainline plug and the ventline plug to the same values that were present following the final drop test.

5.3.5 Damage Assessment #2: of the tested F-294 specimen.

Photograph around the plug closure area, lift lug area. Assess damage.

Attempt to un-torque the plug closure bolts. Record the opening torque.

Attempt the plug removal from the container in Cobalt Operations Facility. If the plug cannot be removed easily, then consider transferring it to an outside contractor for removal of the plug. Monitor this task. Measure deformations of the container - plug closure, upper cavity, lower cavity and any other zone.

Test Plan for F-294 Regulatory Tests

5.3.6 Inspect and dimensional measurements of Dummy C-188's

The dummy C-188's shall be inspected as per guidelines of standard capsule inspection procedure CO-QC/IT-0001. The dimensional measurements of the dummy C-188's shall be carried out. Repeat dimensional measurements as per 5.1.6 and complete additional measurements as instructed by the project engineer.

5.3.7 Helium Leak test of dummy C-188's.

The dummy C-188's shall be helium leak tested as per guidelines of procedure CO-C5/IT-0002 or appropriate instructions as per manufacturer's leak testing equipment. Repeat measurements as per 5.1.7 and complete additional measurements as instructed by the project engineer.

5.3.8 Inspection of F-313 source carrier.

The dimensional measurements of the F-313 shall be carried out. Repeat dimensional measurements as per 5.1.8 and complete additional measurements as instructed by the project engineer.

5.3.9 Radiation Survey

In cell #6, the F-294 test specimen shall be loaded with active C-188 sources in F-313 carrier with approx. 360 kCi of cobalt -60. Source loading diagrams are to be reviewed by project engineer prior to actual source loading. Appropriate consideration shall be given to temperature instrumentation, on the C-188's and the cavity wall of F-294, prior to source loading (See Item 5.1.9).

Radiation survey of the flask and the package shall be carried out separately as per procedure CO-QC/TP-0001. In the radiation survey report, it shall be duly noted that the procedure CO-QC/TP-0001 supersedes DS 0726 Z00, which has been specified in the F-294 technical specification DS 0757 F294.

The cavity of the F-294 shall be purged with Argon.

The torque for the plug closure bolts shall be the same values measured in 5.3.5. The ventline and drainline plugs shall be sealed to allow for retention of argon gas in the F-294 cavity but permit the thermocouples wires to pass.

5.3.10 Normal thermal test.

The F-294 temperature data requirements shall be provided by the project engineer. Prior to C-188 source loading, the F-294 shall be instrumented with thermo-couples in the F-294 cavity and provisions shall be made to measure temperatures of C-188's sources. The balance of the thermocouples shall mounted either prior to source loading or after source loading at the discretion of Manager, Cobalt source production.

Test Plan for F-294 Regulatory Tests

5.3.10.1 Case 1: F-294 Without extra Insulation.

The normal thermal test shall be carried out as per procedure IN/OP 0597 F294 and other written instructions.

5.3.10.2 Case 2: F-294 With extra Insulation.

Extra thermal insulation, as specified by the project engineer, shall be temporarily installed on the F-294 test specimen. The normal thermal test shall be carried out as per procedure IN/OP 0597 F294 and other written instructions.

Note: After radiation surveys and the normal thermal tests have been carried out, the F-294 shall be unloaded in Cell #6.

6. DOCUMENTATION REQUIREMENTS:

Each test specified in section 5 shall be documented by the person conducting the test and verified by Quality Control at the time of the test. The documentation shall be compiled and consist of sketches, charts, data sheets, procedures, written instructions etc. Each test shall clearly identify: pre-drop test, drop test or post -drop test status.

A comprehensive test report shall be prepared by the project engineer. This comprehensive test report shall be compilation of the tests outlined in Section 5.

7. OVERALL TEST PROGRAM ACCEPTANCE CRITERIA

1. The test packaging shall be radiation surveyed prior to drop tests and after the drop tests.

The Design Acceptance Criteria (DAC) shall be 80 % of the regulatory allowable 1000 mrem/ h radiation at 1.0 m. from the surface of the drop tested packaging, based on maximum radioactive contents in the package (Para 71.51 (a) (2) of Ref. [5]).

2. After the drop tests, there shall be no weld fractures or fractures in the primary stainless steel shell that envelopes the lead shielding in the plug and in the container assembly. Fractures in the fillet weld between the fin and container shell or fractures in the fin shall not be a cause of rejection.
3. After the drop tests, there shall be no loss of thermal protection (i.e. no through puncture holes in the fireshields such that the container wall is directly exposed to the flame of fire in the hypothetical thermal test or loss of crush shield). The damage and displacement of the thermal protection is to be less than 10 % of the total insulated area (9260 in²).
4. After the drop tests, the dummy C-188's to meet leaktightness of 1×10^{-7} std. cc/sec. of air.

8. SCHEDULE

It is planned to conduct drop tests at Chalk River Laboratory (CRL), Chalk River, Ontario, Canada during February 1998. The actual day of test cannot be proposed at the time of writing but shall be communicated to USNRC and others as soon as arrangements are finalized.

9. REFERENCES

- [1] SAR Rev. A, Nordion Report: TR-9301-F294 Rev. A.
- [2] USNRC Letter: Cass R. Chappell to J. Stirling: Dec. 8 1994.
- [3] SAR Rev. B, Nordion Report: TR-9301-F294 Rev. B
- [4] USNRC Letter: Cass R. Chappell to J. Stirling: March 18, 1997.
- [5] 10CFR71: Code of Federal Regulations.
- [6] IN/QP 1369 F294: Quality Plan for F-294 Regulatory Tests.
- [7] DS 0757 F294: Technical Specification for F-294 flask.
- [8] DS 0726 Z00: Procedure for radiation integrity for new shipping containers.
- [9] CO-QC/TP-0001: Radiation integrity for new transport packages procedure.
- [10] IN/OP 0019 Z000: Radioactive Material Transport Packaging Inspection and Maintenance Procedure
- [11] IN/OP 0597 F294: Procedure for F-294 steady state thermal test.
- [12] IN/OP 0598 F294: Procedure for helium leak test of cavity.
- [13] CO-C5/TT-0002: In-cell Helium Leak Detection For Industrial Radioactive Sources.

Test Plan for F-294 Regulatory Tests

Table 1: F-294 OVERALL TEST PROGRAM

ITEM	TASK DESCRIPTION	GROUP RESPONSIBLE
1.0	CONDUCT PRE-DROP TESTS AT MDS-NORDION	
1.1	INSPECT F-294 TEST SPECIMEN	CSP, QC, PE*
1.2	WEIGH F-294 TEST SPECIMEN	CSP, QC
1.3	DIM. MEASUREMENT OF F-294 TEST SPECIMEN	CSP, QC
1.4	AIR PRESSURE TEST OF F-294 CAVITY	CSP, QC
1.5	HELIUM LEAK TEST OF F-294 CAVITY	CSP, QC
1.5	PHOTOGRAPHS AS APPROPRIATE	CSP, QC, PE
1.6	FABRICATE DUMMY C-188'S (QTY = 8)	CSP
1.6.1	INSPECT DUMMY C-188'S	QC
1.6.2	HELIUM LEAK TEST DUMMY C-188'S.	PE, QC
1.8	STEADY STATE NORMAL THERMAL TESTS @ 360 kCi. 2 cases: with and without additional insulation	CSP, QC, PE
1.9	RADIATION SURVEYS @ 360 kCi.	CSP, QC
2.0	PREPARE F-294 TEST SPECIMEN	CSP, PE
2.1	ADD DUMMY WEIGHT	CSP, PE
2.2	MOUNTING FOR ACCELEROMETERS	CRL
3.0	DROP TESTS AT CRL, CHALK RIVER, ONTARIO.	CRL
3.1	1.2 m NORMAL FREE DROP TEST	CRL, PE, QC
3.2	30-FOOT FREE DROP TEST SIDE OBLIQUE ORIENTATION	CRL, PE, QC
3.3	PUNCTURE TESTS (40 in. height, PIN DROP TEST) AS APPROPRIATE	CRL, PE, QC
3.4	30-FOOT FREE DROP TEST END DROP ORIENTATION	CRL, PE, QC
3.5	PUNCTURE TESTS (40 in. height, PIN DROP TEST) AS APPROPRIATE	CRL, PE, QC
4.0	POST-DROP TESTS	PE
4.1	DAMAGE ASSESSMENT OF F-294 CONTAINER	CSP, QC, PE
4.2	AIR PRESSURE TEST OF CAVITY	CSP, QC
4.3	HELIUM LEAK TEST OF CAVITY	CSP, QC
4.4	RADIATION SURVEYS	CSP, QC, PE
4.5	NORMAL THERMAL TEST - DEFORMED PACKAGING 2 cases: with and without added insulation.	CSP, QC, PE
4.6	HELIUM LEAK TEST OF DUMMY C-188'S	PE, QC
4.7	DAMAGE ASSESSMENT OF DUMMY C-188'S / F-313 CARRIER	PE, QC
5.0	TEST REPORT	PE, QA

*CSP = Cobalt Source Production

QC = Quality Control (Industrial)

PE = Package Engineering

CRL = Chalk River Laboratory.

Q.A. = Quality Assurance

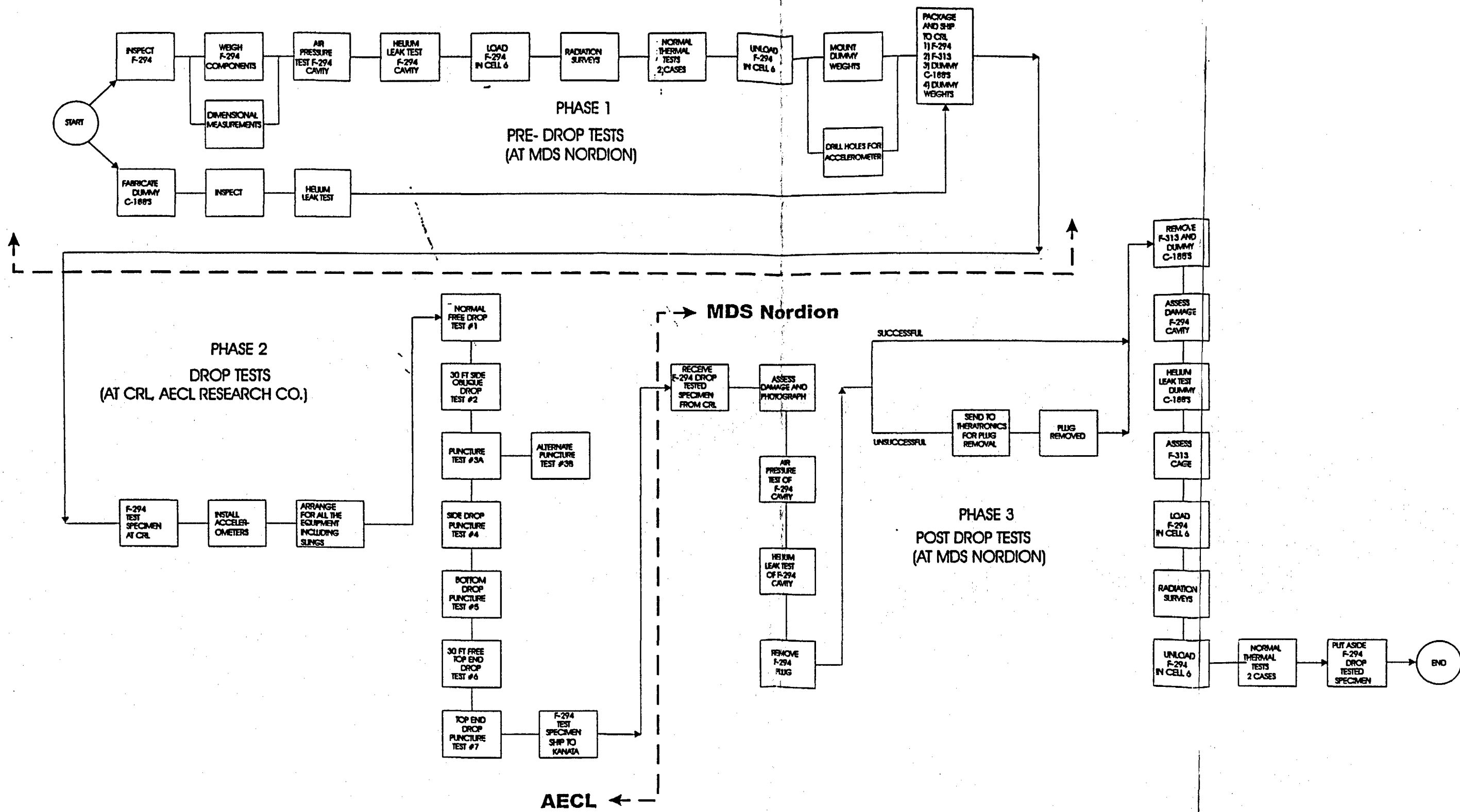


Figure 1: F-294 Test Flowsheet

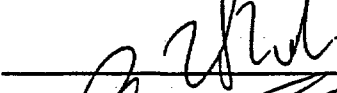
6. **IN/QA 1369 F294: QUALITY PLAN FOR F-294 REGULATORY TESTS**
(REFERENCE [49])

This page left blank intentionally.

Quality Plan for F-294 Regulatory Tests

Signatures

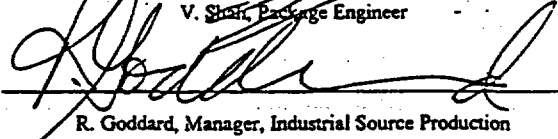
Prepared by:



V. Shih, Package Engineer

Date: 98-01-12

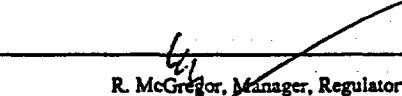
Reviewed by:



R. Goddard, Manager, Industrial Source Production

Date: 98/1/12

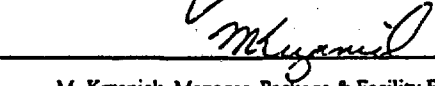
Reviewed by:



R. McGregor, Manager, Regulatory Affairs

Date: 98/01/13

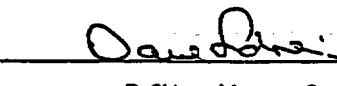
Reviewed by:



M. Krzaniak, Manager, Package & Facility Engineering

Date: 98/01/13

Approved by:



D. Sidney, Manager, Quality Assurance

Date: 98-01-14

Document History

Date	Version	Comments	Prepared by	Reviewed by	Approved by
	1	CCF: A1232-C-00A			

TABLE OF CONTENTS

1. INTRODUCTION..... 3

2. TEST PROGRAM..... 3

2.1 TEST PLAN [1] 3

2.2 TEST SPECIMEN: 3

2.3 ORDER OF TESTS: 3

3. QUALITY PROCESS..... 3

3.1 INSPECTION AND TEST PLAN:..... 3

3.2 TEST REPORT:..... 4

 3.2.1 Test Record for each test. 4

 3.2.2 Review of test records. 4

 3.2.3 Review of test report 4

3.3 TESTS PERFORMED BY ORGANIZATION OTHER THAN MDS-NORDION..... 4

3.4 RETENTION OF RECORDS: 4

4. DEVIATIONS..... 5

5. REFERENCES..... 5

1. INTRODUCTION

The purpose of the quality plan for the F-294 Regulatory tests is to establish that the F-294 test specimen, the tests that were conducted on the F-294 test specimen and the test data meet the prescribed quality requirements specified herein.

2. TEST PROGRAM

2.1 Test Plan [1]

Reference [1] identifies the tests that are planned to be conducted on the F-294 test specimen.

2.2 Test Specimen:

A qualified test specimen shall be used for conducting the regulatory tests. An Inspection Data File (IDF) or a history file shall be available for purpose of demonstrating that the F-294 test specimen has been manufactured to a quality standard or deemed to meet a quality standard as specified in the Technical Specification for F-294 flask [2].

2.3 Order of tests:

Where the order of tests is a regulatory requirement [3], it should be demonstrated that such an order of conducting the tests was met.

3. QUALITY PROCESS

The following quality process is specified.

3.1 Inspection and Test Plan:

The overall Test Plan [1] should be approved by Quality Assurance (QA). All test activities required to verify conformance with test plan are to be organized in advance. A typical test plan, where appropriate and where applicable, shall have the following elements :

1. test methods
2. test schedule and time requirements
3. equipment requirements
4. responsibilities
5. calibration
6. record keeping methods (checklist or lab book)
7. pre-approved criteria for pass or fail

3.2 Test Report:

3.2.1 Test Record for each test.

Each test shall be conducted as per written procedure or written instructions or referenced to a document. The test procedure document shall be appended in the overall Test Plan [1]. The test instructions shall be approved by Quality Assurance (QA). A typical test record shall have the following elements:

- 1) purpose and time of the test
- 2) method of testing
- 3) acceptance or rejection criteria, where applicable.
- 4) measuring instruments, including serial numbers and evidence of calibration where applicable
- 5) direction for inclusion and format of test results
- 6) direction for evaluation of test results, if applicable
- 7) conclusions; state regulatory paragraphs ,where applicable.

3.2.2 Review of test records.

Each test record (i.e. check sheet, test report, or lab book record) shall be reviewed by personnel from Quality Control (QC). A test record shall, as a minimum have 2 independent signatures. The persons who conduct the test or jointly conduct the test shall be one of the signatories under "prepared by": The second signatory shall be a person from QC under "reviewed by":

3.2.3 Review of test report

All test records will be compiled into a test report that will be reviewed by Quality Assurance and approved by the Technical Authority.

3.3 Tests performed by Organization other than MDS-Nordion

Where tests are performed by an organization independent from MDS-Nórdion, this organization shall follow an MDS Nordion approved test plan. As a minimum, the organization shall have written procedures, check sheets, etc. to verify that the tests were conducted as specified in a test plan. The test results shall be documented by this organization in a form of an approved test report.

3.4 Retention of Records:

The records must be maintained for the life of F-294 as per procedure IN/QA 0224 Z000 [5].

4. DEVIATIONS

Deviations will be documented and approved in accordance with procedure QAP AP-14 [4].

5. REFERENCES

[1] IN/QA 1368 F294: Test Plan for F-294 Regulatory Tests.

[2] Technical specification of F-294 Flask : DS-0757 F294

[3] CFR Part 71: USNRC Regulations : Packaging and Transportation of Radioactive Material.

[4] QAP AP-14: Quality Assurance Procedure, Internal Non conformance Disposition.

[5] IN/QA 0224 Z000: Radioactive Material Transport Package Quality Plan.

7. **A-16485-TN-1 DECELERATION MEASUREMENTS DURING DROP TESTS
OF AN F-294 PACKAGING
(REFERENCE [55])**

This page left blank intentionally.



AECL EACL

Engineered Products and Services
Design Document

Classification/
Designation CONTROLLED

DOCUMENT TITLE DECELERATION MEASUREMENTS DURING DROP TESTS
OF THE F-294 TEST PACKAGING

PROJECT/JOB TITLE _____

DOCUMENT TYPE Technical Note

Prepared By	<u><i>John Tromp</i></u> J. Tromp	Date	<u>98/04/01</u>
Reviewed By	<u><i>R. Birchall</i></u> R. Birchall	Date	<u>98/5/29</u>
Approved By	<u><i>C. Kittmer</i></u> C. Kittmer	Date	<u>98/5/29</u>
Accepted By	_____	Date	_____
Accepted By	_____	Date	_____

(Signatories for Rev. 0 only)

REA No. 16485

Document No. A-16485-TN-1

Revision No. 1

Alternate Document No. _____

TABLE OF CONTENTS

	<u>Page</u>
1. INTRODUCTION.....	1
2. INSTRUMENTATION.....	1
3. CALIBRATION.....	1
4. TEST RESULTS.....	1
5. COMMENTS.....	2
6. CONCLUSION.....	6

LIST OF TABLES

- Table 1: Maximum Measured Acceleration of Drops #1-8
 Table 2: Elapse Impact Time of Drops #1-8

LIST OF FIGURES

- Figure 1: Drop Orientation of F-294 for Drops #1, 2, and 3
 Figure 2: Drop Orientation of F-294 for Drops #4, 5, and 6
 Figure 3: Drop Orientation of F-294 for Drops #7 and 8
 Figure 4: Accelerometer Placement on the F-294 Test Packaging
 Figure 5: Orientation of Accelerometers with Respect to Drain Hole
 Figure 6: Acceleration Signals During Impact of Drop #1 from 36 inches
 Figure 7: Acceleration Signals During Impact of Drop #2 from 30 feet
 Figure 8: Acceleration Signals During Impact of Drop #3 from 40 inches onto a Pin
 Figure 9: Acceleration Signals During Impact of Drop #4 from 40 inches onto a Pin
 Figure 10: Acceleration Signals During Impact of Drops #5, 6 and 7 from 40 inches, 30 feet, and 40 inches onto a Pin, Respectively
 Figure 11: Acceleration Signals During Impact of Drop #8 from 40 inches onto a Pin

LIST OF APPENDICES

- Appendix A: Instrumentation Used in the F-294 Test Packaging Drop Tests

DECELERATION MEASUREMENT DURING DROP TESTS OF A F-294 TEST PACKAGING

1. INTRODUCTION

Impact tests were conducted on an F-294 test packaging. The Vibration and Tribology Unit was asked to gather data during the impact of this package to address structural concerns. All drops were performed as requested onto an unyielding surface using various orientations (see Figures 1, 2, and 3).

2. INSTRUMENTATION

The package was instrumented with low impedance accelerometers, capable of measuring 2500 g and withstanding a shock load of 5000 g. The accelerometers were checked out (See Section 3 Calibration) prior to mounting them in the package to verify their operation, since the majority of them would not be accessible for replacement once the package was closed. After the package was closed, the accelerometers were again tested for signal integrity before the drop test. Deceleration signals were stored on a multi-channel tape recorder for later analysis. Figure 4 shows the location of the accelerometers. Figure 5 shows their orientation with respect to the drain plug.

3. CALIBRATION

Calibration certificates for all accelerometers are included in Appendix A.

All accelerometers were tested to verify calibration both before and after the drops. A hand-held shaker was used as an excitation source. This shaker vibrates at 159.2 Hz and produces an acceleration level of 1.0 g. Each accelerometer was mounted on the shaker and with the amplifier adjusted for the correct sensitivity, the resulting output was documented as shown on page 15, Appendix A.

4. TEST RESULTS

The signals stored on tape contain both the deceleration frequency and all natural frequencies of all parts of the package and contents excited on impact. Natural frequencies are usually higher frequencies having higher amplitudes and should therefore be filtered out to reveal the true deceleration frequency.

A strip chart recorder was used to display deceleration trace. Figures 6 to 11 show the signals after being filtered so that anything above 640 Hz is eliminated. Table 1 is a summary of the deceleration data from Figures 6 to 11.

5. COMMENTS

The sensing element of the accelerometer is oriented along its longitudinal axis. Thus, when the accelerometer is oriented in the transverse direction to the direction of drop, no valid measurements can be made. This is shown in Table 1 as N/A for each applicable accelerometer.

5.1 Drop Test #1

Drop orientation is shown as per Figure #1 (Drop #1). Prior to the drop, all accelerometers were functional. However, at the end of the drop, the crush shield moved enough to cause severe damage to the leads of three accelerometers at G-2 resulting in a loss of signal.

Table #1 lists the acceleration test data.

Table #2 lists the elapse impact time data.

5.1.1 Discussion

The acceleration amplitudes listed in Table #1 are derived from the strip chart traces of Figure #6. The Y-axis of the chart represents acceleration amplitude in volts when played back from the tape-recorder. The vertical bars to the left of the traces show the voltage setting of the strip chart recorder for each channel displayed.

Using accelerometer #2525 (channel #1) as an example, the maximum change in voltage measured from the chart is a trace having a negative sense and an amplitude (A) of two divisions. This is multiplied by the voltage sensitivity (V) of 50 mV/division. The accelerometer signals were recorded on tape using a 0-10 volt range, but could only be played back at 0-5 volt range. Therefore, a gain factor (gf) of two needs to be applied to the trace amplitude. The sensitivity (s) of accelerometer #2525 is 1.72 mV/g as per the calibration sheet.

Thus, the maximum acceleration (in g's) = $A * V * gf / s$

where

- A is amplitude (in divisions)
- V is channel voltage sensitivity (in mV)
- gf is tape-recorder gain factor
- s is accelerometer sensitivity (in mV/g)

The horizontal scale of the chart represents time. The chart speed (c) is set at 50 ms/division as seen at the top of the strip chart. The duration (d) of the impact signal (using accelerometer #2525) showed a peak lasting 2.6 divisions. The signal was recorded at a tape speed of 76 cm/s, but the playback speed was reduced by a factor (I) of 16.

Therefore, the elapse impact time (in ms) = $c \cdot d / f$

where

- c is chart speed (in ms/division)
- d is duration of impact signal (in divisions)
- f is tape speed factor

The plate on which the accelerometers at G-4 are mounted, is very thin and only supported around the perimeter of the skid. On impact, this plate vibrates at a measured 115 Hz dominating the impact frequency of about 140 Hz that we are trying to measure.

5.2 Drop Test #2

Drop orientation is shown as per Figure #1 (Drop #2). Prior to the drop, only 9 of the 12 accelerometers were functional. The leads of the three accelerometers at G-2 were not repaired due to in-accessibility and lack of time. For the duration of the tests, signals from these three accelerometers were unavailable. At the end of this drop, 9 accelerometers were still functional.

Table #1 lists the acceleration test data.

Table #2 lists the elapse impact time data.

5.2.1 Discussion

The acceleration amplitudes are derived from the strip chart traces of Figure #7 using the calculations shown in Section 5.1.1. Each of the three charts shown have a common accelerometer trace (#2525). It was used to trigger data acquisition and show the time relationship of all 9 accelerometer signals. This particular signal shows a large positive spike, an indication that the lead was momentarily shorted. The horizontal scale of the chart represents 50 ms/division.

5.3 Drop Test #3

Drop orientation is shown as per Figure #1 (Drop #3). Prior to the drop, 9 of the 12 accelerometers were functional. At the end of the drop, 6 accelerometers were functional. The leads from accelerometers at G-1 were crushed in impact resulting in loss of data.

Table #1 lists the acceleration test data.

Table #2 lists the elapse impact time data.

5.3.1 Discussion

The acceleration amplitudes are derived from the strip chart traces of Figure #8 using the calculations shown in Section 5.1.1. The duration of impact is less defined for this drop. After initial impact, lasting about 9 milliseconds, the flask rotates about the point of impact until the skid makes contact with the concrete pad. This extends the deceleration signal to about 40 ms. The horizontal scale of the chart represents 100 ms/division.

5.4 Drop Test #4

Drop orientation is shown as per Figure #2 (Drop #4). Because the leads of the accelerometers at G-1 were accessible, they were repaired by splicing the leads. Thus 9 of the 12 accelerometers were functional. At the end of the drop, all 9 accelerometers were still functional.

Table #1 lists the acceleration test data.

Table #2 lists the elapse impact time data.

5.4.1 Discussion

The acceleration amplitudes are derived from the strip chart traces of Figure #9 using the calculations shown in Section 5.1.1. The signal from accelerometer #2527 shows a large spike, an indication that the lead was momentarily shorted. The duration of impact is less defined for this drop as well. After initial impact lasting about 5 milliseconds, the flask rotates about the point of impact until the skid makes contact with the concrete pad. This extends the deceleration signal to about 45 ms. The horizontal scale of the chart represents 100 ms/division.

5.5 Drop Test #5

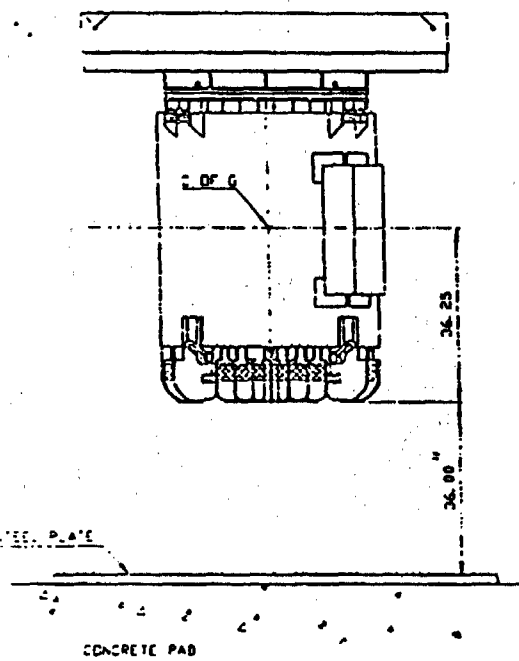
Drop orientation is shown as per Figure #2 (Drop #5). The three accelerometers normally mounted at location G-4 on the middle of the base plate were moved off to the side so that they would not be damaged on impact. The orientation was kept the same as all previous drops. Before and after the drop, all 9 accelerometers were functional.

Table #1 lists the acceleration test data.

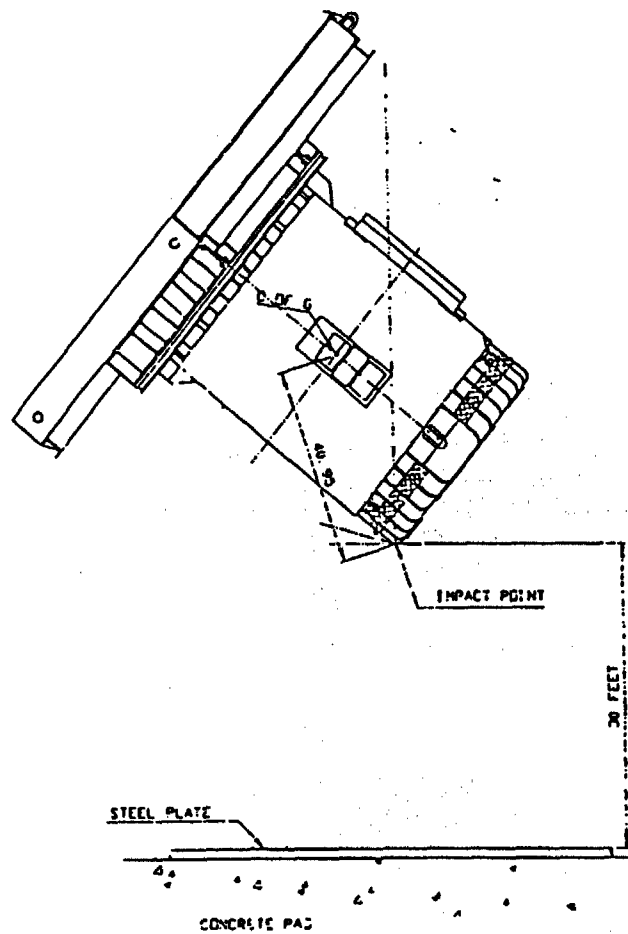
Table #2 lists the elapse impact time data.

5.5.1 Discussion

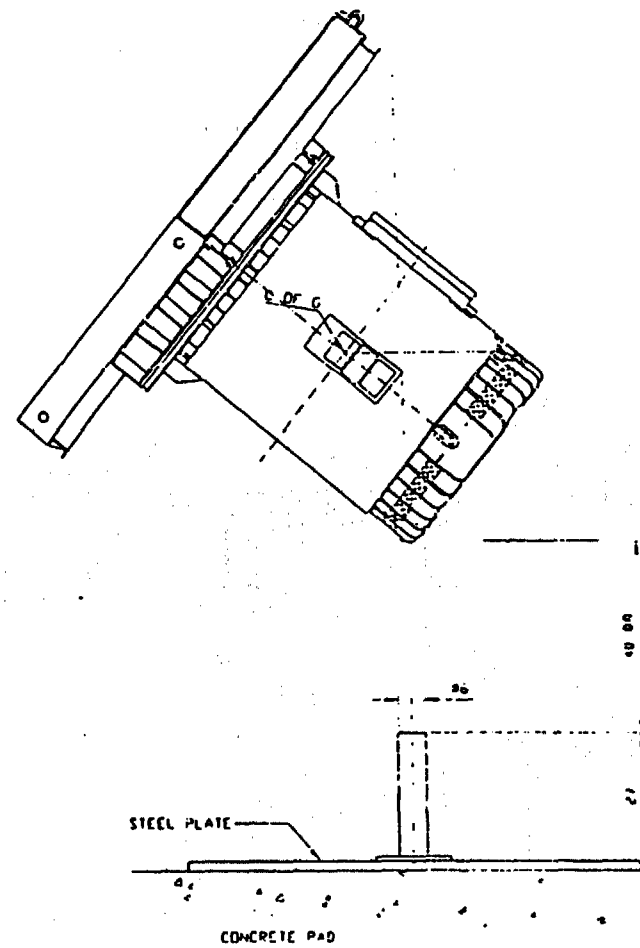
The acceleration amplitudes are derived from the top strip chart traces of Figure #10 using the calculations shown in Section 5.5.1. Accelerometer #4713 mounted on the plate at G-4 was moved off center for this and all subsequent drops. The signal for all subsequent drops shows a frequency of about 500 Hz, making it impossible to obtain meaningful deceleration signals. The horizontal scale of the chart represents 100 ms/division.



Drop # 1

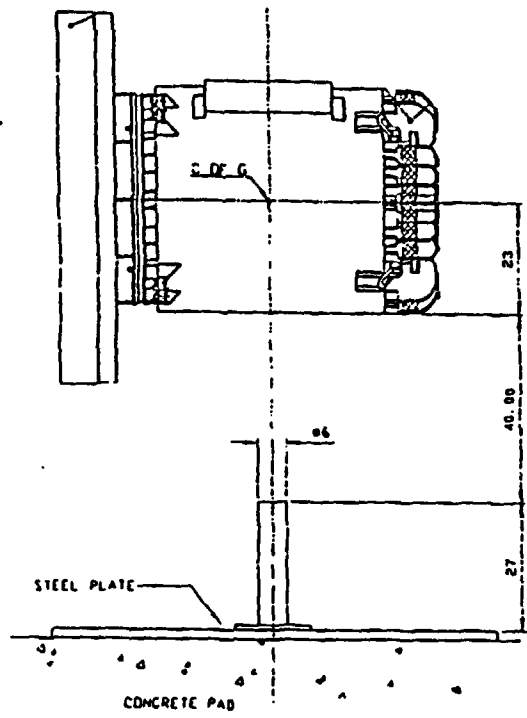


Drop # 2

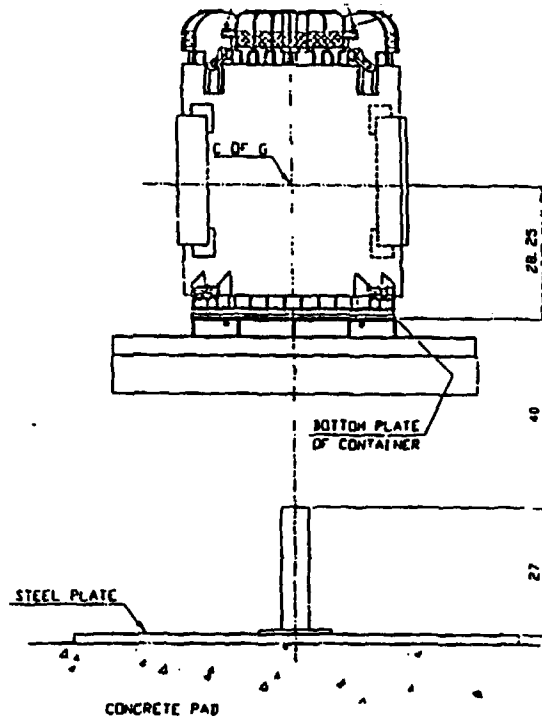


Drop # 3

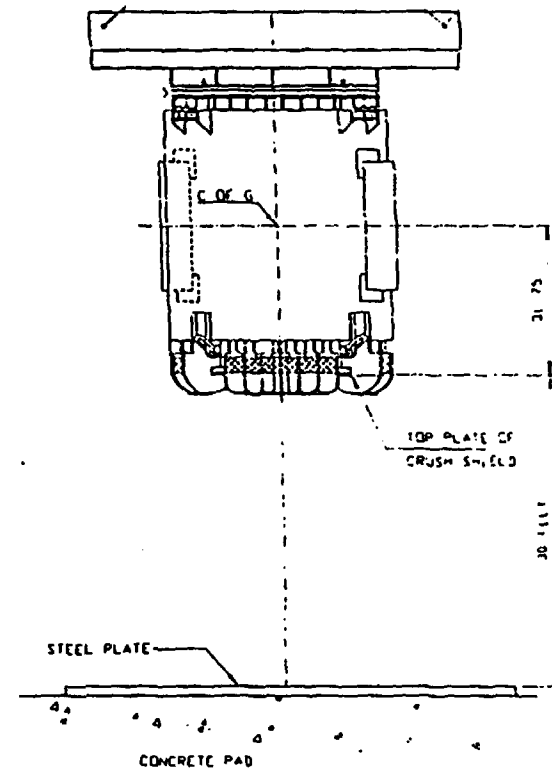
Figure 1: Drop Orientation of F-294 for Drops #1, 2, and 3



Drop # 4

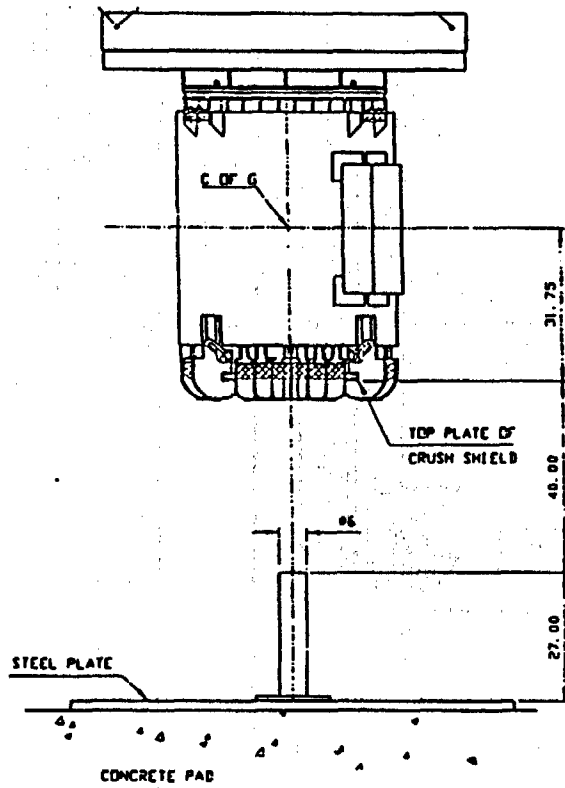


Drop # 5

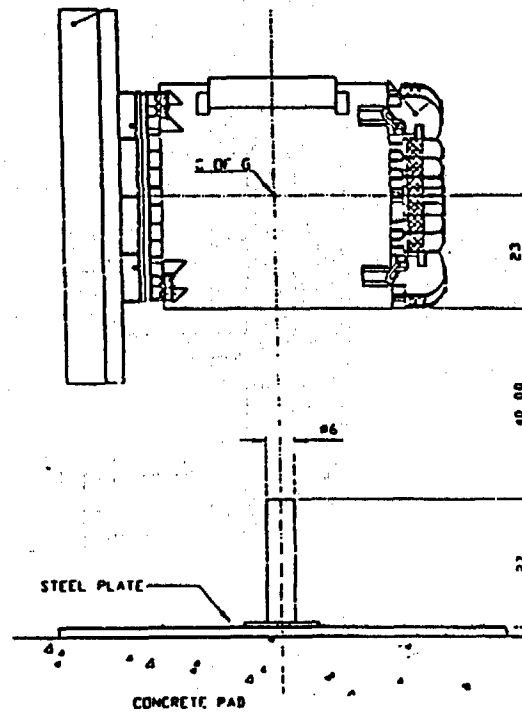


Drop # 6

Figure 2: Drop Orientation of F-294 for Drops #4, 5, and 6



Drop # 7



Drop # 8

Figure 3: Drop Orientation of F-294 for Drops #7 and 8

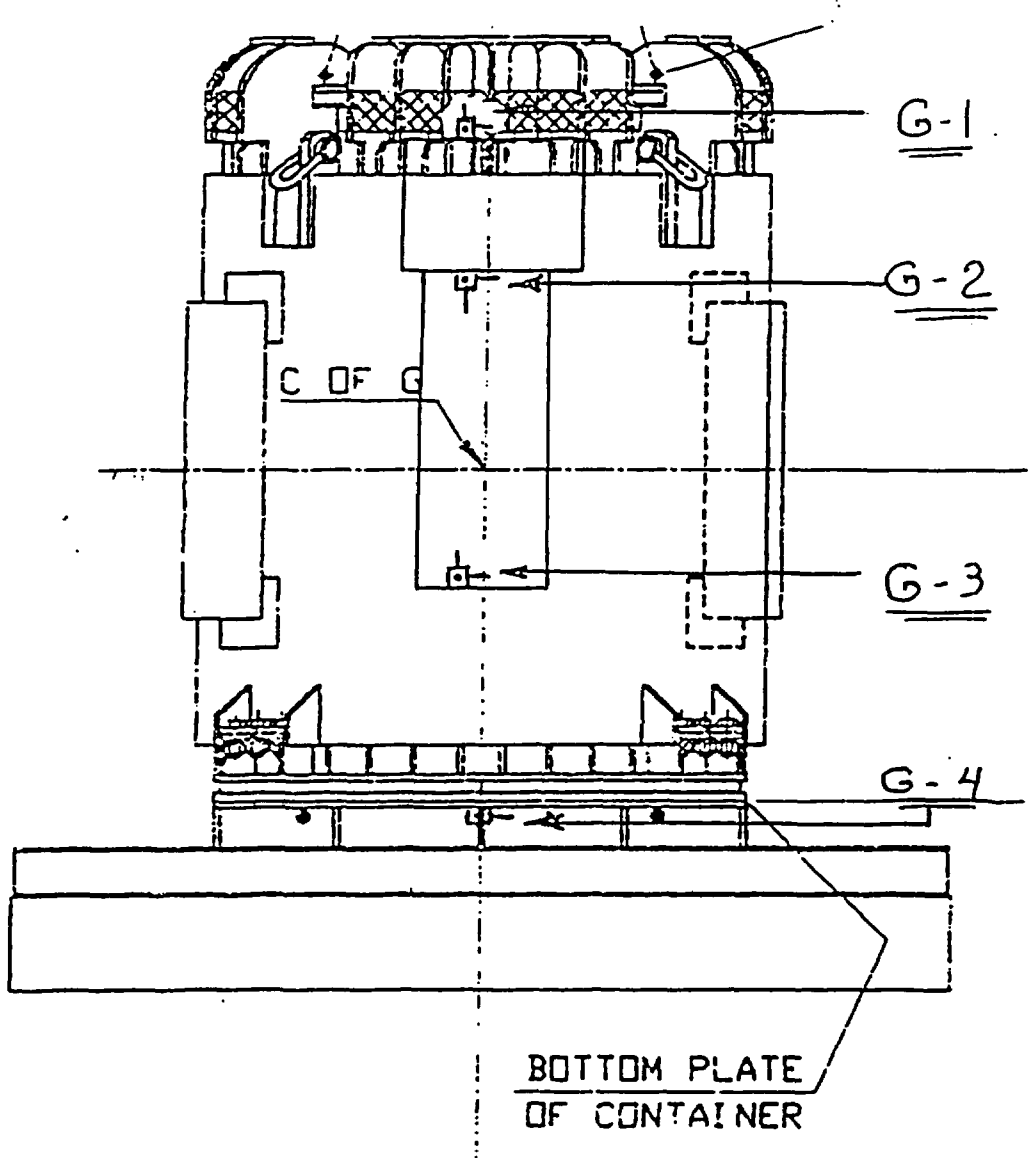


Figure 4: Accelerometer Placement on the F-294 Test Packaging

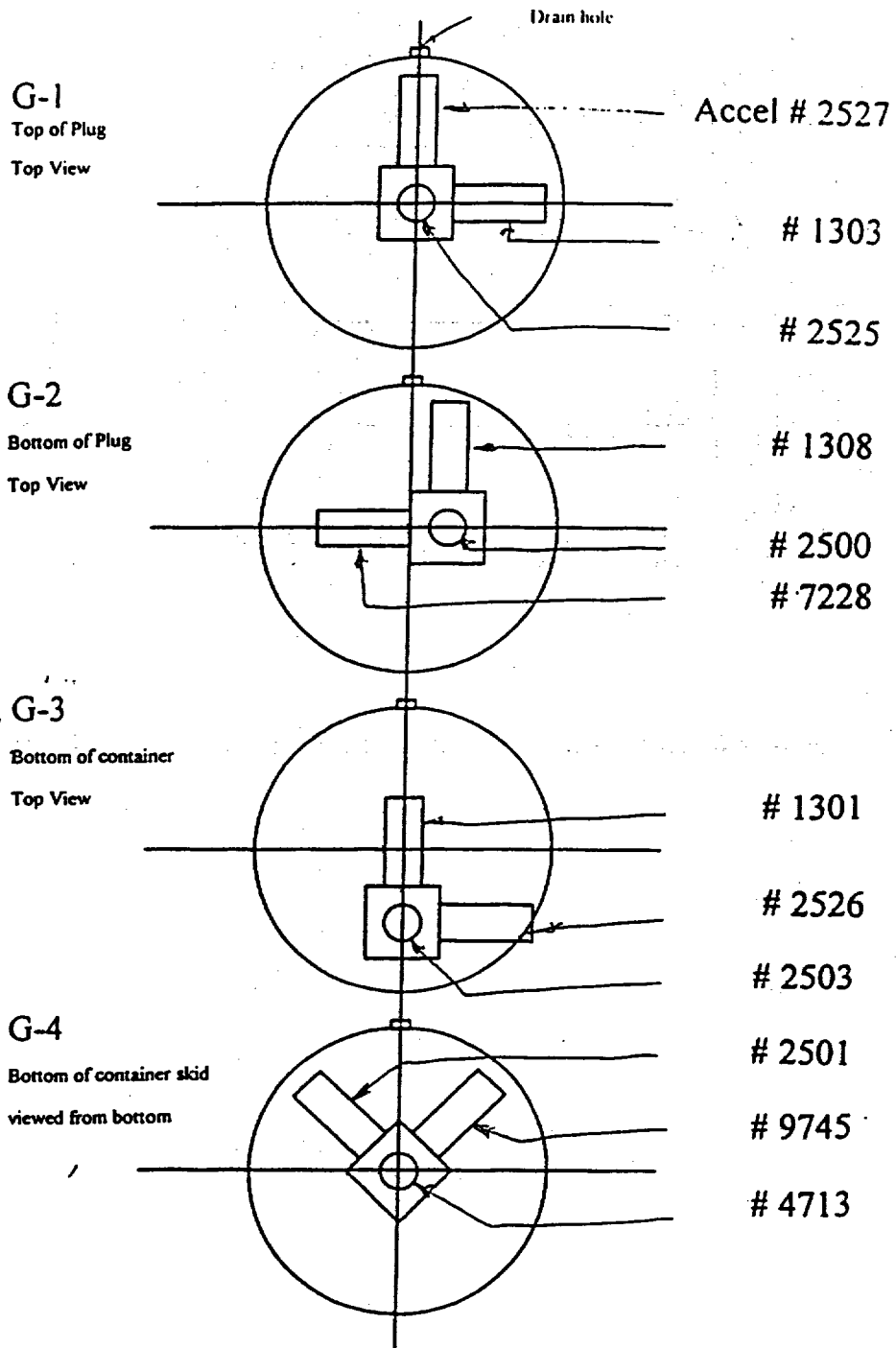


Figure 5: Orientation of Accelerometers with Respect to Drain Hole

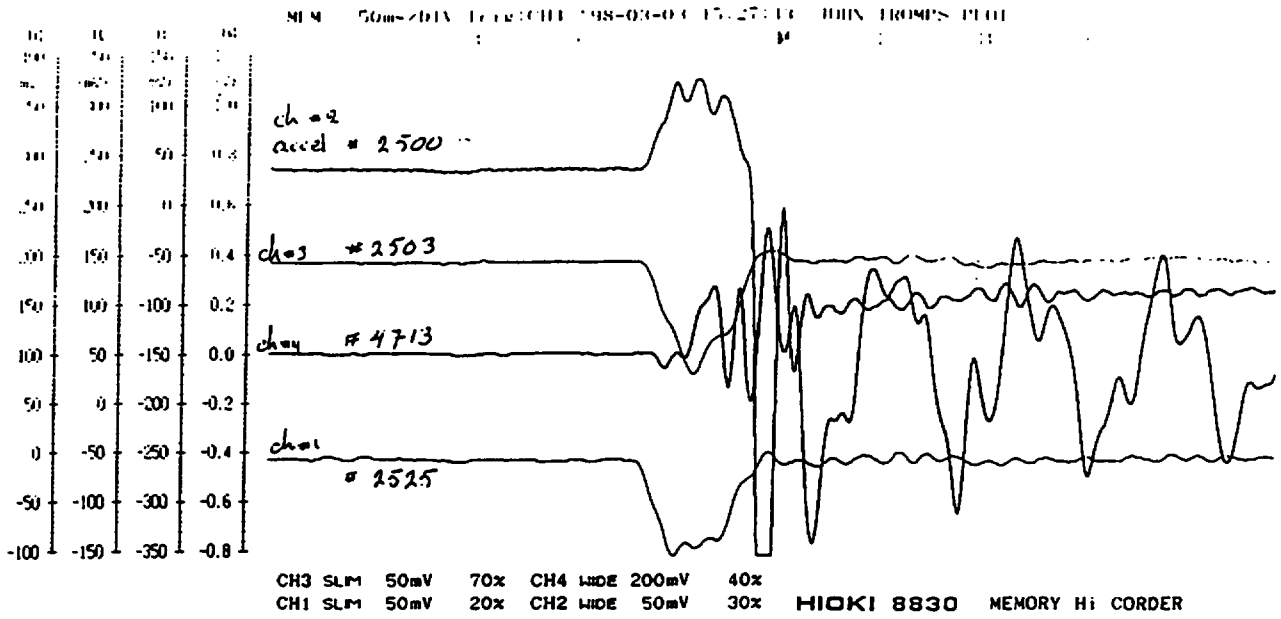
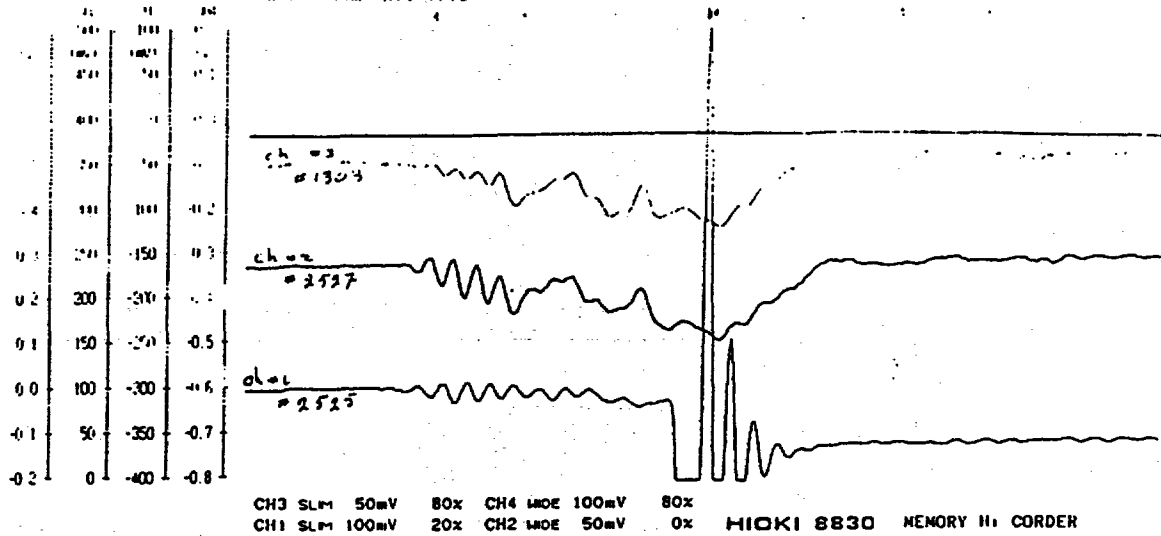


Figure 6: Acceleration Signals During Impact of Drop #1 from 36 inches

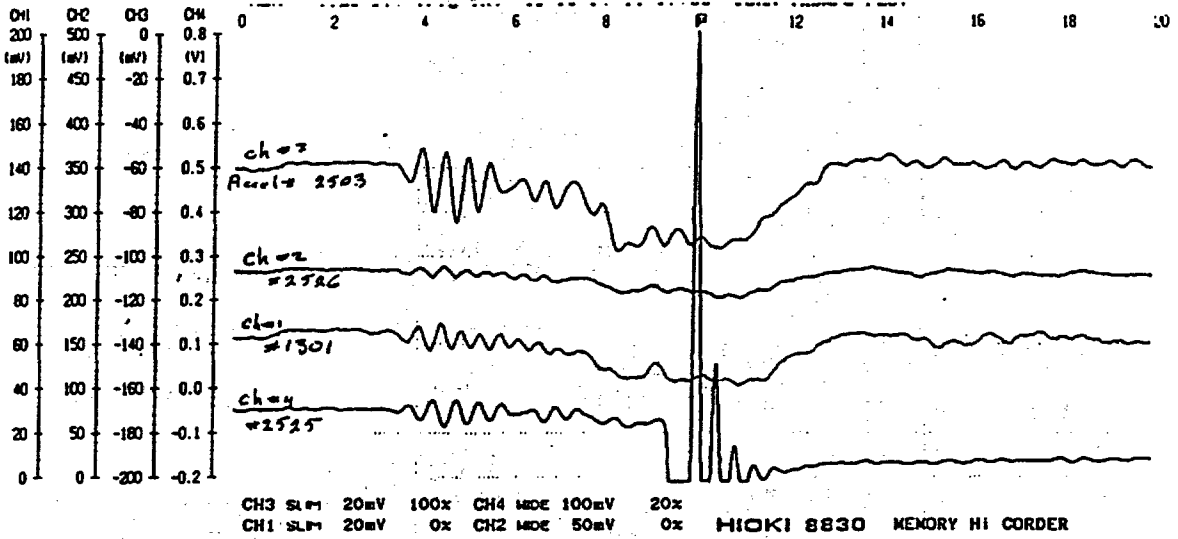
Drop #2

G-1



Drop #2

G-3



Drop #2

G-4

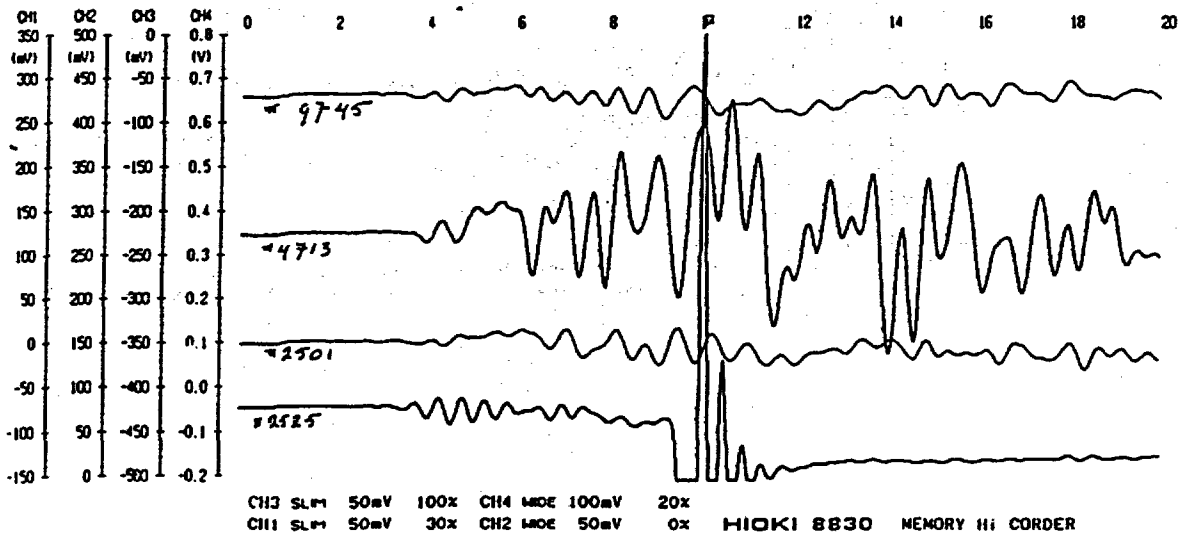
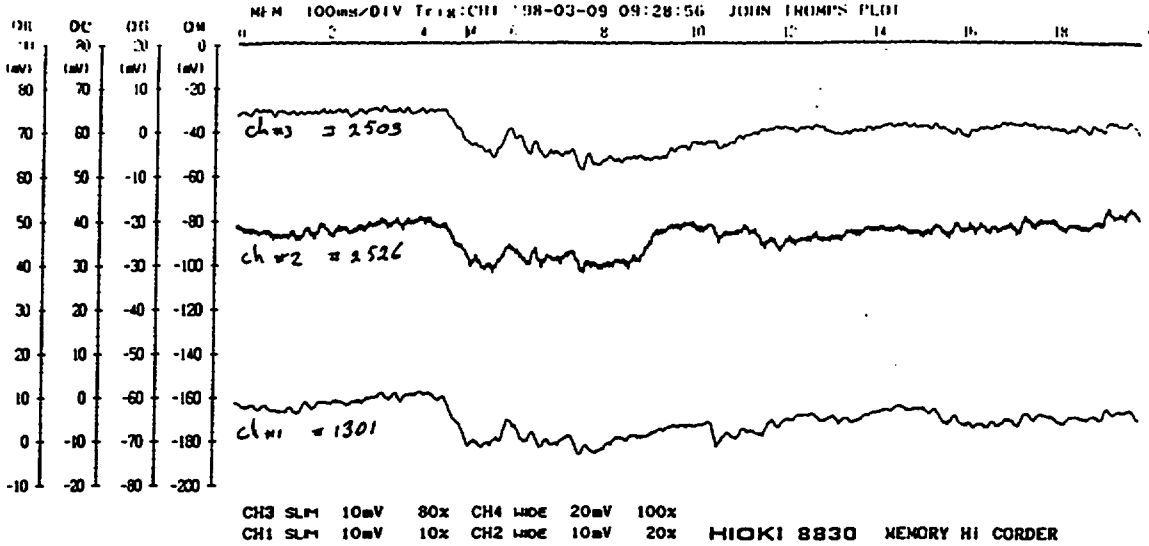


Figure 7: Acceleration Signals During Impact of Drop #2 from 30 feet

Drop #3
G-3



Drop #3
G-4

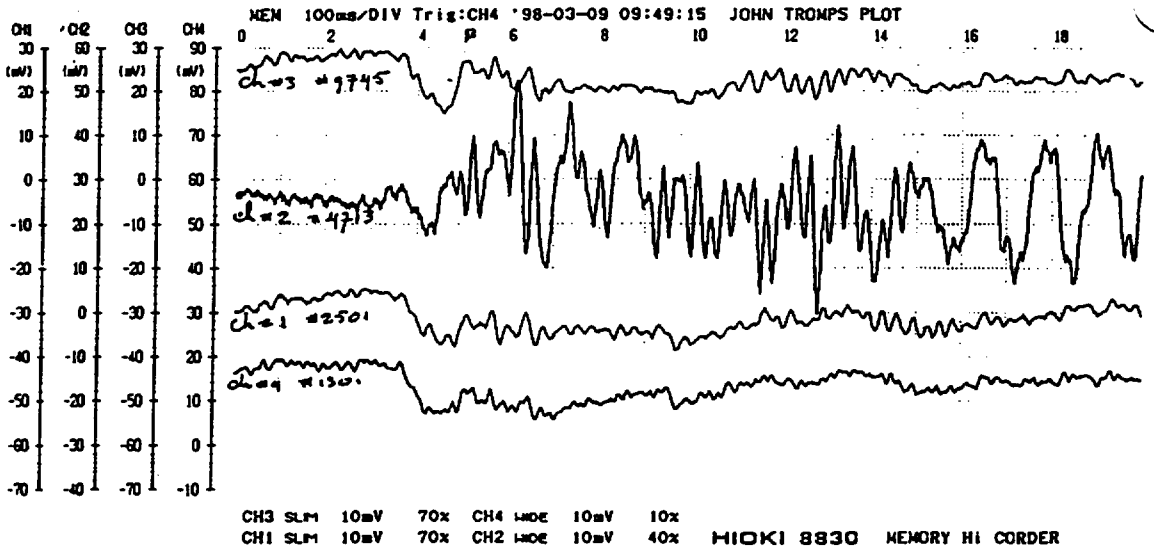
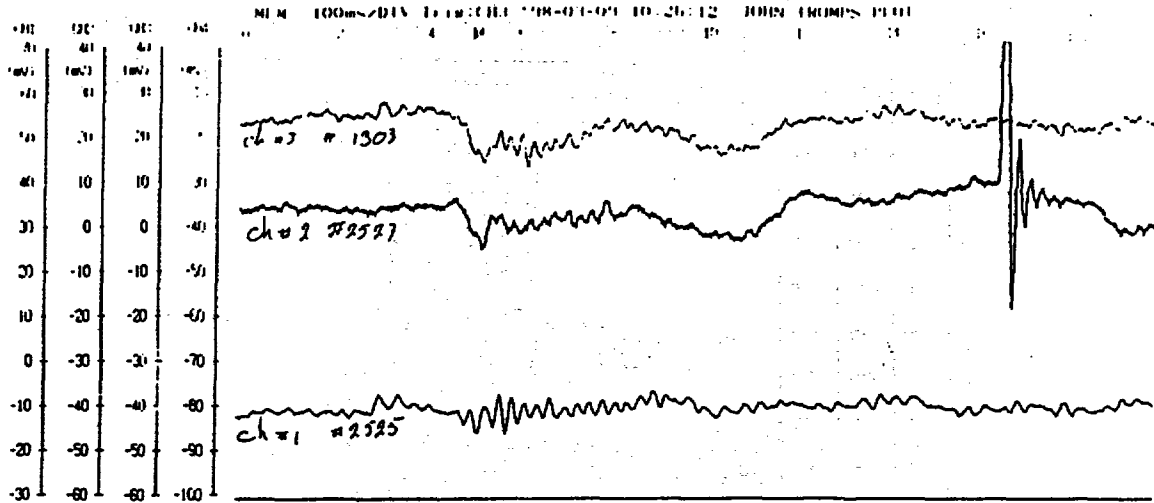


Figure 8: Acceleration Signals During Impact of Drop #3 from 40 inches onto a Pin

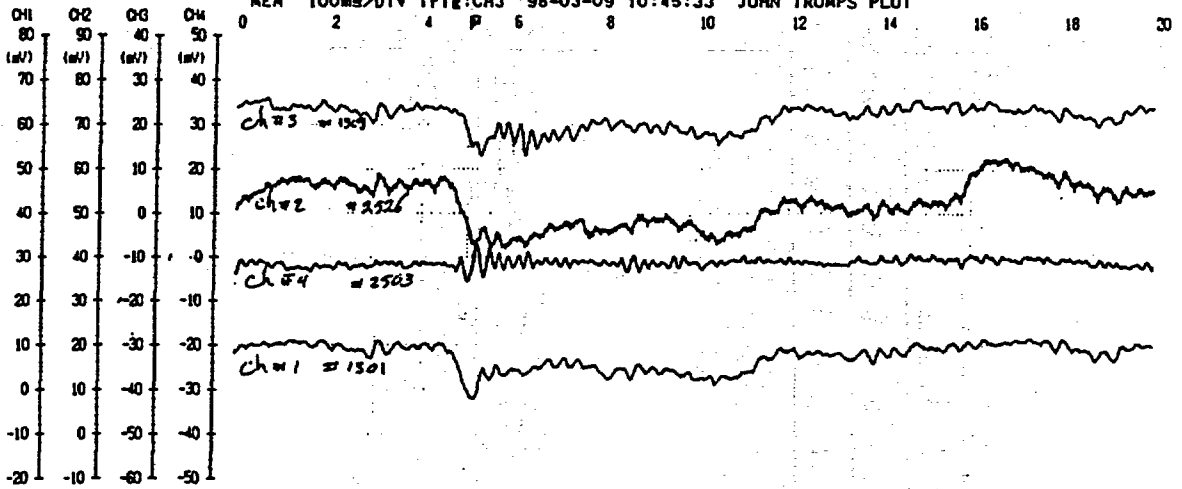
Drop #4

G-1



Drop #4

G-3



Drop #4

G-4

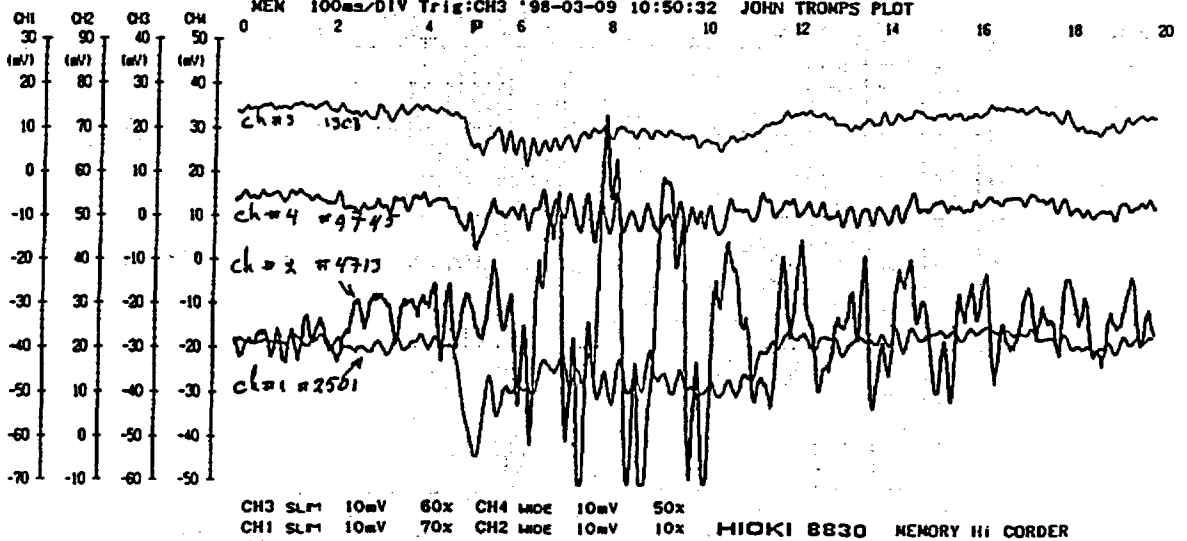
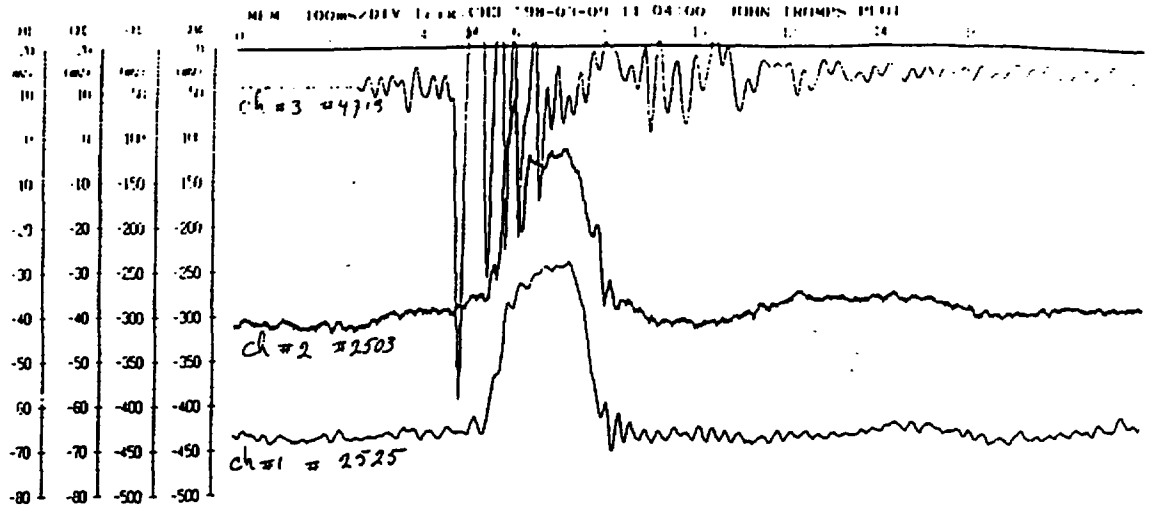
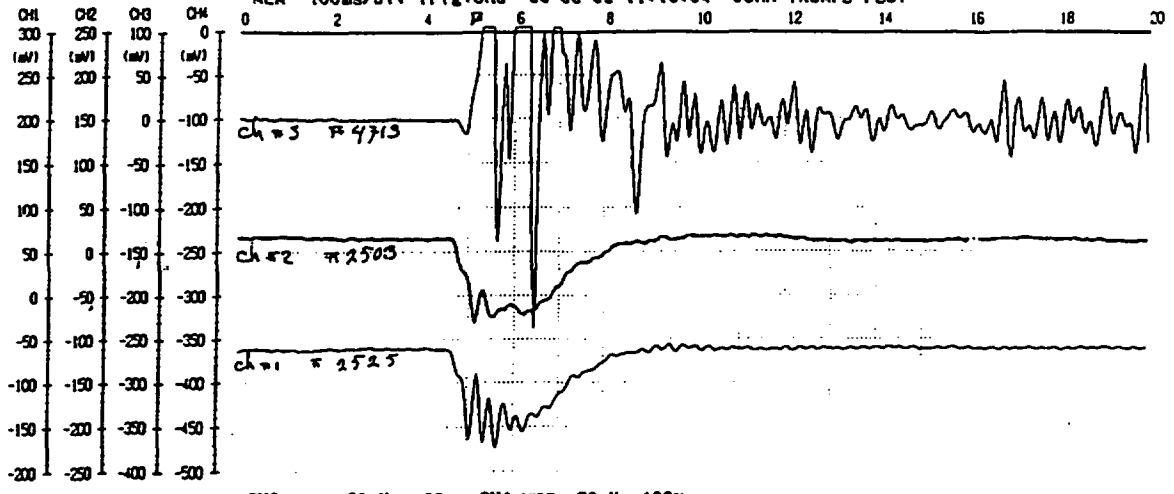


Figure 9: Acceleration Signals During Impact of Drop #4 from 40 inches onto a Pin

Drop # 5



Drop # 6



Drop # 7

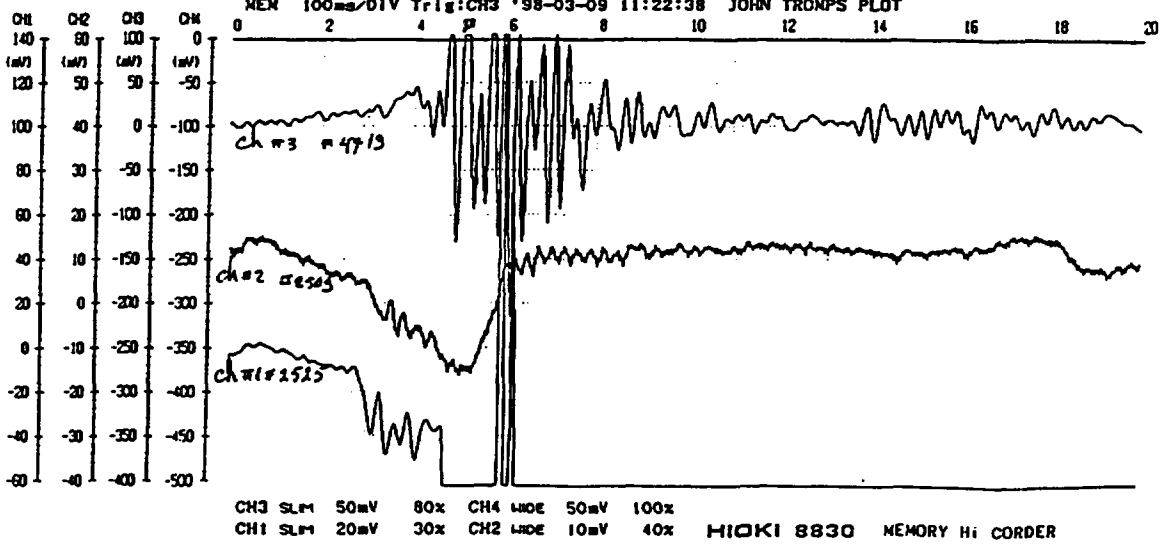
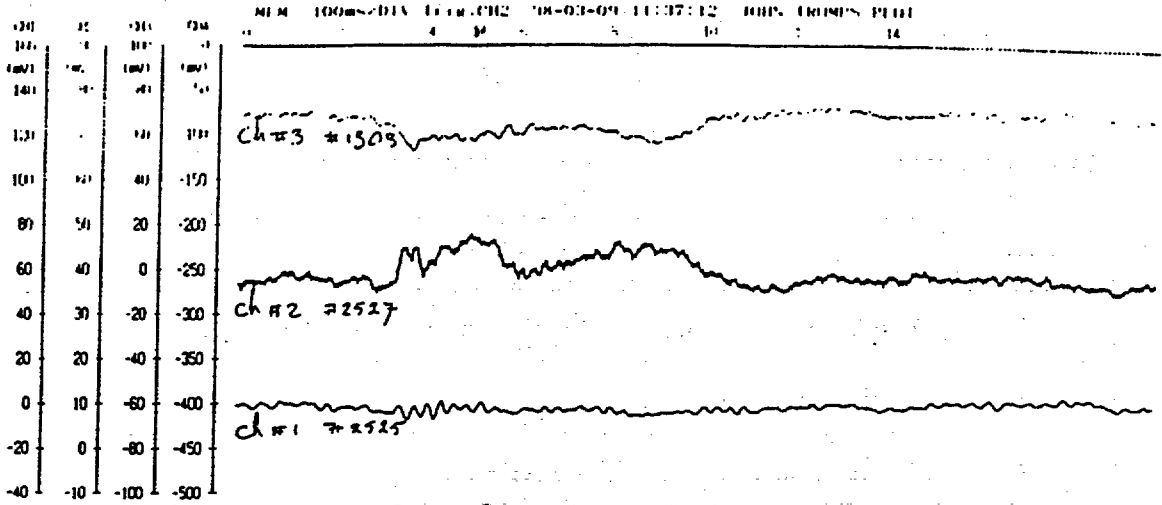
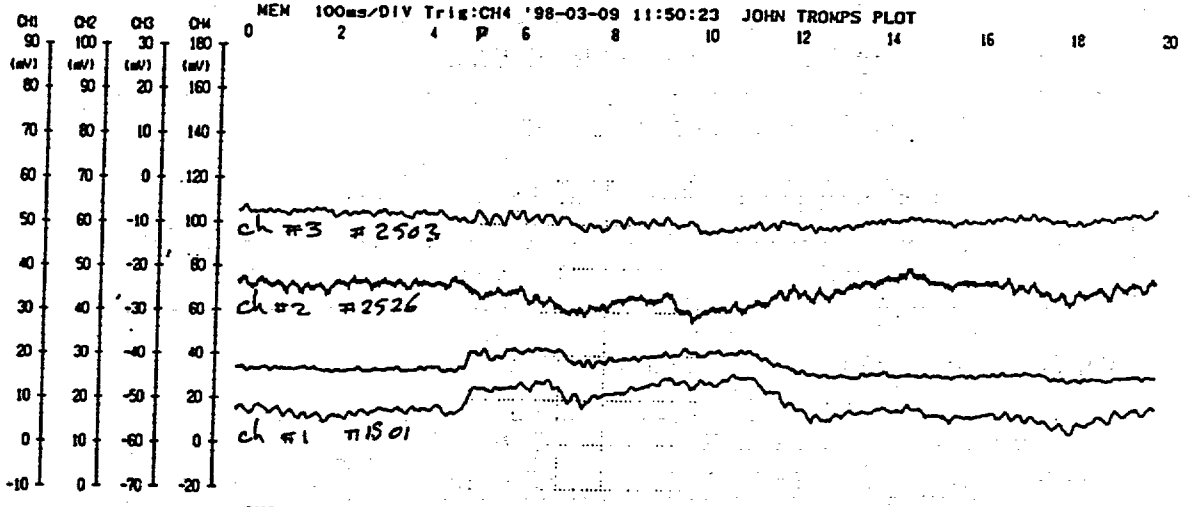


Figure 10: Acceleration Signals During Impact of Drops #5, 6 and 7 from 40 inches, 30 feet, and 40 inches

Drop #8
G-1



Drop #8
G-3



Drop #8
G-4

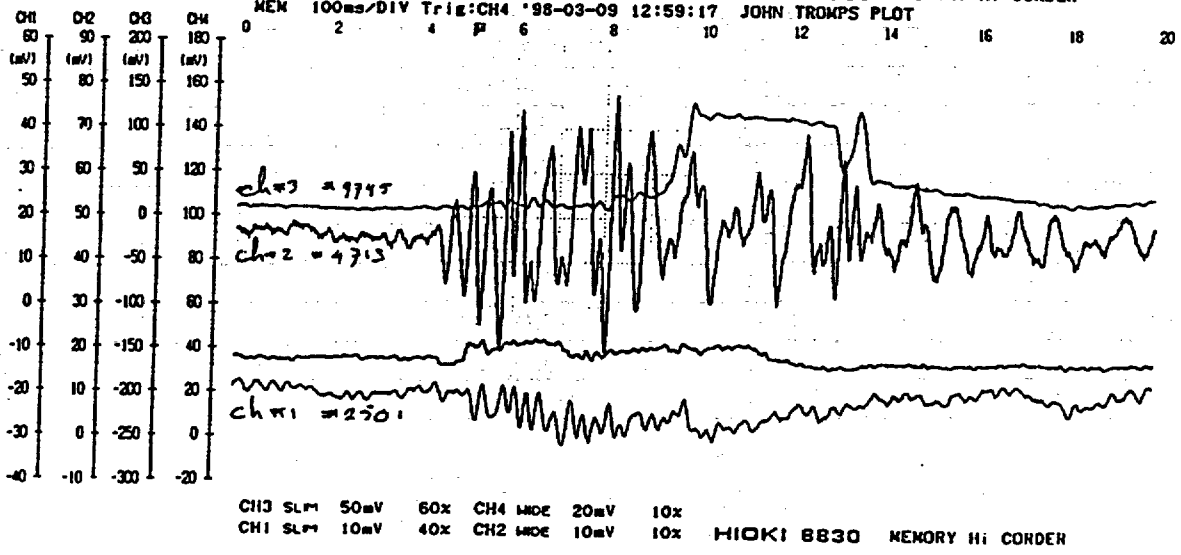


Figure 11: Acceleration Signals During Impact of Drop #8 from 40 inches onto a Pin

APPENDIX A

Instrumentation used in the F-294 Transport Package drop tests:

Item	Description	QA#
1-12	Accelerometers Model #305A05 (calibration sheets attached)	
13	Multi-channel power unit for accelerometers above Model #483A	
14	Magnetic taperecorder TEAC XR7000	456-268
15	Analog Filter Krohn-Hite Model #3342	456-296
16	Analog Filter Krohn-Hite Model #3342	456-302
17	Strip Chart recorder H10K1 8830 (Calibration was verified using a sinusoidal signal from a krohn-hite Oscillator #4023 last calibrated 97/11/24. A 100 Hz signal with an amplitude of 100 mV (RMS) was used.)	

Verification of accelerometer calibration:

Accelerometer (Serial #)	Sensitivity (mV/g)	Date of Calibration	Measured Acceleration (g's)	
			Before Drops	After Drops
2500	1.50	93/04/29	0.96	0.97
7228	2.22	92/01/14	0.96	0.96
1308	1.67	93/04/29	0.96	0.96
2526	1.67	92/01/14	0.98	0.98
2503	1.69	93/04/29	0.98	0.97
1301	1.50	93/04/29	0.95	0.95
2525	1.72	93/04/29	0.93	0.93
1303	1.70	90/05/07	1.00	1.00
2527	1.74	92/04/14	0.95	0.95
2501	1.70	93/04/29	0.93	0.93
4713	2.02	86/04/21	0.97	0.97
9745	1.55	91/12/18	0.96	0.95

Calibration Certificate

Per ISA-RP37.2

Model No. 305A05

Serial No. 1308

PO No. _____ Customer _____

Calibration traceable to NIST thru Project No. 822/251101-93

ICP® ACCELEROMETER
with built-in electronics

Calibration procedure is in compliance with
MIL-STD-45662A and traceable to NIST

CALIBRATION DATA

Voltage Sensitivity 1.67 mV/g ($\frac{2000}{\text{Shook}} g^{-1}$)
 Transverse Sensitivity 2.5 %
 Resonant Frequency 45 kHz
 Time Constant 2.0 s
 Output Bias Level 9.8 V

KEY SPECIFICATIONS

Range 2500 ± g
 Resolution .05 g
 Temp. Range -100/+250 °F

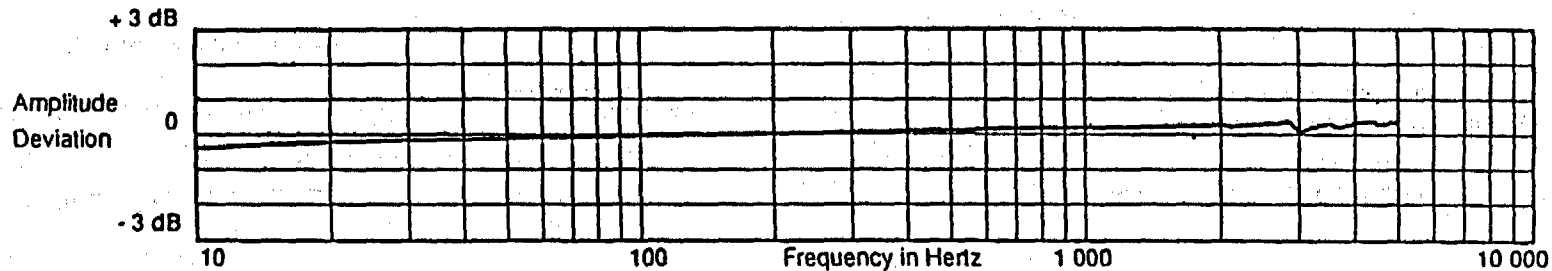
METRIC CONVERSIONS

ms² = 0.102 g
 °C = 5/9 x (°F - 32)

Reference Freq.

Frequency Hz	10	15	30	50	100	300	500	1000	3000	5000		
Amplitude Deviation %	-3.7	-2.8	-1.7	-1.3	0.0	1.2	1.7	2.6	1.4	4.4		

FREQUENCY RESPONSE



Piezotronics, Inc. 3425 Walden Avenue Depew, NY 14043-2495 USA
 716-684-0001

Date 4/29/93

Calibrated by Ron Burke

21

A 1005 1/1

Calibration Certificate

Per ISA-RP37.2

Model No. 305A05

Serial No. 9745

PO No. _____ Customer _____

Calibration traceable to NIST thru Project No. 732/245191-90

ICP® ACCELEROMETER
with built-in electronics

Calibration procedure is in compliance with
MIL-STD-45662A and traceable to NIST

CALIBRATION DATA

Voltage Sensitivity	1.55	mV/g	($\frac{2000}{g_{shock}}$)
Transverse Sensitivity	2.2	%	
Resonant Frequency	45	kHz	
Time Constant	2.0	s	
Output Bias Level	10.8	V	

KEY SPECIFICATIONS

Range	2500	± g
Resolution	.05	g
Temp. Range	-100/+250	°F

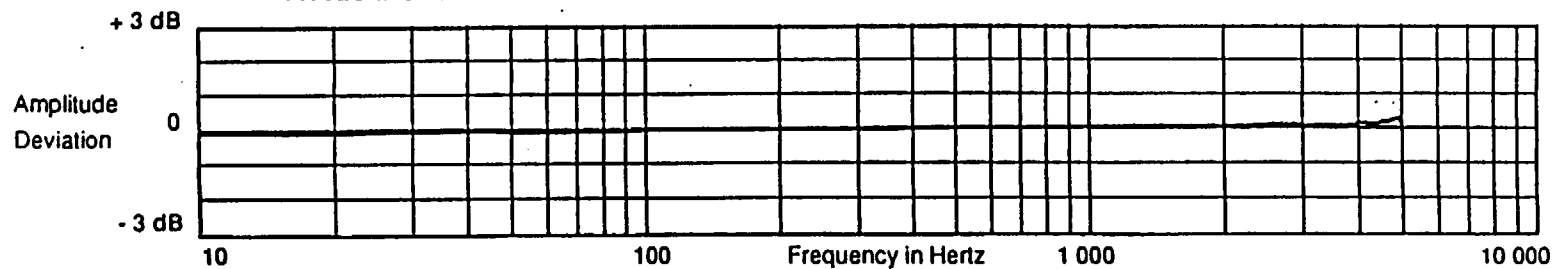
METRIC CONVERSIONS

ms⁻² = 0.102 g
°C = 5/9 x (°F - 32)

Reference Freq.

Frequency	Hz	10	15	30	50	100	300	500	1000	3000	5000		
Amplitude Deviation	%	-1.0	-1.3	-0.5	-0.9	0.0	0.0	.5	.8	1.3	2.6		

FREQUENCY RESPONSE



Piezotronics, Inc. 3425 Walden Avenue Depew, NY 14043-2495 USA
716-684-0001

Date 12/18/91

Calibrated by J Chadwick

12

A 16485-10-1

Calibration Certificate

Per ISA-RP37.2

Model No. 305A05

Serial No. 1301

PO No. _____ Customer _____

Calibration traceable to NIST thru Project No. 822/251101-93

ICP® ACCELEROMETER
with built-in electronics

Calibration procedure is in compliance with
MIL-STD-45662A and traceable to NIST

CALIBRATION DATA

Voltage Sensitivity 1.50 mV/g $\left(\begin{smallmatrix} 2000 \\ \text{Shock} \end{smallmatrix} g'''' \right)$
 Transverse Sensitivity 2.5 %
 Resonant Frequency 45 kHz
 Time Constant 2.0 s
 Output Bias Level 9.8 V

KEY SPECIFICATIONS

Range 2500 ± g
 Resolution .05 g
 Temp. Range -100/+250 °F

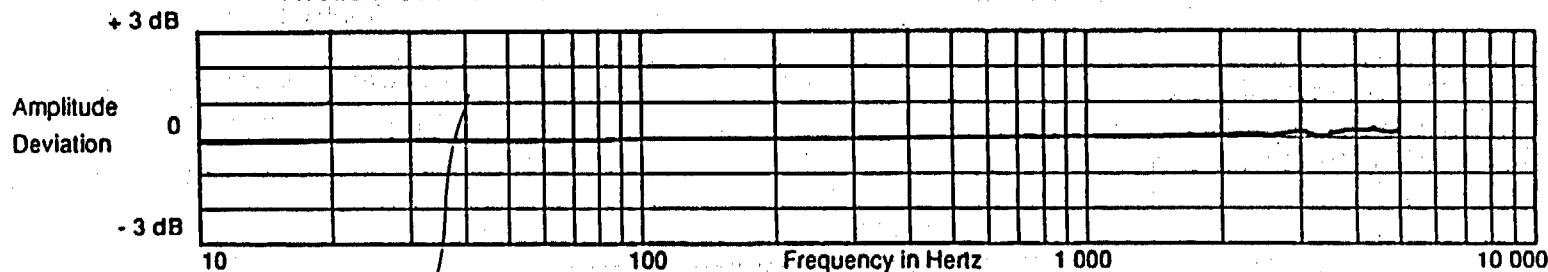
METRIC CONVERSIONS

$ms^{-2} = 0.102 g$
 $^{\circ}C = 5/9 \times (^{\circ}F - 32)$

Reference Freq.

Frequency Hz	10	15	30	50	100	300	500	1000	3000	5000		
Amplitude Deviation %	-1.1	-0.6	-0.1	-1.0	0.0	0.0	.4	.8	2.3	2.3		

FREQUENCY RESPONSE



Piezotronics, Inc. 3425 Walden Avenue Depew, NY 14043-2495 USA
 716-684-0001

Date 4/29/93

Calibrated by Ron Burke

23

A 1051 N 1

Calibration Certificate

Per ISA-RP37.2

Model No. 305A05

Serial No. 2500

PO No. _____ Customer _____

Calibration traceable to NIST thru Project No. 022/251101-93

ICP® ACCELEROMETER
with built-in electronics

Calibration procedure is in compliance with
MIL-STD-45662A and traceable to NIST

CALIBRATION DATA

Voltage Sensitivity	1.50	mV/g	(^{2000 g's} Shock)
Transverse Sensitivity	4.4	%	
Resonant Frequency	45	kHz	
Time Constant	2.0	s	
Output Bias Level	10.3	V	

KEY SPECIFICATIONS

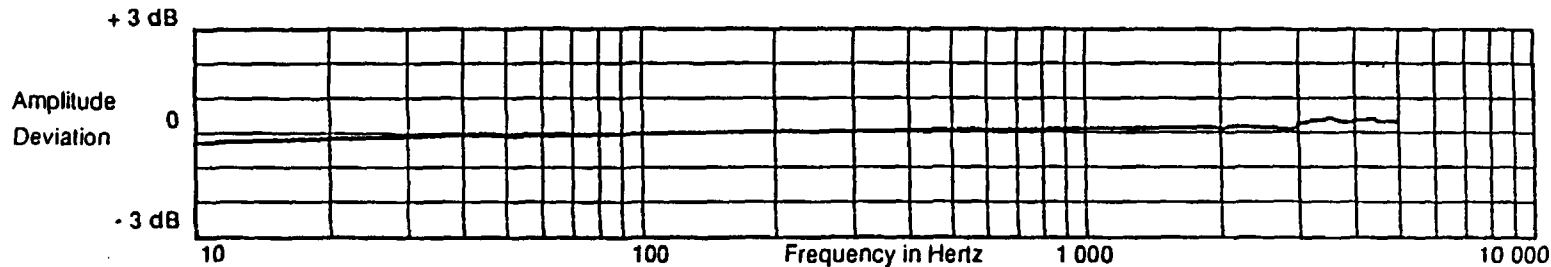
Range	2500	± g
Resolution	.05	g
Temp. Range	-100/+250	°F

METRIC CONVERSIONS
ms⁻² = 0.102 g
°C = 5/9 x (°F - 32)

Reference Freq.

Frequency Hz	10	15	30	50	100	300	500	1000	3000	5000		
Amplitude Deviation %	-3.1	-2.3	-1.1	-1.0	0.0	.7	1.4	1.8	3.3	4.1		

FREQUENCY RESPONSE



Piezotronics, Inc. 3425 Walden Avenue Depew, NY 14043-2495 USA
716-684-0001

Date 4/29/93

Calibrated by Tom Burke

Calibration Certificate

Per ISA-RP37.2

Model No. 305A05

Serial No. 2501

PO No. _____ Customer _____

Calibration traceable to NIST thru Project No. 822/251101-93

ICP® ACCELEROMETER
with built-in electronics

Calibration procedure is in compliance with
MIL-STD-45662A and traceable to NIST

CALIBRATION DATA

Voltage Sensitivity 1.70 mV/g $\left(\begin{smallmatrix} 2000 \\ \text{Shock } g^*s \end{smallmatrix} \right)$
 Transverse Sensitivity 3.9 %
 Resonant Frequency 45 kHz
 Time Constant 2.0 s
 Output Bias Level 9.8 V

KEY SPECIFICATIONS

Range 2500 ± g
 Resolution .05 g
 Temp. Range -100/+250 °F

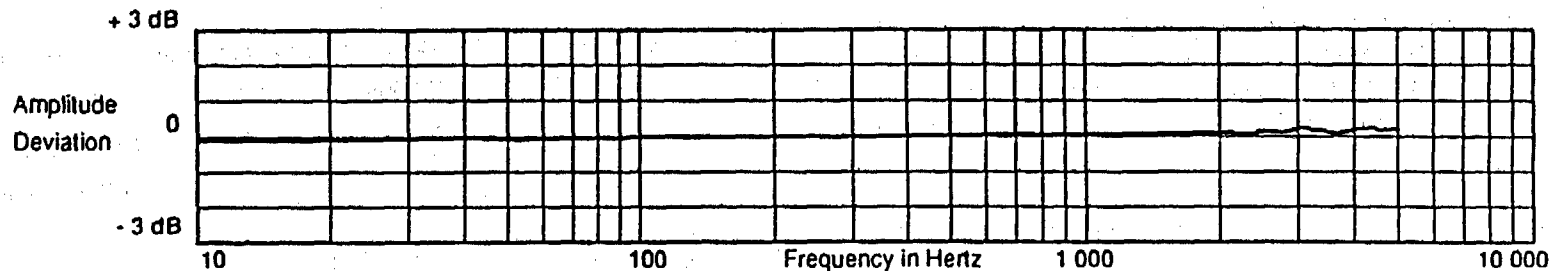
METRIC CONVERSIONS

ms² = 0.102 g
 °C = 5/9 x (°F - 32)

Reference Freq.

Frequency Hz	10	15	30	50	100	300	500	1000	3000	5000		
Amplitude Deviation %	-1.4	-1.1	-0.8	-1.1	0.0	.1	.4	1.0	2.9	2.6		

FREQUENCY RESPONSE



Piezotronics, Inc. 3425 Walden Avenue Depew, NY 14043-2495 USA
716-684-0001

Date 4/29/93

Calibrated by Ron Burke

25

A 10185 1/1

Calibration Certificate

Per ISA-RP37.2

Model No. 305A05

Serial No. 2503

PO No. _____ Customer _____

Calibration traceable to NIST thru Project No. 822/251101-93

ICP® ACCELEROMETER
with built-in electronics

Calibration procedure is in compliance with
MIL-STD-45662A and traceable to NIST

CALIBRATION DATA

Voltage Sensitivity 1.69 mV/g $\left(\frac{2000 \text{ g} \cdot \text{s}}{\text{Shock}} \right)$
 Transverse Sensitivity 1.4 %
 Resonant Frequency 45 kHz
 Time Constant 2.0 s
 Output Bias Level 10.0 V

KEY SPECIFICATIONS

Range 2500 ± g
 Resolution .05 g
 Temp. Range -100/+250 °F

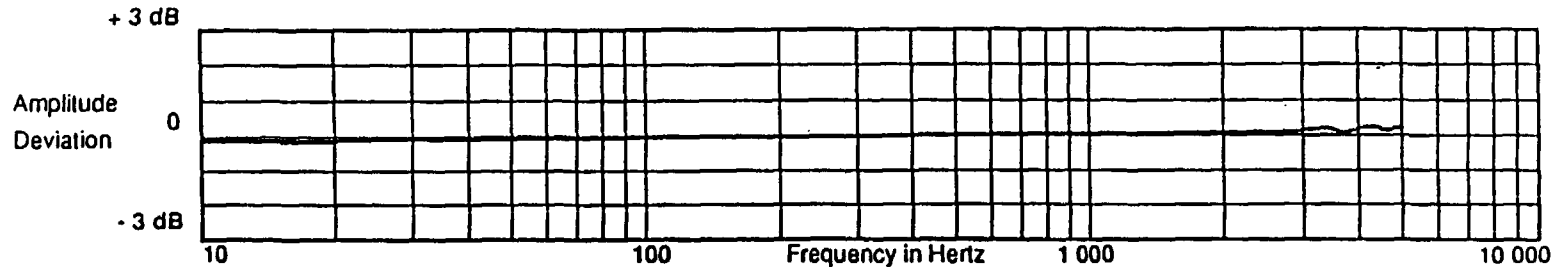
METRIC CONVERSIONS

ms² = 0.102 g
 °C = 5/9 x (°F - 32)

Reference Freq.

Frequency Hz	10	15	30	50	100	300	500	1000	3000	5000		
Amplitude Deviation %	-1.1	-1.4	-.7	-.5	0.0	.3	.7	1.1	2.3	2.7		

FREQUENCY RESPONSE



Piezotronics, Inc. 3425 Walden Avenue Depew, NY 14043-2495 USA
 716-684-0001

Date 4/29/93

Calibrated by Ron Burke

Calibration Certificate

Per ISA-RP37.2

Model No. 305A05

Serial No. 2525

PO No. _____ Customer _____

Calibration traceable to NIST thru Project No. 822/251101-93

ICP® ACCELEROMETER
with built-in electronics

Calibration procedure is in compliance with
MIL-STD-45662A and traceable to NIST.

CALIBRATION DATA

Voltage Sensitivity 1.72 mV/g ($\begin{matrix} 2000 \\ \text{Shock } g \cdot s \end{matrix}$)
 Transverse Sensitivity 2.6 %
 Resonant Frequency 45 kHz
 Time Constant 2.0 s
 Output Bias Level 9.5 V

KEY SPECIFICATIONS

Range 2500 ± g
 Resolution .05 g
 Temp. Range -100/+250 °F

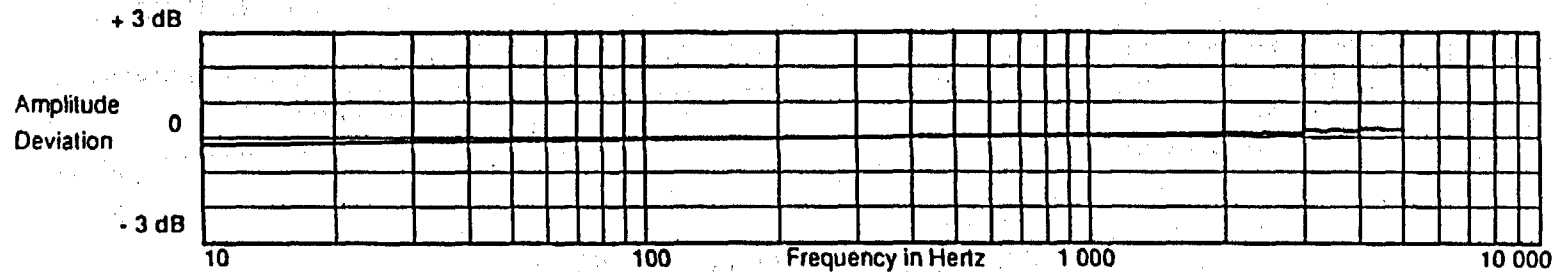
METRIC CONVERSIONS

ms² = 0.102 g
 °C = 5/9 x (°F - 32)

Reference Freq.

Frequency Hz	10	15	30	50	100	300	500	1000	3000	5000		
Amplitude Deviation %	-1.9	-1.6	-1.1	-.9	0.0	.4	.9	1.4	2.9	3.2		

FREQUENCY RESPONSE



Piezotronics, Inc. 3425 Walden Avenue Depew, NY 14043-2495 USA
716-684-0001

Date 4/29/93

Calibrated by Ron Burke

Calibration Certificate

Per ISA-RP37.2

Model No. 305A05

Serial No. 2527

PO No. _____ Customer _____

Calibration traceable to NIST thru Project No. 822/249179-92

ICP® ACCELEROMETER
with built-in electronics

Calibration procedure is in compliance with
MIL-STD-45662A and traceable to NIST.

CALIBRATION DATA

Voltage Sensitivity 1.74 mV/g $\left(\begin{smallmatrix} 2000 \\ \text{Shock } g \cdot s \end{smallmatrix} \right)$
 Transverse Sensitivity 3.6 %
 Resonant Frequency 45 kHz
 Time Constant 2.0 s
 Output Bias Level 10.0 V

KEY SPECIFICATIONS

Range 2500 ± g
 Resolution .05 g
 Temp. Range -100/+250 °F

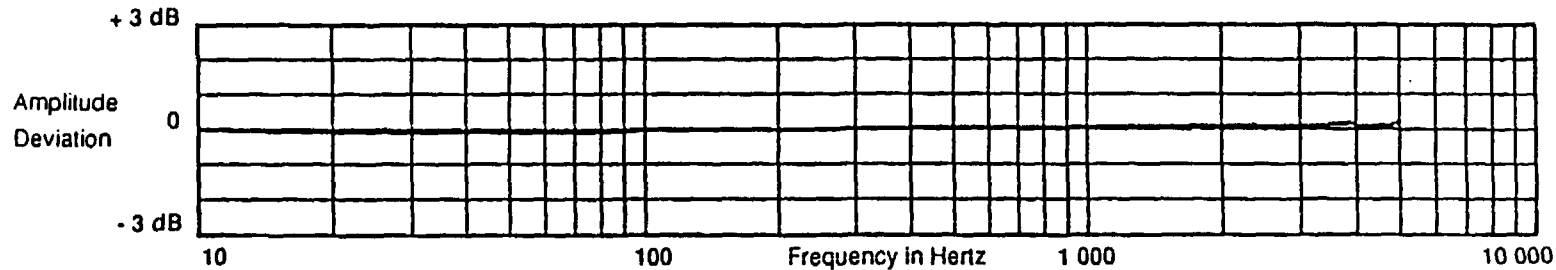
METRIC CONVERSIONS

ms⁻² = 0.102 g
 °C = 5/9 x (°F - 32)

Reference Freq.

Frequency Hz	10	15	30	50	100	300	500	1000	3000	5000		
Amplitude Deviation %	0.0	-0.7	-1.2	-1.0	0.0	.5	.9	1.0	1.6	2.5		

FREQUENCY RESPONSE



Piezotronics, Inc. 3425 Walden Avenue Depew, NY 14043-2495 USA
716-684-0001

Date 1/14/92

Calibrated by J. Schmidt

28

A 16485 T N 1

Calibration Certificate

Per ISA-RP37.2

Model No. 305A05

Serial No. 2526

PO No. _____ Customer _____

Calibration traceable to NIST thru Project No. 822/249179-92

ICP® ACCELEROMETER
with built-in electronics

Calibration procedure is in compliance with
MIL-STD-45662A and traceable to NIST.

CALIBRATION DATA

Voltage Sensitivity 1.67 mV/g $\left(\frac{2000 \text{ g}^2}{8 \text{ hook}} \right)$
 Transverse Sensitivity 1.3 %
 Resonant Frequency 45 kHz
 Time Constant 2.0 s
 Output Bias Level 9.5 V

KEY SPECIFICATIONS

Range 2500 ± g
 Resolution .05 g
 Temp. Range -100/+250 °F

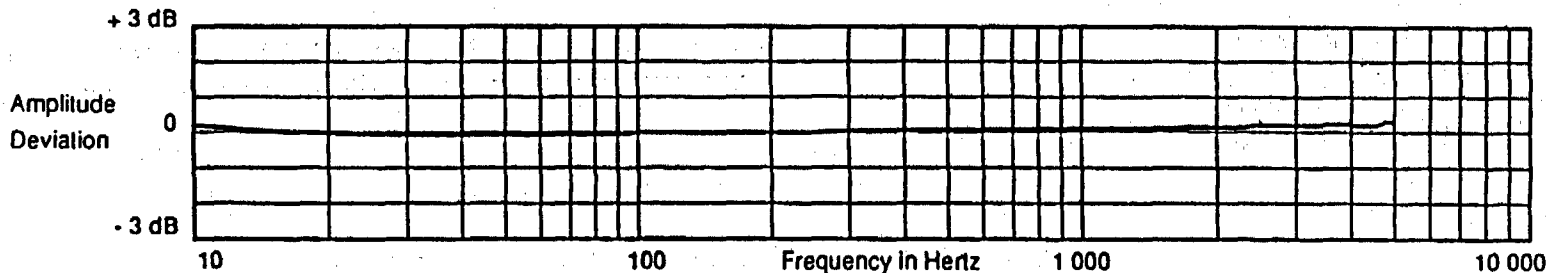
METRIC CONVERSIONS

ms⁻² = 0.102 g
 °C = 5/9 x (°F - 32)

Reference Freq.

Frequency Hz	10	15	30	50	100	300	500	1000	3000	5000		
Amplitude Deviation %	2.4	.3	-1.1	-1.2	0.0	.7	1.1	1.6	2.5	3.6		

FREQUENCY RESPONSE



Piezotronics, Inc. 3425 Walden Avenue Depew, NY 14043-2495 USA
 716-684-0001

Date 1/14/92
 Calibrated by J. Richmond

29

A 164851EN-1

Calibration Certificate

Per ISA-RP37.2

Model No. 305A05

Serial No. 7228

PO No. _____ Customer _____

Calibration traceable to NIST thru Project No. 822/249179-92

ICP® ACCELEROMETER
with built-in electronics

Calibration procedure is in compliance with
MIL-STD-45662A and traceable to NIST

CALIBRATION DATA

Voltage Sensitivity 2.22 mV/g (2000 μ 's Shook)

Transverse Sensitivity 2.5 %

Resonant Frequency 45 kHz

Time Constant 2.0 s

Output Bias Level 9.2 V

KEY SPECIFICATIONS

Range 2500 \pm g

Resolution .05 g

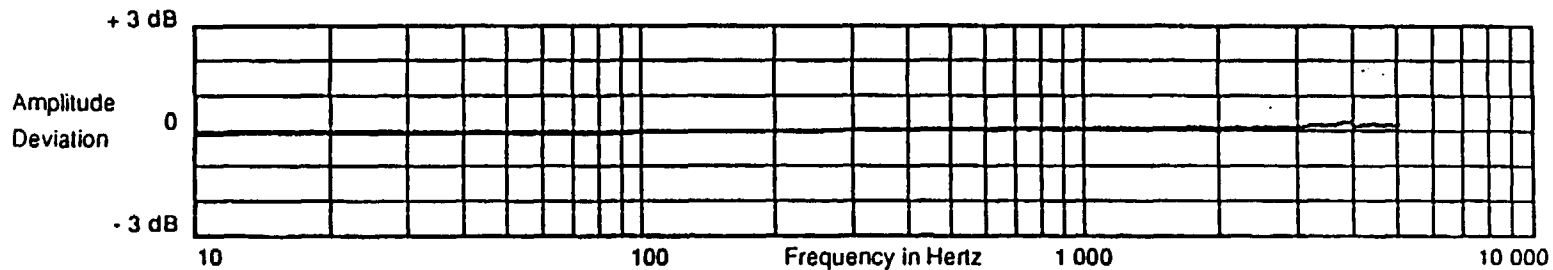
Temp. Range -100/+250 °F

METRIC CONVERSIONS
ms⁻² = 0.102 g
°C = 5/9 x (°F - 32)

Reference Freq.

Frequency Hz	10	15	30	50	100	300	500	1000	3000	5000		
Amplitude Deviation %	-1.0	-1.5	-0.9	-0.8	0.0	.7	.9	1.1	1.9	2.3		

FREQUENCY RESPONSE



Piezotronics, Inc. 3425 Walden Avenue Depew, NY 14043-2495 USA
716-684-0001

Date 1/14/92
Calibrated by J. Richmond

10

A 16485 IN 1

Calibration Certificate

Per ISA-RP37.2

Model No. 305A05

Serial No. 1303

PO No. _____ Customer _____

Calibration traceable to NIST (NBS) thru Project No. 732/243254-89

ICPT™ ACCELEROMETER
with built-in electronics

Calibration procedure is in compliance with
MIL-STD-45662 and traceable to NIST. (NBS)

CALIBRATION DATA

Voltage Sensitivity 1.70 mV/g
 Transverse Sensitivity 2.2 %
 Resonant Frequency 45 kHz
 Time Constant 2.0 s
 Output Bias Level 10.2 V

KEY SPECIFICATIONS

Range 2500 ± g
 Resolution .05 g
 Temp. Range -100/+250 °F

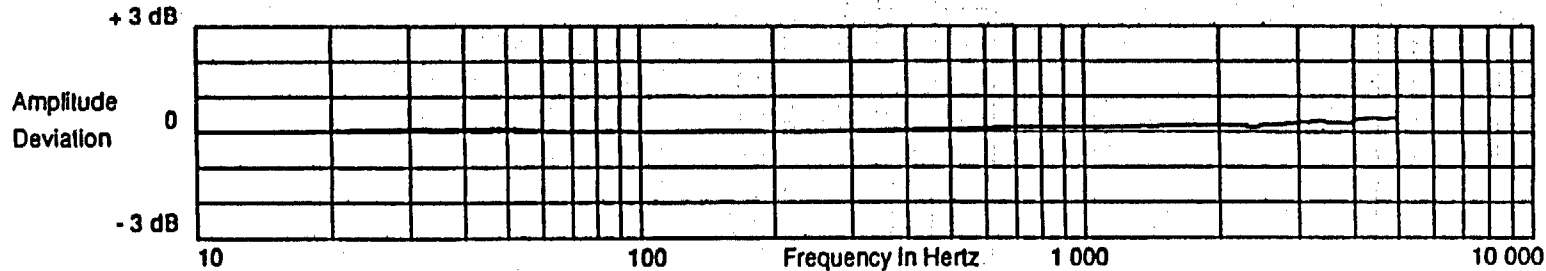
METRIC CONVERSIONS:

ms⁻² = 0.102 g
 °C = 5/9 x (°F - 32)

Reference Freq.

Frequency Hz	10	15	30	50	100	300	500	1000	3000	5000		
Amplitude Deviation %	0.0	.2	1.3	1.3	0.0	.5	1.0	1.6	3.3	4.6		

FREQUENCY RESPONSE



Piezotronics, Inc. 3425 Walden Avenue Depew, NY 14043-2495 USA
 716-684-0001

Date 5/7/90
 Calibrated by P. Jernigan

- 31 -

A 16185 IN 1

Customer _____

 Order No. _____



PIEZOTRONICS

The Calibration procedures of PCB Piezotronics are in compliance with MIL-STD-45662

CALIBRATION DATA
 for
 I. C. P. ACCELEROMETER
 (per I S A S37.2)

Model No. 305A25
 Serial No. 4713
 Range 2,500 g's
 Max Input 5,000 g's
 Max Temp 250 °F

1. VOLTAGE SENSITIVITY 2.02 mv/g @ 100 Hz, 2000 g's PK SHOCK
2. MAXIMUM TRANSVERSE SENSITIVITY 2.7 percent
3. RESONANT FREQUENCY 42 KHz
4. DISCHARGE TIME CONSTANT 2.0 seconds
5. OUTPUT BIAS LEVEL 10.4 Volts
6. FREQUENCY RESPONSE:

Freq. Hz		10	30	50	100	300	500	1000	3000	5000		
Deviation %		-2.7	-1.8	-0.9	0	+1.4	+1.8	+2.5	+3.6	+5.0		

Calibration traceable to NBS through project no. 737/236182-85

PCB PIEZOTRONICS, INC.
 3425 WALDEN AVENUE
 DEPEW, NEW YORK 14043

date 4-21-86
 by John P. Keenan

**8. MDS NORDION F-294 TRANSPORT PACKAGING TESTING
(REFERENCE [56])**



Engineered Products and Services
Design Document

Classification/
Designation CONTROLLED

DOCUMENT TITLE MDS Nordion F-294 Transport Packaging Testing

PROJECT/JOB TITLE F-294 Testing

DOCUMENT TYPE Test Report

Prepared By	<u></u>	Date	<u>98/05/28</u>
	Richard Birchall		
Reviewed By	<u></u>	Date	<u>98/06/03</u>
	Randy Lesco		
Approved By	<u></u>	Date	<u>98.6.3</u>
	Eric Butterworth		
Accepted By	_____	Date	_____
Accepted By	_____	Date	_____

(Signatories for Rev. 0 only)

REA No. 16485

Document No. A-16485-TN-2

Revision No. 0

Alternate Document _____



Engineered Products and Services
Document Status and Revision History

Table with 4 columns: Rev. No., Date, Revision History and ECN Reference, Prepared/Reviewed, and Approved/Accepted. Includes title 'Test Report: MDS Nordion F-294 Transport Packaging Testing' and document details like REA No. 16,485 and Doc. No. A-16485-TN-2.

Table with 5 columns: Issue No., Rev. No., DTS No., Date, ISSUE/STATUS, and BY. A grid for tracking document issues and status.

1. Introduction

Vertical drop tests and puncture tests were performed on the F-294 transport packaging prototype on February 25, 1998, at the AECL drop test facility at Chalk River, Ontario, Canada.

These tests were witnessed by representatives from MDS Nordion, AECB and USNRC.

Seven drop tests were performed, in a variety of orientations, as per a predefined test plan (IN/QA 1368 F294). An unplanned eighth drop test was also performed.

Tri-axial accelerometer blocks were installed on the packaging, in four locations to record deceleration data.

Visual records were made with a video camera and still photography.

Observations were recorded after each drop test.

2. References

AECL document:

1. A-16485-TN-1, "Deceleration Measurements During Drop Tests of the F-294 Transport Packaging".

MDS Nordion documents:

2. Test Plan for F-294 Regulatory Tests, IN/QA 1368 F294
3. Quality Plan for F-294 Regulatory Tests, IN/QP 1369 F294

MDS Nordion drawings:

Drawing #	Title
F629401-002	DROP TEST MODS
F629401-003	PUNCTURE PIN 6" DIA X 16 HIGH
F629401-004	PUNCTURE PIN 6" DIA X 26 HIGH
F629401-005	NORMAL FREE DROP TEST
F629401-006	30 FT FREE DROP TEST
F629401-007	PUNCTURE TEST NO. 1A
F629401-008	PUNCTURE TEST NO. 1B
F629401-009	PUNCTURE TEST NO. 2
F629401-010	PUNCTURE TEST NO. 3
F629401-011	30 FT FREE DROP TEST #2
F629401-012	PUNCTURE TEST #4
F629401-013	WEIGHT ASSY
F629401-014	TUBE
F629401-015	END PLATE
F629401-017	MOUNTING PLATE
F629401-018	MOUNTING PLATE LOWER
F629401-019	F294 TEST SPECIMEN
F629401-020	FLOW DIAGRAM

3. Facilities

AECL (Atomic Energy of Canada Limited) maintains a drop test facility at Chalk River Laboratories (CRL), located at Chalk River, Ontario. The drop test tower is 65 ft high; the maximum drop height is 50 ft. The impact target has a surface area of 48 ft².

The impact target consists of a steel plate mounted on a concrete pad with a total mass of approximately 80 ton. The entire target is embedded in granite bedrock to provide an essentially infinite mass. The steel-reinforced concrete pad is 10 ft by 10 ft by 10 ft deep with a compressive strength of 5000 psi. The steel plate is 8 ft by 6 ft by 4 inches thick, ASTM A203 Grade E. Tapped holes are provided in the top plate for the installation of a high strength plate and puncture bar for impact testing.

(Ref: AECL Dwg. E-4511-2002)

4. Preparation of F-294 prototype

The F-294 packaging prototype was received at Chalk River Laboratories on February 17, 1998. The five-day lead time allowed for the installation of the four tri-axial accelerometer blocks at locations G1, G2, G3 and G4 (Ref: MDS Nordion Dwg. F629401-019).

Photographic record:

9802-23287-1	Accelerometer location G1
9802-23287-2	Accelerometer location G2
9802-23287-3	Accelerometer location G3
9802-23287-4	View of location G3, under the F-313 carrier (F-313 handle later removed and shock buffers added)

The mounting hole for G4 was relocated 1 ft from the centerline, to avoid destruction of the accelerometer during Drop No. 5. This location was used for all drop tests.

A "shock buffer" was installed between the top of the F-313 carrier and the underside of the F-294 closure plug. Also the handle was removed from the F-313 carrier. This was done to prevent damage to the accelerometer installation at G2, during the inverted drops.

Additional work was required to install four safety hoist rings (Welch Part No. 23202) on the shipping skid, to allow for safe inverted lifts on the day of testing. The four 2-inch diameter holes provided (Ref: MDS Nordion Dwg. F629401-002) had to be patched and redrilled to 1-1/2 inch diameter.

The torque wrench used to disassemble and reassemble the F-294 was calibrated. Some oxidation was observed on the closure plug bolts. Due to bending of the crush shield fins, it was not possible to reach the specified 50 ft-lb closing torques for the crush shield to container side-retaining bolts. See Appendix 1 for the recorded torque values and record of torque wrench calibration.

5. Testing

5.1. Test No. 1

Step 5.2.3 – MDS Nordion Test Plan IN/QA 1368 F-294 (1)

Normal Conditions of Transport

Free Drop Test

(Ref: MDS Nordion Dwg. F629401-005)

Conditions:

Drop height = 36 inch
Orientation: Top end drop
Temperature: 6.7 °C
Time of drop: 10:10 a.m.

Photographic record:

9802-23308-1	Accelerometer location G4
9802-23308-2 to 9802-23308-4	F-294, pre-drop
9802-23308-5	Verification of 36 inch drop height, using measured steel rod
9802-23308-6	F-294, pre-drop
9802-23308-7 to 9802-23308-14	F-294, post-drop

Observations:

1. Slight "ripple" on load spreader plate of crush shield.
2. Mesh slightly bent inwards between two fins on crush shield.
3. Up to 0.5 inches of deformation on the crush shield.
4. No other visible change.
5. Setup: Release hook did not release first time.
6. Setup: 36 inch drop height verified visually with bar prior to each two attempts.
7. Additional damage as per photographic records.

5.2. Test No. 2**Step 5.2.4 – MDS Nordion Test Plan IN/QA 1368 F-294 (1)****Hypothetical Accident Condition****30 Feet Free Drop****(Ref: MDS Nordion Dwg. F629401-006)****Conditions:**

Drop height = 30 feet
Orientation: Side oblique ($36\frac{1}{2}^\circ$ from horizontal). Impact point centered around the lift lug fin #4. on the top corner zone of the container
Temperature: 10.2 °C
Time of drop: 1:22 p.m.

Photographic record:

9802-23308-15	Verification of $36\frac{1}{2}^\circ$ angle from horizontal
9802-23308-16 to 9802-23308-20	F-294, pre-drop
9802-23308-21 to 9802-23308-50	F-294, post-drop

Observations:

1. Dummy weight transferred, so both dummy weights are on same side of the fireshield.
2. Measured angle = $36\frac{1}{2}^\circ$ from horizontal. Could not attain 40° drop angle, due to C.O.G. of F-294 packaging.
3. Crush shield deformed on impact face.
4. Shipping skid deformed on impact face.
5. Fixed skid mostly intact; horizontal crack (on skid) located below nameplate. Horizontal crack (on skid) also at location at lead weights.
6. Nine broken welds on inner fin attachment of the crush shield.
7. Three side crush shield to container fasteners are loose.
8. Some welds intact on shipping skid.
9. Fireshield deformed on impact face.
10. Balance of fireshield intact.
11. Upper fireshield intact. No damage.
12. Shipping skid landed just outside the steel pad but on reinforced concrete pad.
13. Side/top of the container (Lift lug fin #4) zone impacted on the steel pad.
14. Setup: 30 foot drop height verified with plumb line prior to first attempt. Subsequent attempts used visual mark/reference point to platform on drop tower.
15. Setup: First two attempts, release hook did not function (limit of release hook is slightly exceeded).
16. Setup: Third attempt (1:22 p.m.) successful.
17. Setup: Manual release for release hook used for this and all subsequent tests.
18. Additional damage as per photographic records.

5.3. Test No. 3**Step 5.2.5 – MDS Nordion Test Plan IN/QA 1368 F-294 (1)**

(Step 5.2.5 of Test Plan identified Test #3A and Test #3B. Neither of these were performed. It was decided that this test (Test No.3) would be more damaging and would be referred to as Test #3C.)

Hypothetical Accident Condition**Puncture Test**

(Ref: MDS Nordion Dwg. F629401-007, F629401-008)

Conditions:

Drop height = 40 inches from top of 26 inch high puncture pin (67 inches from plate)
Orientation: Side oblique (36½° from horizontal). Center-of-gravity on target pin.
Temperature: 9.9 °C
Time of drop: 2:15 p.m.

Photographic record:

9802-23308-51 to 9802-23308-60	F-294, post-drop
-----------------------------------	------------------

Observations:

1. Severe local deformation of crush shield.
2. Crack on fireshield on impact point.
3. Upper fireshield intact.
4. All bolting intact.
5. One (strip) piece of metal broke free (approx. ½ inch wide by 8 inch long).
6. Lift lug severely deformed.
7. Puncture pin damaged (to be switched for next test)
8. 26 inch high puncture pin used.
9. The puncture pin fastening to the steel pad was checked before and after the test. The puncture pin did not move during the test.
10. The puncture pin top face was damaged during the test.
11. Setup: Rigging on one point only.
12. Setup: 40 inch over puncture pin drop height, verified visually with measured bar.
13. Setup: Crush shield was not partially detached prior to test, as had been shown in MDS Nordion Dwg. F629401-007 and F629401-008.
14. Instrumentation: One accelerometer missing at location G2(top of cavity).
15. Additional damage as per photographic records.

5.4. Test No. 4**Step 5.2.6 – MDS Nordion Test Plan IN/QA 1368 F-294 (1)****Hypothetical Accident Condition****Puncture Test****(Ref: MDS Nordion Dwg. F629401-009)****Conditions:**

Drop height = 40 inches from top of 26 inch high puncture pin (67 inches from plate)
Orientation: Side drop
Impact target: Cylindrical fireshield
Temperature: 9.2 °C
Time of drop: 3:10 p.m.

Photographic record:

9802-23308-61 to 9802-23308-62	Verification of 40 inch drop height, using measured steel rod
9802-23308-63 to 9802-23308-65	F-294, post-drop
9802-23308-66 to 9802-23308-68	Further photos of damage from Test No. 3

Observations:

1. Severe local deformation and shearing in circular pattern.
2. Both layers (walls) of fireshield penetrated.
3. Dished head through puncture. Area cut is $\frac{2}{3}$ of circumference of puncture pin.
4. Approx. 2 inch displacement of entire shell (deformed zone).
5. 6 inch diameter puncture.
6. Approx. 10½ to 11 inch diameter deformed zone.
7. The shipping skid did not bottom out first.
8. 26 inch high puncture pin (second pin) was used.
9. The puncture pin fastening to the steel pad was checked before and after the test. The puncture pin did not move during the test.
10. The pin face was not damaged after the test.
11. Setup: Orientation rotated 45° from that as shown on MDS Nordion Dwg. F629401-009.
12. Setup: Through-holes on puncture pin mounting plate (backup puncture pin) enlarged to $\frac{15}{16}$ inches to accommodate bolts.
13. Setup: 40 inches over puncture pin drop height, verified visually with measured bar.
14. Instrumentation: Accelerometer G2 is non-functional (inside top of plug).
15. Additional damage as per photographic records.

5.5. Test No. 5**Step 5.2.7 – MDS Nordion Test Plan IN/QA 1368 F-294 (1)****Hypothetical Accident Condition****Puncture Test****(Ref: MDS Nordion Dwg. F629401-010)****Conditions:**

Drop height = 40 inches from top of 26 inch high puncture pin (67 inches from plate)
Orientation: Bottom drop
Impact target: Bottom of container fixed skid
Temperature: 9.5 °C
Time of drop: 3:48 p.m.

Photographic record:

9802-23308-69	Verification of 40 inch drop height, using measured steel rod
9802-23308-70 to 9802-23308-76	F-294, post-drop

Observations:

1. Local deformation, no penetration.
2. Deformation indentation zone similar to pin diameter.
3. Deformation zone 10 inches diameter.
4. 26 inch high puncture pin (second pin) used.
5. The puncture pin fastening to the steel pad was checked before and after the test. The puncture pin did not move during the test.
6. The pin face was not damaged after the test
7. Setup: 40 inches over puncture pin drop height, verified visually with bar.
8. Additional damage as per photographic records.

5.6. Test No. 6**Step 5.2.8 – MDS Nordion Test Plan IN/QA 1368 F-294 (1)****Hypothetical Accident Condition****30 Feet Free Drop****(Ref: MDS Nordion Dwg. F629401-011)****Conditions:**

Drop height = 30 feet
Orientation: Inverted (top end drop). Puncture pin is removed from drop test pad.
Temperature: 9.4 °C
Time of drop: 4:40 p.m.

Photographic record:

9802-23308-77	F-294, pre-drop
9802-23308-78 to 9802-23308-84	F-294, post-drop

Observations:

1. Crush shield as per photographs
2. Crush shield top retaining bolts still in place. Crush shield retained (jammed) on top of the container.
3. Part of crush shield top ring missing.
4. Most severe deformation on half of circumference.
5. Most crush shield fins attached. Some crush shield fins with broken pieces. Some fins flattened.
6. Fireshield intact. Slight outward bowing along top circumference.
7. Setup: Puncture pin removed.
8. Setup: 30 foot drop height verified with plumb line.
9. Additional damage as per photographic records.

5.7. Test No. 7**Step 5.2.9 – MDS Nordion Test Plan IN/QA 1368 F-294 (1)****Hypothetical Accident Condition****Puncture Test****(Ref: MDS Nordion Dwg. F629401-012)****Conditions:**

Drop height = 40 inches from top of 26 inch high puncture pin (67 inches from plate)
Orientation: Inverted (top end drop). 26 inch puncture pin is reinstalled on drop test pad.
Impact target: Top of crush shield
Temperature: 8.9 °C
Time of drop: 5:00 p.m.

Photographic record:

9802-23308-85	Verification of 40 inch drop height, using measured steel rod
9802-23308-86 to 9802-23308-89	F-294, post-drop

Observations:

1. 6 inch diameter main deformation, 16 inch diameter gradual deformation.
2. No penetration. However foot print of the pin on the upper plate of the crush shield.
3. Approx. 2 inches vertical deformation.
4. 26 inch high puncture pin (second pin) was used.
5. The puncture pin fastening to the steel pad was checked before and after the test. The puncture pin did not move during the test.
6. The puncture pin face was not damaged after the test.
7. Setup: 40½ inches over puncture pin height, verified visually with bar.
8. Additional damage as per photographic records.

5.8. Test No. 8

(Additional test not listed in the Test Plan to assess effect of reinforced area of the outer fireshield shell)

Hypothetical Accident Condition

Puncture Test

(Similar to Ref: MDS Nordion Dwg. F629401-009)

Conditions:

Drop height = 40 inches from top of 26 inch high puncture pin (67 inches from plate)
Orientation: Side puncture on nameplate (Centre-of-gravity on fireshield).
Temperature: 7.2 °C
Time of drop: 5:28 p.m.

Photographic record:

9802-23308-90	Target area, showing removal of nameplate
9802-23308-91	F-294, pre-drop
9802-23308-92 to 9802-23308-94	F-294, post-drop

Observations:

- Shipping skid cleared the steel pad (impact plate).
- Packaging remained balanced on pin (pin penetrated fireshield).
- 1 foot diameter deformation by 1½ inch deep.
- $\frac{2}{3}$ circumference (of 6 inch diameter indent) penetrated.
- 26 inch high puncture pin (second pin) used.
- The puncture pin fastening to the steel pad was checked before and after the test. The puncture pin did not move during the test.
- The puncture pin top face was not damaged after the drop test.
- The shipping skid landed on the reinforced concrete pad just outside the steel pad. The shipping skid did not bottom out first.
- Setup: 40 inches over puncture pin drop height, verified visually with bar.
- Setup: Nordion Identification, Radioactive Caution, and Heat Emitter plates were removed from the impact target zone on the container.
- Additional damage as per photographic records.

6. Accelerometer Data

Reference:

A-16485-TN-1, "Deceleration Measurements During Drop Tests of the F-294 Transport Packaging"

- Deceleration data is summarized on Table 1 of A-16485-TN-1, page 7.
- Where two values are given for a particular accelerometer block for a drop test, the maximum acceleration M , is calculated as:

$$M = \sqrt{a^2 + b^2}$$

where a , b are the acceleration values.

- Where three values are given for a particular accelerometer block for a drop test, the maximum acceleration M , is calculated as:

$$M = \sqrt{a^2 + b^2 + c^2}$$

where a , b , c are the acceleration values.

This is used to provide the following table:

Table 1: Maximum Absolute Decelerations for F-294 Transport Packaging
 [g's]

	1	2	3	4	5	6	7	8
G1	116	136 ²	LOS	20	46	132 ³	60	22
G2	113	LOS	LOS	LOS	LOS	LOS	LOS	LOS
G3	130	66	25	26	58	118	32	14
G4	277 ¹	73	23	35	0	0	50	15

Legend: LOS = Loss Of Signal (cable cut)

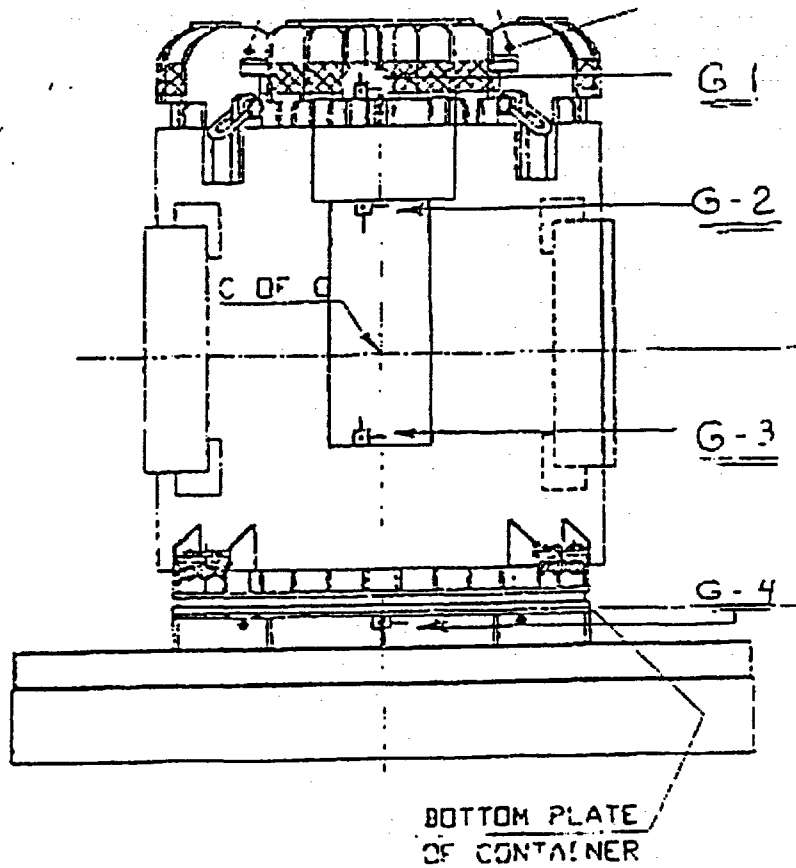


Figure 1 — Locations of Accelerometers

Notes:

1. The very high G4 value, for Test No. 1, is not valid. G4 is mounted on the bottom of container fixed skid, a thin plate supported around the perimeter of the skid, acting as a diaphragm. As per Figure 6 of A-16485-TN-1, page 9, the maximum level attained by G4 does not occur until after the initial impact.

The crush shield does not significantly deform during this test. The rigidity of the F-294 package in this orientation & drop speed is a possible cause for the high deceleration value observed.

2. Test No. 2 is the first 30 foot drop. G1 is very near the impact point for Test No. 2. It is observed to measure the highest deceleration value. G3 and G4 are located further away from the impact point. The crush shield fins on the impact target are greatly deformed, helping to reduce the maximum deceleration value.
3. Test No. 6 is the second 30 foot drop. The maximum value attained by G1, for Test No.6, is similar to that maximum attained for the first 30 foot drop, Test No. 2. Again, the crush shield fins on the impact target are greatly deformed, helping to reduce the maximum deceleration value.

Appendix 1

Recorded Opening and Closing Torques for F-294 Packaging

1. The torque wrench used, Snap-On model QC3R250, serial number 0897600912, range 0-250 ft-lb, was calibrated by AECL using a TWA-1000 Torque Analyzer, on February 24, 1998.

(calibration record attached)

2. The TWA-1000 Torque Analyzer, serial number 21900, was calibrated by McCann Equipment on 05/07/1997.

(calibration record attached)

3. Opening and closing torques were recorded. Opening torques are not accurate as there was an oxidation build-up, causing a "snap action" when opening the bolts.

Measured closing torques are exactly the specified value (preset on the torque wrench), within the torque wrench tolerance. Torques were confirmed by a second person.

4. Closing torques were measured on February 24, 1998.

5. Closing torque values (specified and measured):

Main closure plug to container inner shell assembly: 100 ft-lb
Crush shield to container top retaining bolts: 200 ft-lb
Crush shield to container side retaining bolts: 50 ft-lb
Cylindrical fireshield to fixed skid: 200 ft-lb

Vent-line caps and drain-line cap were removed to permit accelerometer cables to pass through.

(other fasteners were not disturbed, torque values as-delivered by MDS Nordion)

Torque Record - Norion F-294 Packaging

Main closure plug to container inner shell assembly

Torque = 100 ft-lb

OPEN CLOSE

1	150				
2	200				
3	200				
4	175				
5					
6					
7	200				
8	200				
9	200				
10	210				
11	200				
12	175				
13	220				
14	200				
15	150				
16	100				

Crush shield to container top retaining bolts

Torque = 200 ft-lb

OPEN CLOSE

1	120				
2	120				
3	185				
4	220				
5	185				
6					
7					
8					

Crush shield to container side retaining bolts

Torque = 50 ft-lb

OPEN CLOSE

1	30				
2	30				
3	30				
4	30				
5					
6					
7					
8					

Fixed skid to shipping skid (removable skid)

Torque = 200 ft-lb

OPEN CLOSE

1					
2					
3					
4					
5					
6					
7					
8					

Cylindrical fireshield to fixed skid

Torque = 200 ft-lb

OPEN CLOSE

1	220				
2	220				
3	240				
4	240				
5	220				
6	240				
7					
8					

Ventline blind cap

Torque = 20 ft-lb

OPEN CLOSE

1					
2					

Drainline blind cap

Torque = 20 ft-lb

OPEN CLOSE

1					
---	--	--	--	--	--

Millwright: Eddy L. ...

Second: My Biel

Date: February 24, 1958

TORQUE WRENCH CALIBRATION RECORD

A-16485-TN

Make	Model	Range	Serial No.	Inst. No.
Snap-on	QC3R250	0-250 ft.lb	0297600912	Page 17
Procedure: As per Torque analyzer manual			Accuracy: Clockwise	
Owner: Colin Guthrie			± 4% From 20% of full scale to full scale.	

Test Equipment Used		
Inst. No.	Description	Use
456-722	Torque Analyzer TWA-1000 (SERIAL NUMBER 21900)	Standard ind.

Applied Torque(display) Units: ft.lb.			Dial indication(wrench) (Pre-set click type) Units: ft.lb.			
No.1	No.2	No.3	No.1	No.2	No.3	Accuracy % FS (avg of 3)
49.5	49.8	50.0	50	50	50	+0.09
100.2	101.0	100.2	100	100	100	-0.19
151.0	149.5	150.7	150	150	150	-0.16
199.0	199.3	200.1	200	200	200	-0.21
251.0	249.8	250.2	250	250	250	-0.13

Comments: No 409 QA number was on this wrench.

Name: C.R. LADE <i>CR LaDe</i>	Date: 98 Feb 24
-----------------------------------	-----------------

Nom/Name: Atomic Energy of Canada Ltd.
 Cert No.: 101624

CERTIFICAT D'ÉTALONNAGE CERTIFICATE OF CALIBRATION

ÉQUIPEMENT McCANN

9501 Côte de Liesse
 Dorval, Québec
 Canada, H9P 2N9

Tel: (514) 636-6344

Fax: (514) 636-0365

Référence:	Numéro de Série:
Model No.: TWA-1000 40315	Serial No.: 21900
Capacité Maximale:	Precision: .25% of Reading
Maximum Capacity: 1000 N/M	Accuracy: +/- 1 Digit
Technicien:	Température ambiante:
Technician: Stephen Lawson	Ambiant Temperature: 20.8 C.

<u>Nominales</u>	<u>Reeles</u>	<u>Nominales</u>	<u>Reeles</u>
<u>Nominal</u>	<u>Actual</u>	<u>Nominal</u>	<u>Actual</u>
100.00	99.99	600.00	600.20
200.00	200.02	700.00	700.27
300.00	300.08	800.00	800.31
400.00	400.10	900.00	900.39
500.00	500.13	1000.00	1000.47

Les limites indiquées et l'équipement de vérification utilisé pour cet étalonnage sont approuvés par le Conseil national de recherches - Canada ou par le National Institute of Standards and Technology des E.-U. (ou les deux).

The limits shown and the test equipment used for this calibration comply with the requirements of the National Research Council, Canada and/or the National Institute of Standards and Technology, U.S.A.

Tolérance de mesure de l'équipement de vérification utilisé:
 Uncertainty of measurement of the test equipment used is: 0.025% F.S.D.

ÉTALONS UTILISES/TRANSFER STANDARDS

Poutrelle D'étalonnage No. de Serie/

Test Beam Serial Number: 15066

Donnees de Retracedabilite/Traceability Data: B13274, B13090, B13064
 B03489, B03485

Poids/Weights: 771, 774, 775, 776, 777, 778, 779, 780, 1022, 1031

Donnees de Retracedabilite/Traceability Data: NIST #VT93-402

Multimetre/Multimeter: Fluke 8840A s/n: 5061012

Donnees de Retracedabilite/Traceability Data: Report #0581388

Date D'étalonnage/Calibration Date: 05/07/1997

Date de Recertification/Recertification Due: 05/07/1998

Superviseur D'assurance Qualite:

Q.A. Supervisor: John Greig



MONTREAL:
 9501 Côte de Liesse
 Dorval, Qué. H9P 2N9
 Tél.: (514) 636-6344
 Fax: (514) 636-0365

TORONTO:
 2395 Drew Rd. #4
 Mississauga, Ont. L5S 1T2
 Tel.: (905) 677-3336
 Fax: (905) 677-4333

WINNIPEG:
 1489 Dublin Ave.
 Winnipeg, Man. R3E 3G8
 Tel.: (204) 774-2277
 Fax: (204) 774-2358

VANCOUVER:
 #7 - 7533 - 135th Street
 Surrey, B.C. V3W 0N6
 Tel.: (604) 596-4077
 Fax: (604) 596-6479

SPÉCIALISTES EN OUTILS À TORSION • RÉPARATION ET CALIBRATIONS
TORQUE TOOL SPECIALISTS • REPAIRS AND RECALIBRATIONS

**Servicing The Aircraft, Construction, Industrial,
 Marine & Mining Industries**
**Desservons: Avionnerie, Construction, Industrie,
 Marine et Industries minières**

NORBAR • CHICAGO PNEUMATIC • COLUMBUS McKINNON • RAYMOND • ENERPAC • RECOULES

A-16485-TN-2
 Rev. 0
 Page 19

Atomic Energy of Canada Ltd.

CERT# 101624

DESCRIPTION: TWA-1000
MODEL NUMBER: 40315
SERIAL NUMBER: 21900
TESTER: Fluke 8840A Digital Multimeter
 S/N: 5061012

We certify that all the goods detailed above have been inspected and tested and unless otherwise stated above, conform with the drawings, specifications, and orders of the customer and with all appropriate official standards which are in force. The equipment used for the purpose of calibration is directly traceable to the National Research Council of Canada and/or the National Institute of Standards and Technology, U.S.A.

DATE OF CALIBRATION: 05/07/1997

RECERTIFICATION DATE: 05/97/1998

Stephen Lawson
Technician

APPENDIX 2.10.11
DETERMINATION OF THE MAXIMUM DAMAGING DROP TEST
ORIENTATION FOR F-294 TRANSPORT PACKAGE

CONTENTS

1. INTRODUCTION	3
2. FAILURE CRITERIA	3
3. END DROP – TOP ORIENTATION	3
3.1 ORIENTATION.....	3
3.2 ENERGY ABSORPTION	4
3.3 G-LOADS.....	4
3.4 COMMENTS.....	5
3.4.1 Note #1	5
3.4.2 Note # 2.....	5
3.4.3 Note #3.....	5
3.4.4 Note #4.....	5
3.4.5 Note #5.....	5
3.4.6 Note #6.....	6
3.5 SUMMARY	6
4. CORNER DROP – TOP ORIENTATION	6
4.1 ORIENTATION.....	6
4.2 MODE OF PRIMARY IMPACT	6
4.2.1 Energy Absorption During Primary Impact.....	7
4.2.2 G-Loads Based on Primary Impact.....	7
4.3 SECONDARY IMPACT.....	7
4.4 COMMENTS.....	8
4.4.1 Note #1	8
4.4.2 Note # 2.....	8
4.4.3 Note #3.....	9
4.4.4 Note #4.....	9
4.4.5 Note #5.....	9
4.4.6 Note #6.....	9
4.5 SUMMARY	10
5. OBLIQUE DROP – SIDE ORIENTATION	10
5.1 ORIENTATION.....	10
5.2 MODE OF PRIMARY IMPACT	10
5.2.1 Energy Absorption During Primary Impact.....	11
5.2.2 G-loads based on Primary impact.....	11
5.3 SECONDARY IMPACT.....	11
5.4 COMMENTS.....	12
5.4.1 Note #1	12
5.4.2 Note #2.....	12
5.4.3 Note #3.....	13
5.4.4 Note #4.....	13
5.4.5 Note #5.....	13
5.4.6 Note #6.....	13
5.5 SUMMARY	13

6. OVERVIEW OF DAMAGE IN THREE DIFFERENT DROP TEST ORIENTATIONS..... 14
6.1 IN THE END DROP – TOP ORIENTATION..... 14
6.2 IN THE CORNER DROP TOP ORIENTATION (57° TO HORIZONTAL)..... 14
6.3 IN OBLIQUE DROP – SIDE ORIENTATION (15° TO HORIZONTAL) 15
7. DISCUSSION 15
8. CONCLUSIONS..... 15

1. INTRODUCTION

The F-294 package can be dropped in any of the six designated free drop test orientations shown in Figure 2.10.11-F1. The drop orientations are identified as:

- Orientation #1.1 end drop – top
- Orientation #1.2 end drop – bottom
- Orientation #2 side drop
- Orientation #3.1 corner drop – top
- Orientation #3.2 corner drop – bottom
- Orientation #4.1 oblique drop – side

Out of six combinations of drop test orientations listed above, from the viewpoint of the integrity of shielding and the containment system, it is concluded that the end drop – top (#1.1), corner drop – top (#3.1) and oblique drop – side (#4.1) orientations are more critical drop orientations than the end drop – bottom (#1.2), side drop (#2) and corner – bottom (#3.2) drop orientations. The main justification for this is:

1. The top, top corner and the side oblique drop orientations affect the containment system and could potentially result in the loss of the top closure plug or the crush shield.
2. The F-294 components such as the crush shield and the closure plug are bolted and are therefore weaker than the welded fin connections at the bottom of the F-294.

In order to determine the maximum damaging drop test orientation, two methods are used: 1) quantitative and 2) qualitative. Three drop test orientations are considered 1) end drop – top, 2) corner drop – top, and 3) oblique drop – side. Also, the failure criteria, as per section 2, is used to evaluate each drop test orientation

2. FAILURE CRITERIA

- 1) Loss of closure plug is unacceptable as the containment system will fail and the shielding integrity will not be met;
- 2) Failure of primary shell or primary shell welds (other than fin welds) is unacceptable as the subsequent fire test to follow will expose the lead shielding directly to hot gases or flames.
- 3) Loss of thermal protection is unacceptable as the radiative heat uptake of the container will be increased in the fire test and therefore lead melt safety margin will be eroded.

3. END DROP – TOP ORIENTATION

3.1 ORIENTATION

The angle between the line between centre of gravity (COG) and the impact point (or plane) and the horizontal test pad is 90°. See Figure 2.10.11-F2. So, the weight of the package, centre of gravity directly over impact point, is centric. Therefore, upon primary impact, potential energy (PE) due to 30-ft drop is translated to kinetic energy. In other words, during the primary impact, there is no rotation of the package and no rotational energy component.

3.2 ENERGY ABSORPTION

- 1) The impact is characterized as hard impact. Entire top face of the container is impacted. Meaning high G's and short deformation (distance between centre of gravity and impact point or plane = 36.25 in.).
- 2) All 28 fins of the crush shield come into play; The fins impact is characterized as impact on *straight-edge*. 66.8 % of PE is absorbed by crush shield fins. The deformation of the fins is expected to be 2.0 in.
- 3) There are 36 container fins: 4 lift lug fins (1.25 in. thick). 8, 1/2-inch thick and 24, 3/8-inch thick. 8, 1/2-inch thick and 24, 3/8-inch thick container fins come into play and between them absorb 33.2% of PE. The deformation is expected to be 1.8 in.
- 4) So, between the crush shield and the container fins, 100% PE is absorbed.
- 5) The total deformation is expected to be of the order of 3.8 in. (i.e., 2.0 + 1.8 in.). As the lift lug fin is recessed from the initial impact point (at time = 0) by at least 6 in., the lift lug fins of the container do not come into play as the impact front is arrested at 3.8 in. from the initial impact point. Consequently, the peak loads are transferred to the container top conical region via twenty-four 3/8-inch thick and eight 1/2-inch thick fins.

3.3 G-LOADS

Based on Davis Methodology G-load estimates are low (200 g's). Based on comparison to similar packages G-loads are estimated to be 800 g's. Its expected that the G-loads of the order of 800 g's; however it may exceed 800 g's as the impact is characterized as hard.

What is the impact of high g-loads on the top zone component integrity? Or what is the G-load capability of the components? See Table 2.10.11-T1

Table 2.10.11-T1
G-load Capability: End Drop - Top Orientation

Component	Sub-component	Top drop g's	Comments (Section 3.4)
Closure Plug			Note #1 (see Fig. 2.10.11-F3)
	Bolts	1,186	
	Threaded Hole	670	
Container			
	Weld Group	1,194	Note #2 (see Fig. 2.10.11-F3)
	Top Flange	1,744	
	Lift Lug Base Zone	344	Note #3 (see Fig. 2.10.11-F4)
	Cavity End Cap	198	Note #4 (see Fig. 2.10.11-F5)
Crush shield			Note #5
	Bolts (16)	50	
	Other Features	Trapped	
Cylindrical fireshield			Note #6
	Bolts (8)	551	
	Other Features	Trapped	

3.4 COMMENTS

3.4.1 Note #1

The closure plug has 16 fasteners (UNBRAKO Socket Head Screws). The size of fasteners is 1 in. Dia. - UNC. In the top end drop, the closure plug bolts are loaded in tension as the closure plug is pulling away from the rest of the container (see Fig. 2.10.11-F3). Calculations for G-loads are presented in Appendix 2.10.14.

3.4.2 Note #2

Due to lead slump, the weld group WCC1, WCC2, WCC7, WCC3 and WF1 is impacted.

See Fig. 2.10.11-F3. Calculations for G-loads are presented in appendix 2.10.14 of SAR. Assuming the weld group is loaded collectively. WF1 are the external fin/shell fillet welds. The fins convert the shell from non-stiffened plain shell to stiffened composite shell. As the lead slumps, the welds are stressed collectively but not necessarily equally. After lead slump, the deformed shape of the conical shell will approximate orange peel configuration.

3.4.3 Note #3

There are four lift lug fins, one in each quadrant of the conical shell. At the base of lift lug fins, the primary shell is reinforced. Upon impact, the impact front (crush front) advances as a function of time, it appears that the crush front is arrested 3.8 in. from initialization. As the lift lug fins are at least 6 in. from the initial plane, the lift lugs will not be impacted. If the four lift lugs are affected in any way, then the primary shell may suffer shear fracture at approximately 344 g's [Pure shear failure. (Shear area $172 \text{ in}^2 \times 70,000 \text{ UTS psi} \times 0.6/\text{weight of } 21,000 \text{ lb.} = 344 \text{ g's}$). The factor 0.6 is for converting UTS to U shear stress (USS)].

In the current design of F-294, the base of the lift lug has been re-designed (double shell, etc. beefed up) Consequently, this failure path has very low possibility.

3.4.4 Note #4

In the top end drop, the bottom plate of the cavity is loaded with deceleration loads due to the lead weight distributed (slump) over the plate. Its estimated that, based on 0.5 in. thick Hastelloy plate, the plate is capable of withstand 198 g's. As the plate bends, the curvature will enable to withstand lots more G's. As the bottom of cavity is 46.25 in. from the impact point or plane, the G-loads at the bottom of the cavity will be substantially reduced compared to G-loads at the closure plug bolt area. The end cap is more likely to bend (become dished rather than fracture). If the lead slumps, the displacement of lead shielding is not a major concern as the F-294 is over-shielded.

3.4.5 Note #5

There are 16 fasteners (1 inch dia. SAE Gr. 8) joining the crush shield to the container at the top zone. In the top end drop eight fasteners are loaded in compression, while the remaining eight are loaded in shear. The G-load capability of the crush shield fasteners is estimated to be 50 g's.

The crush shield is impacted first. As the impact progresses, it is crushed between the rest of the container and the drop test pad. Consequently, the crush shield is trapped between the top of the container inclusive of the cylindrical fireshield and the drop test pad.

Also after the top end drop, we may find the crush shield friction welded to the top of the container.

3.4.6 Note #6

There are eight fasteners (1 inch Dia. SAE Gr. 8) joining the cylindrical fireshield to the container at the bottom fixed skid zone. Two fasteners at each of the corners (4) of the fixed skid. In the top end drop, eight fasteners are loaded in tension. The g-load capability has been calculated in Appendix 2.10.14 of SAR Revision 3.

The crush shield is impacted first. As the impact progresses, the cylindrical fireshield is decelerated. The cylindrical fireshield is trapped between the deformed crush shield and the fixed skid.

3.5 SUMMARY

- 1) Despite the fact that all the potential energy (PE) is estimated to be absorbed between crushshield fin impact limiters and the container fins, the impact is characterized as hard. Consequently, high G-loads, low deformation and short duration is to be expected. Therefore the impulsive (instantaneous force x time) loads will be of significant magnitude.
- 2) Closure between the container and the plug shall be maintained for up to 1200 g's. 1200 g's is based on static UTS.
- 3) Despite the fact that crush shield fasteners have all sheared, the crush shield shall be retained and trapped between the top of the container and the drop test pad. As the top fireshield is integral with the crush shield, the top fireshield shall be retained (no loss of thermal protection).
- 4) The cylindrical fireshield shall be retained and trapped between the fixed skid and the deformed crush shield (no loss of thermal protection).
- 5) Due to lead slump, the welds at the top zone of the containers are collectively loaded. One of the external welds (WCC1 or WCC3 or WF1) could fracture. Also, the shell could fracture. In this failure path scenario, the lead shielding could be exposed directly to fire test to follow (hot gases and or flame).
- 6) As the lift lug fin is sufficiently recessed from the final impact front, the base of the lift lug fin is not impacted.

4. CORNER DROP – TOP ORIENTATION

4.1 ORIENTATION

The container shall be suspended 57° from the horizontal (see Figure 2.10.11-F6). The top corner zone, centered around the lift lug fin, is to be impacted. So the weight of the package, centre of gravity (CG) directly over impact point, is centric. Therefore, upon primary impact, potential energy (PE) due to 30-ft drop is translated to kinetic energy. In other words, during the primary impact there is no rotation of the package and no rotational energy component

4.2 MODE OF PRIMARY IMPACT

The order in which the components are impacted when the impact front advances is as follows:

- 1) Crush shield fins – Peak loads transmitted to top four container/crush shield joint pads (eight fasteners on top face and remaining eight fasteners on side face). Peak load may shear all or some of the 16 fasteners. [Note: The reactive force may detach the crush shield. Crush shield tries to “fly” off. However, during the primary impact the crush shield shall be trapped between the container driving down and the drop test pad.]
- 2) The two container fins supporting the joint pad come into play.
- 3) As the impact front advances, the next component to come into play is the lift lug fin. The peak loads from the lift lug are transmitted to the base of the lift lug zone. These loads may shear (fracture) the primary shell.

- 4) The next component to come into play are the container fins.
- 5) The top corner of the cylindrical fireshield is the next component to come into play.
- 6) The top closure zone is the last component to come into play.

4.2.1 Energy Absorption During Primary Impact

- 1) The top corner of the container is impacted. The impact is characterized as medium- hard impact. Meaning medium G's and medium deformation Δ . See Fig. 2.10.11-F7 for G versus Δ curve. Distance between centre of gravity and impact point or plane = 41.1 in.
- 2) Only 10 of total 28 fins of the crush shield come into play; the fin impact is characterized as impact on curved-edge. Estimated 36% of PE is absorbed by crush shield fins. The deformation of the fins is expected to be 2.7 in.
- 3) There are 36 container fins: 4 lift lug fins (1.25 in. thick). 8 0.5 in. thick and 24 3/8 in. thick. One lift lug fin of the container is the first container fin to come into play as it is closest to the advancing impact front. It is estimated to absorb 10.3% of PE. The deformation is expected to be 1.2 in.
- 4) So between crush shield and 1 container fin (lift lug fin), it is estimated 46 % PE is absorbed. The remaining 54 % has to be absorbed by the container fins + container body /closure plug and cylindrical fireshield assembly.
- 5) The total deformation is expected to be of the order of > 3.7 in. (i.e. 2.7 + 1. in.) perhaps around 5 in. As the lift lug fin is impacted, the peak loads are transferred to the container top conical region lift lug base zone via 1 lift lug fin.

4.2.2 G-Loads Based on Primary Impact

Based on Davis Methodology, G-load estimates are low (340 g's). Based on comparison to similar packages G-loads are estimated to be 800 g's. It is expected that the G-loads shall be of the order of 800 g's.

What is the impact of G-loads on the components? Or what is the G-load capability of the components?
See Table 2.10.11-T2

4.3 SECONDARY IMPACT

After the primary impact, the F-294 shall be subjected to secondary bounce, followed by secondary impact as per Figure 2.10.11-F8. The secondary bounce shall be up to y feet (where y = up to 4 ft.). As the F-294 does the secondary bounce of y ft., at y ft. elevation, there are two scenarios:

- i) If all the fasteners of the crush shield joint have fractured (sheared), the fully detached crush shield shall "take -off" (i.e., propelled by reaction forces which have not been fully dissipated), only to be retained by the long fins which are located between the container side fins and the cylindrical fireshield.
- ii) If some of the fasteners have fractured, the partially detached crush shield shall be swung open around a hinge. Once again, the crush shield shall be restrained from opening by long fins or the "friction welded" top deformed zone.

**Table 2.10.11-T2
G-load Capability: Corner Drop – Top Orientation**

Component	Sub-Component	Top Corner Drop G's	Comments (section 4.4)
Closure Plug			Note #1
	Bolts	913	
	Threaded Hole	642	
Container			
	Weld Group	1,050	Note #2
	Top Flange	1,248	
	Lift Lug Base Zone	86	Note #3
	Cavity End Cap	245	Note #4
Crush Shield			Note #5
	Bolts (16)	50	
	Other Features	Appears Trapped	Note #5
Cylindrical Fireshield			Note #6
	Bolts (8)	500	
	Other Features	Trapped	Note #6

4.4 COMMENTS

4.4.1 Note #1

The closure plug has 16 fasteners (UNBRAKO Socket Head Screws). The size of fasteners is 1 in. Dia. – UNC. In the top corner drop, the closure plug bolts are loaded in tension & shear as the closure plug is pulling away from the rest of the container. It is estimated that the closure plug would maintain closure up to 913 g's.

4.4.2 Note # 2:

Due to lead slump, in the top corner zone, only 1/4 to 1/3 of the full circumference of the container is impacted. Due to lead slump, the weld group WCC1, WCC2, WCC7, WCC3 and WF1 is impacted. Calculations for G-loads are presented in Appendix 2. assuming the weld group is loaded collectively. WF1 are the external fin/shell fillet welds. The fins convert the shell from non-stiffened plain shell to stiffened composite shell. As the lead slumps, the welds are stressed collectively but not necessarily equally. After lead slump, the deformed shape of the conical shell will approximate orange peel configuration.

4.4.3 Note #3

There are four lift lugs fins, one in each quadrant of the conical shell. At the base of lift lug fins, the primary shell is reinforced. Upon impact, the impact front (crush front) advances as a function of time, ONE (of four) lift lug will be impacted. Consequently, the primary shell may suffer shear fracture at approximately 86 g's [Pure shear failure. (Shear area $43 \text{ in}^2 \times 70,000 \text{ UTS psi} \times 0.6 / \text{weight of } 21,000 \text{ lb.} = 86 \text{ g's}$). The factor 0.6 is for converting UTS to U Shear Stress (USS)].

In the current design of the F-294, the base of the lift lug has been re-designed (double shell ,etc. beefed up) Consequently, this failure path has very low possibility.

4.4.4 Note #4

In the top corner drop, the bottom plate of the cavity is loaded with deceleration loads due to the lead weight distributed (slump) over the plate. Its estimated that, based on 0.5 in. thick Hastelloy plate, the plate is capable of withstanding 245 g's. As the plate bends, the curvature will enable it to withstand lots more G's. As the bottom of cavity is 55 in. from the impact point or plane, the G-loads at the bottom of the cavity will be substantially reduced compared to G-loads at the closure plug bolt area. The end cap is more likely to bend (become dished rather than fracture). If the lead slumps, the displacement of lead shielding is not a major concern as the F-294 is over-shielded.

4.4.5 Note #5

There are 16 fasteners (1 inch Dia. SAE Gr. 8) joining the crush shield to the container at the top zone. In the top end drop eight fasteners are loaded in compression, while the remaining eight are loaded in shear. The G-load capability as per following calculation:

Step #1: in tension:	P1	= $8 \times 150,000 \text{ psi} \times 0.551 \text{ in}^2 = 661,200 \text{ lb.}$
Step #2: in shear:	P2	= $8 \times 150,000 \text{ psi} \times 0.6 \times 0.551 \text{ in}^2 = 396,720 \text{ lb.}$
Step #3: allowable	P	= $P1 + P2 = 1,057,920 \text{ lb.}$
Step #4.	G	= $1,057,920 \text{ lb.} / 21,000 \text{ lb.} = 50 \text{ g's}$

During the primary impact, the crush shield is impacted first. As the impact progresses, the crush shield is trapped between the top of the container inclusive of the cylindrical fireshield and the drop test pad. Also, after the top corner drop, we may find the crush shield is partially "friction welded" to the top of the container.

4.4.6 Note #6

There are eight fasteners (1 inch. Dia. SAE Gr. 8) joining the cylindrical fireshield to container at the bottom fixed skid zone. Two fasteners at each of the corners (4) of the fixed skid. In the top corner drop eight fasteners are loaded in tension. The g-load capability has been calculated:

Step #1: in tension:	P1	= $8 \times 150000 \text{ psi} \times 0.551 \text{ in}^2 = 661,200 \text{ lb.}$
Step #2.	G	= $661,200 \text{ lb.} / \text{weight of fireshield } 1,200 \text{ lb.} / 1.1 = 500 \text{ g's}$

The crush shield is impacted first. As the impact progresses, the cylindrical fireshield is decelerated. The cylindrical fireshield is trapped between the deformed crush shield and the fixed skid. So there is no loss of side thermal protection.

4.5 SUMMARY

- 1) In the top corner drop attitude, the impact is characterized as medium-hard. Only 46% of the total PE is estimated to be absorbed between crush shield fin impact limiters and the container fins. Consequently, medium G-loads, high deformation and long duration is to be expected. Therefore, the impulsive (instantaneous force x time) loads will be of significant magnitude around the lift lug fin.
- 2) Closure between the container and the plug shall be maintained for up to 900 g's. 900 g's is based on static UTS. Its concluded that closure shall be maintained.
- 3) During the primary impact, the crush shield shall be retained and trapped between the top of the container and the drop test pad. As the top fireshield is integral with crush shield, the top fireshield shall be retained. (No loss of thermal protection). However, the crush shield may be "lost: during the secondary impact, depending upon the magnitude of reaction forces. In this failure path scenario, the puncture test to follow could further detach the crush shield and cause loss of top thermal protection.
- 4) The cylindrical fireshield shall be retained and trapped between the fixed skid and the deformed crush shield. (no loss of thermal protection.)
- 5) Due to lead slump, the welds at the top zone of the containers are collectively loaded. One of the external welds (WCC1 or WCC3 or WF1) could fracture. Also the shell could fracture. In this failure path scenario, the lead shielding could be exposed directly to hot gases and or flame of the fire test to follow.
- 6) As the lift lug fin is the second component to be impacted, peak loads are transmitted from the lift lug fin to the base of the primary shell of the container. It is possible that the primary shell could fracture locally.

5. OBLIQUE DROP – SIDE ORIENTATION

5.1 ORIENTATION

The container shall be suspended 15° from the horizontal. See Figure 2.10.11-F9. The top side corner zone, centered around the lift lug fin is to be impacted. So the weight of the package acting on the line of centre of gravity (CG) is not coincidental over impact point i.e., eccentric/oblique drop. Therefore, upon primary impact, potential energy (PE) due to 30-ft drop is translated to kinetic energy + rotational energy.

5.2 MODE OF PRIMARY IMPACT

The order in which the components are impacted when the impact front advances is as follows:

- 1) Crush shield fins: Peak loads are transmitted to top four container/crush shield joint pads (eight fasteners on top face and remaining eight fasteners on side face). Peak load may shear all or some of 16 fasteners.
[Note: The reactive force may detach the crush shield. Crush shield tries to "fly" off. However during the primary impact, the crush shield shall be trapped between the container driving down and the drop test pad.]
- 2) As the impact front advances, the next components to come in play are the lift lug fin and the top corner of the cylindrical fireshield. The peak loads from the lift lug are transmitted to the base of the lift lug zone. These loads may shear (fracture) the primary shell.
- 3) The top and side container fins, the top closure zone, the container shell and the lead shielding are the last components to come into play.

5.2.1 Energy Absorption During Primary Impact

- 1) The top/side corner of the container is impacted. The impact is characterized as medium impact. Meaning medium G's and high deformation Δ . See Fig. 2.10.11-F7 for G versus Δ curve. Distance between centre of gravity and impact point or plane = 41 in.
- 2) Only six of total 28 fins of the crush shield come into play; the fin impact is characterized as impact on curved-edge. Estimated 15% of PE is absorbed by crush shield fins. The deformation of the fins is expected to be 2.4 in.
- 3) There are 36 container fins: four lift lug fins (1.25 in. thick). eight, 0.5 in. thick and 24, 3/8 in. thick.
One lift lug fin of the container is the first container fin to come into play as it is closest to the advancing impact front. It is estimated to absorb 10% of PE. The deformation is expected to be 1.2 in.
- 4) The cylindrical fireshield: for deformation 0.1 in. over 30-inch length, the cylindrical fireshield shall absorb 4.5% of PE.
- 5) So between crush shield, one container lift lug fin and the cylindrical fireshield, it is estimated 30% PE is absorbed. The remaining 70% has to be absorbed by the container fins + container body/closure plug + lead shielding and cylindrical fireshield assembly.
- 6) The total deformation is expected to be of the order of 4 in. (i.e., 2.4 + 1 in.). As the lift lug fin is impacted, the peak loads are transferred to the container top conical region lift lug base zone via one lift lug fin.

5.2.2 G-loads based on Primary impact

Based on comparison to similar packages, G-loads are estimated to be 1000 g's.

What is the impact of G-loads on the components? Or what is the G-load capability of the components? See Table 2.10.11-T3.

5.3 SECONDARY IMPACT

- 1) After the primary impact, the F-294 shall be subjected to secondary bounce, followed by secondary impact as per Figure 2.10.11-F10. The secondary bounce shall be y feet (where y = up to 2 ft.). As the F-294 does the secondary bounce of y ft., at y ft. elevation, there are two scenarios:
 - i). If all the fasteners of the crush shield joint have fractured (sheared), the fully detached crush shield shall "take -off" (i.e., propelled by reaction forces which have not been fully dissipated), only to be restrained by the long fins which are located between the container side fins and the cylindrical fireshield.
 - ii). If only some of the fasteners have fractured, the partially detached crush shield shall be swung open around a hinge. Once again the crush shield shall be restrained from opening by long fins or the "friction welded" top deformed zone.

**Table 2.10.11-T3
G-load Capability: Side Oblique Drop Orientation**

Component	Sub-Component	Side Oblique Drop	Comments (section 5.4)
		G's	
Closure Plug			Note #1
	Bolts	912	
	Threaded Hole	904	
Container			
	Weld Group	1,580	Note #2
	Top Flange	2,200	
	Lift Lug Base Zone	86	Note #3
	Cavity End Cap	430	Note #4
Crush Shield			Note #5
	Bolts (16)	46	
	Other Features	Appears Trapped	Note #5
Cylindrical Fireshield			Note #6
	Bolts (8)	480	
	Other Features	Trapped	Note #6

5.4 COMMENTS

5.4.1 Note #1

The closure plug has 16 fasteners (UNBRAKO Socket Head Screws). The size of fasteners is - 1 in. Dia. - UNC. In the SIDE OBLIQUE drop, the closure plug bolts are loaded in tension and shear as the closure plug is pulling away from the rest of the container.

It is estimated that the closure plug would maintain closure up to 912 g's.

5.4.2 Note #2

Due to lead slump, in the side oblique zone, 1/3 to 1/2 of the full circumference of the container is impacted. Due to lead slump, the weld group WCC1, WCC2, WCC3, WCC, WCC5, WCC7, WCL1 and WF1 resist this impact. G-loads are calculated assuming the weld group is loaded collectively and only welds in the bottom half of the container shell are effective. WF1 are the external fin/shell fillet welds. The fins convert the shell from non-stiffened plain shell to stiffened composite shell. As the lead slumps, the welds are stressed collectively but not necessarily equally. After lead slump, the deformed shape of the conical shell will approximate orange peel configuration.

5.4.3 Note #3

There are four lift lugs fins, one in each quadrant of the conical shell. At the base of lift lug fins, the primary shell is reinforced. Upon impact, the impact front (crush front) advances as a function of time, ONE (of four) lift lug will be impacted. Consequently the primary shell may suffer shear fracture at approximately 86 g's [Pure shear failure. (Shear area $43 \text{ in}^2 \times 70,000 \text{ UTS psi} \times 0.6 / \text{weight of } 21,000 \text{ lb.} = 86 \text{ g's}$). The factor 0.6 is for converting UTS to U Shear Stress (USS)].

In the current design of F-294, the base of the lift lug has been re-designed (double shell etc. beefed up) Consequently, this failure path has very low possibility.

5.4.4 Note #4

In the side oblique drop, the bottom plate of the cavity is loaded with deceleration loads due to the lead slump. Its estimated that, based on 0.5 in. thick Hastelloy plate, the plate is capable of withstanding 430 g's. As the plate bends, the curvature will enable to withstand lots more G's. As the bottom of cavity is 55 in. from the impact point or plane, the G-loads at the bottom of the cavity will be substantially reduced compared to G-loads at the closure plug bolt area. The end cap is more likely to bend (become dished rather than fracture). If the lead slumps, the displacement of lead shielding is not a major concern as the F-294 is over-shielded.

5.4.5 Note #5

There are 16 fasteners (1 in. Dia. SAE Gr. 8) joining the crush shield to the container at the top zone. In the top end drop eight fasteners are loaded in compression, while the remaining eight are loaded in shear. The G-load capability is calculated to be 46 g's.

During the primary impact, the crush shield is impacted first. As the impact progresses, the crush shield is trapped between the top of the container and the drop test pad. Also after the side oblique drop, we may find the crush shield is partially "friction welded" to the top of the container.

5.4.6 Note #6

There are eight fasteners (1 in. Dia. SAE Gr. 8) joining the cylindrical fireshield to container at the bottom fixed skid zone. Two fasteners at each of the corners (4) of the fixed skid. In the top corner drop eight fasteners are loaded in tension. The g-load capability is estimated to be 480 g's.

The crush shield is impacted first. As the impact progresses, the cylindrical fireshield is decelerated. The cylindrical fireshield is trapped between the deformed crush shield and the fixed skid, so there is no loss of side thermal protection.

5.5 SUMMARY

- 1) In the side oblique drop attitude, the impact is characterized as medium-hard. Only 30% of the total PE is estimated to be absorbed between crush shield fin impact limiters, the container fins and the cylindrical fireshield Lead slump will absorb the balance of the PE. Consequently medium G-loads, high deformation and long duration is to be expected. Therefore the impulsive (instantaneous force x time) loads will be of significant magnitude around the lift lug fin.
- 2) Closure between the container and the plug shall be maintained for up to 912 g's. 912 g's is based on static UTS. Its concluded that closure shall be maintained.

- 3) During the primary impact, the crush shield shall be retained and trapped between the top of the container and the drop test pad. As the top fireshield is integral with crush shield, the top fireshield shall be retained (no loss of thermal protection). However the crush shield may be "lost" during the secondary bounce, depending upon the magnitude of reaction forces. In this failure path scenario, the puncture test to follow could further detach the crush shield and cause loss of top thermal protection.
- 4) The cylindrical fireshield shall be retained and trapped between the fixed skid and the deformed crush shield (no loss of side thermal protection).
- 5) Due to lead slump, the welds at the top and side zone of the containers are collectively loaded. However, the G-load capability of the weld group is relatively high (1,580 g's). The event "One of the container external welds (WCC1 or WCC3 or WF1) could fracture due to poor weld, asymmetric loading etc. "is a real possibility. Also the shell could fracture. In this failure path scenario, the lead shielding could be exposed directly to hot gases and or flame of the fire test to follow.
- 6) As the lift lug fin is the second component to be impacted, peak loads are transmitted from the lift lug fin to the base of the primary shell of the container. It is possible that the primary shell could fracture locally.

6. OVERVIEW OF DAMAGE IN THREE DIFFERENT DROP TEST ORIENTATIONS

6.1 *IN THE END DROP – TOP ORIENTATION*

- 1) Due to shearing of threads of the bolt hole, the closure plug is most likely to fail and be displaced in the top end drop orientation compared to other drop test orientations. As only static UTS was used to compute g-load capability, and as Dynamic UTS/Static UTS = 2, the closure plug in most likelihood will not come loose and be displaced.
- 2) Due to lead slump, the primary shell may be overstressed and subject welds to fracture. This is considered a low probability. The area under the lift lug fin is unlikely to be impacted.
- 3) Despite the fact that the crush shield fasteners are sheared, the loss of crush shield is unlikely as the crush shield is expected to be "friction welded" to the container as it crushes. Therefore no loss of top thermal protection.
- 4) The cylindrical fireshield is not likely to be lost. No loss of side thermal protection.

6.2 *IN THE CORNER DROP TOP ORIENTATION (57° TO HORIZONTAL)*

- 1) The closure plug is not likely to fail; however it may be displaced leading to radiation streaming. As the F-294 is over-shielded, this is not major concern.
- 2) Due to lead slump, 1/3rd or 1/4 of the primary shell and the welds in the top corner zone are subjected to stresses. In top corner attitude, as there is smaller area of impact, the stresses are high (compared to top end drop attitude). However, there are other mitigating circumstances that suggest that the stresses may not be quite high:
 - i) G-loads in top corner attitude will be lower than the G-loads in the top drop attitude as the top corner drop attitude has longer distance (41.1 in.) of CG from the impact point than the top end drop attitude (36.5 in.).
 - ii) The lead slump does not directly impact the top corner impact zone as the lead slump is sheltered by the inner cavity structure.

The impact of the lift lug and subsequent transfer of peak loads to the base of the lift lug is a different and unique situation. It is most likely that the lift lug may cause sufficient stresses as

to fracture the primary shell. This is considered the worst case scenario for the top corner drop orientation.

- 3) The crush shield fasteners are going to shear and fail; however the crush shield may be "friction welded" to the container fins. In a secondary bounce, the crush shield may "take off", thus causing loss of top thermal protection only to be restrained by long fins of the crush shield.
- 4) The cylindrical fireshield is not likely to be lost. No loss of side thermal protection.

6.3 *IN OBLIQUE DROP – SIDE ORIENTATION (15° TO HORIZONTAL)*

- 1) The closure plug is not expected to be lost but it shall be displaced sufficiently to cause radiation streaming. This radiation streaming shall be worse than the top corner drop test orientation.
- 2) Due to lead slump, the primary shell shall be stressed; however as the load is spread over larger area, the primary shell is unlikely to fracture.

The impact of the lift lug and subsequent transfer of peak loads to the base of the lift lug is a different and unique situation. It is most likely that the lift lug may cause sufficient stress as to fracture the primary shell. This is considered the worst case scenario for the side oblique drop orientation.

- 3) The crush shield fasteners will definitely shear. Upon secondary bounce the crush shield shall be caused to eject and separate from the rest of the container. Thus causing loss of thermal protection in the top zone.
- 4) Cylindrical fireshield is unlikely to be lost. No loss of the side thermal protection.

7. DISCUSSION

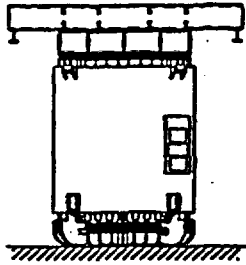
- 1) Loss of closure plug event is low probability in any drop test orientation. The ranking in which drop test orientation that this event is most likely is as follows:
Top end drop: Most likely
- 1.1) Displacement of closure plug event leading to radiation streaming. (The ranking is as follows):
Side oblique drop orientation: most likely
- 2) Fracture of primary shell container welds event: Overall low probability.
Top end drop: Most likely
- 2.2) Fracture of lift lug base zone:
Top corner or Side oblique drop orientation: Equally likely
- 3) Loss of crush shield, Loss of top thermal protection: high probability.
Side oblique drop orientation: Most likely.
- 4) Loss of cylindrical fireshield, loss of side thermal protection: very low probability.
Side oblique drop orientation: Most likely.

8. CONCLUSIONS

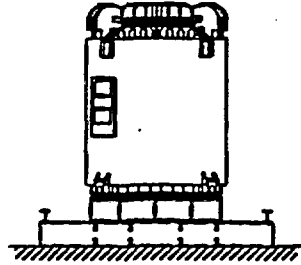
The most damaging drop test orientation is side oblique drop orientation for the following reasons:

- 1) The loss of crush shield event has a very high probability of taking place in the side oblique drop orientation compared to top corner drop orientation.
- 2) The displacement of closure plug event leading to radiation streaming.
- 3) Fracture of the primary shell under the lift lug base; Equal likelihood in side oblique or top corner drop orientations.

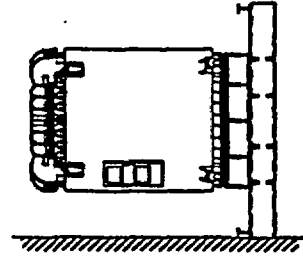
Figure 2.10.11-F1
Drop Test Orientations



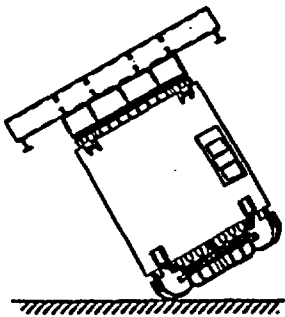
DROP ORIENTATION
#1.1
TOP END DROP



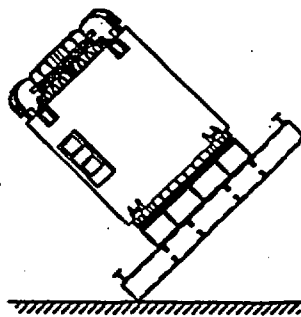
DROP ORIENTATION
#1.2
BOTTOM END DROP



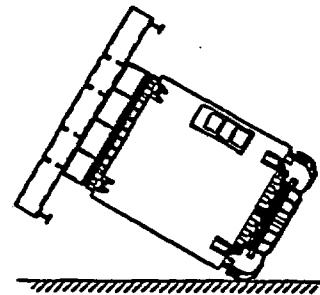
DROP ORIENTATION
#2
SIDE DROP



DROP ORIENTATION
#3.1
TOP CORNER DROP



DROP ORIENTATION
#3.2
BOTTOM CORNER DROP



DROP ORIENTATION
#4
OBLIQUE

Figure 2.10.11-F2
F-294 End Drop - Top Orientation (i.e., Inverted)

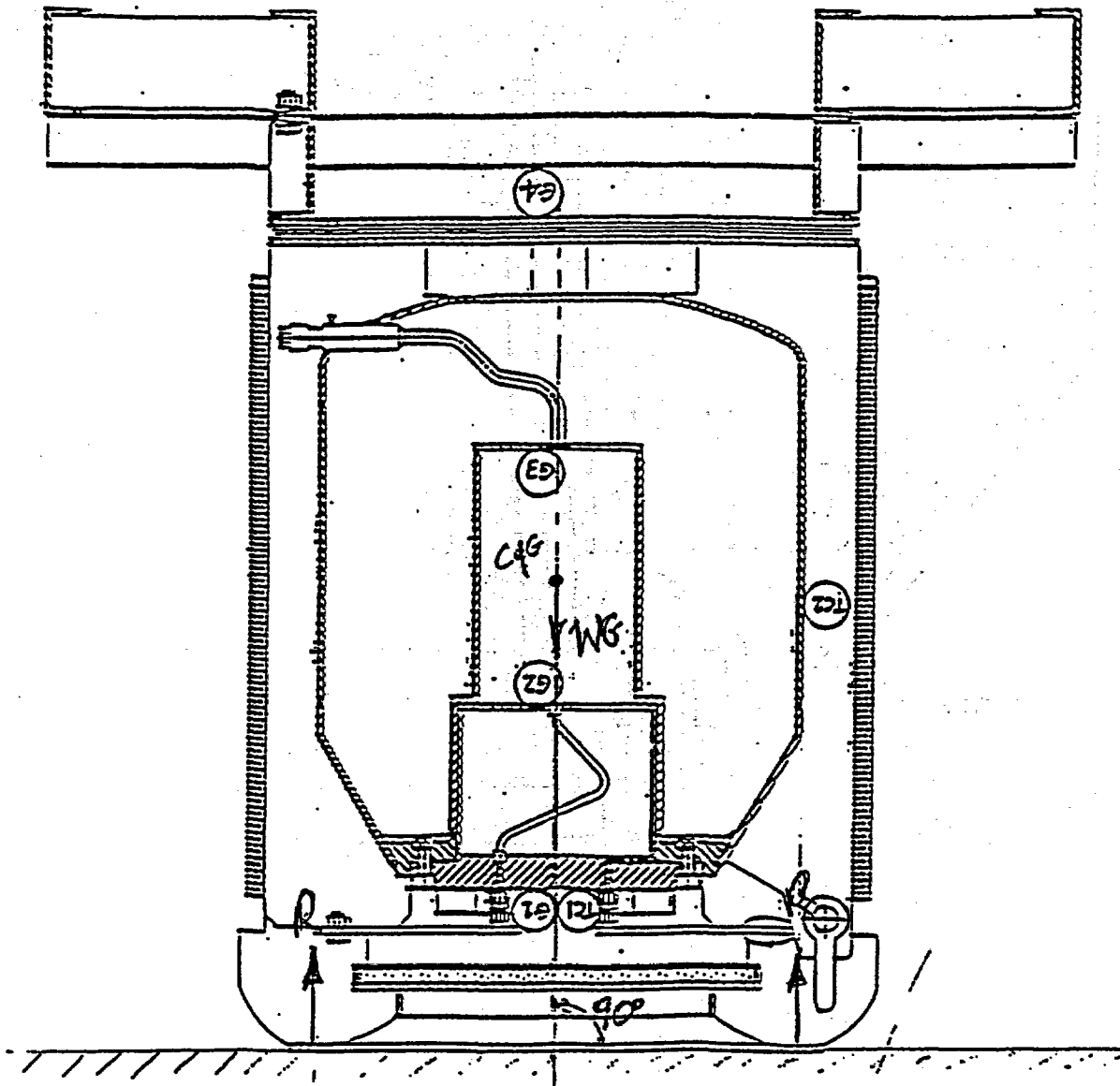


Figure 2.10.11-F3
F-294 Container Welds under Deceleration Load

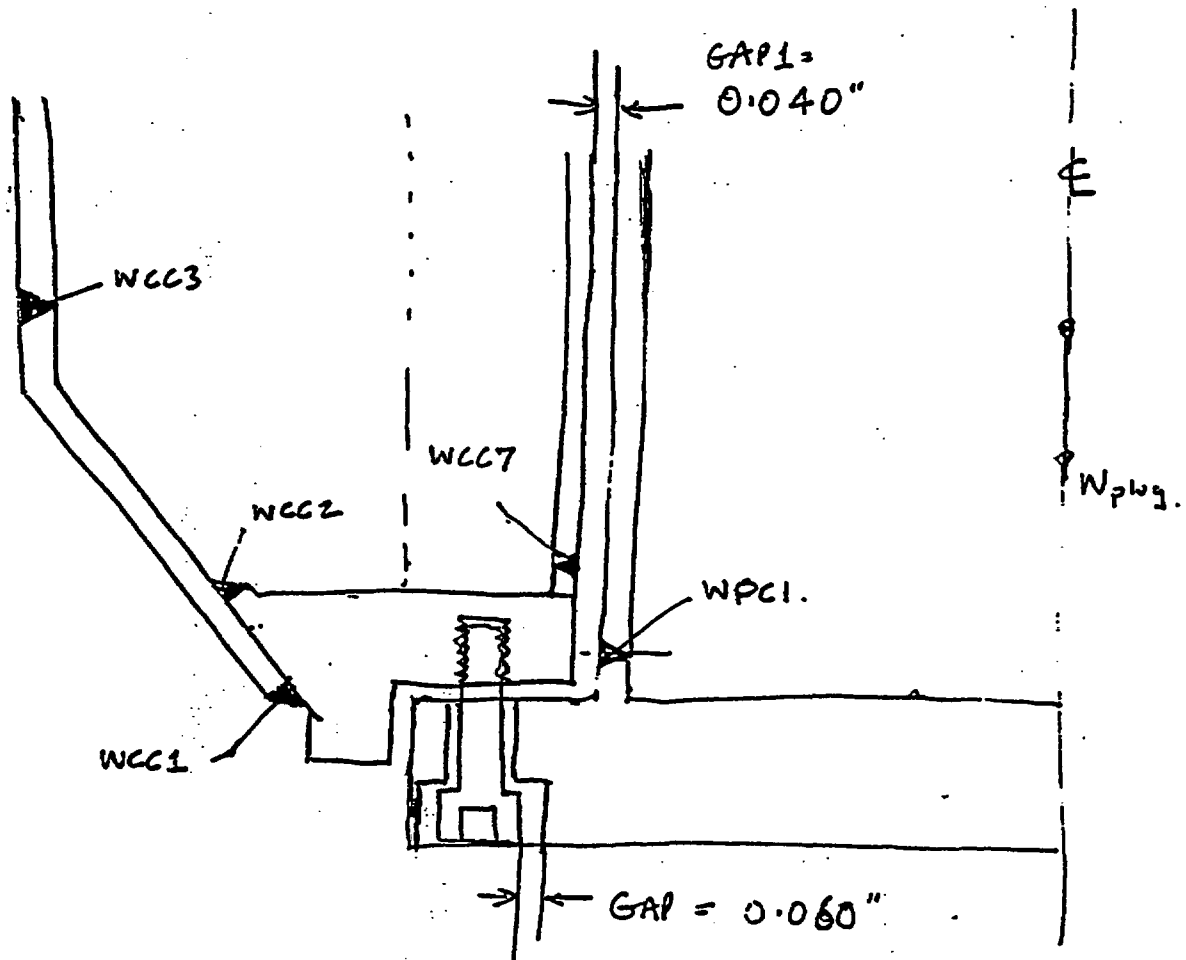


Figure 2.10.11-F4
Lift Lug Region of F-294 Test Packaging and F-294 Transport Package

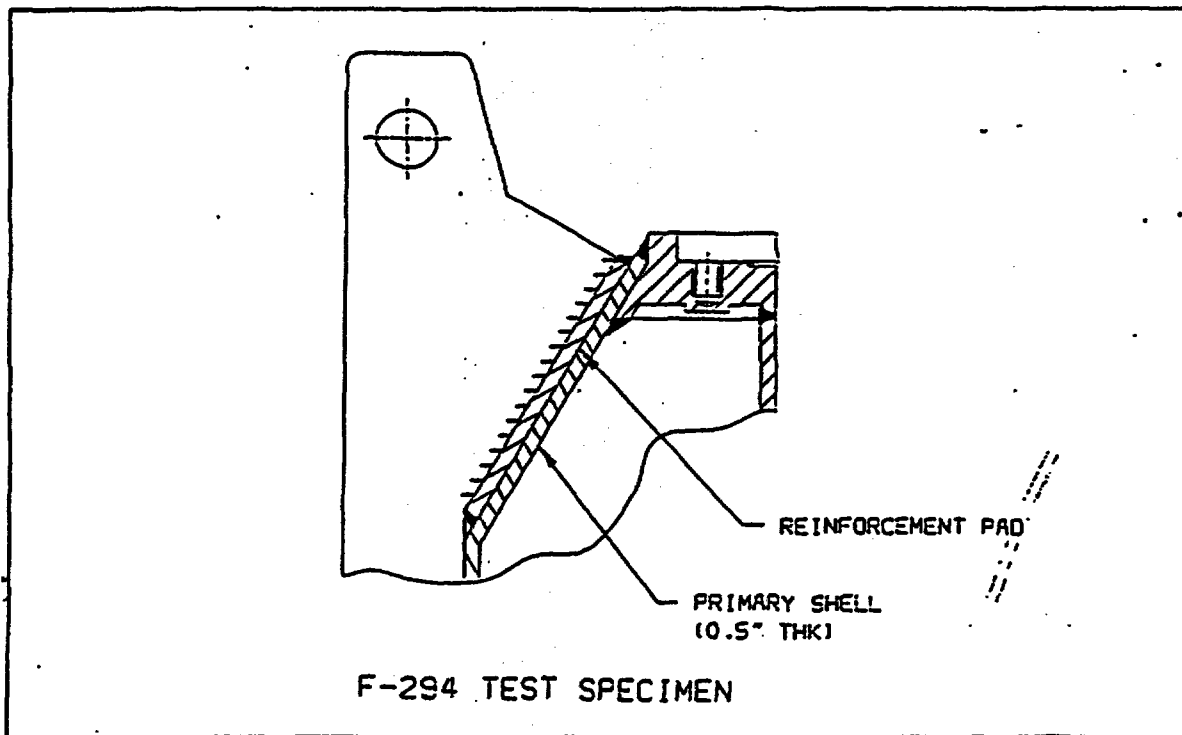
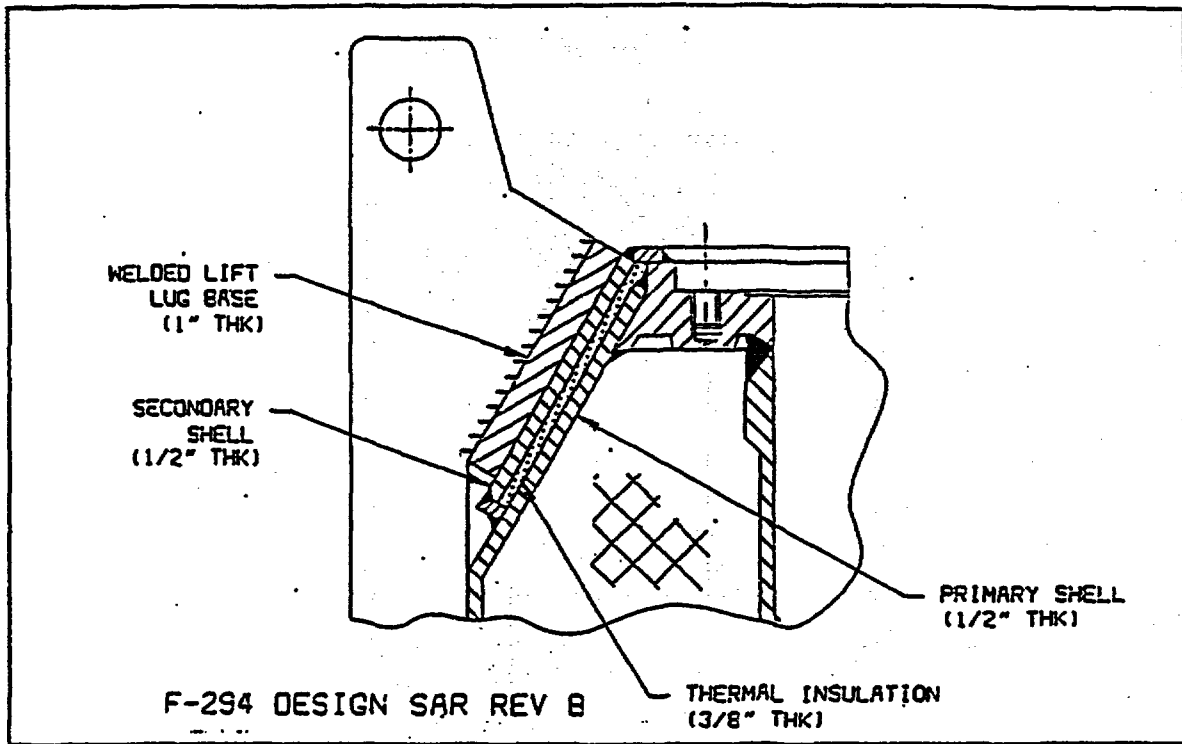


Figure 2.10.11-F5
F-294 Cavity and Cap under Deceleration Loads

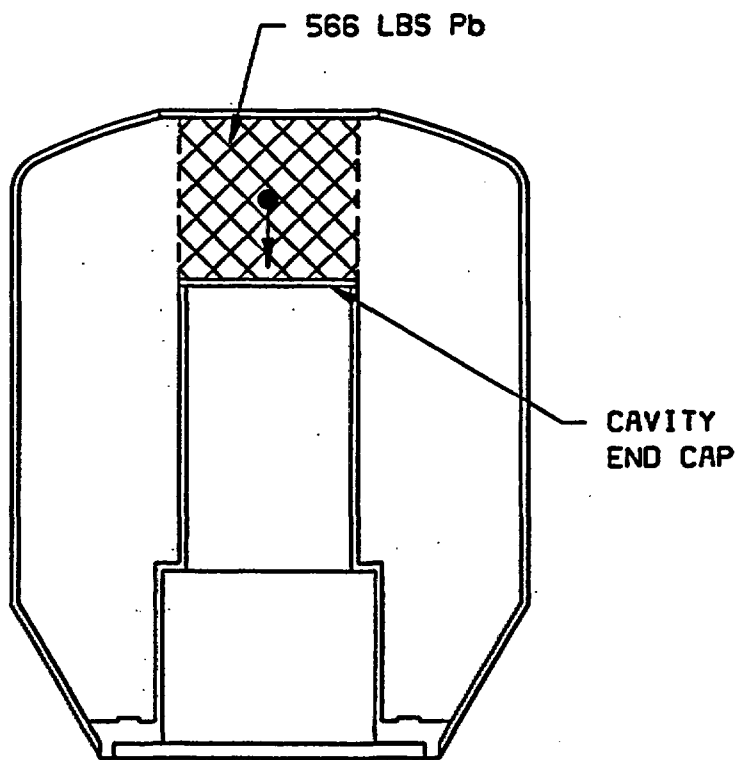


Figure 2.10.11-F7
Deceleration (g's) versus Deformation Characteristic for Various Drop Orientations

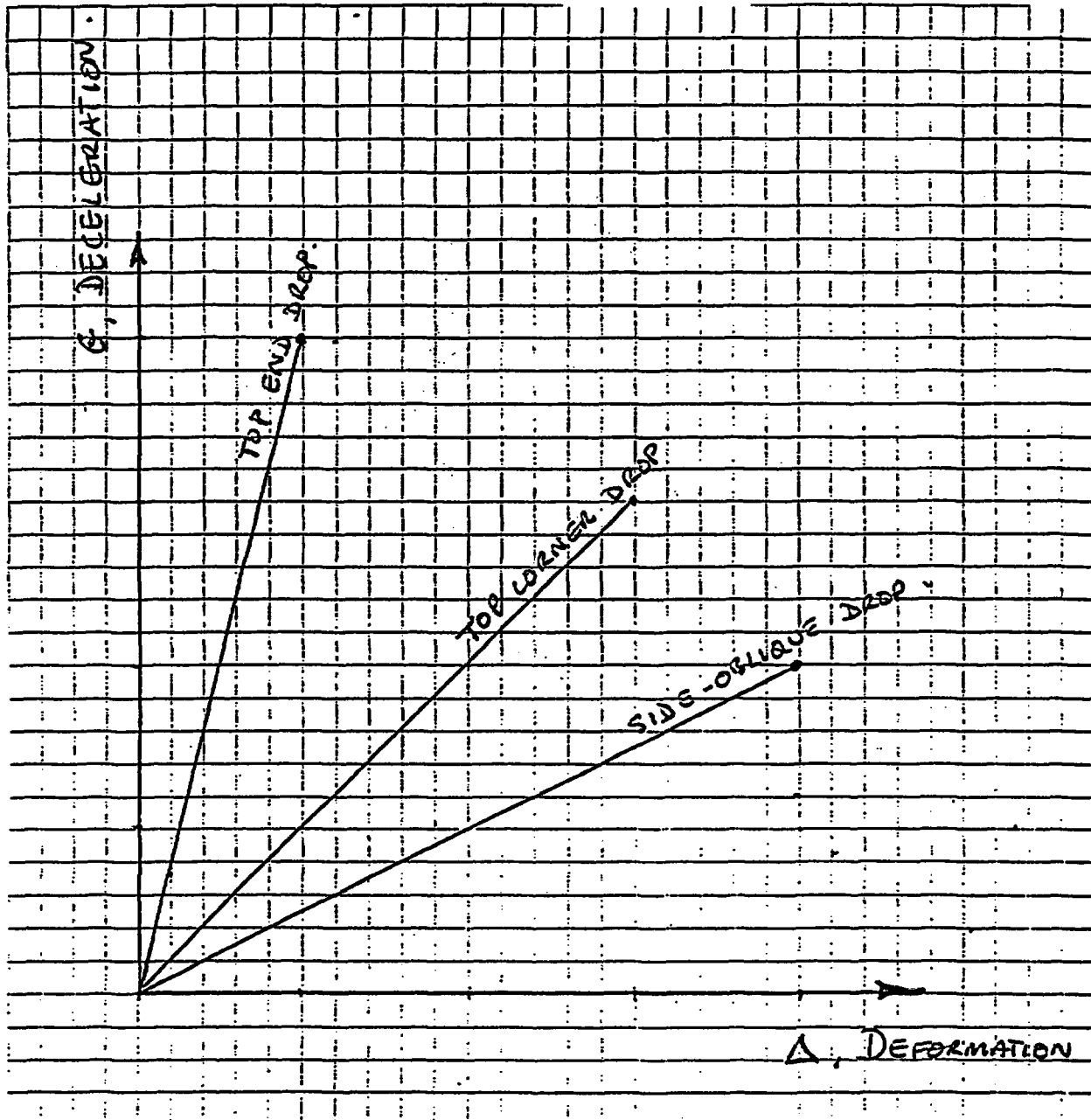


Figure 2.10.11-F8
F-294 Secondary Impact in Top Corner Drop Orientation

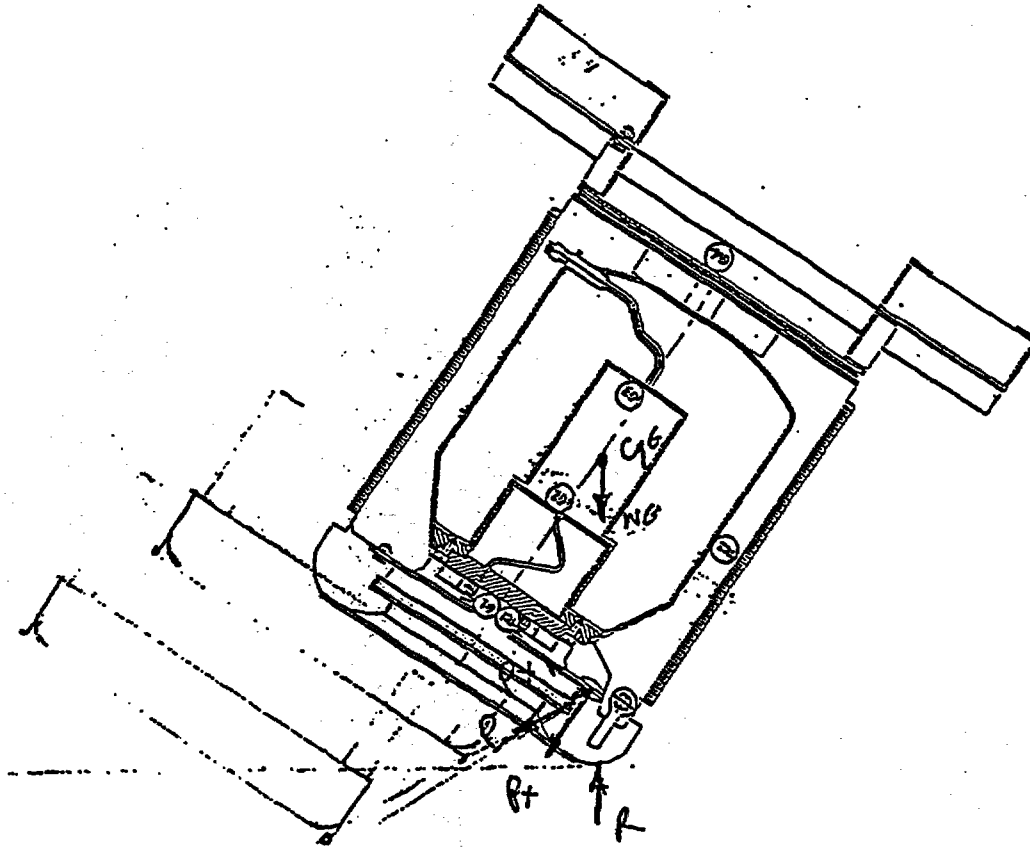
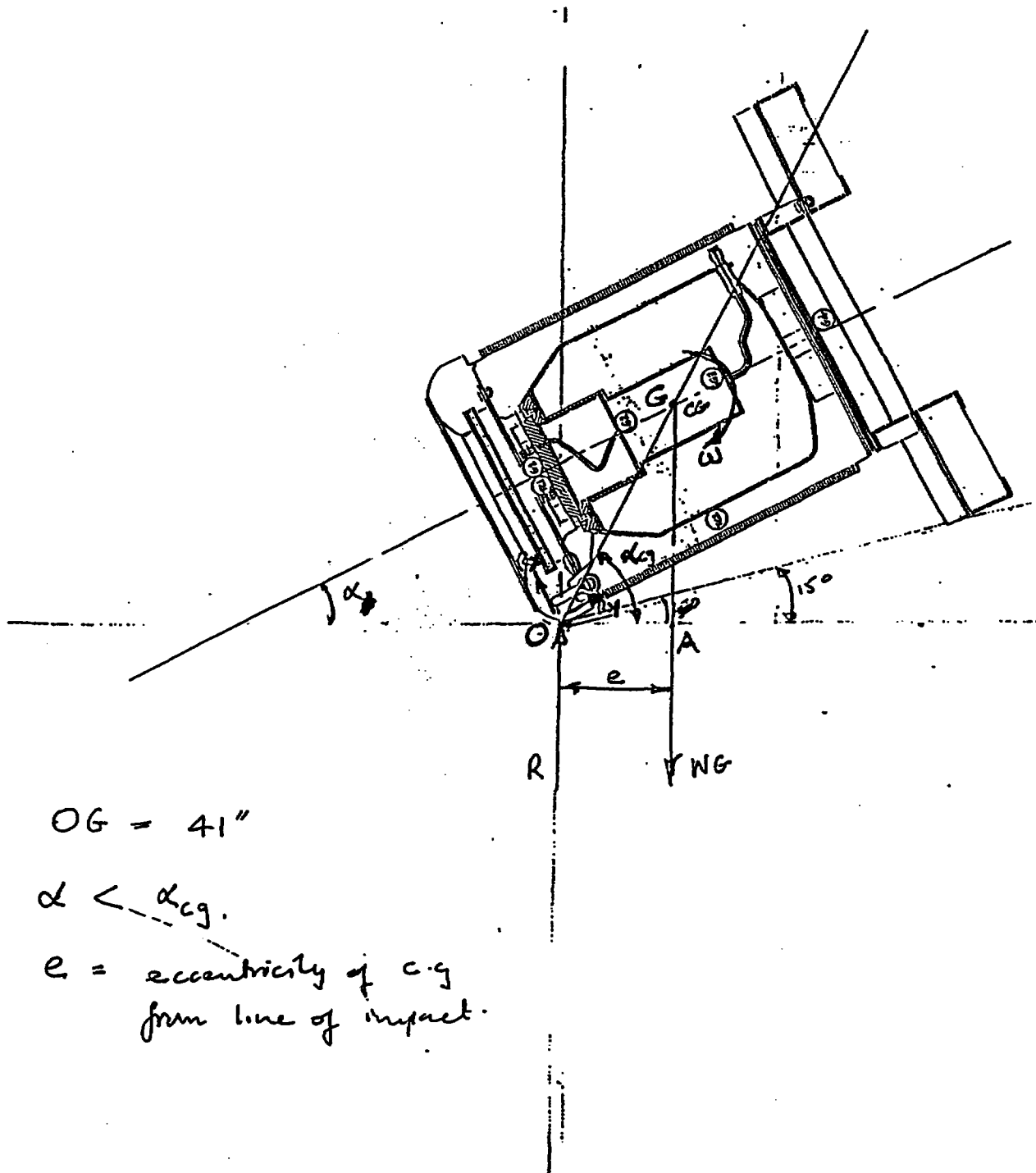


Figure 2.10.11-F9
F-294 in Side Oblique Drop (15° to Horizontal)



$OG = 41''$

$\alpha < \alpha_{cg}$

$e =$ eccentricity of c.g.
from line of impact.

Figure 2.10.11-F10
F-294 Secondary Impact in Side-Oblique Drop Orientation

